uOttawa

L'Université canadienne
Canada's university

FACULTÉ DES ÉTUDES SUPÉRIEURES ET POSTOCTORALES

uOttawa

L'Université canadienne
Canada's university

FACULTY OF GRADUATE AND POSDOCTORAL STUDIES

Chao Wang

AUTEUR DE LA THÈSE / AUTHOR OF THESIS

Ph.D. (Electrical and Computer Engineering)

GRADE / DEGREE

School of Information Technology and Engineering

FACULTÉ, ÉCOLE, DÉPARTEMENT / FACULTY, SCHOOL, DEPARTMENT

Photonic Generation and Processing of Microwave Arbitrary Waveforms Based on Advanced Fiber Bragg Gratings

TITRE DE LA THÈSE / TITLE OF THESIS

J. Yao

DIRECTEUR (DIRECTRICE) DE LA THÈSE / THESIS SUPERVISOR

CO-DIRECTEUR (CO-DIRECTRICE) DE LA THÈSE / THESIS CO-SUPERVISOR

J. Albert

T. Yeap

H. Schriemer

Gary W. Slater

Le Doyen de la Faculté des études supérieures et postdoctorales / Dean of the Faculty of Graduate and Postdoctoral Studies

PHOTONIC GENERATION AND PROCESSING OF MICROWAVE ARBITRARY WAVEFORMS BASED ON ADVANCED FIBER BRAGG GRATINGS

By

Chao Wang

A thesis submitted in partial fulfillment of the requirements for the degree of

Doctor of Philosophy

Ottawa-Carleton Institute of Electrical and Computer Engineering
School of Information Technology and Engineering
Faculty of Engineering
University of Ottawa

December 2010

Your file Votre référence
ISBN: 978-0-494-79733-4
Our file Notre référence
ISBN: 978-0-494-79733-4

ACKNOWLEDGMENTS

First of all, I would like to express my great gratitude towards my Ph. D thesis advisor Professor Jianping Yao for providing me the research environment, continuous support, valuable directions and superb guidance throughout this work. He has been a source of constant encouragement and enthusiasm. Without his trust and encouragement, this work would have never been possible.

Special thanks to Dr. Fei Zeng, for his generosity in passing down his knowledge and countless inspiring conversations. Sincere thanks to his invaluable help, both inside and outside the laboratory.

Enormous appreciations are to Sebastian Blais, for his technical guidance and fruitful discussions. With his help, I was able to start the first lab work on the FBG fabrication.

I would also like to thank the following people, who are current or former colleagues working with me in the Microwave Photonics Research Laboratory at the School of Information Technology and Engineering, University of Ottawa: Qing Wang, Yu Yan, Hao Chi, Yitang Dai, Honglei Guo, Wangzhe Li, Xihua Zou, Haiyun Xia, Hongqian Mu, Shilong Pan and Ming Li. Their strong supports and generous help greatly improved my research work. I will always cherish the good memories of working with them.

Finally, I am greatly indebted to my beloved wife Qi Zheng, for her immeasurable love and the biggest support, physically and mentally, to my study.

TABLE OF CONTENTS

ACKNOWLEDGMENTS I

TABLE OF CONTENTS II

LIST OF FIGURES IV

LIST OF TABLES XI

LIST OF ACRONYMS XII

ABSTRACT XV

CHAPTER 1 INTRODUCTION 1

1.1. Background review 1

1.2. Major contribution of this thesis 9

1.3. Organization of this thesis 14

CHAPTER 2 THEORETICAL OVERVIEWS 16

2.1. Dispersion-induced frequency-to-time mapping 16

2.1.1 Mathematical description 17

2.1.2 Practical implementation 21

2.1.3 Impact of higher-order dispersion 24

2.2. Fiber Bragg gratings 26

2.2.1. Mathematical model of a fiber Bragg grating 26

2.2.2. Synthesis of a fiber Bragg grating 29

2.2.3. Fabrication of fiber Bragg gratings 32

CHAPTER 3 PHOTONIC GENERATION OF MICROWAVE ARBITRARY WAVEFORMS USING FBGS 34

3.1 Photonic microwave arbitrary waveform generation based on optical spectral shaping and frequency-to-time mapping 35

3.1.1. FBG as an optical spectral shaper 37

3.1.2. FBG as a frequency-to-time mapper 71

3.1.3. FBG as a multifunctional device for both spectral shaping and frequency-to-time mapping 98

3.1.4. FBG as a multifunctional device for spectral shaping, frequency-to-time mapping and time shifting 108

3.2 Photonic microwave arbitrary waveform generation based on Fourier-transform optical pulse shaping 130

3.2.1. Time-domain Fourier-transform pulse shaping for micorwave arbitrary waveform generation 131

3.2.2. Frequency-domain Fourier-transform pulse shaping for microwave arbitrary waveform generation 149

CHAPTER 4 PHOTONIC PROCESSING OF MICROWAVE ARBITRARY WAVEFORMS USING FBGS 159

4.1. Photonic microwave delay-line filter for microwave waveform processing 160

4.1.1. Principle of photonic microwave multi-tap delay-line filter 160

4.1.2. Nonuniformly-spaced photonic microwave multi-tap delay-line filter for arbitrary microwave waveform matched filtering 162

4.2. Photonic microwave filter based on optical filter response to microwave filter response conversion. 174

CHAPTER 5 SUMMARY AND FUTURE WORK 202

5.1. Summary 202

5.2. Future work 203

LIST OF REFERENCE 205

PUBLICATION LIST 229

VITA 233

LIST OF FIGURES

Fig. 2.1. Schematic diagram showing the frequency-to-time mapping in a dispersive device. ...16

Fig. 2.2. Schematic diagram showing the higher-order dispersion induced nonlinear frequency-to-time mapping. 25

Fig. 2.3. Simulation results showing the synthesis method for strongly chirped fiber Bragg gratings. 31

Fig. 2.4. A phase mask is applied as a component of the interferometer for FBG fabrication. Normally incident UV beam diffracted into two ±1 orders....32

Fig. 3.1. General diagram of a photonically assisted microwave arbitrary waveform generation system based on coherent optical pulse shaping. 34

Fig. 3.2. Schematic diagram of a photonic microwave arbitrary waveform generation system based on optical spectral shaping and dispersion-induced frequency-to-time mapping. 36

Fig. 3.3. (a) Block diagram of the proposed all-fiber UWB signal generation system. (b) All-fiber optical spectral shaper configuration. MLFL: mode-locked fiber laser; EDFA: erbium-doped fiber amplifier; PD: photodetector; OC: optical coupler; TOF: tunable optical filter. 40

Fig. 3.4. UWB monocycle pulse generation. (a) Optical power spectrum after spectral shaping. (b) Spectrum of the incident ultrashort pulse. (c) Generated UWB pulse. (d) Power spectrum of the generated monocycle pulse. 44

Fig. 3.5. UWB doublet pulse generation. (a) Optical power spectrum after spectral shaping. (b) Generated UWB doublet pulse. (c) Power spectrum of the generated UWB pulse. 45

Fig. 3.6. Block diagram of the UWB signal generation system incorporating a balanced photodetector to remove the based band pedestal. MLFL: mode-locked fiber laser; SMF: single-mode fiber; OC: optical coupler; ATT: attenuator; DL: delay line; BPD: balanced photodetector. 47

Fig. 3.7. Schematic diagram of the conventional superimposed chirped fiber Bragg gratings. The Fabry-Perot cavity has a constant cavity length. The reflection response has a constant FSR. 49

Fig. 3.8. The proposed superimposed chirped fiber Bragg gratings with different chirp rates. The Fabry-Perot cavity has a wavelength-dependent cavity length. The reflection response has a chirped FSR. 50

Fig. 3.9. (a) Schematic diagram of the proposed microwave chirped pulse generation system. (b) SI-CFBG-based chirped FSR optical spectral filter. 51

Fig. 3.10. (a) Measured (solid line) and the simulated (dashed line) reflection spectra and (b) reflection group delay response of the proposed SI-CFBG. 54

Fig. 3.11. (a) Measured pulse profile and instantaneous carrier frequency of the generated chirped microwave pulse. (b) Autocorrelation waveform of the generated chirped microwave pulse. 56

Fig. 3.12. Schematic diagram showing an all-fiber optical spectral filter based on LCFBG-incorporated Sagnac loop mirror. FC: fiber coupler; TDL: tunable delay line; LCFBG: linearly chirped fiber Bragg grating; PC: polarization controller. 60

Fig. 3.13. Simulation results. The intensity spectra of the shaped optical pulse with (a) a symmetrical FSR (ΔL_0=0), (c) an increasing FSR (ΔL_0=9.7 mm), and (e) a decreasing FSR (ΔL_0=6.9 mm). The generated time-domain waveforms with (b) a symmetrical chirp rate and a zero central frequency, (d) a negative chirp rate and a central frequency of 22.3 GHz, and (f) a positive chirp rate and a central frequency of 16.1 GHz. 65

Fig. 3.14. Experiment setup for the generation of chirped microwave pulses based on spectral shaping and frequency-to-time mapping. (MLFL: mode-locked fiber laser; SMF: single-mode fiber, EDFA: erbium-doped fiber amplifier, OSA: optical spectrum analyzer, PD: photodetector, OSC: oscilloscope). 67

Fig. 3.15. The optical spectra of (a) input ultrashort pulse, and (b) the fabricated LCFBG (reflection). 67

Fig. 3.16. Experimental results. (a) Spectral response of the Sagnac loop mirror with a decreasing FSR. (b) Generated waveform with a positive chirp rate (dotted line: ideal Gaussian envelope). (c) Instantaneous RF frequency (solid line: linear fitting, circle: obtained from experimental result). (d) Compressed pulse by autocorrelation. 68

Fig. 3.17. Experimental results. (a) Spectral response of the Sagnac loop mirror with an increasing FSR. (b) Generated waveform with a positive chirp rate (dotted line: ideal Gaussian envelope). (c) Instantaneous RF frequency (solid line: linear fitting, circle: obtained from experimental result). (d) Compressed pulse by autocorrelation. Inset shows

the autocorrelation of a chirped pulse with the same chirp rate but an ideal Gaussian envelope. 70

Fig. 3.18. Schematic diagram of the proposed chirped microwave pulse generation system. PLS: pulsed laser source; SLF: Sagnac loop filter; HDD: high-order dispersive device; PD: photodetector. 75

Fig. 3.19. Simulation results for a chirped microwave pulse generation system using a dispersive device with the second-order dispersion only. (a) Envelope and optical instantaneous carrier frequency of the two chirped optical pulses {solid line: $r_1(t)$, dotted line: $r_2(t)$}; (b) Amplitude and RF carrier frequency of the generated microwave pulse..... 81

Fig. 3.20. Simulation results for a chirped microwave pulse generation system using a dispersive device with both the second- and third-order dispersion. (a) Envelope and optical instantaneous carrier frequency of the two chirped optical pulses {solid line: $r_1(t)$, dotted line: $r_2(t)$}; (b) Amplitude and RF carrier frequency of the generated chirped microwave pulse. 82

Fig. 3.21. Instantaneous RF carrier frequency of the generated chirped pulses under different second- and third-order dispersion. 83

Fig. 3.22. Schematic diagram showing the NL-CFBG generation using strain-gradient beam tuning technique. (a) Right-angled triangle cantilever beam. (b) Bending of the grating with the beam. LCFBG: linearly chirped fiber Bragg grating. 84

Fig. 3.23. Simulation results: group delay characteristics of the generated NL-CFBG at different beam displacements. 87

Fig. 3.24. Experimental setup of the proposed chirped microwave pulse generation system based on nonlinear frequency-to-time mapping. (a) System configuration; (b) the two-tap SLF; (c) the normalized transmission response of the SLF. (MLFL: mode-locked fiber laser, SLF: Sagnac loop filter, NL-CFBG: nonlinearly chirped fiber Bragg grating, EDFA: erbium-doped fiber amplifier, PD: photodetector, OC: optical coupler, PC: polarization controller, PMF: polarization maintaining fiber, OSC: oscilloscope.) 88

Fig. 3.25. Measured optical spectrum of the shaped optical pulse. The inset shows the spectrum of input optical pulse before spectral shaping. 89

Fig. 3.26. Measured results: (a) reflection spectra and (b) group delay responses of the generated NL-CFBG under different beam deflections. (dotted line: zero deflection; solid line: 2 mm deflection; dash-dot line: 5 mm deflection.) 90

Fig. 3.27. Experimental results. (a) Pulse profile and (b) instantaneous frequency in the case of 2-mm beam deflection. (c) Pulse profile and (d) instantaneous frequency in the case of 5-mm beam deflection. {Circle in (b) and (d): obtained from experimental results, dashed line in (b) and (d): theoretical prediction by (3-30).} 91

Fig. 3.28. Autocorrelation waveforms of the generated chirped microwave pulses. (a) Beam displacement is 2 mm. (b) Beam displacement is 5 mm. Insets: generated chirped microwave pulse. 93

Fig. 3.29. Generated microwave waveforms with different modulation depth under different second-order dispersion of (a) 580, (b) 648, (c) 700, and (d) 820 ps^2 95

Fig. 3.30. Required second-order dispersion to generate a temporal waveform with an optimal modulation depth at different time delays 96

Fig. 3.31. Schematic diagram showing the proposed microwave arbitrary waveform generator using a single LCFBG. MLFL: mode-locked fiber laser, LCFBG: linearly chirped fiber Bragg grating, PD: photo detector 100

Fig. 3.32. Refractive index modulation and reflection spectrum for a strongly chirped fiber Bragg grating 102

Fig. 3.33. Flow chart for the design and fabrication of an LCFBG with arbitrary magnitude response 104

Fig. 3.34. Measured reflection spectra and group delay responses of the fabricated LCFBGs for (a) chirped microwave pulse generation and (b) UWB monocycle pulse generation. 106

Fig. 3.35. Arbitrary waveform generation results. (a) Shaped spectrum by an LCFBG for chirped microwave pulse generation. (b) The generated chirped microwave pulse. (c) Shaped spectrum by a second LCFBG for UWB monocycle pulse generation. (d) The generated UWB monocycle pulse. 107

Fig. 3.36. A large TBWP microwave pulse generator using an SD-CFBG. MLFL: mode-locked fiber laser, SD-CFBG: spatially discrete chirped fiber Bragg grating, EDFA: Erbium-doped fiber amplifier, PD: photodetector 112

Fig. 3.37. Illustration of the design and fabrication of an SD-CFBG. (a) An SD-CFBG implemented based on axial fiber shifting during the fabrication process. (b) The group delay response and the impulse response of the produced SD-CFBG 113

Fig. 3.38. Experiment result: the measured group delay response of the fabricated SD-CFBG for linearly chirped microwave pulse generation. 120

Fig. 3.39. Experimental result: the generated linearly chirped microwave pulse (solid line) and the instantaneous frequency (circle line).....121

Fig. 3.40. Calculated autocorrelation of the generated linearly chirped microwave pulse.....122

Fig. 3.41. Experiment result: the measured group delay response of the fabricated SD-CFBG for nonlinearly chirped microwave pulse generation. The dashed line shows the cubic curve fitting result.....124

Fig. 3.42. Experimental result: the generated nonlinearly chirped microwave pulse (solid line) and the instantaneous frequency (circle line). Dashed line: quadratic curve fitting of the instantaneous frequency.....124

Fig. 3.43. Calculated autocorrelation of the generated nonlinearly chirped microwave pulse...125

Fig. 3.44. Step-chirped microwave pulse generation. (a) The designed fiber shifting function. (b) The measured group delay response of the fabricated SD-CFBG. (c) The generated step-chirped microwave pulse (solid line) and the instantaneous frequency (circle line). Dashed line: discrete linear fitting of the instantaneous frequency.....126

Fig. 3.45. (a) Measured reflection spectral response and (b) the group delay response of the fabricated SD-CFBG for nonlinearly microwave pulse generation.....130

Fig. 3.46. Schematic diagram of a typical temporal pulse shaping system for microwave arbitrary waveform generation. MLFL: mode-locked fiber laser; EOM: electro-optic modulator; PD: photodetector.....131

Fig. 3.47. Schematic diagram of an unbalanced TPS system for microwave pulse generation based on frequency multiplication. MLFL: mode-locked fiber laser, LCFBG: linearly chirped fiber Bragg grating, MZM: Mach-Zehnder modulator, PD: photodetector.....135

Fig. 3.48. The unbalanced TPS system can be modeled as a typical TPS system followed by a residual dispersion element. MLFL: mode-locked fiber laser, LCFBG: linearly chirped fiber Bragg grating, MZM: Mach-Zehnder modulator, PD: photodetector.....136

Fig. 3.49. Simulation results. (a) Output signal from the typical TPS system. (b) The optical spectrum of the signal in (a). (c) The frequency-multiplied microwave signal at the output of the entire system.....141

Fig. 3.50. Simulated output microwave pulses from the unbalanced TPS systems based on DSB modulation {(a), (b), (c)} and DSB-SC modulation {(d), (e), (f)}.....142

Fig. 3.51. Experimentally generated frequency-multiplied microwave pulses with different multiplication factors.....143

Fig. 3.52. Calculated frequency multiplication factor and output pulse duration as a function of the residual dispersion. 145

Fig. 3.53. Simulation result. The output signal of the typical TPS system with both the GVD and TOD. 148

Fig. 3.54. Schematic diagram of a conventional frequency-domain Fourier-transform optical pulse shaping system. 150

Fig. 3. 55. Schematic diagram of the proposed Fourier-transform optical pulse shaping system using a single LCFBG. USPL: ultra-short pulsed laser, LCFBG: linearly chirped fiber Bragg grating 152

Fig. 3.56. The reflection spectrum and the group delay response of the fabricated LCFBG. Solid line: measured spectrum; dotted line: desired spectrum. 155

Fig 3.57. The magnitude and group delay response of the entire pulse shaping system. Solid line: measured magnitude response; dotted line: desired magnitude response. 156

Fig. 3.58. Measured impulse response of the entire pulse shaping system. 157

Fig. 3.59. Synthesized triangular pulse (calculated using the measured LCFBG magnitude and group delay response). 157

Fig. 4.1. General diagram of a photonic microwave filter for microwave waveform processing. 159

Fig. 4.2. A diagram showing a generic photonic microwave delay-line filter with a finite impulse response. 161

Fig. 4.3. A diagram showing a nonuniformly-spaced photonic microwave delay-line filter by using an SD-CFBG. 166

Fig. 4.4. The frequency response of the desired bandpass filter. 169

Fig. 4.5. The tap coefficients (a) and time delays (b) of the designed nonuniformly-spaced FIR filter. 169

Fig. 4.6. The calculated frequency responses (both magnitude and phase) of the nonuniformly-spaced FIR filter (solid lines) and the regular uniformly-spaced FIR filter (dashed lines) 170

Fig. 4.7. (a) Simulated reflection spectral response and (b) the group delay response of the designed SD-CFBG. 171

Fig. 4.8. (a) The temporal shape and (b) the spectrum of the input linearly chirped microwave pulse to be compressed. 172

Fig. 4.9. The compressed pulse at the output of the designed photonic microwave filter. 173

Fig. 4.10. Schematic diagram of the proposed photonic microwave filter based on optical filter response to microwave filter response conversion. SSBM: single-sideband modulator; OSF: optical spectral filter. 175

Fig. 4.11. Normalized magnitude spectrum of the linearly chirped microwave pulse with a TBWP of 80. 186

Fig. 4.12. Reflection magnitude response and group-delay response of the LCFBGs for the implementation of (a) a POF, (b) a CMF, and (c) an MIF. 187

Fig. 4.13. Correlations outputs of the three filters for (a) a noise-free chirped microwave pulse, and (b) a chirped microwave pulse with an additive white Gaussian noise. (The correlation peak height is normalized.) 188

Fig. 4.14. Experimental setup of the proposed system. TLS: tunable laser source; PC: polarization controller; MZM: Mach-Zehnder modulator; FBG: fiber Bragg grating; VNA: vector network analyzer; PD: photodetector. 189

Fig. 4.15. Designed FBG for the implementation of the optical phase filtering. (a) Reflection spectra, (b) group delay responses. (Solid lines: experimental results; dashed lines: simulation results) 192

Fig. 4.16. Experimental results: optical spectra of the gratings and the optical signals. (Solid line: transmission of FBG1; dashed line: reflection of FBG2; dotted line: single-sideband modulated optical signal) 193

Fig. 4.17. Experimental results: frequency response of the microwave filter. (a) Magnitude transmission response (Solid line: measured response; dashed line: desired response); (b) measured phase response. Inset: parabolic phase response after subtracting the linear phase component (Dashed line: quadratic curve-fitting; dotted line: theoretical prediction). 194

Fig. 4.18. Temporal waveforms. (Blue dotted line: original microwave pulse; red solid line: compressed microwave pulse). Inset: zoom-in view of the envelopes of the compressed microwave pulses. 196

Fig. 4.19. Simulation results: reflection spectrum and group delay of a broadband linearly chirped FBG. 199

Fig. 4.20. Simulated reflection spectrum and group delay responses of a broadband nonlinearly chirped FBG. 200

LIST OF TABLES

TABEL 3.1. Experimental Parameters and Results 143

TABLE 4.1. Performance Measures for Different Filters 189

TABLE 4.2. Comparison of System Performances 197

LIST OF ACRONYMS

AOM	Acousto-Optic Modulator
ASE	Amplified Spontaneous Emission
AWG	Arrayed Waveguide Grating
BPD	Balanced Photodetector
CMF	Complex Matched Filter
CMT	Coupled-Mode Theory
CW	Continuous Wave
DCF	Dispersion Compensating Fiber
DE	Dispersion Element
DLP	Discrete Layer Peeling
DSB	Double Sideband
DSB-SC	Double Sideband with Suppressed Carrier
DST	Direct Space-to-Time
EDFL	Erbium-doped fiber laser
EOM	Electro-Optic Modulator
FBG	Fiber Bragg Grating
FIR	Finite Impulse Response
FP	Fabry-Perot
FSR	Free Spectral Range
FWHM	Full Width at Half Maximum
GLM	Gelfand-Levitan-Marchenko

GVD	Group Velocity Dispersion
IM	Intensity Modulation/Modulator
LCFBG	Linearly Chirped Fiber Bragg Grating
LCM	Liquid Crystal Modulator
LD	Laser Diode
LTI	Linear Time Invariant
MIF	Modified Inverse Filter
MLFL	Mode-Locked Fiber Laser
MZI	Mach-Zehnder Interferometer
MZM	Mach-Zehnder Modulator
NL-CFBG	Nonlinearly Chirped Fiber Bragg Grating
OCDMA	Optical Code Division Multi-Access
OSA	Optical Spectrum Analyzer
OSC	Oscilloscope
OSF	Optical Spectral Filter
OVA	Optical Vector Analyzer
PC	Polarization Controller
PD	Photodetector
PIC	Photonic Integrated Circuit
PM	Phase Modulation/Modulator
PMF	Polarization Maintaining Fiber
POF	Phase-Only Filter
PSR	Peak-to-Sidelobe Ratio
RF	Radio Frequency

SD-CFBG	Spatially Discrete Chirped Fiber Bragg Grating
SI-CFBG	Superimposed Chirped Fiber Bragg Grating
SLF	Sagnac Loop Filter
SLM	Spatial Light Modulator
SMF	Single-Mode Fiber
SNR	Signal-to-Noise Ratio
SOD	Second-Order Dispersion
SS-FTM	Spectral Shaping and Frequency-to-Time Mapping
SSB	Single Sideband
TBWP	Time-Bandwidth Product
TDL	Tunable Delay Line
TMM	Transfer Matrix Method
TOD	Third-Order Dispersion
TOF	Tunable Optical Filter
TPS	Temporal Pulse Shaping
UB-TPS	Unbalanced Temporal Pulse Shaping
UWB	Ultra-Wide Band
UV	Ultraviolet
VNA	Vector Network Analyzer
WDM	Wavelength Division Multiplexing

ABSTRACT

Photonic generation and processing of microwave arbitrary waveforms has been a topic of interest recently. Compared with the electronic techniques, photonics techniques provide the capabilities of generating and processing high-frequency and large-bandwidth microwave waveforms which cannot be fulfilled by the electronic techniques. In this thesis, techniques to generate and process microwave arbitrary waveforms in the optical domain using advanced fiber Bragg gratings (FBGs) are investigated, with an emphasis on the system architectures in which FBGs are employed as spectral shapers and dispersive elements.

The thesis consists of two main parts. In the first part, we investigate the generation of a microwave arbitrary waveform using advanced FBGs. Two techniques to generating microwave arbitrary waveforms based on coherent optical pulse shaping are investigated. The first technique is based on optical spectral shaping and frequency-to-time mapping. The use of an FBG as an optical filter to achieve spectral shaping, as a dispersive element to achieve frequency-to-time mapping, and as a multifunctional device to perform both optical spectral shaping and frequency-to-time mapping is investigated. In the second technique, the photonic microwave arbitrary waveform generation is realized based on Fourier-transform pulse shaping. Time-domain Fourier-transform pulse shaping is first studied, where a pair of linearly chirped FBGs is employed as dispersive elements to temporally stretch and compress the input optical pulse. Fourier-transform pulse shaping is also implemented in the frequency domain, where a linearly chirped FBG functioning as both an optical spectral shaper and a conjugate dispersive element pair to perform pulse stretching and pulse compression is employed.

In the second part, we investigate the photonic processing of a microwave arbitrary waveform using advanced FBGs. A photonic microwave filter is usually used to process microwave signals in the optical domain. Two different photonic microwave filters are explored. The first filter is a nonuniformly spaced photonic microwave multi-tap delay-line filter, which is designed to have a quadratic phase response to achieve matched filtering of a frequency-chirped microwave waveform. A spatially-discrete chirped fiber Bragg grating (SD-CFBG), which can be designed to arbitrarily control the tap coefficients and the time delays, is utilized in the multi-tap delay-line filter to achieve the desired microwave filter response. The second photonic microwave filter is implemented based on optical filter response to microwave filter response conversion in which an FBG with the desired magnitude and phase response is employed as the optical filter. The employment of the photonic microwave filter for matched filtering of a frequency-chirped microwave waveform is demonstrated.

CHAPTER 1 INTRODUCTION

1.1. Background review

Microwave photonics is an interdisciplinary area that studies the interaction between microwave and lightwaves, for applications such as broadband wireless access networks, wireless sensors networks, radar and instrumentation [1-4]. Photonic generation and processing of arbitrarily shaped microwave/millimetre-wave (mm-wave) waveforms has been of a topic of interest recently, especially in the area of microwave photonics [5-6]. Thanks to advantages of the high speed and the broad bandwidth offered by optics, photonically assisted techniques provide the capabilities of generating and processing microwave and mm-wave arbitrary waveforms at a much higher frequency and broader bandwidth which may not be easily accomplished by conventional electronic techniques due to the limited speed and bandwidth of electronic devices.

Photonic microwave arbitrary waveform generation is usually achieved in the optical domain based on coherent optical pulse shaping. Numerous techniques have been proposed and demonstrated to achieve optical pulse shaping for photonic microwave arbitrary waveform generation. For example, photonically assisted microwave arbitrary waveform generation has been realized based on direct space-to-time (DST) pulse shaping in the spatial domain [7-12]. A DST pulse shaper operates to convert a spatially distributed pattern directly to a temporally distributed pattern. By controlling the amplitude, pulse-to-pulse spacing and repetition rate of the optical pulse sequence, a microwave or mm-wave waveform exhibiting arbitrary phase and amplitude modulation can be obtained.

A microwave or mm-wave arbitrary waveform can also be generated based on optical pulse shaping in the time domain using a temporal pulse shaping (TPS) system [13-22]. A typical TPS system consists of a pair of conjugate dispersive elements and an electro-optic modulator (EOM) located between the two dispersive elements. A transform-limited ultrashort optical pulse is temporally stretched by the first dispersive element, modulated by a designed microwave drive signal or pattern at the EOM, and then completely compressed by the second dispersive element. Both intensity modulation [15, 17, 20] and phase modulation [14, 18, 21-22] have been employed in the TPS systems. At the output of the TPS system, a temporal waveform that is the Fourier transform of the modulation signal is obtained. The key advantage of this technique is that an ultra-fast microwave or mm-wave waveform can be generated using a relatively low-speed microwave modulating signal.

Another widely-used technique to achieving microwave arbitrary waveform generation in the optical domain is based on optical spectral shaping of a transform-limited ultrashort optical pulse followed by dispersion-induced frequency-to-time mapping. The frequency-to-time mapping, also known as the real-time Fourier transformation [23-30], can be explained by the well-known analogy between the paraxial diffraction of optical beams in space and the dispersion of ultrashort pulses in time (time-space duality) [26, 31-36]. In a microwave arbitrary waveform generation system based on spectral shaping and frequency-to-time mapping (SS-FTM), an optical spectral shaper is usually used to shape the optical power spectrum of the input ultrashort optical pulse. A dispersive element is applied to perform the frequency-to-time mapping. The spectrally shaped and temporally stretched optical pulse is then fed to a high-speed photodetector (PD) which performs optical to electrical conversion. At the output of the system, a microwave waveform with the shape identical to that of the shaped optical spectrum

is obtained. The SS-FTM-based pulse shaping provides a straight-forward method for the generation of microwave arbitrary waveforms [6, 37-39]. The key feature of this technique is that the temporal pulse shaping is performed in the frequency domain, which is easy to be implemented by using an optical spectral filter. By properly designing the spectral response of the optical filter, microwave arbitrary waveforms can be generated after the frequency-to-time mapping in the dispersive device.

The key device in a microwave arbitrary waveform generation system based on SS-FTM is the optical spectral shaper or optical filter. Over the past few decades, a number of approaches for spectral shaping of an ultrafast optical pulse have been proposed. A widely adopted method for optical pulse shaping is implemented in the spatial domain based on spatial masking of the spatially dispersed optical spectrum [40-41], where a spatial light modulator (SLM) is usually used to manipulate the optical spectrum component of the input ultrafast optical pulse. Several different types of SLMs have been developed for ultrafast pulse shaping, including fixed spatially patterned amplitude and phase masks [42] and programmable SLMs, such as liquid crystal modulator (LCM) arrays [43-44] and acousto-optic modulators (AOMs) [45-47]. The advantage of using a programmable SLM is that the filter response can be reconfigured in real time with the help of a computer [37, 39].

It is known that the optical spectrum of an input optical pulse train generated by a mode-locked laser is usually in the form of discrete spectral lines. In a typical optical pulse shaping system, the spectral lines are manipulated in groups rather than individually, resulting in waveform bursts that are separated in time with low repetition rate. This is mainly due to the practical difficulty in building a pulse shaping system capable of resolving individual spectral line for an optical pulse train with a repetition rate below 1 GHz. To resolve this problem, spectral line-by-

line manipulation technique has been intensively investigated recently. Spectral line-by-line phase manipulation was first experimentally demonstrated by a hyperfine wavelength-division multiplexing (WDM) filter with 5-GHz line spacing in an optical code division multi-access (O-CDMA) system [48] and with 12.4-GHz spacing in a photonic radio-frequency (RF) arbitrary waveform generation experiment [49]. Complete amplitude and phase line-by-line pulse shaping experiments have been performed by use of a high-resolution diffraction-grating-based pulse shaper, which is capable of resolving individual spectral lines of an optical pulse train from an actively mode-locked fiber laser with a repetition rate of 8.5 GHz [50] or from a phase-modulated CW laser with a repetition rate of 9 GHz [51]. In [51], the line-by-line optical spectral shaper consists of a 2 × 128 pixel LCM array to independently tailor both the amplitude and phase of each spectral line. Spectral line-by-line optical pulse shaping has found wide applications in optical frequency comb generation [52], optical arbitrary pulse-train generation [53], optical arbitrary waveform generation [54-56] and microwave arbitrary waveform generation [57-58].

The key advantage of the SLM-based spatial domain optical pulse shaping techniques is that the system is reconfigurable with a high update rate. However, drawbacks associated with these techniques include the need for high-quality free-space optical elements with strict tolerances in the alignment. Therefore, an essentially alignment-free, integrated-optic configuration is desirable to simplify the implementation, particularly in the optical communications band near 1550 nm in which integrated-optic devices and techniques are well developed.

An arrayed waveguide grating (AWG), which was originally developed as an optical multiplexer/demultiplexer for applications in wavelength division multiplexed (WDM) systems [59-60], has been proved to be a promising candidate to achieve optical spectral shaping in a

very compact manner. Optical pulse shaping by use of AWGs was first proposed and demonstrated in [61-62]. The decomposed optical spectrum can be phase and/or amplitude modulated by a transmission [61] or reflection [62] spatial filter, which is integrated to the waveguide. This concept has also been applied to achieve direct space-to-time ultrashort optical pulse shaping in an integrated-optic configuration, where a modified AWG and an integrated spatially patterned mask are applied [10]. The spatial mask is employed to directly control the excitation profile of the guides in the waveguide array. Instead of using an integrated spatial filter/mask, by incorporating a separate time delay for each waveguide channel, an AWG in a recirculating feedback configuration can be used to realize a wavelength-selective time delay or phased-array antennas [63-64]. If appropriate attenuators are also involved in the feedback path for each spectral channel to perform amplitude modulation of the spectrum of the input broadband optical pulse, the AWG with a recirculating configuration can be applied to achieve photonic microwave arbitrary waveform generation based on discrete frequency-to-time mapping [6]. Due to the relatively low optical spectral resolution of the AWG, however, the frequency lines are manipulated in groups rather than individually. If the optical resolution is increased by increasing the size of the AWG, line-by-line optical spectral shaping can also be performed by using an AWG in a more compact way compared to the free-space-optics-based line-by-line optical spectral shaping. More recently, optical arbitrary waveform generation via line-by-line optical spectral shaping by exactly replicating the target waveform's complex spectrum (both amplitude and phase) has been reported by using AWG-based waveform shapers [65-66]. The synthesis of arbitrary waveform is achieved by applying phase and amplitude modulation to each line (mode) of an input optical frequency comb. The high-speed phase and amplitude modulators with bandwidths equal to the optical resolution of the AWG

are integrated into each channel of the AWG. However, the AWG-based optical pulse shaping approaches rely on complex waveguide elements [65-66], such as integrated phase and/or amplitude modulators, to achieve the desired spectral filter response. They are practically limited by the strict fabrication requirements.

In the optical pulse shaping systems based on SLMs and AWGs, since the spectral shaping is implemented in either free space or integrated waveguides, coupling the shaped waveforms back into an optical fiber would introduce considerable loss and limit the potential for practical applications. The solution is to use all-fiber optical spectral filters, which have the advantages of lower loss and good compatibility with other fiber-optics devices. In addition, an all-fiber system has high potential for integration. Recently, several photonic microwave arbitrary waveform generation systems have been demonstrated in an all-fiber fashion [38, 49, 67]. In [49], for example, a fiber-optic WDM filter with a channel spacing of 6.2 GHz is used to separate the individual frequency lines/modes of an input ultrashort pulse train. The output from each of the WDM filter channels is sent through both an electro-optic intensity and a phase modulator such that the relative intensity and phase between channels can be controlled. Thus, arbitrary waveforms can be synthesized by controlling the amplitudes and phases of the individual frequency modes. All-fiber arbitrary waveform generation can also be achieved by superposing a set of properly weighted and time-delayed optical sample pulses, which are generated from a single input optical pulse by using a uniform-FBG array in conjunction with a multi-channel delay-line device to achieve amplitude weighting and time delaying [38]. The similar concept has been previously proposed based on a free-space multi-stage interferometer [68].

Note that the output at a channelized photonic arbitrary waveform generator, such as that based on an AWG [6, 65-66], a wavelength-division-multiplexer [49], or a uniform FBG array [38], is actually the sampled version of the desired temporal waveform. The number of resolvable temporal spots in the output waveform is identical to the number of waveguide/fiber channels. In addition, the photonic microwave arbitrary waveform generation systems in [6, 65-66] were usually implemented using multiple optical devices, which makes the systems complicated with high coupling loss. The optical spectral shaping devices are also difficult to fabricate, such as a complex AWG or an FBG array. Thus it is desirable to find an all-optical approach for microwave arbitrary waveform generation that relies on a simple fiber-optic pulse shaper.

A key device in a fiber-optics-based optical pulse shaping system is the fiber Bragg grating (FBG). FBGs have been intensively investigated in the last few decades and different types of FBGs have been proposed [69]. Their unique filtering properties and versatility as in-fiber devices have been illustrated by their use in a variety of lightwave applications [70]. One of the most interesting fields of application of FBGs is microwave photonics, where an FBG with properly designed spectral response can be employed to generate and process microwave and mm-wave signals [71]. Since the magnitude response and the phase response (or group delay response) of an FBG can be precisely designed, both intensity and phase modulation of the input optical spectrum (complete optical spectral shaping) can be achieved in a single FBG. This feature makes FBG an excellent candidate of simple fiber-optic spectral shaper for microwave arbitrary waveform generation, with the advantage of simpler configuration, better stability, and better compatibility with other fiber-optic devices.

On the other hand, it is also desirable that the optically generated microwave waveforms can be processed in the optical domain, to take advantage of the high speed and broad bandwidth

offered by optics. FBGs have also found extensive applications in broadband photonic microwave signal processing systems [72]. It has been well demonstrated that optical delay-line filters are very powerful and widely used for processing high-frequency and broad-bandwidth microwave signals [73]. The first reported work on fiber delay-line filters for microwave signal processing can be traced back to 1976, when Wilner and Van de Heuvel first found that the low loss and the large bandwidth of optical fibers are ideal for broadband microwave signal processing [74]. This opens up new perspective toward the implementation of high-resolution and wide-band all-optical microwave signal processors. In the past few years, extensive efforts have been directed to the design and realization of photonic microwave delay-line filters with different structures to achieve different functionalities [75-96]. Thanks to the spectral filtering and temporal delaying (dispersion) properties, different FBGs have been extensively applied in the photonic microwave multi-tap delay-line filters to realize the tap weighting and time delaying [97-114]. Photonic processing of microwave signals with FBGs offers new capabilities of achieving tunable or reconfigurable operation through optical wavelength control. Moreover, these in-fiber signal processors are inherently compatible with other well-developed fiber-optic microwave photonics devices and systems.

Considering the various advantages provided by FBGs, in this thesis we focus on the investigation of photonic generation and processing of microwave arbitrary waveforms based on advanced FBGs. By applying the well-developed grating design algorithms, such as the inverse-scattering algorithms [115-116], FBGs with the desired magnitude and phase responses can be precisely synthesized. Meanwhile, the state-of-the-art FBG fabrication techniques enable the inscription of the designed FBGs with complex refractive index profile into photosensitive fibers with very high accuracy [69, 117-121]. Therefore, the use of FBGs becomes a promising

and achievable solution for photonically assisted microwave arbitrary waveform generation and processing.

1.2. Major contribution of this thesis

The major contributions of this thesis are to propose and demonstrate novel all-optical techniques to generate and process microwave arbitrary waveforms using advanced FBGs. Compared to other photonically assisted microwave arbitrary waveform generation and processing techniques based on free-space optics, the use of advanced FBGs makes the system more compact, with lower cost and fully compatible with other fiber-optic devices.

(Note that most of the presented work consists of material re-written from various published articles.)

In the first part of the thesis, photonic generation of microwave arbitrary waveforms based on advanced FBGs is investigated. Two techniques to generating microwave arbitrary waveforms based on coherent optical spectral shaping are investigated. The first technique is based on optical spectral shaping and frequency-to-time mapping (SS-FTM) [34]. The use of an FBG as an optical spectral shaper to achieve spectral shaping, as a dispersive element to achieve frequency-to-time mapping, and as a multifunctional device to perform both optical spectral shaping and frequency-to-time mapping is investigated.

Since the spectral characteristics (both the magnitude and phase responses) of an FBG can be tailored, it can be employed in an SS-FTM-based microwave arbitrary waveform generation system as an optical spectral shaper. Various configurations employing an FBG-based optical spectral shaper are proposed and demonstrated. We have proposed an ultra-wide band (UWB)

pulse generation system based on spectral shaping of an optical ultrashort pulse using FBGs. This work has been published in IEEE Photonics Technology Letters [122]. UWB is an attractive technology for short-range and high data-rate wireless communication systems [123-125]. The choice of the UWB pulse shapes is critical to the performance of UWB systems. Gaussian monocycle and doublet pulses have been considered promising candidates for UWB communication systems [126]. To photonically generate UWB monocycle and doublet pulses, an optical spectral filter that consists of a tunable optical bandpass filter and two uniform FBGs with different center wavelengths and bandwidths is used to achieve a spectral response corresponding to a UWB monocycle or doublet pulse [122]. After linear frequency-to-time mapping in a dispersive element, a temporal UWB monocycle or doublet pulse with a shape that is a scaled version of the shaped spectrum is generated.

Chirped microwave pulses have found wide applications in modern radar systems [127], in spread-spectrum communications [128] and in microwave computed tomography [129]. In an SS-FTM-based microwave arbitrary waveform generation system, an optical spectral filter that has a spectral response with an increasing or decreasing free spectral range (FSR) is required to shape the optical spectrum of the input ultrashort optical pulse for chirped microwave pulse generation. We have proposed and demonstrated an optical spectral filter that consists of two superimposed chirped fiber Bragg gratings (SI-CFBGs) with different chirp rates. The SI-CFBGs form a distributed Fabry-Perot cavity with a cavity length linearly dependent on the resonance wavelength, thus a spectral response with a linearly increasing or decreasing FSR is obtained. By properly selecting the chirp rates and longitudinal offset of the two superimposed chirped FBGs, a linearly chirped microwave pulse with a high central frequency and large chirp rate could be generated after linear frequency-to-time mapping in a dispersive element. This

work has been published in IEEE Photonics Technology Letters [130]. In [130], since the two chirped FBGs need to be written in a single optical fiber, the fabrication process is complicated. In addition, the longitudinal offset between the two chirped FBGs is fixed once the two chirped FBGs are fabricated; therefore the central frequency and the chirp profile of the generated chirped microwave pulse cannot be tuned. To solve these problems, we have recently proposed an all-fiber optical spectral shaper that has a varying FSR using only one single chirped FBG. The optical spectral shaper is implemented based on a chirped-FBG-incorporated Sagnac-loop mirror. By tuning the time delay in the fiber loop, the central frequency and chirp profile of the generated chirped microwave pulse can be both tailored. This work has been published in Journal of Lightwave Technology [131].

It is well known that a chirped FBG would exhibit large dispersion when used in reflection mode. In an SS-FTM-based microwave arbitrary waveform generation system, a chirped FBG can also act as a dispersive element to perform the frequency-to-time mapping. Based on this idea, we can find another way to generate chirped microwave pulses, which is based on spectral shaping using a uniform sinusoidal spectral filter, i.e., a Sagnac-loop filter (SLF) [132] or a Mach-Zehnder interferometer (MZI) [133], followed by the nonlinear frequency-to-time mapping using a high-order dispersive device having both the second- and third-order dispersion. We have produced a nonlinearly chirped fiber Bragg grating (NL-CFBG) with a tunable nonlinear group delay response (third-order dispersion) to serve as the high-order dispersive device to perform the nonlinear frequency-to-time mapping for the generation of chirped microwave pulses. This work has been published in IEEE Transactions on Microwave Theory and Techniques [132].

The spectral shaping and frequency-to-time mapping are usually achieved using two separated devices in all the previous approaches [6, 26, 37, 39, 122, 130-132], the system becomes complicated, costly, and with high loss. To improve the system performance, we have proposed to use a single linearly chirped fiber Bragg grating (LCFBG) as a multifunctional device to perform both optical spectral shaping and frequency-to-time mapping. We can control the spectral response of an LCFBG by designing the grating refractive index modulation profile. Therefore, the LCFBG can be designed to have a magnitude response corresponding to the target temporal waveform for spectral shaping. At the same time, due to the inherent linear group delay response, the LCFBG also performs the linear frequency-to-time mapping. This work has been published in IEEE Photonics Technology Letters [134]. Most recently, we have proposed an optical approach to generate microwave arbitrary waveforms using a spatially-discrete chirped fiber Bragg grating (SD-CFBG) as a multifunctional device. Compared with the LCFBG used in [134], the SD-CFBG provides one extra feature: the mapped temporal waveform can be further time shifted. A large time-bandwidth product arbitrary microwave waveform can be generated based on simultaneous spectral slicing, frequency-to-time mapping, and temporal shifting of the input optical pulse in the single SD-CFBG. This work has been published in Journal of Lightwave Technology [135].

The second technique to achieve photonic microwave arbitrary waveform generation is based on Fourier-transform pulse shaping, which can be implemented in either the time domain or the frequency domain. We have proposed and demonstrated an unbalanced time-domain Fourier-transform pulse shaping system to generate high-frequency microwave waveforms based on continuously tunable microwave frequency multiplication. The unbalanced temporal Fourier-transform pulse shaping system consists of an EOM and a pair of LCFBGs having opposite

dispersion, but non-identical in magnitude. The entire system can be modeled as a typical balanced temporal pulse shaping system for real-time Fourier transformation followed by a residual dispersive element for a second real-time Fourier transformation. This work has been published in IEEE Photonics Technology Letters [136]. On the other hand, Fourier-transform pulse shaping can also be implemented in the frequency domain using an optical spectral filter. We have demonstrated a simplified frequency-domain Fourier-transform optical pulse shaping system based on a single LCFBG. The LCFBG in the system was functioning as an optical spectral shaper and at the same time as a conjugate dispersive element pair to perform pulse stretching and pulse compression. The use of a single LCFBG guarantees an exact cancellation of the dispersion, making the pulse shaping system have a better pulse shaping accuracy with a greatly simplified structure. This work has been published in IEEE Photonics Technology Letters [137].

In the second part of this thesis, photonic processing of a microwave arbitrary waveform using advanced FBGs is investigated. One of the most important microwave waveform processing functions is matched filtering [127]. A photonic microwave filter can be used to achieve matched filtering of a microwave waveform in the optical domain. Two different types of photonic microwave filters are explored. The first filter is a nonuniformly-spaced photonic microwave multi-tap delay-line filter. We have demonstrated an FBG-based nonuniformly-spaced delay-line filter to achieve matched filtering of a chirped microwave waveform. An SD-CFBG, which can be designed to arbitrarily control the tap coefficients and the time delays, is utilized in the system to achieve the desired microwave filter response. We also investigate another photonic microwave filter based on optical filter response to microwave filter response conversion by using a single-sideband (SSB) modulator and an FBG. The FBG with the user-

defined magnitude and phase response is employed as the optical spectral filter. The optical filter response is then transferred to the response of the microwave filter through SSB modulation and optical heterodyne detection at a high-speed PD [138-139]. Based on this idea, a photonic microwave filter with a nonlinear phase response has been implemented to achieve matched filtering of a frequency-chirped microwave waveform. This work has been published in IEEE Transactions on Microwave Theory and Techniques [138].

1.3. Organization of this thesis

This thesis consists of two main parts. In the first part, we investigate the photonic generation of a microwave arbitrary waveform using advanced FBGs. In the second part, we investigate the photonic processing of a microwave arbitrary waveform using advanced FBGs

Specifically, in Chapter 1, a brief review of the background of photonic generation and processing of microwave arbitrary waveforms is first presented. The major contributions of this research work are then summarized. In Chapter 2, theoretical basis of the proposed FBG-based microwave arbitrary waveform generation and processing techniques is presented. Specifically, dispersion-induced frequency-to-time mapping is first discussed in Section 2.1. In Section 2.2, a brief study of theoretical and practical issues in the field of fiber Bragg gratings is presented. In Chapter 3, photonic generation of microwave arbitrary waveforms based on coherent optical pulse shaping using advanced FBGs is investigated. Two different techniques for microwave arbitrary waveform generation are investigated and experimentally demonstrated. Photonic processing of microwave arbitrary waveforms using advanced FBGs is investigated in Chapter 4. Two different photonic microwave filters are demonstrated to achieve matched filtering of

microwave arbitrary waveforms. Finally, a conclusion is drawn in Chapter 5 with some recommendations for future work.

CHAPTER 2 THEORETICAL OVERVIEWS

2.1. Dispersion-induced frequency-to-time mapping

It is known that a duality exists between the spatial Fraunhofer diffraction and the propagation of a temporal signal in a dispersive device under the second-order dispersion approximation [32, 140]. The time-space duality shows that a dispersive element which provides quadratic phase modulation in the time domain is the analogue of a thin lens in the space domain. The time-space duality has led to an interesting conclusion that if a transform-limited ultrashort optical pulse passes through a dispersive element, the dispersed optical pulse has a shape that is proportional to the optical power spectrum of the input optical pulse, as illustrated in Fig. 2.1. This is the so-called dispersion-induced frequency- or wavelength-to-time mapping (FTM or WTM). Since the output pulse from the dispersive element has a temporal envelope that is the Fourier transform of the input optical pulse envelope, the frequency-to-time mapping in a dispersive element is also known as real-time Fourier transformation [25]. These two terms are used interchangeably in this thesis.

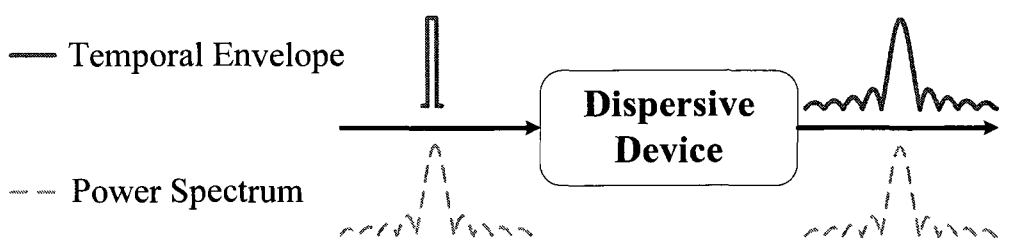

Fig. 2.1. Schematic diagram showing the frequency-to-time mapping in a dispersive device.

Frequency-to-time mapping has laid the foundation for the first technique we investigate for photonic microwave arbitrary waveform generation. In a photonic microwave arbitrary

waveform generation system based on spectral shaping and frequency-to-time mapping (SS-FTM), a user-defined optical spectral filter is employed to shape the optical power spectrum of the input short optical pulse. A temporal waveform with a shape identical to the shaped spectrum is obtained thanks to the frequency-to-time mapping in a dispersive element. In this section, the principle of dispersion-induced frequency-to-time mapping is first reviewed. Practical consideration of the implementation of the mapping process and the impact of higher-order dispersion on the mapping process are also discussed.

2.1.1 Mathematical description

It is known that a dispersive element, such as a single-mode fiber (SMF) or a chirped fiber Bragg grating (CFBG), can be modeled as a linear time-invariant (LTI) system with a transfer function given by

$$H(\omega) = |H(\omega)| \exp[-j\Phi(\omega)] \tag{2-1}$$

where $|H(\omega)|$ and $\Phi(\omega)$ are the magnitude and phase response of the dispersive element at angular frequency ω, respectively. We can assume that this transfer function has a nearly flat magnitude response $|H(\omega)|$ over an interested spectral bandwidth $\Delta\omega$ centered at an optical carrier frequency ω_0. This assumption is always true for a SMF over tens of nm bandwidth or for an LCFBG with a flat reflection within the reflection bandwidth. This treatment allows us to concentrate on the pulse distortion purely introduced by the dispersion (phase response).

Mathematically, the phase response $\Phi(\omega)$ can be expanded in Taylor series in the vicinity of ω_0 as

$$\Phi(\omega) = \Phi_0 + \dot{\Phi}_0(\omega - \omega_0) + \frac{1}{2}\ddot{\Phi}_0(\omega - \omega_0)^2 + \frac{1}{6}\dddot{\Phi}_0(\omega - \omega_0)^3 + \cdots \quad (2\text{-}2)$$

where $\Phi_0 = \Phi(\omega_0)$ is the phase constant at the carrier angular frequency, $\dot{\Phi}_0 = \left.\frac{d\Phi(\omega)}{d\omega}\right|_{\omega=\omega_0}$ is the group delay, $\ddot{\Phi}_0 = \left.\frac{d^2\Phi(\omega)}{d\omega^2}\right|_{\omega=\omega_0}$ is defined as the second-order dispersion (SOD), and $\dddot{\Phi}_0 = \left.\frac{d^3\Phi(\omega)}{d\omega^3}\right|_{\omega=\omega_0}$ denotes the third-order dispersion (TOD). Note that $\ddot{\Phi}_0$ is also called first-order dispersion (FOD) in some literatures since the first-order derivative of phase term $\dot{\Phi}_0$ actually gives the group delay. In this research work, however, $\ddot{\Phi}_0$ is called the second-order dispersion, or group velocity dispersion (GVD), since it is the second-order derivative of phase term and the first-order derivative of group delay; $\dddot{\Phi}_0$ is called the third-order dispersion or dispersion slope.

In the second-order dispersion approximation, in which the dispersion terms higher than the second-order are ignored within the spectral bandwidth of interest, the transfer function $H(\omega)$ can be approximated as

$$H(\omega) \cong |H(\omega)| \exp(-j\Phi_0) \exp(-j\dot{\Phi}_0\omega) \exp\left(-j\frac{1}{2}\ddot{\Phi}_0\omega^2\right) \quad (2\text{-}3)$$

It is worth noting that in (2-3) ω is used to replace $\omega - \omega_0$ in (2-2). Here ω is the relative angular frequency with respect to the central optical frequency of interest ω_0. This is equivalent to shifting the central optical carrier frequency to base band (down conversion), which makes it easier to analyze the system spectral response.

According to the LTI system theory, the corresponding impulse response $h(t)$ of the dispersive element can be obtained by taking the inverse Fourier transform of the above transfer function,

$$h(t) = \tilde{F}^{-1}\left[H(\omega)\right] \propto \exp\left[j\frac{1}{2\ddot{\Phi}_0}\left(t-\dot{\Phi}_0\right)^2 \right] \tag{2-4}$$

Note that the constant items are ignored in (2-4). For simplicity, we also use t to replace $t-\dot{\Phi}_0$ in the following analysis, which is equivalent to ignoring the average pulse delay $\dot{\Phi}_0$ and allows us to focus on the pulse distortion induced by the second-order dispersion $\ddot{\Phi}_0$.

Let $x(t)$ and $y(t)$ be the complex envelopes of the input and output optical pulses of a dispersion element with an impulse response $h(t)$, respectively. If the spectral bandwidth of the input optical pulse is narrower than the effective bandwidth of the dispersion device $\Delta\omega$, the envelopes $y(t)$ and $x(t)$ can be related by the convolution operation, that is, $y(t) = x(t) * h(t)$. Considering the impulse response in (2-4), we can rewrite the output pulse $y(t)$ as

$$\begin{aligned} y(t) &= \int_{-\infty}^{+\infty} x(t')h(t-t')dt' \propto \int_{-\infty}^{+\infty} x(t')\exp\left[j\frac{1}{2\ddot{\Phi}_0}(t-t')^2 \right]dt' \\ &\propto \exp\left(j\frac{t^2}{2\ddot{\Phi}_0} \right)\int_{-\infty}^{+\infty} x(t')\exp\left(j\frac{1}{2\ddot{\Phi}_0}t'^2 \right)\exp\left(-j\frac{1}{\ddot{\Phi}_0}tt' \right)dt' \end{aligned} \tag{2-5}$$

where t' is the convolution integral variable. Here we assume that

$$\left| \frac{\ddot{\Phi}_0}{(\Delta t_0)^2} \right| >> 1 \tag{2-6}$$

where Δt_0 is the time width of the incident ultrashort pulse $x(t)$.The assumption in (2-6) is also known as the temporal Fraunhofer approximation. It means that the second-order dispersion of the dispersive device $\ddot{\Phi}_0$ (in ps^2/rad) should be sufficiently large to temporally separate the spectral components of the incident pulse such that the time duration of the broadened pulse is much larger than that before experiencing the dispersion. Under the assumption given by (2-6), equation (2-5) can be approximated by

$$\begin{aligned} y(t) &\propto \exp\left(j\frac{t^2}{2\ddot{\Phi}_0}\right)\int_{-\infty}^{+\infty} x(t')\exp\left(-j\frac{t}{\ddot{\Phi}_0}t'\right)dt' \\ &\propto \exp\left(j\frac{t^2}{2\ddot{\Phi}_0}\right)X(\omega)\Big|_{\omega=\frac{t}{\ddot{\Phi}_0}} \end{aligned} \tag{2-7}$$

where $X(\omega) = \tilde{F}[x(t)]$ is the Fourier transform of the input temporal pulse $x(t)$. It is clearly shown in (2-7) that the output temporal pulse envelope is proportional to the spectrum of the input pulse with a phase factor. Therefore, dispersion-induced frequency-to-time mapping is obtained.

The result obtained above can be understood intuitively by considering the dispersion stretching effect. The chromatic dispersion introduced by the dispersive device causes a frequency-dependent linear time delay to the input optical pulse. Sufficient dispersion must be provided to temporally separate the spectral components of the input optical pulse and realize the unique mapping from the frequency domain to the time domain.

The frequency-to-time mapping relationship is determined by the second-order dispersion of the dispersive element. The second-order dispersion (or GVD) can be expressed in three different forms

$$\ddot{\Phi}_{\lambda} = \frac{d\tau}{d\lambda} \qquad (in\ ps/nm) \tag{2-8a}$$

$$\ddot{\Phi}_{\omega} = \frac{d\tau}{d\omega} = \frac{d^2\Phi}{d\omega^2} \quad (in\ ps^2/rad) \tag{2-8b}$$

$$\ddot{\Phi}_{\nu} = \frac{d\tau}{d\nu} \qquad (in\ ps^2) \tag{2-8c}$$

where $\ddot{\Phi}_{\lambda}$, $\ddot{\Phi}_{\omega}$, $\ddot{\Phi}_{\nu}$ are related by

$$\ddot{\Phi}_{\lambda} = -\frac{2\pi c}{\lambda^2}\ddot{\Phi}_{\omega} = -\frac{c}{\lambda^2}\ddot{\Phi}_{\nu} \tag{2-8d}$$

where λ is the optical wavelength, ω is the optical angular frequency, ν is the optical frequency, and τ is the time delay introduced by the dispersive element, which is given by

$$\tau = \frac{d\Phi}{d\omega} = -\frac{\lambda^2}{2\pi c}\frac{d\Phi}{d\lambda} \tag{2-9}$$

Then the mapping relationship between the time variable (Δt) and the frequency or wavelength variable ($\Delta\omega$, $\Delta\lambda$) is expressed as

$$\Delta t = \ddot{\Phi}_{\nu}\Delta\nu = \ddot{\Phi}_{\omega}\Delta\omega = \ddot{\Phi}_{\lambda}\Delta\lambda \tag{2-10}$$

2.1.2 Practical implementation

Equation (2-7) provides the theoretical basis for the dispersion-induced frequency-to-time mapping. For practical implementations, however, a few more issues have to be addressed.

First, the frequency-to-time mapping or real-time Fourier transform is usually performed in the coherent regime and restricted to work with a Fourier transform-limited input ultrashort optical pulse only. A Fourier transform-limited pulse, or more commonly known as transform-limited

or bandwidth-limited pulse, is usually an ultrashort optical pulse that has the minimum possible time duration for a given spectral bandwidth. The transform-limited pulse has a constant phase (chirp free) across the whole pulse window. Its complex field can be expressed as

$$E(t) = |E(t)| \exp(j\omega_0 t) \exp(j\varphi_0) \tag{2-11}$$

where $|E(t)|$ is the pulse envelope, ω_0 is the central angular frequency, and φ_0 is the time-independent phase constant. On the contrary, an optical pulse, which is not transform-limited, usually has a time-dependent phase term $\varphi(t)$, resulting in an instantaneous frequency sweep (chirp) across the pulse window. The amplitude spectrum of the transform-limited pulse is the Fourier transformation of the temporal envelope, which is, however, not valid for a non-transform-limited optical pulse.

Transform-limited optical pulses are usually generated by mode-locked lasers [141]. In this research work, a passive mode-locked fiber laser from IMRA is employed as the optical source to generate transform-limited optical pulses for frequency-to-time mapping. Another well-established approach to generate transform-limited ultrashort optical pulses is based on electro-optic phase modulation of a CW laser and subsequent phase-to-intensity conversion in a dispersive medium [142-143].

Note that the frequency-to-time mapping can also be performed in the incoherent regime. In this scenario, a transform-limited optical pulse is no longer required. Recently, frequency-to-time mapping using an incoherent optical source was reported [144], where the optical source can be an amplified spontaneous emission (ASE) source and a light emitting diode (LED) source. Incoherent frequency-to-time mapping has also been applied in photonic microwave arbitrary

waveform generation [145]. The incoherent frequency-to-mapping may reduce the system cost, but at the price of a significantly higher noise added to the generated microwave waveform. This is because a fixed phase relation exists between the different spectral components of the electric field of a coherent source. However, there is no phase correlation between the optical-frequency components of an incoherent source. The applicability of an incoherent pulse shaping systems depends on their signal-to-noise ratio (SNR). A consistent statistical analysis of incoherent pulse shaping has been reported recently [146], where a full statistical study of the SNR of incoherent pulse shaping is presented.

Second, the dispersive element used to perform the frequency-to-time mapping can be a single-mode fiber (SMF), a dispersion compensating fiber (DCF), or a linearly chirped fiber Bragg grating (LCFBG), as long as the so-called temporal Fraunhofer approximation given by (2-6) is satisfied. In this thesis, both the dispersive fiber and the LCFBG have been used as the dispersive element. Basically, dispersive fibers (both SMF and DCF) feature truly broad bandwidth, relatively low insertion loss and flat transmittance. To provide sufficient dispersion, a very long fiber is required, which makes the system bulky with high loss, suffering from the effect of polarization mode dispersion. On the other hand, the use of an LCFBG provides a compact solution for dispersion-induced frequency-to-mapping. However, there are several factors that limit the performance of LCFBGs as a perfect dispersive element. These factors are the insertion loss, limited bandwidth, deviations from linearity of the group delay and group delay ripple (GDR). Among these parameters, GDR, which is a result of the interference between the broadband reflection due to the edge of the grating and the distributed nature of the grating reflection [69], may have non-neglectable impact on the frequency-to-time mapping process. Ideally, the GDR of a LCFBG can be significantly reduced by applying apodization

during the grating fabrication process. However, an apodized LCFBG usually exhibits pseudoperiodic GDRs due to the errors in grating period and the index modulation deviations resulting from imperfections in the fabrication process [147]. A detailed study of the grating GDRs on the performance of a microwave pulse generation system based on spectral-shaping and frequency-to-time mapping has been reported recently [148], where the GDRs are modeled using a sinusoidal distribution with different amplitudes and periods. Their results show that the system performance degradation due to the GDRs in the chirped FBG is small, as long as the frequency of the GDRs is larger than that of the generated microwave waveform.

2.1.3 Impact of higher-order dispersion

Frequency-to-time mapping or real-time Fourier transform has been discussed in Subsection 2.1.1, where the second-order dispersion approximation is applied and all the higher order dispersion is ignored. Therefore, a linear frequency-to-time mapping process occurs. The second-order dispersion approximation is valid for a SMF with a moderate length and a linearly chirped FBG. For some applications, however, the length of the SMF used as a dispersive element is very long, and higher-order dispersion has to be taken into account [149]. Note that the mapping process will work so as long as the temporal Fraunhofer approximation (2-6) is satisfied. In this scenario, the frequency-to-time mapping is no longer linear due to the higher-order dispersion. Nonlinear frequency-to-time mapping is analyzed in this section.

Assume that a transform-limited ultrashort optical pulse $x(t)$ is sent to a dispersive element incorporating both the second-order and higher-order dispersion. A dispersed optical pulse $y(t)$ is obtained at the output of the dispersive element due to the nonlinear frequency-to-time

mapping. The schematic diagram of a dispersive element with both the second-order and higher-order dispersion is shown in Fig. 2.2.

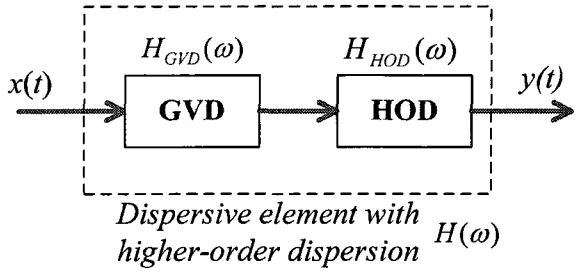

Fig. 2.2. Schematic diagram showing the higher-order dispersion induced nonlinear frequency-to-time mapping.

If the higher-order dispersion is considered, the transfer function of the dispersive element can be written as

$$H(\omega) = |H(\omega)| \exp\left(-j\frac{1}{2}\ddot{\Phi}_0\omega^2\right)\exp\left[-j\sum_{k=3}^{\infty}\left(\frac{1}{k!}\overset{k}{\Phi}_0\,\omega^k\right)\right] \\ = H_{GVD}(\omega)H_{HOD}(\omega) \tag{2-12}$$

where $\overset{k}{\Phi}_0 = \left.\frac{d^k\Phi(\omega)}{d\omega^k}\right|_{\omega=\omega_0}$ is the k*th*-order dispersion, $H_{GVD}(\omega) = |H(\omega)| \exp\left(-j\frac{1}{2}\ddot{\Phi}_0\omega^2\right)$ and $H_{HOD}(\omega) = \exp\left[-j\sum_{k=3}^{\infty}\left(\frac{1}{k!}\overset{k}{\Phi}_0\,\omega^k\right)\right]$. Therefore, the dispersive element can be modeled as a cascade of two dispersive elements, a first dispersive element having only the second-order dispersion (or GVD) and a second having all higher-order dispersion, with the transfer functions given by $H_{GVD}(\omega)$ and $H_{HOD}(\omega)$, respectively. A nonlinear mapping relationship incorporating higher-order dispersion is given [149]

$$\omega = \frac{t}{\ddot{\Phi}_0} - \sum_{k=3}^{\infty}\left[\frac{\overset{k}{\Phi}_0}{(k-1)!\left(\ddot{\Phi}_0\right)^k}t^{k-1}\right] \tag{2-13}$$

where ω is the optical frequency and t is the time.

2.2. Fiber Bragg gratings

FBGs were first discovered by Hill and his coworkers at the Communications Research Centre in Ottawa, Canada, back to 1978 [121, 150]. Since then, extensive efforts have been contributed to the investigation of FBG technology. The most interesting feature of FBGs is their flexible spectral characteristics. Other advantages offered by FBGs over competing optical devices include all-fiber geometry, low insertion loss, high return loss or extinction, and low cost. FBGs have been developed into critical optical components for many applications, such as in fiber-optic communications, optical sensor systems, and optical signal processing.

Recently, FBGs have attracted more and more interests in the area of microwave photonics, where different types of FBGs with properly designed spectral responses are employed to generate and process microwave and mm-wave signals in the optical domain [71]. In this research work, FBGs are playing the key roles in our proposed photonic microwave arbitrary waveform generation and processing systems. In this section, a brief review of the theoretical basis of FBGs is presented. The issues associated to FBG fabrication are also discussed.

2.2.1. Mathematical model of a fiber Bragg grating

An FBG is basically a section of optical fiber in which the refractive index in the core is perturbed forming a periodic index modulation profile so that certain wavelengths are transmitted while the other wavelengths are reflected. Typical FBGs have grating periods of a few hundred nanometers (nm), which allows mode coupling between two counter-propagation modes in the fiber core. Another type of fiber grating is called long-period gratings (LPGs),

which usually have periods in the order of hundreds of microns (μm), allowing mode coupling between a core mode and cladding modes. In this case, the core mode and the cladding modes are propagating in the same direction. In this thesis, we only focus on the first type of FBGs which reflects light over a narrow wavelength range and transmit all the other wavelengths.

When the Bragg condition is fulfilled, we have maximum mode coupling or reflection. The center wavelength of reflection is then called Bragg wavelength λ_B, which is related to the grating period by [69]

$$\lambda_B = 2n_{eff}\Lambda \tag{2-14}$$

where Λ is the grating period and n_{eff} is the effective refractive index of the optical fiber. By modulating the periodic index perturbation in amplitude and/or phase, we may obtain an FBG with different spectral response.

The relationship between the spectral characteristics of an FBG and the corresponding grating refractive index modulation profile can be described by the coupled-mode theory (CMT) [151-153]. CMT is a straightforward, intuitive, and powerful tool for obtaining quantitative information on the spectral properties (both the magnitude and phase) for an FBG with a given structure.

Let $A(z)$ and $B(z)$ to be two counter-propagating modes in the fiber core. According to the CMT, one mode will be coupled to another thanks to the periodic refractive index perturbation. A simplified coupled-mode equation can be given [152]

$$\frac{dR}{dz} = j\hat{\sigma}R(z) + j\kappa S(z)$$
$$\frac{dS}{dz} = -j\hat{\sigma}S(z) - j\kappa^* R(z) \tag{2-15}$$

where $R(z) = A(z)\exp(j\delta z - \phi/2)$, $S(z) = B(z)\exp(-j\delta z + \phi/2)$, $\delta = \beta - \pi/\Lambda$ is the propagation constant detuning from the mode propagation constant β , ϕ describes the grating chirp, κ is the "ac" coupling coefficient and $\hat{\sigma}$ is the general "dc" (period-averaged) self-coupling coefficient.

For a single-mode uniform Bragg reflection grating, closed-form solutions can be obtained for (2-15). In such a case, the amplitude reflection coefficient, ρ, for an FBG of a length L is given by

$$\rho = \frac{-\kappa \sinh\left(\sqrt{\kappa^2 - \hat{\sigma}^2}L\right)}{\hat{\sigma}\sinh\left(\sqrt{\kappa^2 - \hat{\sigma}^2}L\right) + j\sqrt{\kappa^2 - \hat{\sigma}^2}\cosh\left(\sqrt{\kappa^2 - \hat{\sigma}^2}L\right)} \tag{2-16}$$

Then the group delay response τ_ρ and dispersion d_ρ (in ps/nm) for a light reflected off the grating can be obtained from the phase of the amplitude reflection coefficient, $\theta_\rho = phase(\rho)$

$$\tau_\rho = \frac{d\theta_\rho}{d\omega} = -\frac{\lambda^2}{2\pi c}\frac{d\theta_\rho}{d\lambda} \tag{2-17}$$

$$d_\rho = \frac{d\tau_\rho}{d\lambda} = -\frac{2\pi c}{\lambda^2}\frac{d^2\theta_\rho}{d\omega^2} \tag{2-18}$$

In order to tailor the spectral characteristics of an FBG, a refractive index modulation technique called apodization can be used. Apodization is a word often mentioned in filter design.

Specifically, when applied to fiber grating filter design, the word "apodization" means gradually increasing the index modulation strength and hence the coupling coefficient with penetration into, as well as gradually decreasing on exiting from the grating [69]. Several apodization profiles, e.g., Gaussian, raise-cosine and super-Gaussian, are usually used to reduce the sidelobe level in the grating reflection spectrum. Apodization technique is also desirable in fabricating chirped fiber Bragg gratings, to eliminate the group delay ripples.

When dealing with FBGs with complicated coupling coefficient and chirp, no simple closed-form solution exists for the coupled-mode equation in (2-15). In this scenario, some numerical methods are employed. One of the most commonly used numerical methods for FBG response calculation is the piecewise-uniform transfer matrix method (TMM) [152, 154], which is implemented based on identifying matrices for each uniform section of the grating, and then multiplying all the sub matrices to get a single matrix describing the whole grating. In this research work, the FBGs (both uniform FBGs and chirped FBGs) are all calculated using this transfer matrix method.

2.2.2. Synthesis of a fiber Bragg grating

The synthesis of an FBG is to find the complex coupling coefficient or the refractive index modulation profile that corresponds to a given grating spectral response. The synthesis problem of a fiber grating is complicated, especially when compared with the well-known direct problem of computing the grating reflection response from a known grating structure (refractive index modulation profile). The simplest approach to solving grating synthesis problem was based on the first-order Born approximation where a Fourier transform relationship exists between the grating magnitude response and the refractive index modulation function [155]. This method,

however, is only suitable for weakly coupled gratings. Another feasible numerical method for FBG synthesis is the Gelfand-Levitan-Marchenko (GLM) inverse scattering algorithm [156]. This approach is accurate but only works for an FBG whose reflection coefficient is a rational function.

In 1999, Feced *et al.* proposed the so-called discrete layer-peeling (DLP) algorithm for the synthesis of fiber Bragg gratings [115]. To improve the clarity and efficiency of the DLP algorithm, a further study has been implemented to simplify the DLP synthesis method [157]. The DLP method is fast and accurate. In fact, it is even as simple as the direct problem. A comprehensive study on the DLP method and its application in optical filter design can be found in [158]. In this thesis, the synthesis of all uniform-period FBGs is implemented using the DLP method.

The numerical methods [115, 155-158] are suitable in the design of uniform-period or weakly chirped fiber gratings. In this research work, strongly chirped fiber Bragg gratings with desired reflection characteristics are usually required in the proposed microwave arbitrary waveform generation and processing systems. Therefore, we propose a simple and effective method to synthesize a highly-reflective and strongly-chirped FBG with nearly arbitrary reflection magnitude response. Since amplitude-only refractive index modulation is required, the designed LCFBG can be easily realized with the state-of-the-art FBG fabrication technique.

The proposed synthesis method for strongly chirped fiber Bragg gratings is based on an accurate mapping of the refractive index apodization to the grating reflection response, which is illustrated in Fig. 2.3. We can first set up the mapping relationship between the refractive index modulation profile and the grating response by imprinting a linearly varying index modulation

profile into the optical fiber using a linearly chirped phase mask, as shown in Fig. 2.3(a), to fabricate a calibration grating and measuring the grating reflection response, with the simulated grating response plotted in Fig. 2.3(b). By comparing the target grating reflection response with the measured grating response in Fig. 2.3(c), the desired index modulation function is obtained, as shown in Fig. 2.3(d). Finally, by applying the desired index modulation using the same phase mask, a strongly chirped fiber Bragg grating with the target reflection response can be obtained, as shown in Fig. 2.3(e). Note that for a chirped grating with a symmetrical spectral response, a symmetrical triangular index modulation function is preferred to build the calibration grating at the beginning.

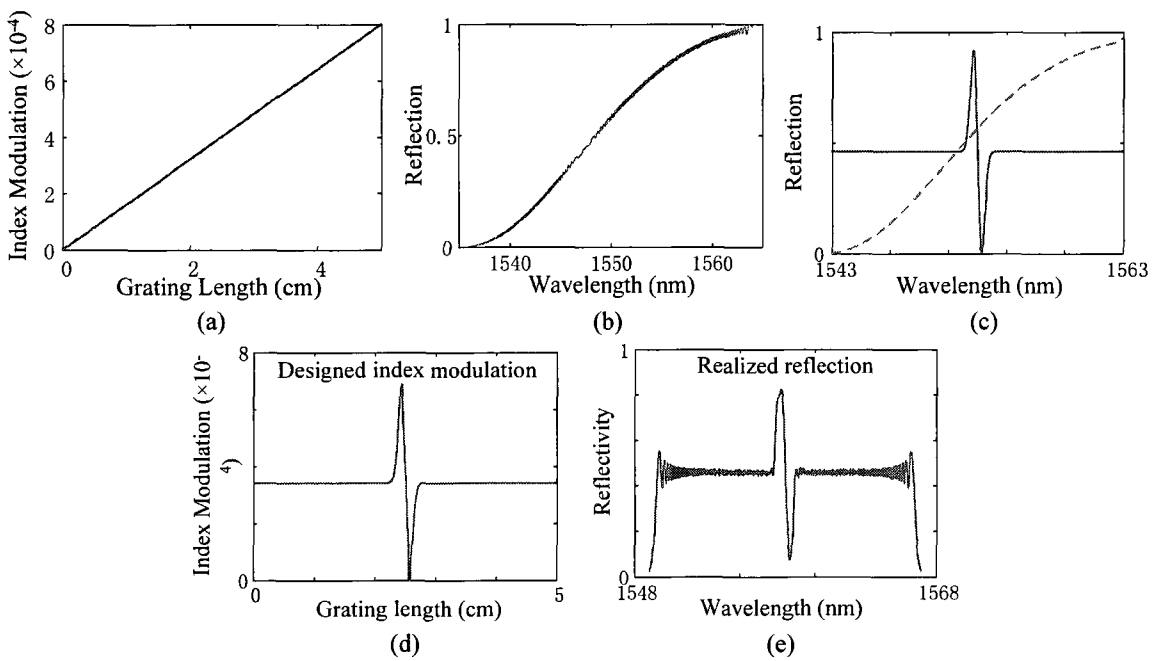

Fig. 2.3. Simulation results showing the synthesis method for strongly chirped fiber Bragg gratings.

A more detailed study on the synthesis of strongly chirped fiber Bragg gratings with the user-defined spectral response for microwave arbitrary waveform generation is presented in Section 3.1.3. The proposed synthesis method is verified by experimental demonstrations.

2.2.3. Fabrication of fiber Bragg gratings

Various methods have been proposed for the fabrication of fiber Bragg gratings [69]. The FBG fabrication techniques can be generally classified into two main categories: those that are interferometric [159] and those are noninterferometric, based on simple exposure to ultraviolet (UV) radiation periodically along a piece of fiber [160]. In this research work, phase mask technique, which belongs to the first category, is employed to fabricate all the designed FBGs. A phase mask is applied as a component of the interferometer, as shown in Fig. 2.4.

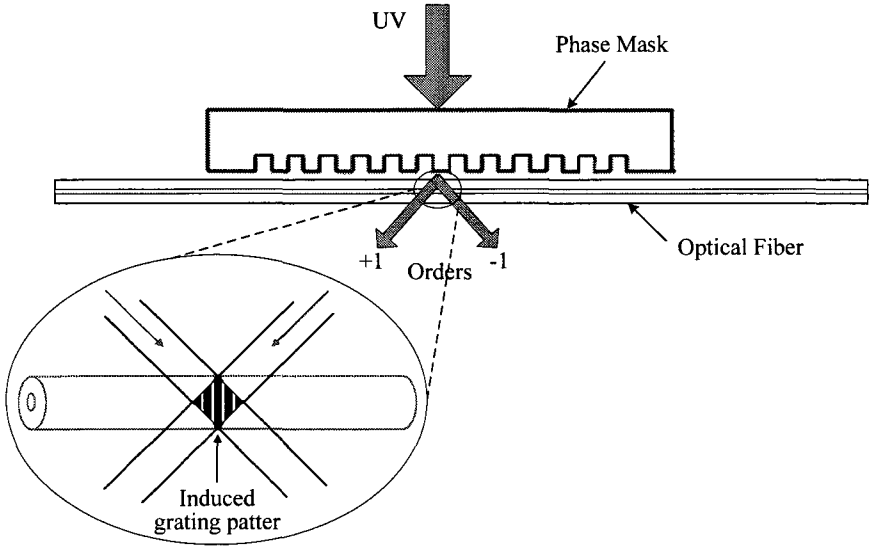

Fig. 2.4. A phase mask is applied as a component of the interferometer for FBG fabrication. Normally incident UV beam diffracted into two ±1 orders.

A phase mask is actually a relief grating which is often fabricated by holographic exposure or e-beam lithography in a fused silica plate. In order to maximize the efficiency of the grating fabrication, the phase mask is properly designed such that the zeroth order radiation is minimized and the two first-order radiations are maximized [161]. When the UV radiation is incident on the phase mask, the two first-order radiations will interfere, as shown in Fig. 2.4. If

a photosensitive fiber is exposed to the interference pattern, the refractive index of the fiber core will be changed and a grating is produced.

In order to inscribe a long grating into a photosensitive optical fiber, a long phase mask may be used. By scanning the UV beam along the phase mask, a long grating with its length determined by the length of the phase mask can be produced. Moreover, by adjusting the intensity of the UV writing beam along the length of grating, or keeping the UV beam intensity constant but controlling the scanning velocity, the radiation intensity and hence the transfer characteristics of the fiber grating can be tailored. In other words, apodization is implemented.

Note that by scanning the UV writing beam along a uniform phase mask, amplitude-only refractive index modulation can be implemented. To realize some special transfer characteristics of the grating, however, both amplitude and phase index modulation are usually required. In such a case, a moving fiber technique can be applied to introduce phase shift to the index modulation profile [162]. In this scheme, when the UV beam is scanning across a fixed phase mask, the fiber is also moving slowly relative to the phase mask with a moving distance determined by the phase mask period and the desired phase shift. In fact, the moving fiber technique can be applied to apodize a fiber grating. It can also be used to introduce a chirp to a uniform fiber grating by controlling the fiber moving velocity corresponding to the UV beam scanning velocity, with the given the UV beam width and the phase mask period [162].

CHAPTER 3 PHOTONIC GENERATION OF MICROWAVE ARBITRARY WAVEFORMS USING FBGS

High-frequency and large-bandwidth microwave and millimeter-wave (mm-wave) arbitrary waveform generation has become an important research area that has numerous scientific and industrial applications, such as in UWB and multiple-access communication systems, electronic countermeasures, and pulsed radar systems. Photonically assisted microwave arbitrary waveform generation techniques provide the capability of generating high-frequency and broadband microwave arbitrary waveforms which may not be easily accomplished by conventional electronic techniques. Basically, a microwave waveform with the desired shape can be generated from an ultrashort optical pulse based on coherent optical pulse shaping in the optical domain followed by the optical-electrical conversion in a high-speed photodetector.

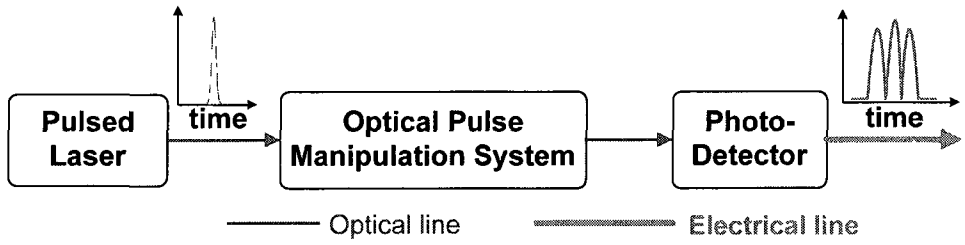

Fig. 3.1. General diagram of a photonically assisted microwave arbitrary waveform generation system based on coherent optical pulse shaping.

Fig. 3.1 shows the general structure of a photonically assisted microwave arbitrary waveform generator. An ultrashort optical pulse from a pulsed laser source is sent to a properly designed optical pulse manipulation system, where the optical pulse is shaped in the optical domain by

different means. A microwave waveform with the desired shape is finally obtained after the optical-electrical conversion in a fast photodetector. Note that the bandwidth of the photodetector actually limits the frequency of the generated microwave waveform. An ultrafast photodetector with a bandwidth as high as 300 GHz has been reported [163].

Optical pulse shaping is the key process in the presented microwave arbitrary waveform generation systems. In this chapter, techniques to achieve microwave arbitrary waveform generation based on optical pulse shaping in FBG-based all-fiber platforms are investigated. The techniques implemented using pure fiber optics offer advanced features of smaller size, lower loss, better stability and higher potential for integration when compared with those implemented using free-space optics. The presented microwave arbitrary waveform generation techniques can be generally classified into the following two categories: 1) photonic microwave arbitrary waveform generation based on optical spectral shaping and frequency-to-time mapping (SS-FTM), and 2) photonic microwave arbitrary waveform generation based on Fourier-transform optical pulse shaping.

3.1 Photonic microwave arbitrary waveform generation based on optical spectral shaping and frequency-to-time mapping

Among the various photonic microwave arbitrary waveform generation techniques, optical spectral shaping of a transform-limited ultrashort optical pulse followed by frequency-to-time mapping in a dispersive element has been demonstrated to be a promising technique to generate high-frequency and broadband microwave waveforms with arbitrary shapes. A schematic diagram showing an SS-FTM-based photonic microwave arbitrary waveform generation system is illustrated in Fig. 3.2. An ultrashort optical pulse generated from a pulsed laser source has a

broad optical spectrum (the bandwidth is normally more than 10 nm). The broadband optical pulse is first sent to an optical spectral filter with a properly designed spectral response. The spectrum-shaped optical pulse is then passing through a dispersive medium, such as a length of dispersive fiber or a chirped FBG. As we have discussed in Section 2.1.1, dispersion-induced frequency-to-time mapping occurs in the dispersive medium. The dispersed optical pulse has an envelope identical to the shaped optical power spectrum. A microwave waveform is finally obtained at the output of a high-speed photodetector. Therefore, by properly designing the spectral response of the optical spectral filter according to the target temporal waveform, a microwave waveform with the desired shape is obtained. A key feature of this technique is that the temporal pulse shaping is performed in the frequency-domain, which is easy to implement using an optical spectral filter.

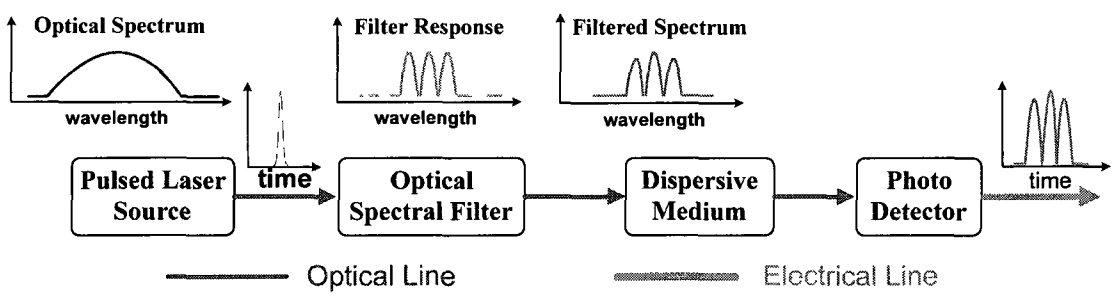

Fig. 3.2. Schematic diagram of a photonic microwave arbitrary waveform generation system based on optical spectral shaping and dispersion-induced frequency-to-time mapping.

As an important in-fiber device, FBGs are playing key roles in the presented photonic microwave arbitrary waveform generation systems. Since both the magnitude response and the phase response (or group delay response) of an FBG can be precisely designed, the intensity and phase modulation of the input optical spectrum can be achieved in the FBG. In this thesis, the use of an FBG as an optical spectral shaper to achieve spectral shaping, as a dispersive

element to achieve frequency-to-time mapping, and as a multifunctional device to perform both optical spectral shaping and frequency-to-time mapping is investigated.

3.1.1. FBG as an optical spectral shaper

As we have discussed in Section 2.2, the spectral response of an FBG working on the reflection mode can be tailored by properly controlling the refractive index modulation profile during the grating fabrication process. Therefore, an FBG can be employed as an efficient optical spectral filter to achieve nearly arbitrary optical spectral shaping. Various configurations for FBG-based all-fiber optical spectral shaping have been proposed for the generation of different microwave waveforms, such as an ultra-wideband pulse and a frequency-chirped microwave pulse.

3.1.1.1. All-fiber ultra-wideband pulse generation based on spectral shaping and dispersion-induced frequency-to-time mapping

This section is a revised version of the following published paper.

Article title: All-fiber ultrawideband pulse generation based on spectral-shaping and dispersion-induced frequency-to-time conversion

Authors: Chao Wang, Fei Zeng, and Jianping Yao

Published in IEEE Photonics Technology Letters, vol. 19, no. 3, pp. 137-139, Feb. 2007.

I. *Introduction*

Ultra-wideband (UWB) is an attractive technology for short-range high data-rate wireless communication systems. Being different from conventional narrowband wireless

communications, in which the signals are modulated on a carrier with a specific frequency, such as IEEE 802.11, UWB impulse radio spreads signals to cover a very wide range of spectrum. The key advantages of UWB technology include huge bandwidth, weak spectrum intensity, multipath immunity, high data rates and low equipment cost [123, 164]. As defined by the US Federal Communications Commission (FCC), UWB signals must occupy a 10-dB bandwidth of 500 MHz or more, or a fractional bandwidth greater than 20% of the centre frequency, within the 7.5-GHz spectrum from 3.1 to 10.6 GHz for unlicensed use of indoor and hand-held UWB devices with an effective power level of less than -41.3 dBm/MHz [165].

Due to the extremely low emission power regulated by the FCC, the current UWB systems can operate with a distance limited to 10 m. To integrate such indoor and isolated UWB wireless networks into the existing wired optical access networks, UWB-over-fiber technology is considered as a promising solution, thanks to advantageous properties such as broad bandwidth and low loss offered by the state-of-the-art optical fibers [125]. In addition, to distribute UWB signal over fiber, it is also desirable that the UWB impulse signals can be generated directly in the optical domain to avoid costly electrical to optical conversion.

On the other hand, the choice of the UWB pulse shapes is critical to the performance of the UWB systems. Gaussian monocycle and doublet pulses, which are defined as the first- and second-order derivative of a Gaussian pulse, respectively, have been considered promising candidates for UWB communications, since they are easy to generate and have better bit-error and multipath performance [166]. Many approaches have been proposed to generate Gaussian monocycle and doublet pulses [167-169]. Most of them are based on electronics circuits. For UWB-over-fiber applications, it is desirable the pulses can be generated directly in the optical domain. Several pioneer works have been recently proposed to generating UWB pulses in the

optical domain. In [170], UWB monocycle pulses are generated using a hybrid system, which consists of a gain-switched Fabry-Perot (FP) laser diode to generate an optical pulse train, and a microwave differentiator to produce the required monocycle pulse in the electrical domain. Our research group has proposed an all-fiber technique to generate UWB signals using an optical phase modulator in combination with a dispersive fiber [171]. The phase-modulation (PM) signal is converted to intensity-modulation (IM) signal when distributing over the dispersive fiber. The PM-IM conversion has a frequency response corresponding to a bandpass filter, which is used to shape the spectrum profile of a Gaussian pulse, leading to the generation of UWB doublet. More recently, various optical UWB pulse generation techniques have been reported by different groups [124, 172-176].

In fact, UWB pulses can also be generated based on optical spectral shaping and the subsequent frequency-to-time mapping using a Fourier-transform device. Fourier-transform optical spectral shaping and dispersive stretching techniques were implemented to generate adaptive broadband microwave arbitrary waveforms [37, 39]. Such technique of spectral-temporal mapping was previously used to measure optical fiber dispersion and to evaluate an optical source spectrum [177]. The dispersion-induced frequency-to-time mapping based on the space-time duality has been introduced in Section 2.1. A comprehensive theoretical analysis can be found in [25].

In this research work, we proposed a novel approach to generating and distributing UWB monocycle and doublet pulses based on all-fiber spectral shaping and frequency-to-time conversion. In our approach, the optical power spectrum of a femtosecond pulse from a passively mode-locked fiber laser (MLFL) is spectrum shaped by an all-fiber optical spectral shaper, to obtain a spectral shape corresponding to a Gaussian monocycle or doublet pulse. A length of SMF is then used to act as a dispersive device to perform the frequency-to-time

conversion. A UWB monocycle or doublet pulse is obtained at the output of a high-speed PD. The key difference between this approach and the approaches in [37, 39] is that the optical spectral shaping is performed using all-fiber components which has the advantages of smaller size, lower loss, and higher potential for integration using the photonic integrated circuit (PIC) technology.

II. *Principle*

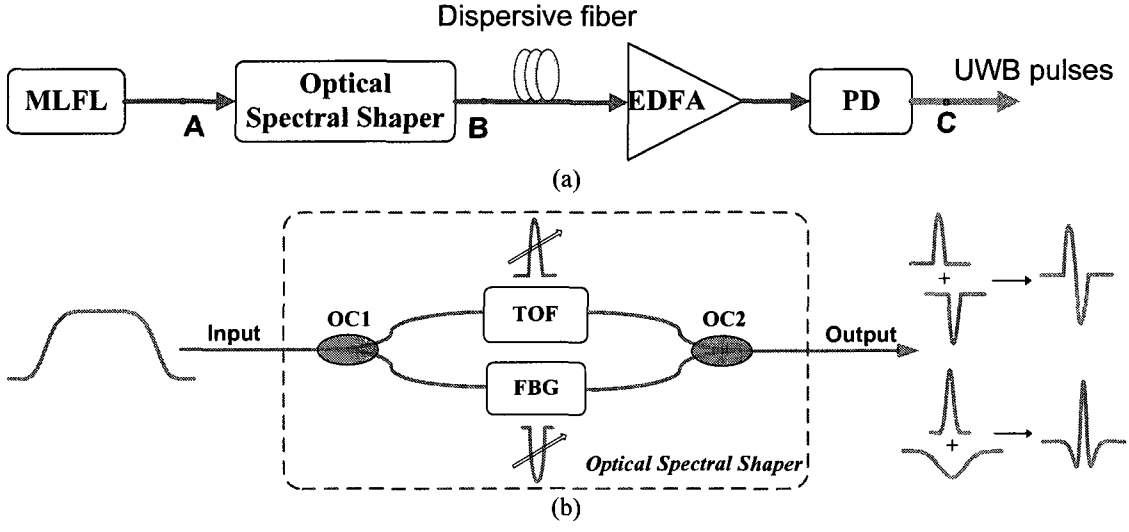

Fig. 3.3. (a) Block diagram of the proposed all-fiber UWB signal generation system. (b) All-fiber optical spectral shaper configuration. MLFL: mode-locked fiber laser; EDFA: erbium-doped fiber amplifier; PD: photodetector; OC: optical coupler; TOF: tunable optical filter.

The block diagram of the proposed UWB pulse generation system is illustrated in Fig. 3.3. A transform-limited ultrashort pulse train from the MLFL is spectrally shaped by an all-fiber spectral shaper. The spectral shaper is designed such that it shapes the optical power spectrum of the ultrashort pulse to be the user-designed Gaussian monocycle or doublet. The spectrally shaped pulse is then sent to a length of dispersive fiber to perform the frequency-to-time mapping. The total chromatic dispersion must be properly determined according to the mapping relationship between the spectral bandwidth and the temporal pulsewidth [25]. After the optical-

to-electrical conversion at a high-speed PD, a temporal electrical monocycle or doublet pulse is obtained. Thanks to the frequency-to-time mapping in the dispersive fiber, the generated UWB pulse has a shape that is a scaled version of the user-designed optical spectrum.

To obtain an optical power spectrum with a shape corresponding to a Gaussian monocycle or doublet, we use an all-fiber optical spectral shaper, as shown in Fig. 3.3(b). The ultrashort pulse train from the MLFL source is divided into two branches by an optical coupler (OC1), with a coupling ratio determined by user-defined spectrum shaping requirement. The spectrum of the ultrashort pulse from Port 1 is shaped by a tunable optical filter (TOF); the spectrum of the ultrashort pulse from Port 2 is spectrally shaped by an FBG operating on the transmission mode. The FBG is acting as a band stop filter with a center wavelength that can also be slightly tuned by applying tension. The pulses after spectral-shaping from the two arms are then recombined by a 3-dB optical coupler (OC2). Since the spectra of the two filters are complementary, the power spectrum of the ultrashort pulse is shaped to have a user-designed Gaussian monocycle or doublet.

This all-fiber optical spectral shaper can be configured to generate UWB monocycle or doublet pulses by adjusting the spectral widths and the center wavelengths of the two optical filters (TOF and FBG). To obtain a power spectrum corresponding to a UWB monocycle, the bandwidths of two optical filters should be controlled to be approximately identical. In addition, a proper wavelength difference between the central wavelengths of the two optical filters is required to ensure a good time separation between the two temporal pulses after frequency-to-time mapping, as shown in Fig. 3.3(b). For UWB monocycle, the positive and negative spectral peaks at the output of the spectral shaper should be identical, which is realized in our system by controlling the coupling ratio of OC1 to account for the different insertion losses of the two

optical filters. On the other hand, to achieve a power spectrum corresponding to a UWB doublet, the optical spectral shaper has to be reconfigured by using another FBG with a broader spectral bandwidth. The center wavelength of the TOF is tuned to be identical to that of the second FBG, as also shown in Fig. 3.3(b). Again, the coupling ratio of OC1 is adjusted to ensure that the spectrum meets the UWB doublet requirement [166]. Thus, the combination of the two inversed spectra gives an over all power spectrum corresponding to a UWB monocycle or doublet.

In the all-fiber spectral shaper, the incident ultrashort pulse is spectrally filtered in the two different paths. The optical lengths of the two arms have to be carefully controlled to guarantee a good temporal synchronization of the spectrum-shaped optical pulses from the two paths. In fact, the continuous tuning of the wavelength spacing between the two central wavelengths would lead to the continuous change of the time delay difference between two polarity-reversed pulses thanks to the frequency-time mapping. Therefore, electrical waveforms other than the UWB monocycle or doublet may also be generated.

It is worth noting that the proposed spectral shaper is based on a Mach-Zehnder interferometer (MZI) structure. However, we intend to introduce large time delay between the two arms, which is much larger than the coherent length of the applied pulsed laser source. Therefore, temporal interference is inherently avoided even though a coherent optical source is used. The pulse shaping system is free from the instability introduced by an interferometer.

The spectrum shaping operation in the all-fiber spectral shaper is implemented in an open-loop fiber link without close-loop iterations, which makes the system very simple with high stability. In addition, the optical spectral shaper is implemented using all-fiber components, which makes the system compact with low loss and provides the possibility of integration using PIC

technology. Although the use of the TOF and the FBG filters would make the system sensitive to environmental changes such as temperature and vibration, an integrated version of the system with temperature control and proper packaging would easily tackle the problem.

III. *Experiment*

The proposed UWB pulse generation system, as shown in Fig. 3.3, is experimentally implemented. The MLFL can generate a transform-limited ultrashort optical pulse train with a 3-dB pulsewidth of about 550 fs and a 3-dB spectral bandwidth of about 8 nm. The ultrashort pulse from the MLFL is spectrally filtered by the all-fiber spectral shaper. To generate a UWB monocycle, the input pulse spectrum from Port 1 of OC1 is shaped by a TOF, which is a reflection bandpass filter with a tunable range of 1460–1575 nm and an average 3-dB bandwidth of 0.2 nm. In the first experiment, the central wavelength of TOF is set at 1557.71 nm, which is mainly determined by the central wavelength of the fabricated FBG. The input spectrum from Port 2 of OC1 is shaped by an FBG with 0.25-nm bandwidth and a center wavelength of 1558.2 nm. The spectrum-shaped pulses are then combined at OC2. In the experiment, the coupling ratio of OC1 is 70 : 30, that is, 70% of the input power is sent to the upper branch, since TOF has higher insertion loss.

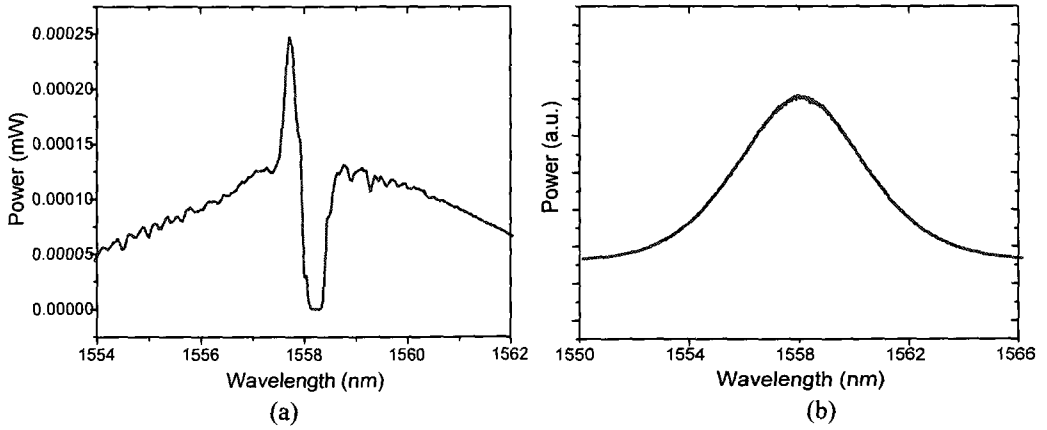

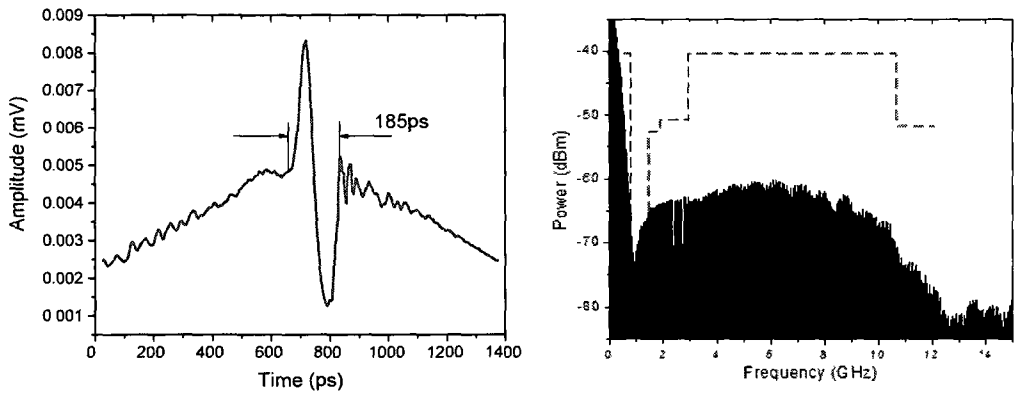

(c) (d)

Fig. 3.4. UWB monocycle pulse generation. (a) Optical power spectrum after spectral shaping. (b) Spectrum of the incident ultrashort pulse. (c) Generated UWB pulse. (d) Power spectrum of the generated monocycle pulse.

The optical spectrum at the output of the optical spectral shaper (Point B) is measured by an optical spectrum analyzer. As shown in Fig. 3.4(a), the shaped optical spectrum exhibits a monocycle pulse shape, but is superimposed on a broader Gaussian-like pedestal, which is the spectrum of the original pulse from the MLFL (as shown in Fig. 3.4(b) for comparison). The spectrally shaped optical pulse is then applied to a 10-km SMF to perform the frequency-to-time mapping. The total chromatic dispersion of the SMF is about 170 ps/nm. The electrical pulse at point *C* is obtained at the output of a 45-GHz PD and measured by a high-speed sampling oscilloscope, with the result shown in Fig. 3.4(c). The generated signal is stable and 5 times averaging is performed. We can clearly see that the pulse has the same shape as the optical spectrum at the output of the optical spectral shaper. The full-width at half-maximum (FWHM) of the generated monocycle pulse is about 185 ps. The spectrum of the generated pulse is also measured by an electrical spectrum analyzer, as illustrated in Fig. 3.4(d). The FCC mask is also plotted in the figure in dash line. It can be seen that the spectrum has a central frequency of 6 GHz with a 10-dB bandwidth of 9 GHz, from 1.5 to 10.5 GHz. The fractional bandwidth is about 150%, which well meets the FCC requirement of 20%.

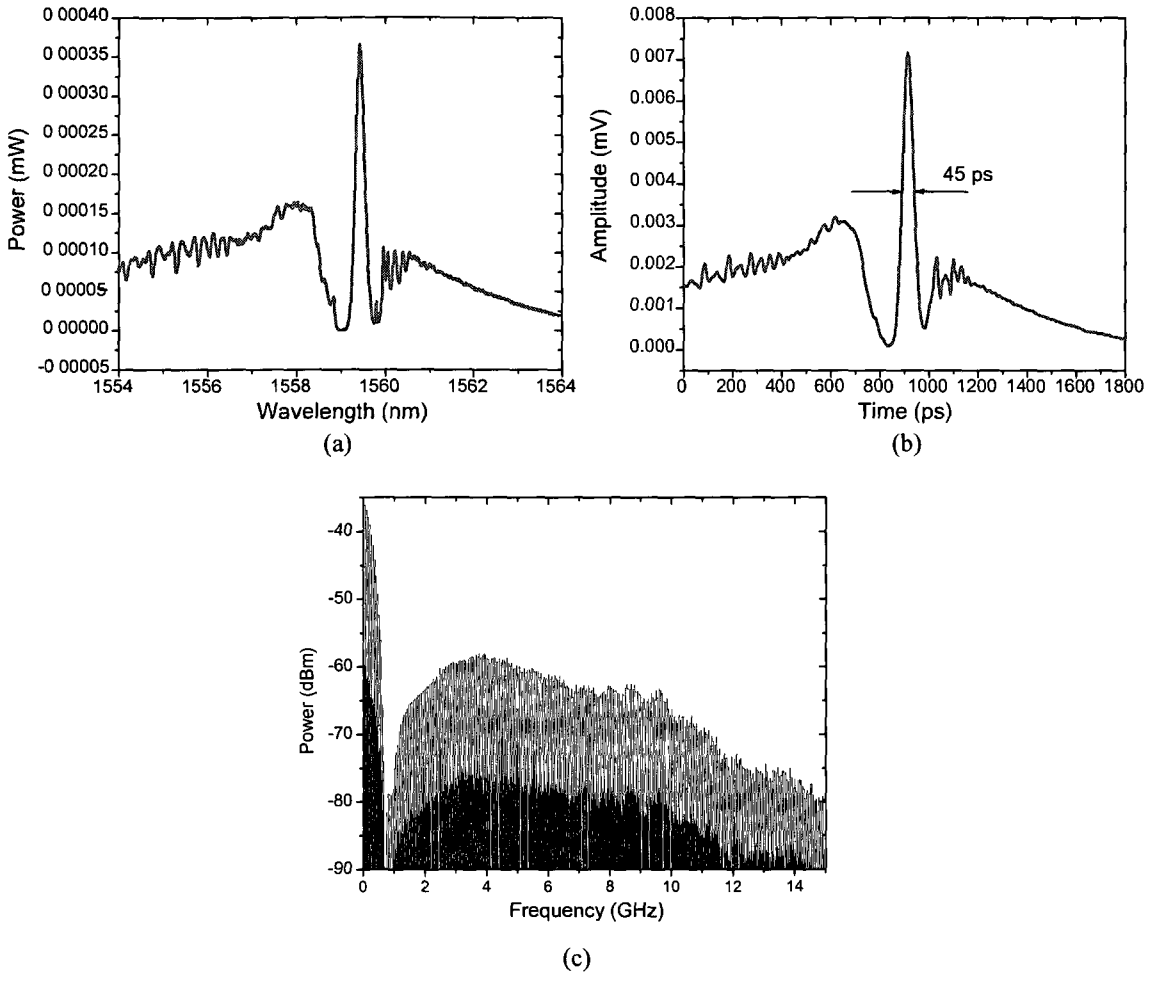

Fig. 3.5. UWB doublet pulse generation. (a) Optical power spectrum after spectral shaping. (b) Generated UWB doublet pulse. (c) Power spectrum of the generated UWB pulse.

To generate a UWB doublet pulse, the optical spectral shaper has to be reconfigured. The input pulse from Port 1 of OC1 is spectrally shaped by the TOF, with the center wavelength set at 1559.45 nm. In the other optical path, the input pulse spectrum is shaped by a new FBG with a broader bandwidth of 0.45 nm centered at 1559.4 nm. Again, the coupling ratio of OC1 needs to be adjusted. This is done by using a new optical coupler with a coupling ratio of 80 : 20. Fig. 3.5(a) shows the optical power spectrum right after the optical spectral shaper. It has a shape corresponding to a Gaussian doublet. After distribution over 10-km SMF, a UWB doublet pulse is generated thanks to the dispersion-induced frequency-to-time mapping. As shown in Fig.

3.5(b), the generated UWB doublet pulse has an FWHM of about 45 ps, which is again superimposed on a broad Gaussian-like pedestal. Fig. 3.5(c) illustrates the power spectrum of the generated UWB doublet pulse, which has a 10-dB bandwidth of about 9.5 GHz, from 1.5 to 11 GHz.

IV. *Discussion*

From the above experimental results, one may notice that in addition to the desired UWB spectrum, there is a baseband spectral component with a bandwidth of less than 1 GHz, as shown in Fig 3.4(d) and Fig 3.5(c), which is resulted from the wide temporal Gaussian-like pedestal (baseband component). A broadband DC block can be used to eliminate the pedestal superimposed on the desired UWB monocycle pulse. Another solution to reduce this baseband component is to use an MLFL with a narrower pulsewidth.

In fact, in order to remove completely the unwanted Gaussian-like pedestal (base band component), a two-arm structure incorporating a balanced photodetector (BPD) has been reported recently [178]. As shown in Fig. 3.6, in the upper arm, the designed optical spectral shaper is applied to tailor the input optical power spectrum. The desired pulse shape is imprinted on the spectrum of the broadband source (spectral pedestal). In the lower arm, no spectral shaping is performed. An optical delay line (DL) and a variable attenuator (ATT) are used to balance the amplitude and the relative delay of the two waveforms from the two arms. After the balanced photodetection, the unwanted temporal pedestal can be removed, leading to the generation of a desired UWB signal that has both positive and negative parts. Note that balanced photodetection can be employed to remove base band components in any microwave waveform generation systems based on optical spectral shaping and frequency-to-time mapping.

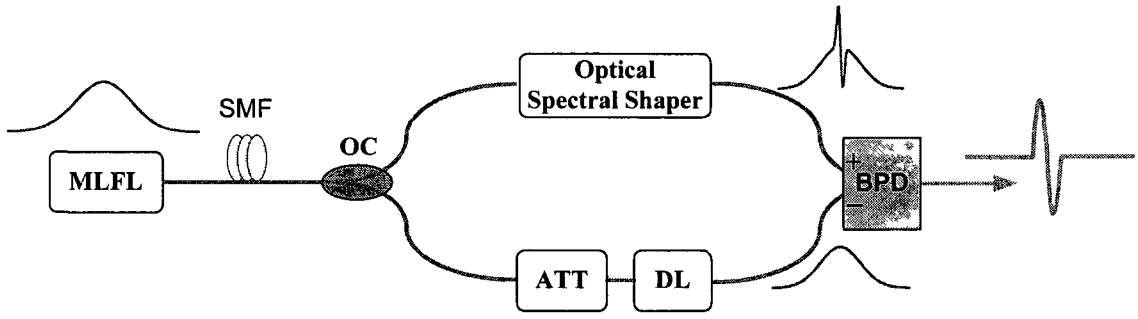

Fig. 3.6. Block diagram of the UWB signal generation system incorporating a balanced photodetector to remove the based band pedestal. MLFL: mode-locked fiber laser; SMF: single-mode fiber; OC: optical coupler; ATT: attenuator; DL: delay line; BPD: balanced photodetector.

V. *Conclusion*

In conclusion, an all-fiber approach to generating UWB monocycle and doublet pulses has been proposed and experimentally demonstrated in this research work. The proposed technique was based on spectral shaping of an ultrashort optical pulse in an all-fiber optical spectral shaper and dispersion-induced frequency-to-time mapping in a dispersive fiber. By configuring the fiber-optic spectral shaper, UWB monocycle or doublet pulse was generated. To generate other waveforms, the spectral shaper has to be reconfigured to produce an optical spectrum corresponding to the required temporal waveform. The frequency-to-time mapping was implemented using a length of SMF, which provides an added advantage: the UWB pulse is not only generated, but also distributed to a remote site through the optical fiber, which would find potential applications in UWB over fiber systems.

3.1.1.2. Photonic generation of chirped microwave pulses based on SS-FTM using superimposed chirped fiber Bragg gratings

This section is a revised version of the following published paper.

Article title: Photonic generation of chirped microwave pulses using superimposed chirped fiber Bragg gratings

Authors: Chao Wang, and Jianping Yao

Published in IEEE Photonics Technology Letters, vol. 20, no. 11, pp. 882-884, Jun. 2008.

I. *Introduction*

In modern microwave radar systems, pulse compression techniques using frequency-chirped or phase-encoded pulses have been widely used to increase the time-bandwidth-product (TBWP) of the transmitted signals. The pulsewidth is significantly compressed at the receiver end by matched filtering leading to an improved radar range resolution and detection distance [127]. Chirped electrical pulses have also found their applications in spread-spectrum communications [128] and in chirped-pulse microwave computed tomography [179]. Conventionally, a chirped microwave pulse is generated in the electrical domain using electronic circuitry [180-182]. However, the major limitations associated with these electrical techniques are the low central frequency and small TBWP. At the current stage of development of radar and communications systems, a central frequency up to the tens or even hundreds of gigahertz is often required [127].

As a promising alternative, photonic generation of high-frequency and broadband chirped microwave pulses has been an active topic, thanks to the broad bandwidth and high speed offered by optics. A few techniques to generating chirped microwave pulses in the optical domain have been proposed recently. In [183], for example, a chirped microwave pulse is generated by beating two chromatically dispersed optical pulses obtained by passing a

broadband ultrashort pulse through two chirped fiber Bragg gratings with different chirp rates in an MZI geometry.

Chirped microwave pulses can also be generated based on optical spectral shaping and dispersion-induced frequency-to-time mapping, as illustrated in Fig. 3.2. In this scenario, the optical spectral shaper should have a spectral response with a varying (increasing or decreasing) FSR, which is called chirped FSR in this research work. Therefore, our efforts here will focus on the design of an FBG-based optical spectral filter with a chirped FSR for optical spectral shaping. In this research work, we propose an optical spectral filter which consists of two superimposed chirped fiber Bragg gratings (SI-CFBGs) having different chirp rates.

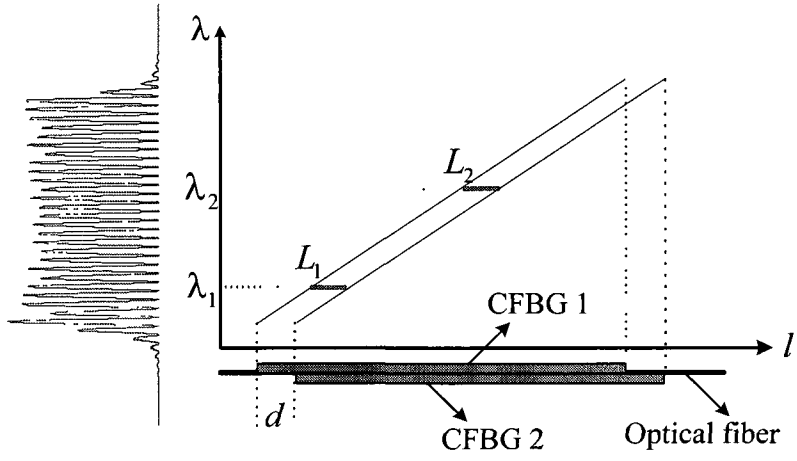

Fig. 3.7. Schematic diagram of the conventional superimposed chirped fiber Bragg gratings. The Fabry-Perot cavity has a constant cavity length. The reflection response has a constant FSR.

It is known that a conventional SI-CFBG, also called chirped moiré grating (CMG) [184], consists of two superimposed linearly chirped FBGs with identical chirp rates, as illustrated in Fig. 3.7. The two LCFBGs have a small longitudinal offset *d*. The conventional SI-CFBG can be considered as an in-fiber distributed Fabry-Perot cavity with a fixed (wavelength-independent) cavity length, which is identical to the offset *d*, therefore a spectral response with a

fixed FSR would be resulted. The simulated reflection spectral response of the SI-CFBG is also plotted in Fig. 3.7. Such grating device has been widely applied in multiband optical filtering [185], multi-wavelength fiber laser [186] and optical pulse repetition-rate multiplication [187].

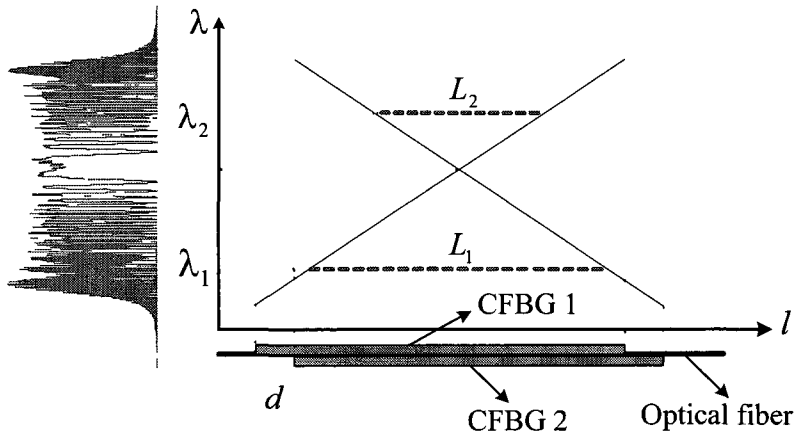

Fig 3 8. The proposed superimposed chirped fiber Bragg gratings with different chirp rates The Fabry-Perot cavity has a wavelength-dependent cavity length. The reflection response has a chirped FSR.

To obtain an optical spectral filter with a chirped FSR, however, the superimposed CFBGs should have different chirp rates to make the Fabry-Perot cavity have a cavity length linearly dependent on the resonance wavelength, thus a spectral response with a chirped FSR would be obtained, as shown in Fig. 3.8. By properly selecting the chirp rates and longitudinal offset of two chirped FBGs, linearly chirped microwave pulses with high frequency and large chirp rate can be generated after linear frequency-to-time mapping in a dispersive element. In addition, since no MZI-based optical interference is involved in the approach, the system is more compact with a better resistance to the environmental perturbations when compared with the approach in [183].

II. *Principle*

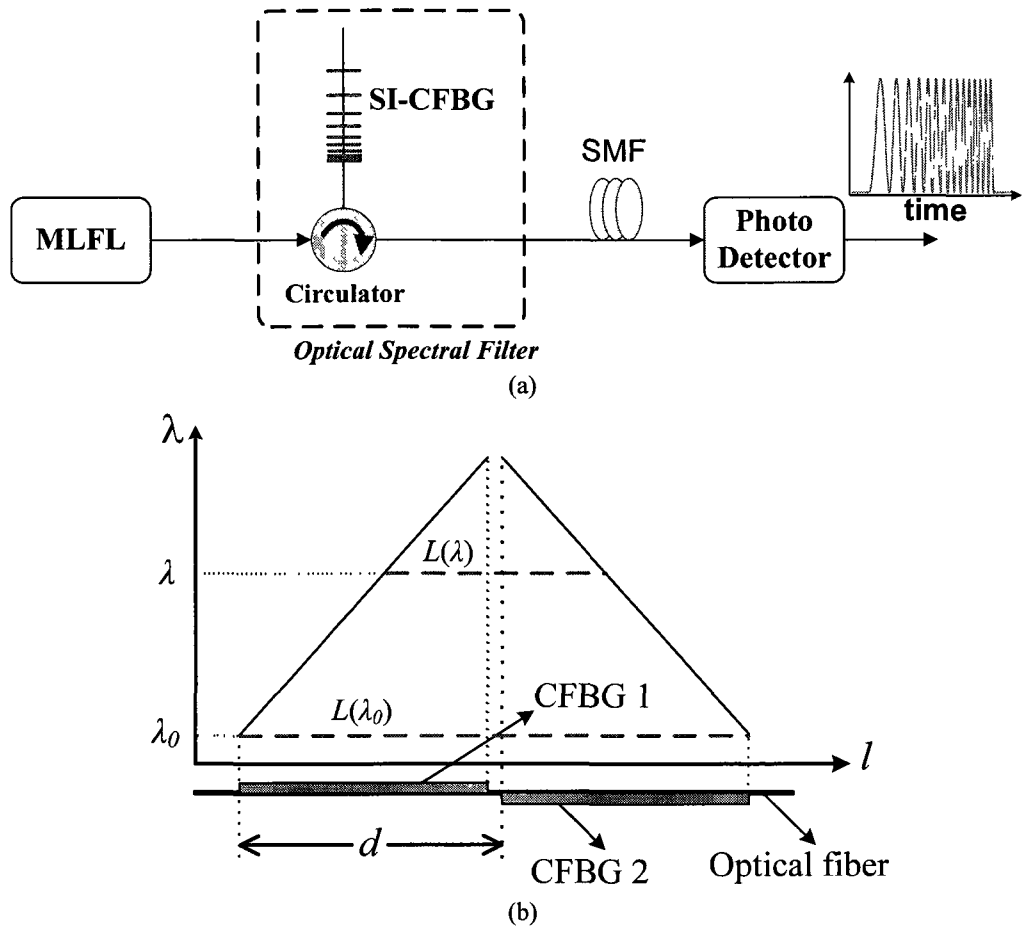

Fig. 3.9. (a) Schematic diagram of the proposed microwave chirped pulse generation system. (b) SI-CFBG-based chirped FSR optical spectral filter.

The block diagram of the proposed chirped pulse generation system is illustrated in Fig. 3.9(a). Similar to the set up described in Section 3.1.1.1, a transform-limited ultrashort optical pulse train from a MLFL is first spectrally shaped by an SI-CFBG-based optical filter with a chirped FSR. The spectrally filtered pulse is then sent to a length of SMF to perform the linear frequency-to-time mapping, which leads to the generation of a linearly chirped microwave pulse at the output of a PD.

To obtain a spectral response with a chirped FSR, the SI-CFBG is designed and fabricated by superimposing two LCFBGs with different chirp rates into a same fiber with a proper

longitudinal offset d, as shown in Fig. 3.9(b). Distributed Fabry–Perot interference is then obtained in the fiber due to the reflections of the two LCFBGs. This generates an in-fiber optical filter with an FSR inversely proportional to the cavity length. Since the two LCFBGs have different linear chirp rates, the equivalent cavity length varies linearly with respect to the resonance wavelength. As a result, the FSR is not constant anymore but is increasing or decreasing with respect to the resonance wavelength.

From Fig. 3.9(b), we can easily find that the equivalent cavity length L is linearly proportional to the wavelength λ within the filter bandwidth

$$L(\lambda) = \frac{C_1 - C_2}{C_1 C_2}(\lambda - \lambda_0) + d \tag{3-1}$$

where C_1 and C_2 are the chirp rates of the two LCFBGs (in nm/mm), d is the longitudinal offset between the two gratings, and λ_0 is the start wavelength. Then the FSR of the distributed Fabry-Perot filter can be determined from the cavity length as

$$FSR \cong \frac{\lambda_0^2}{2nL(\lambda)} \tag{3-2}$$

where n is the refractive index of the fiber. After the dispersion-induced linear frequency-to-time mapping, the FSR is mapped to the temporal period of the generated chirped microwave pulse, namely $\Delta\tau$, with a mapping relationship $\lambda \to t/\ddot{\Phi}_\lambda$ according to (2-10), where $\ddot{\Phi}_\lambda$ (in ps/nm) is the total accumulated dispersion of the SMF.

For simplicity, the instantaneous RF carrier frequency of the generated temporal microwave pulse f_{RF} can be approximated by the reciprocal of the temporal period $\Delta\tau$ as

$$f_{RF}(t) \propto \frac{1}{\Delta\tau} \propto 2n\left(\frac{C_1 - C_2}{C_1 C_2}\frac{t}{\lambda_0^2 \ddot{\Phi}_\lambda^{\ 2}} + \frac{d}{\lambda_0^2 \ddot{\Phi}_\lambda} + \frac{C_2 - C_1}{C_1 C_2 \lambda_0 \ddot{\Phi}_\lambda}\right) \tag{3-3}$$

It can be seen that the instantaneous RF carrier frequency of the generated microwave pulse is linearly proportional to time, therefore it is linearly chirped. For a given length of SMF (the total dispersion $\ddot{\Phi}_\lambda$ is fixed), the central carrier frequency of the generated chirped pulse at $t = 0$ is only dependent upon the grating longitudinal offset d. On the other hand, the chirp rate of generated pulse is determined by the chirp rates of the two LCFBGs. Therefore, by appropriately designing the longitudinal offset and the chirp rates of the LCFBGs, linearly chirped microwave pulses with a high central frequency and a large chirp rate can be generated.

III. *Experiment*

The setup shown in Fig. 3.9 is then experimentally evaluated. In the experiment, a transform-limited Gaussian pulse with a FWHM of 550 fs generated from an MLFL is sent to the SI-CFBG through a three-port optical circulator. The central wavelength of the ultrashort pulse is 1558.5 nm, and the 3-dB spectral bandwidth is 8 nm. The SI-CFBG is fabricated using a frequency-doubled argon–ion laser operating at 244 nm. Two LCFBGs are superimposed in a photosensitive fiber with a small longitudinal spacing, as shown in Fig. 3.9(b). The superimposed LCFBGs with equal but opposite chirp rates ($C_1 = -C_2$) would be preferred due to the following considerations: 1) Only a single chirped phase mask is required to fabricate two gratings; 2) Biggest FSR change and hence the largest microwave frequency chirp rate can be obtained from the two oppositely chirped FBGs; 3) Superimposing two LCFBGs with the same bandwidth will ensure a maximum bandwidth usage because the effective reflection bandwidth of the SI-CFBG is roughly equal to the common reflection bandwidth of the two LCFBGs.

Based on these considerations, two LCFBGs with opposite chirp rates of ± 0.1 nm/mm and an identical grating length of 10 mm are written with a longitudinal offset of 12 mm. The center Bragg wavelength of the two LCFBGs is 1558.3 nm, which is selected to match the center wavelength of the ultrashort pulse. To produce distributed Fabry–Perot resonance, each grating has a weak reflection (≈30%).

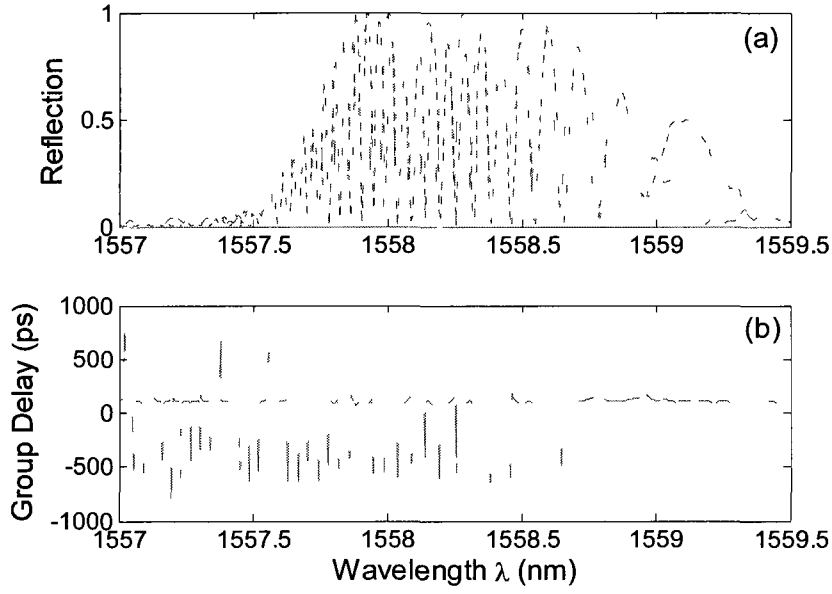

Fig. 3.10. (a) Measured (solid line) and the simulated (dashed line) reflection spectra and (b) reflection group delay response of the proposed SI-CFBG.

Fig. 3.10(a) shows the measured normalized reflection spectrum of the SI-CFBG. Simulation results by using the piecewise-uniform transfer matrix approach [154] are also plotted as the dashed line in Fig. 3.10(a) for comparison. The experimental result matches well with the simulation results. It is shown that an SI-CFBG with a reflection spectrum having a monotonically increasing FSR is obtained, which can be used to spectrally shape the power spectrum of the input broadband ultrashort pulse. Note that the measured spectrum has a limited

modulation depth, especially for shorter wavelength, compared with the simulation result. This mainly owes to the limited resolution of the used optical spectrum analyzer.

Fig. 3.10(b) shows the measured group delay response of the SI-CFBG. A nearly constant group delay is observed, ensuring the dispersion-free spectral filtering, which is usually required in a pulse shaping system based on spectral-shaping and frequency-to-time mapping [25]. The result can be understood intuitively by considering the dispersion cancellation due to two LCFBGs with equal but opposite chirp rates. One may notice that some group delay peaks at the reflection notch wavelengths are also observed. These group delay peaks are actually the measurement errors due to the very low power at the reflection spectral notches. It is important to note that the group delay peaks due to the optical resonance have negligible impact on the time-domain optical pulse shaping because the optical power reflected from these resonance notches is negligible.

The incident ultrashort pulse is spectrum-shaped by the SI-CFBG, which is then mapped to a chirped temporal waveform thanks to linear frequency-to-time mapping in a 58-km SMF ($\ddot{\Phi}_{\lambda}$ = 957 ps/nm). A linearly chirped microwave pulse is experimentally generated at the output a 45 GHz photodetector and measured by a high-speed sampling oscilloscope, with the single sampling result shown in Fig. 3.11(a). The FWHM of the pulse envelope is around 1250 ps. Fig. 3.11(a) also shows the instantaneous RF carrier frequency within the main pulsewidth, which is calculated by Hilbert transform [188] and shown by the open-circle curve, with a linear fitting curve plotted as the dotted line. It is shown that the instantaneous frequency changes almost linearly across the pulse with a central frequency of 15 GHz and a chirp rate of 0.0217 GHz/ps, which agrees very well with the theoretically predicted chirp rate of 0.0238 GHz/ps by (3-3). A

TBWP as large as 37.5 is obtained. To generate a linearly chirped microwave pulse with a larger TBWP and higher frequency, two superimposed LCFBGs with larger chirp rates and longer offset should be used. Practically, the achievable RF frequency and TBWP are only limited by the bandwidth of the high-speed PD.

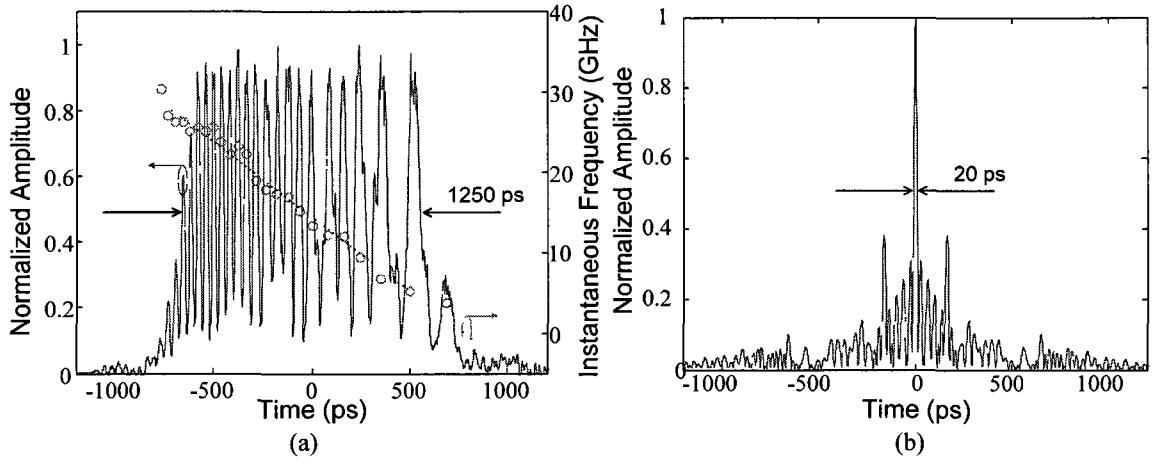

Fig. 3.11. (a) Measured pulse profile (single samping) and instantaneous carrier frequency of the generated chirped microwave pulse. (b) Claculated autocorrelation waveform of the generated chirped microwave pulse.

In a pulsed microwave radar system, chirped pulse compression is usually implemented through matched filtering at the receiver end. Mathematically, the matched filtering operation is identical to an autocorrelation operation given by

$$A(t) = y(t) * y(-t) = \int_{-\infty}^{\infty} y(t+\tau) \cdot y(\tau) d\tau \qquad (3\text{-}4)$$

where * denotes the convolution operation. Fig. 3.11(b) shows the autocorrelation trace of the generated chirped microwave pulse, which is obtained by digitally calculating the autocorrelation between the measured chirped pulse and the reference pulse according to (3-4). The FWHM of the autocorrelation trace is around 20 ps. Therefore, a pulse compression ratio of 62.5 is achieved.

IV. *Conclusion*

As a conclusion, a novel approach to generating a linearly chirped microwave pulse based on spectral filtering and linear frequency-to-time mapping was proposed and experimentally demonstrated. The key component in the proposed system is the SI-CFBG, which was fabricated by superimposing two LCFBGs with identical but opposite chirp rates in a photosensitive fiber with a proper longitudinal offset. The SI-CFBG has a Fabry-Perot resonance response with a chirped FSR. By using a linear dispersive device to perform the frequency-to-time mapping, a linearly chirped microwave pulse with a high carrier frequency and large TBWP was generated. The proposed technique is quite simple, which can find wide applications in modern radar, communications, and instrumentation systems.

3.1.1.3. Tunable chirped microwave pulse generation based on SS-FTM using a Sagnac loop mirror incorporating a linearly chirped fiber Bragg grating

This section is a revised version of the following published paper.

Article title: Chirped microwave pulse generation based on optical spectral shaping and wavelength-to-time mapping using a Sagnac-loop mirror incorporating a chirped fiber Bragg grating

Authors: Chao Wang, and Jianping Yao

Published in IEEE/OSA Journal of Lightwave Technology, vol. 27, no. 12, pp. 3336-3341, Aug. 2009.

I. *Introduction*

Photonic generation of high-frequency and broadband chirped microwave pulses based on spectral shaping using an SI-FBG-based optical filter with a chirped FSR and frequency-to-time mapping in a dispersive element has been investigated in Section 3.1.1.2. Since two LCFBGs need to be written in a single optical fiber, the fabrication process is complicated. In addition, the longitudinal offset between the two LCFBGs is fixed once the two gratings are fabricated; therefore, the central carrier frequency and the chirp profile of the generated chirped microwave pulse cannot be tuned.

In this section, we investigate a simple approach to optically generating a chirped microwave pulse with a tunable carrier frequency and chirp profile based on spectral shaping and frequency -to-time mapping. The proposed optical spectral filter is an LCFBG-incorporated Sagnac-loop mirror, which has a spectral response with a linearly increasing or decreasing FSR. A linearly chirped microwave pulse can be generated after the linear frequency-to-time mapping in a dispersive element. Our efforts here focus on the tuning of the carrier frequency and the chirp profile of the generated chirped microwave pulses.

A Sagnac loop mirror incorporating a uniform FBG with a constant FSR has been studied in details [189] employed for applications such as in a multi-wavelength fiber laser [190]. To the best of our knowledge, however, this is the first time that an LCFBG-incorporated Sagnac loop mirror with a varying FSR is employed to generate chirped microwave pulses. Since only one LCFBG is needed, the proposed filter, compared with the filter presented in Section 3.1.1.2, has the advantages of simpler configuration and lower insertion loss. In addition, by tuning the time delay in the Sagnac loop mirror, the central frequency and the sign of chirp rate of the generated chirped microwave pulses can be controlled.

II. *Principle*

The principle of the proposed chirped microwave pulse generation system is first presented. The schematic diagram of the proposed system is quite similar to that illustrated in Fig. 3.2. A transform-limited ultrashort optical pulse generated by a pulsed optical source, e.g., a MLFL, is first spectrally shaped by an optical spectral filter. The filter is designed to have a spectral response identical to the shape of the target microwave pulse to be generated. The spectrum-shaped optical pulse is then sent to a dispersive element to perform the linear frequency-to-time mapping. At the output of a high-speed photodector, a microwave pulse with the shape identical to that of the shaped optical spectrum is obtained.

To generate a linearly chirped microwave pulse, the optical spectral filter should have a spectral response with a linearly increasing or decreasing FSR. In this research work, we propose an all-fiber optical spectral filter with a linearly varying FSR, which is based on a Sagnac loop mirror with an LCFBG incorporated in the fiber loop. Fig. 3.12 shows the schematic of the proposed optical spectral filter based on an all-fiber Sagnac loop mirror. The Sagnac loop mirror is constructed from a fused 3-dB fiber coupler (FC) spliced to the terminals of the LCFBG, which is located approximately at the central point of the fiber loop. A tunable delay-line (TDL) is located in the fiber loop to finely tune the time-delay difference between two fiber lengths L_1 and L_2. A fiber-optic polarization controller (PC) is also placed in the loop to adjust the fringe visibility of the interference pattern at the output of the loop. A three-port optical circulator is used to direct the ultrashort pulse into the loop mirror and to output the spectrum-shaped pulse for frequency-to-time mapping in the dispersive element.

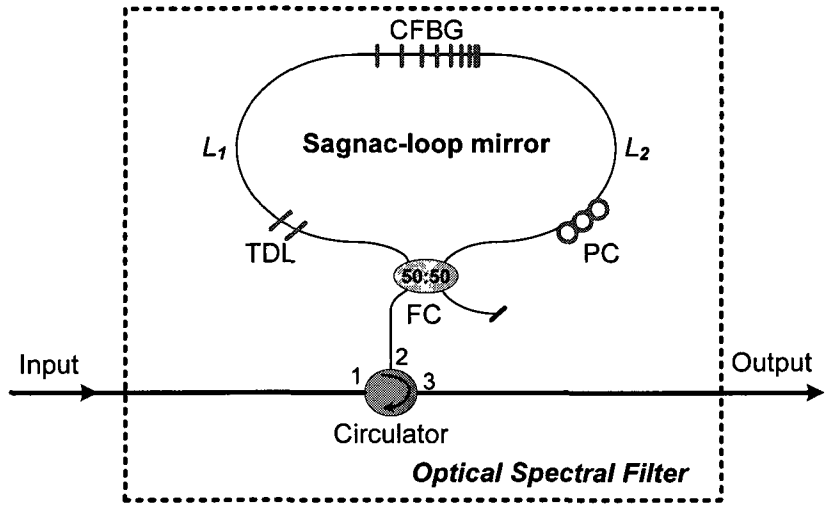

Fig. 3.12. Schematic diagram showing an all-fiber optical spectral filter based on LCFBG-incorporated Sagnac loop mirror. FC: fiber coupler; TDL: tunable delay line; LCFBG: linearly chirped fiber Bragg grating; PC: polarization controller.

Mathematically, the FBG-incorporated Sagnac loop mirror can be modeled as a two-tap delay-line filter. For an all-fiber optical pulse shaping system, it is more convenient to describe the filter response as a function of optical wavelength λ. Then, the transfer function of the Sagnac loop mirror is expressed as

$$T(\lambda)=\frac{1}{2}W(\lambda)\times\left[1+\cos\left(\frac{2\pi n_{eff}}{\lambda}2\Delta L\right)\right],\left(|\lambda-\lambda_0|\le\frac{B_\lambda}{2}\right) \tag{3-5}$$

where $W(\lambda)$ is the intensity reflection spectrum of the LCFBG with a bandwidth B_λ, and n_{eff} is the effective refractive index of the fiber core. $\Delta L = L_1 - L_2$ is the fiber length difference, with L_1 and L_2 measured from the center of the LCFBG to the fiber coupler along the clockwise and counter-clockwise paths, as shown in Fig. 3.12. The fiber length difference ΔL comes from two sources: the wavelength-independent path difference ΔL_0 and the wavelength-dependent fiber length difference introduced by the chirp of the LCFBG $\Delta L(\lambda)$. ΔL_0 can be

controlled to be either a positive or a negative value by tuning the TDL in the fiber loop. $\Delta L(\lambda)$ is determined by the bandwidth and the chirp parameter of the applied LCFBG and can be calculated using $\Delta L(\lambda) = \delta\lambda / C$, where $\delta\lambda$ (in nm) is the wavelength detuning from the center wavelength λ_0, and C (in nm/cm) is the chirp parameter of the LCFBG. Then the spectral transfer function $T(\lambda)$ can be rewritten as

$$T(\lambda) \cong \frac{1}{2} W(\lambda) \times \left\{ 1 + \cos\left[\frac{4\pi n_{eff}}{\lambda_0^2} \lambda \left(|\Delta L_0| \pm \frac{\delta\lambda}{C} \right) \right] \right\} \tag{3-6}$$

where the positive sign and negative sign correspond to the positive and negative value of ΔL_0. Since a linearly chirped FBG is located in the fiber loop, the optical signals with different wavelengths will be reflected from different positions in the LCFBG. The path different between the clockwise and counter-clockwise direction is wavelength-dependent. As a result, an optical spectral filter with a wavelength-dependent FSR is obtained. In other words, an interference fringe pattern is generated within the bandwidth of the LCFBG, with a varying FSR due to the chirp of the LCFBG. In our analysis, the FSR of the optical spectral filter response, defined as the wavelength separation between two adjacent fringes, is a function of the wavelength and can be expressed as [190]

$$FSR = \frac{\lambda^2}{2n_{eff} |\Delta L|} \cong \frac{{\lambda_0}^2}{2n_{eff} \left| \frac{\delta\lambda}{C} + \Delta L_0 \right|} \tag{3-7}$$

According to (3-7), by properly choosing the parameters of the LCFBG and by controlling the TDL in the fiber loop, the FSR of the Sagnac loop-mirror-based optical spectral filter can be controlled. For simplicity, we assume that the input ultrashort optical pulse is a Dirac delta

function $\delta(t)$. Therefore, the intensity spectrum of the shaped optical pulse at the output of the Sagnac loop mirror is identical to the intensity transfer function of the optical spectral filter in (3-6).

After the spectrum-shaped optical pulse propagates through the dispersive element and is detected by the high-speed PD, the shaped spectrum is mapped into a temporal microwave pulse as $T(\lambda) \rightarrow y(t)$, thanks to the dispersion-induced frequency-to-time mapping. According to the mapping relationship of $\lambda = t / \ddot{\Phi}_\lambda$, the converted time-domain waveform is given by

$$y(t) \propto \frac{1}{2} W\left(\frac{t}{\ddot{\Phi}_\lambda}\right)\left\{1+\cos\left[\frac{4\pi n_{eff}}{\lambda_0^{\,2}\ddot{\Phi}_\lambda} t\left(|\Delta L_0| \pm \frac{\delta t}{C\ddot{\Phi}_\lambda}\right)\right]\right\} \tag{3-8}$$

where $\ddot{\Phi}_\lambda$ (in ps/nm) is the second-order dispersion or group velocity dispersion (GVD), δt is the time detuning from the center of the temporal waveform, which is given by the mapping relationship $\delta\lambda \rightarrow \delta t / \ddot{\Phi}_\lambda$. The time-domain pulse duration of the generated microwave pulse is determined by the window function $W(t/\ddot{\Phi}_\lambda)$, and is calculated by $\Delta T = B_\lambda \ddot{\Phi}_\lambda$. Considering that the pulse width of the real input ultrashort optical pulse is not zero, the detected pulse envelope should be modified by an envelope $r(t)$

$$y(t) \propto \frac{1}{2} \times r(t) \times W\left(\frac{t}{\ddot{\Phi}_\lambda}\right)\left\{1+\cos\left[\frac{4\pi n_e}{\lambda_0^2\ddot{\Phi}_\lambda} t\left(|\Delta L_0| \pm \frac{\delta t}{C\ddot{\Phi}_\lambda}\right)\right]\right\} \tag{3-9}$$

where $r(t)$ is the pulse envelope after the input pulse passing through the dispersive element. Assuming that the input ultrashort optical pulse has a Gaussian envelope given by $g(t) \propto \exp(-t^2/t_0^{\,2})$, where t_0 is the half pulsewidth at $1/e$ maximum. Then, the envelope of

output pulse from a dispersive element will maintain the Gaussian shape but with a broadened pulsewidth of $\left|\ddot{\Phi}_v\right|/t_0$ [191], where $\ddot{\Phi}_v$ (in ps^2) is another definition of the second-order dispersion ($\ddot{\Phi}_v = (\lambda^2/c)\ddot{\Phi}_\lambda$). Actually, the envelope is a scaled version of the spectrum envelope of the input pulse, which is mapped to the time domain, thanks to the dispersion-induced frequency-to-time mapping in the LCFBG [26].

The instantaneous microwave carrier frequency of the generated waveform can be obtained from the phase term of (3-9), which is expressed as

$$f_{RF}(\delta t) = \frac{1}{2\pi} \times \frac{d\Psi}{dt} = \frac{2n_{eff}\Delta L_0}{\lambda_0^2 \ddot{\Phi}_\lambda} \pm \frac{2n_{eff} \cdot \delta t}{C\lambda_0^2 \ddot{\Phi}_\lambda^2} \tag{3-10}$$

It can be seen from (3-10) that the generated microwave pulse is linearly chirped. For a given dispersive element, the central RF carrier frequency of the generated chirped microwave pulse, defined by $f_{RF}(\delta t)\big|_{\delta t=0} = 2n_{eff}\Delta L_0 /(\lambda_0^2 \ddot{\Phi}_\lambda)$, is only determined by the absolute value of wavelength-independent fiber length difference ΔL_0 . In other words, a chirped microwave pulse with a symmetrical, linearly increasing, or decreasing frequency chirp can be generated by simply tuning the fiber length difference ΔL_0 . The chirp rate of the generated microwave pulse is defined by

$$R_{RF} = \frac{df_{RF}(\delta t)}{d\delta t} = \pm \frac{2n_{eff}}{C\lambda_0^2 \ddot{\Phi}_\lambda^2} \tag{3-11}$$

Thus the chirp rate R_{RF} is only dependant upon the chirp parameter of the LCFBG. The positive sign and negative sign of the chirp rate correspond to the positive and negative value of

ΔL_0, respectively. Therefore, by appropriately controlling the TDL and choosing the chirp parameter of the LCFBG, a linearly chirped microwave pulse with a high central frequency and a tunable chirp profile can be generated.

It is known that the pulse compression ratio is determined by the TBWP of the transmitted microwave pulse [127]. A large TBWP can be obtained due to the frequency chirping in the generated microwave pulse. In our proposed system, the TBWP of the generated chirped microwave pulse is estimated by

$$TBWP = R_{RF}\Delta T^2 = 4\frac{n_{eff}}{\lambda_0^2}C \cdot l^2 \qquad (3\text{-}12)$$

where l is the length of the LCFBG. It is shown that the TBWP is independent of the dispersion in the system but is solely determined by the parameters of the LCFBG. For an LCFBG with a given chirp parameter, for example, a longer grating leads to a larger TBWP.

III. *Results and Discussions*

Numerical simulations and a proof-of-concept experiment are carried out to verify the proposed approach. In the simulations, a transform-limited ultrashort Gaussian pulse with a FWHM of 550 fs and with a central wavelength of 1558 nm is used as the input optical pulse. The LCFBG has a length of 1 cm with a chirp rate of 2.0 nm/cm. A proper Gaussian apodization is applied to the LCFBG in the simulations. The optical spectral response of the LCFBG-incorporated Sagnac loop mirror is calculated according to (3-6).

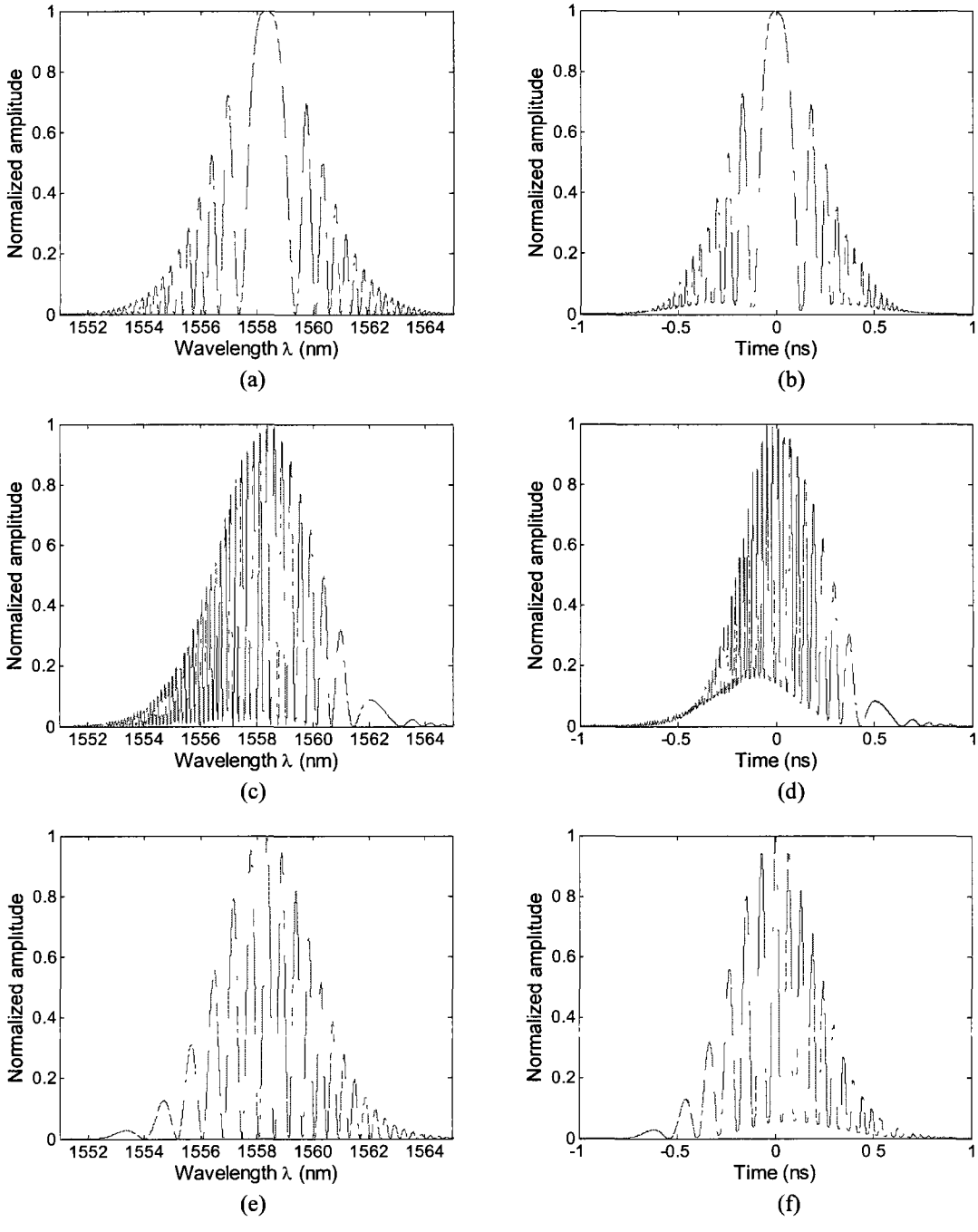

Fig. 3.13. Simulation results. The intensity spectra of the shaped optical pulse with (a) a symmetrical FSR (ΔL_0 =0), (c) an increasing FSR (ΔL_0 =9.7 mm), and (e) a decreasing FSR (ΔL_0 =6.9 mm). The generated time-domain waveforms with (b) a symmetrical chirp rate and a zero central frequency, (d) a negative chirp rate and a central frequency of 22.3 GHz, and (f) a positive chirp rate and a central frequency of 16.1 GHz.

Different values of ΔL_0 are chosen by tuning the TDL in the fiber loop, leading to the optical spectral response with a symmetrical, monotonically increasing, or monotonically decreasing FSR, as shown in Fig. 3.13(a), (c), and (e). After the linear frequency-to-time mapping in a 30.8-km SMF ($\ddot{\Phi}_\lambda = 538$ ps/nm), time-domain waveforms with different central frequencies are generated, as shown in Fig. 3.13(b), (d), and (f). The chirp rates of generated microwave waveforms are ± 0.023 GHz/ps, which matches well with the theoretical prediction by (3-11). Note that the calculated time-domain waveforms have a poorer modulation depth compared with the shaped optical spectra, especially for the cases of smaller FSR as shown in Fig. 3.13(c) and (d). This is mainly caused by the dispersion mismatch for the specific FSR in the frequency-to-time mapping process [132].

An experimental demonstration based on the setup shown in Fig. 3.14 is then implemented to verify the proposed approach for chirped microwave pulse generation. In the experiment, we still use the passive MLFL to generate a transform-limited ultrashort Gaussian pulse with a FWHM of 550 fs. The central wavelength of the pulse is 1558.3 nm, and the 3-dB spectral bandwidth is 8 nm, as shown in Fig. 3.15(a). The input pulse is sent to the LCFBG-incorporated Sagnac loop mirror. The LCFBG is fabricated using our frequency-doubled argon-ion laser operating at 244 nm. The LCFBG has a length of 1 cm with a chirp rate of 2.0 nm/cm. To ensure that the light waves are fully reflected by the LCFBG in the fiber loop, the fabricated LCFBG has a strong reflection as high as 98%. The center Bragg wavelength of the LCFBG is 1558.1 nm, which is selected to match the center wavelength of the ultrashort optical pulse. The reflection spectrum of the fabricated LCFBG is also shown in Fig. 3.15(b).

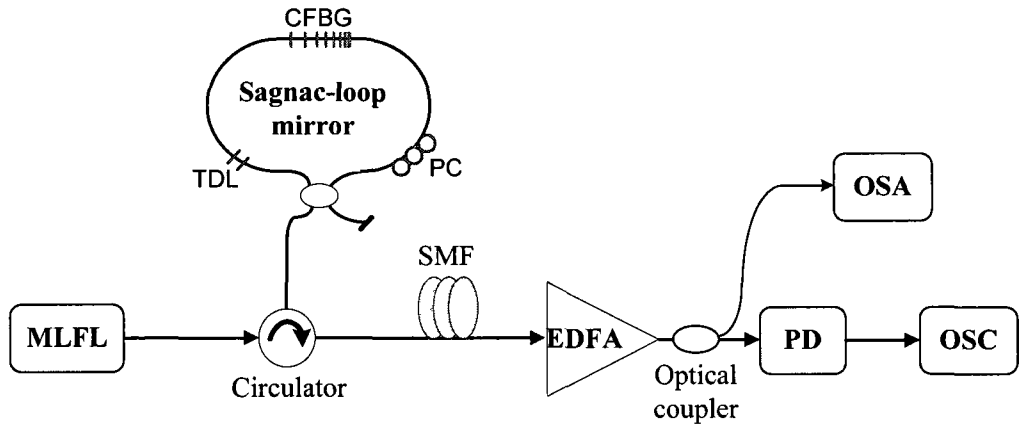

Fig. 3.14. Experiment setup for the generation of chirped microwave pulses based on spectral shaping and frequency-to-time mapping. (MLFL: mode-locked fiber laser; SMF: single-mode fiber, EDFA: erbium-doped fiber amplifier, OSA: optical spectrum analyzer, PD: photodetector, OSC: oscilloscope).

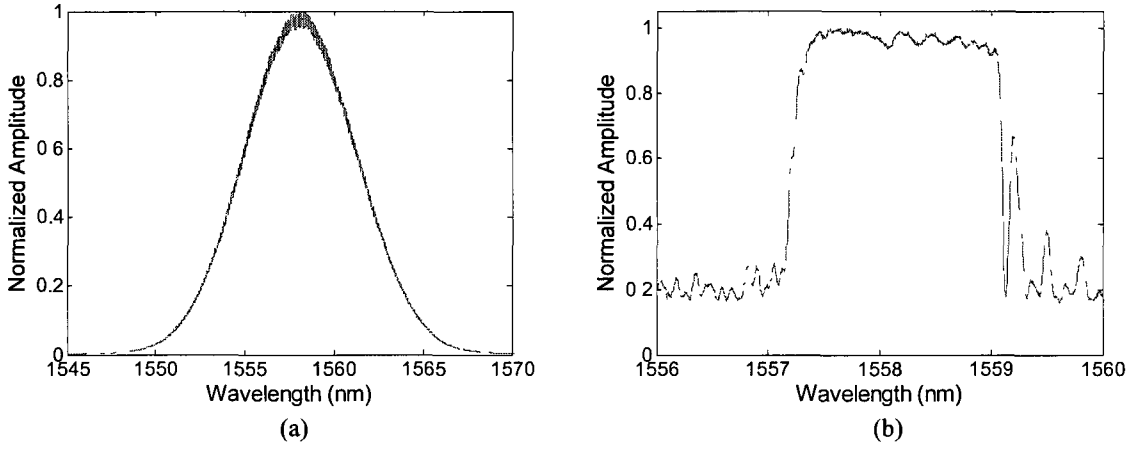

Fig. 3.15. The optical spectra of (a) input ultrashort pulse, and (b) the fabricated LCFBG (reflection).

The experimental results are measured both in the frequency domain using an optical spectrum analyzer (OSA) with a wavelength resolution of 0.01 nm and in the time domain using a sampling oscilloscope with a bandwidth of 63 GHz. In the experiment, we first choose the fiber loop to have a positive length difference of $\Delta L_0 = 9.2$ mm by controlling the TDL. Fig. 3.16 (a) shows the measured reflection spectral response of the LCFBG-incorporated Sagnac loop mirror. It is shown that an optical spectral filter with a decreasing FSR is obtained, which is then used to spectrally shape the power spectrum of the input ultrashort optical pulse. It is worth

noting that the measured reflection spectra have a reduced modulation depth. This is mainly caused by the limited resolution of the optical spectrum analyzer.

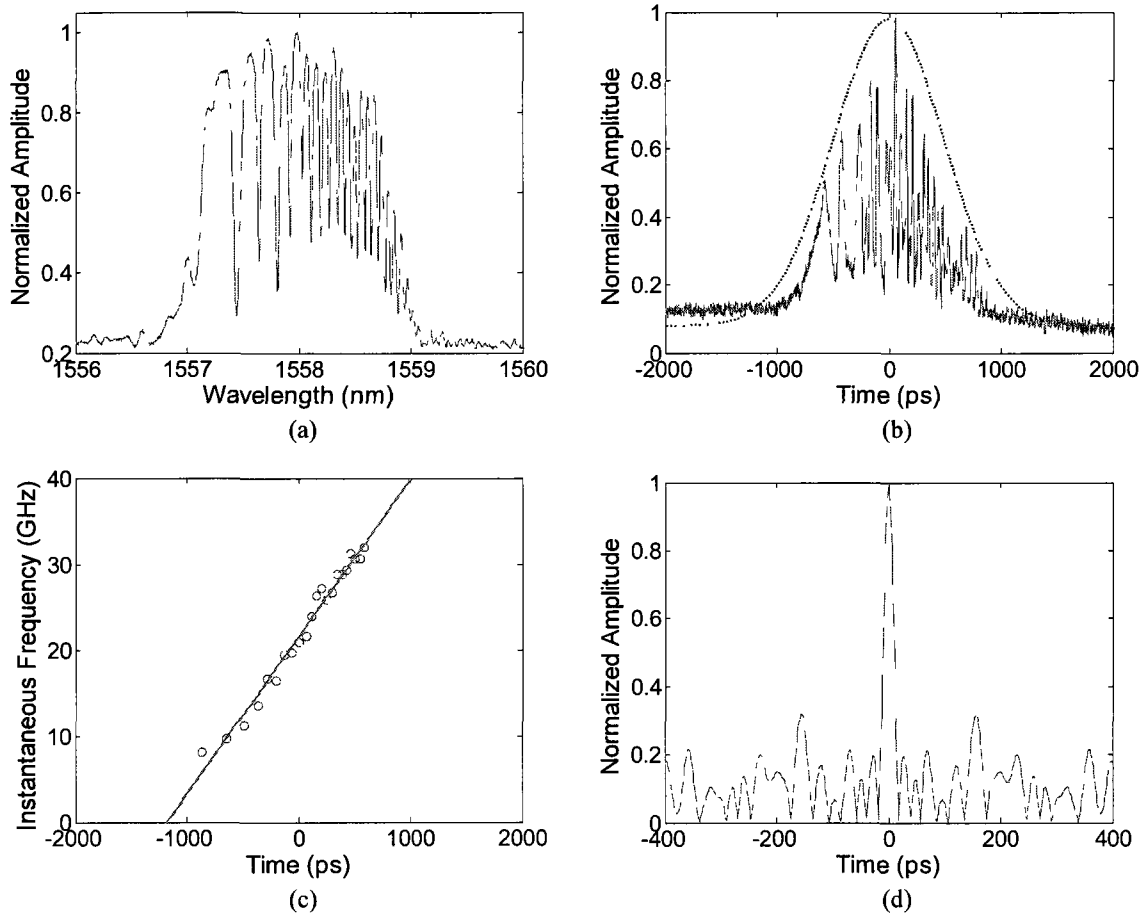

Fig. 3.16. Experimental results. (a) Spectral response of the Sagnac loop mirror with a decreasing FSR. (b) Generated waveform with a positive chirp rate (single sampling measurement). The dotted line shows the ideal Gaussian envelope. (c) Instantaneous RF frequency (solid line: linear fitting, circle: obtained from experimental result). (d) Compressed pulse by autocorrelation.

The spectrum of the shaped optical pulse is then mapped to a chirped temporal waveform, thanks to the linear frequency-to-time mapping in a 30.8-km SMF ($\ddot{\Phi}_{\lambda}$ = 538 ps/nm). A positively chirped microwave pulse is experimentally generated, as shown in Fig. 3.16(b) (single sampling measurement). The dotted line shows the ideal Gaussian pulse envelope. The FWHM of the generated pulse envelope is around 1150 ps. The circles in Fig. 3.16(c) show the

instantaneous microwave carrier frequencies within the main pulsewidth, calculated from the experimental result by Hilbert transform [188]. It is shown that a linearly increasing carrier frequency is obtained with a central frequency of 20.2 GHz and a positive chirp rate of 0.02 GHz/ps, which agree well with the theoretical predictions by (3-10). A linear fitting curve is also shown in Fig. 3.16(c) to illustrate the linear frequency chirping. According to the time-domain waveform and its carrier frequency distribution, the TBWP of the generated chirped microwave pulse is estimated to be around 44.8, which agrees well with the theoretically predicted TBWP of 49.4 by (3-12). Fig. 3.16(d) shows the compressed pulse with an FWHM of 21 ps, which is obtained by calculating the autocorrelation of the generated microwave pulse according to (3-4). By comparing the FWHMs of the waveforms in Figs. 3.16(b) and (d), a pulse compression ratio as large as 54.7 is obtained.

Then the tuning of the chirp profile is investigated. In the experiment, the Sagnac-loop mirror with a reflection spectrum having an increasing FSR is also achieved when we choose the fiber loop to have a negative length difference of ΔL_0 = -11.3 mm by tuning the TDL in the loop. A linearly chirped microwave pulse with a higher central frequency of 24.5 GHz and a negative chirp rate of -0.022 GHz/ps is then experimentally generated after the frequency-to-time mapping in the 30.8-km SMF. The experimental results are shown in Fig. 3.17. The TBWP of the generated chirped microwave pulse is estimated to be around 41, which is close to the value of the first generated chirped pulse. In fact, the TBWP is only determined by the parameters of the LCFBG according to (3-12).

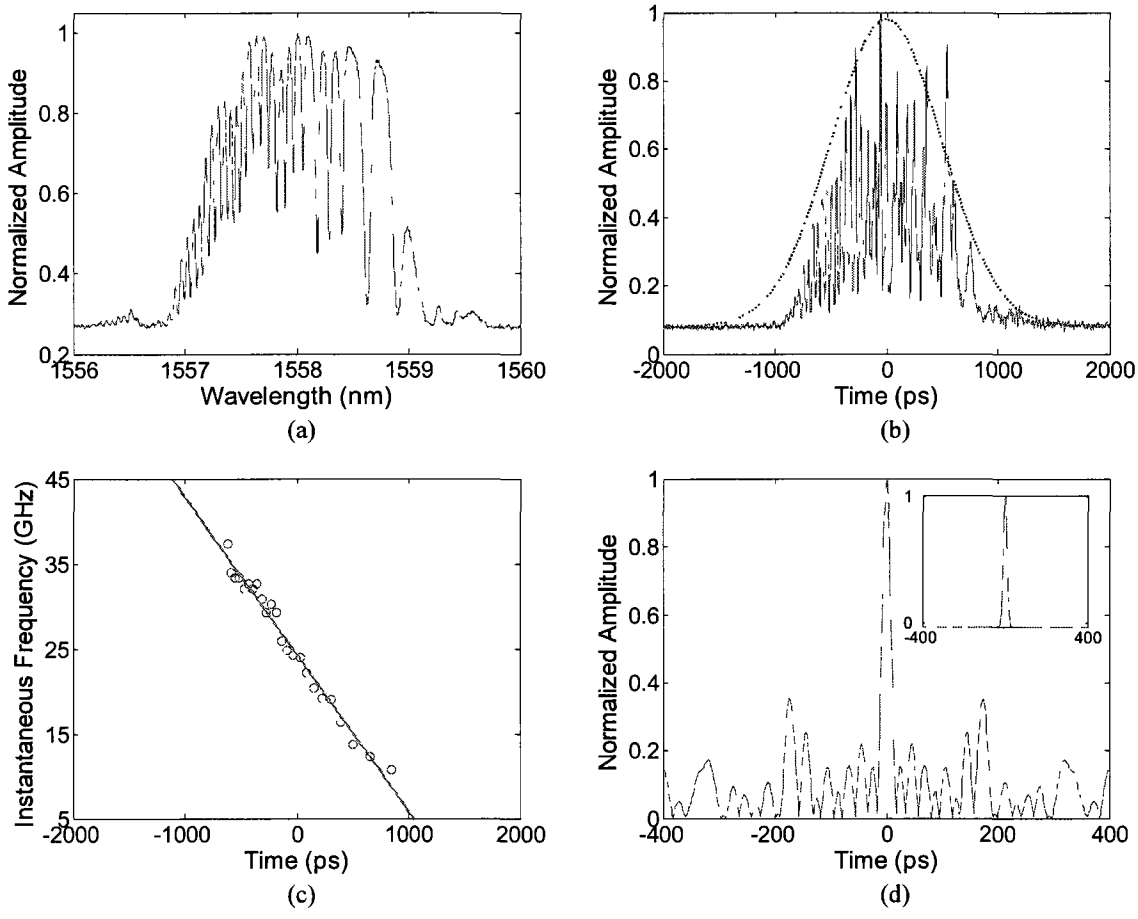

Fig. 3.17. Experimental results. (a) Spectral response of the Sagnac loop mirror with an increasing FSR. (b) Generated waveform with a positive chirp rate (dotted line: ideal Gaussian envelope). (c) Instantaneous RF frequency (solid line: linear fitting, circle: obtained from experimental result). (d) Compressed pulse by autocorrelation. Inset shows the autocorrelation of a chirped pulse with the same chirp rate but an ideal Gaussian envelope.

Fig. 3.17(d) shows the autocorrelation result. A compression ratio of 56.5 is achieved. Compared with the autocorrelation result for a chirped microwave with the same chirp profile but an ideal Gaussian envelope, as shown in the inset of Fig. 3.17(d), although the width of the autocorrelation waveform is maintained unchanged, higher level sidelobes are observed in the experiment, which are resulted from the non-Gaussian-like envelope of the generated waveform. One possible solution to eliminate the autocorrelation sidelobes is to use an LCFBG with a Gaussian-shape reflection spectrum, to ensure the spectrum of the shaped optical pulse to also

have a Gaussian envelope, leading to the generation of a temporal waveform with a Gaussian envelope after the linear frequency-to-time mapping.

IV. *Conclusion*

We have proposed and experimentally demonstrated a new approach to optically generating linearly chirped microwave pulses based on optical spectral shaping and linear frequency-to-time mapping. The key component in the proposed system is the LCFBG-incorporated Sagnac-loop mirror, which has a spectral response with an increasing or decreasing FSR and is employed to act as the optical spectral filter to shape the spectrum of the input ultrashort optical pulse. By using a linear dispersive element, such as a length of SMF in our experimental demonstration, to perform the linear frequency-to-time mapping, a linearly chirped microwave pulse with a high central frequency and tunable chirp profile was generated. The central carrier frequency and the chirp rate of the generated chirped microwave pulse can be controlled by simply tuning the time delay in the Sagnac loop mirror. The proposed approach has the advantage of simpler design, which can find applications in high-speed communications and modern radar systems.

3.1.2. FBG as a frequency-to-time mapper

This section is a revised version of the following published paper.

Article title: Photonic generation of chirped millimeter-wave pulses based on nonlinear frequency-to-time mapping in a nonlinearly chirped fiber Bragg grating

Authors: Chao Wang, and Jianping Yao

Published in IEEE Transactions on Microwave Theory and Techniques, vol. 56, no. 2, pp. 542-553, Feb. 2008.

In Section 3.1.1, FBGs have been employed as the optical spectral shapers to implement photonic microwave arbitrary waveform generation based on SS-FTM. It is also well known that a chirp FBG exhibits large dispersion when used in reflection mode [192]. The use of LCFBGs for dispersion compensation has been intensively investigated over the past decades [193-198]. In fact, in the SS-FTM-based photonic microwave arbitrary waveform generation system as shown in Fig. 3.2, an LCFBG can also act as a dispersive medium to perform the dispersion-induced frequency-to-time mapping. In this section, the use of an LCFBG as a frequency-to-time mapper is investigated.

To perform linear frequency-to-time mapping, a dispersive element with only the second-order dispersion or GVD should be employed. On the other hand, a dispersive element with both the second- and higher-order dispersion could be employed to implement nonlinear frequency-to-time mapping. An important feature of using a high-order dispersive element in an SS-FTM system is that a chirped microwave pulse can also be generated using a simple optical filter having a uniform sinusoidal spectral response (with a fixed FSR) due to the high-order dispersion induced nonlinear frequency-to-time mapping. In this research work, the nonlinear frequency-to-time mapping is achieved using a specially designed nonlinearly chirped fiber Bragg grating (NL-CFBG). Photonic generation of a chirped microwave pulse based on nonlinear frequency-to-time mapping in a NL-CFBG is investigated.

I. *Introduction*

In most of the previous studies, the dispersive device used to perform the frequency-to-time mapping was a length of SMF [122] or an LCFBG [25]. Since the high-order dispersion of the dispersive device is negligible within the operation bandwidth, only second-order dispersion (or GVD) induced linear frequency-to-time mapping could be realized. The generated microwave waveform has a shape that is identical to the shaped optical spectrum. In other words, only chirp-free microwave pulses can be generated using a dispersive device with only the second-order dispersion if the optical spectral filter has a uniform sinusoidal spectral response [199]. Therefore, to generate a chirped microwave pulse, one may use either a uniform sinusoidal spectral filter with a dispersive device having both the second- and high-order dispersion, or an optical spectral filter having a chirped spectral response (varying FSR) with a dispersive device having only the second-order dispersion, as have been presented in Section 3.1.1.2 and 3.1.1.3.

In this research work, we assume that the optical spectral filter has a uniform sinusoidal spectral response with a fixed FSR, which is much easier to implement than the optical filter with a chirped spectral response. Therefore, our efforts will be directed to investigate the use of a NL-CFBG with tunable high-order dispersion for the generation of chirped microwave pulses based on nonlinear frequency-to-time mapping. Although high-order dispersion can be obtained by a very long SMF, its limitations are obvious: the third-order dispersion of a SMF is very small; to obtain large enough third-order dispersion, a very long fiber is required, which makes the system bulky with high loss. In addition, in a very long optical fiber, the effect of polarization mode dispersion cannot be ignored, which would affect the system performance. On the other hand, the use of a NL-CFBG instead of a long SMF makes the system more compact, and more importantly, enables a flexible dispersion management. The NL-CFBG used in the proposed system is produced from a regular LCFBG using a simple and low-cost technique based on

strain-gradient beam tuning technique. To the best of our knowledge, it is the first time that the technique is used to convert an LCFBG to a NL-CFBG.

In our proposed system, a uniform optical sinusoidal spectrum is obtained by spectrally filtering a broadband transform-limited ultrashort optical pulse using a two-tap Sagnac loop filter [200]. The generation of a chirped microwave pulse is then realized by nonlinear frequency-to-time mapping in a NL-CFBG. The central frequency of the generated chirped pulse is dependent upon the second-order dispersion of the NL-CFBG for a Sagnac loop filter with a given FSR, whereas the chirp rate of the generated pulse is determined by both the second- and high-order dispersion. Since the dispersion of the NL-CFBG can be easily controlled, our approach provides the flexibility to tailor the frequency profile of the generated chirped microwave pulses, such as the central carrier frequency and chirp rate. In addition, since no MZI-based optical interference is involved in the approach, the system is more compact with a better resistance to environmental changes.

II. *System Configuration and Theoretical Analysis*

Chirped microwave pulses can be generated based on spectral shaping and frequency-to-time mapping using either a chirped spectral filter with linear frequency-to-time mapping or a uniform spectral filter with nonlinear frequency-to-time mapping. The technique presented here is based on nonlinear frequency-to-time mapping. In the proposed approach, the power spectrum of a broadband ultrashort pulse is shaped by an all-fiber two-tap Sagnac loop filter that has a sinusoidal spectral response. The nonlinear frequency-to-time mapping is then implemented using a dispersive device with both tunable second- and third-order dispersion. As

a result, a high-frequency chirped microwave pulse can be generated with a tunable central frequency and chirp rate.

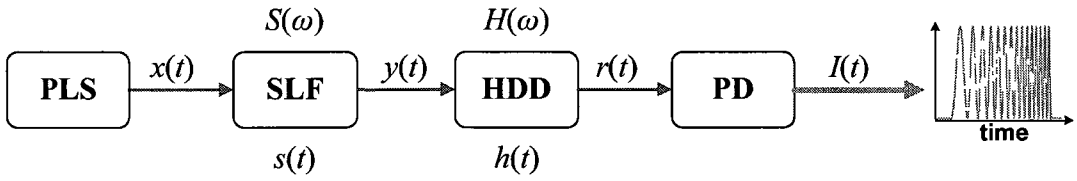

Fig. 3.18. Schematic diagram of the proposed chirped microwave pulse generation system. PLS: pulsed laser source; SLF: Sagnac loop filter; HDD: high-order dispersive device; PD: photodetector.

The operation principle of the proposed techniques is illustrated in Fig. 3.18. The system consists of an ultrashort pulsed laser source (usually a MLFL), a two-tap Sagnac loop filter, a high-order dispersive device, and a high-speed photodetector. In our analysis, both the second- and third-order dispersion are considered. Theoretically, we can assume that the ultrashort optical pulse from the pulsed laser source is a transform-limited Gaussian pulse with an amplitude A_0, a optical carrier angular frequency ω_0, and a half pulsewidth t_0 at the $1/e$ maximum. The envelop of the optical pulse can be expressed as

$$x(t) = A_0 \exp\left(-\frac{t^2}{t_0^2}\right) \tag{3-13}$$

In the system, the Sagnac loop filter with a single length of polarization maintaining fiber can be modeled as a two-tap delay-line filter with an impulse response given by

$$s(t) = \frac{1}{2}\left[\delta(t) + \delta(t-\tau_0)\right] \tag{3-14}$$

where $\delta(t)$ is a Dirac delta function, τ_0 is the time delay difference between the two taps. The Sagnac loop filter can be considered as a LTI filter, after propagating through the filter, the

envelop of the spectrum-shaped optical pulse, $y(t)$, is given by calculating the following convolution

$$y(t) = x(t) * s(t) = \frac{1}{2} A_0 \left\{ \exp\left(-\frac{t^2}{t_0^2} \right) + \exp\left[-\frac{(t-\tau_0)^2}{t_0^2} \right] \right\} \tag{3-15}$$

where * denotes convolution operation.

The spectrum-shaped optical pulse is then sent to a dispersive device, which can also be modeled as an LTI system with a transfer function $H(\omega) = |H(\omega)| \exp[-j\Phi(\omega)]$. As we have discussed in Chapter 2, the phase response of the transfer function, namely, $\Phi(\omega)$, can be expanded in the vicinity of the central frequency ω_0. Assume that the third-order and higher order dispersion are negligible within the pulse spectral bandwidth, the transfer function can then be approximated as

$$H(\omega) \cong |H(\omega)| \exp\left[-j\left(\frac{1}{2}\ddot{\Phi}(\omega-\omega_0)^2 + \frac{1}{6}\dddot{\Phi}(\omega-\omega_0)^3 \right) \right] \tag{3-16}$$

where $\ddot{\Phi} = d^2\Phi(\omega)/d\omega^2 \,|_{\omega=\omega_0}$ (in ps^2) and $\dddot{\Phi} = d^3\Phi(\omega)/d\omega^3 \,|_{\omega=\omega_0}$ (in ps^3) are defined as the second- and third-order dispersion at the central frequency, respectively. Since we mainly focus on the pulse shape change due to the dispersion effect, the so-called retarded frame is used and the average group delay $\dot{\Phi}$ is ignored [191]. It is important to note that the approximation in (3-16) is good when the higher-order dispersion within the pulse spectral bandwidth satisfies

$$|\overset{4}{\Phi}\omega^4 / 24| << \pi \tag{3-17}$$

where $\overset{4}{\Phi} = d^4\Phi(\omega)/d\omega^4\,|_{\omega=\omega_0}$ is defined as the fourth-order dispersion in this work. Note that in the following analysis, ω is used to replace $\omega-\omega_0$, as discussed in Section 2.2.1. Here ω is the relative angular frequency with respect to the central frequency of the optical carrier ω_0.

Let $r(t)$ be the complex envelope of the output optical pulse from the dispersive device. The Fourier transform of $r(t)$ is then written as

$$\begin{aligned}\tilde{R}(\omega) &= \tilde{Y}(\omega)H(\omega) \\ &= \frac{1}{2}A_0\left|H(\omega)\right|\sqrt{\pi}\tau_0\exp\left(-\frac{\tau_0^{\,2}}{4}\omega^2\right) \\ &\quad\times\left[1+\exp(-j\omega\tau_0)\right]\exp\left[-j\left(\frac{1}{2}\ddot{\Phi}\omega^2+\frac{1}{6}\dddot{\Phi}\omega^3\right)\right]\end{aligned} \tag{3-18}$$

where $\tilde{Y}(\omega)$ is the Fourier transform of $y(t)$. Then the related temporal pulse envelope $r(t)$ can be obtained by taking the inverse Fourier transform,

$$r(t) = \tilde{F}^{-1}\left[\tilde{R}(\omega)\right] = r_1(t)+r_2(t) \tag{3-19}$$

where

$$r_1(t) = \frac{A_0\left|H(\omega)\right|\tau_0}{4\sqrt{\pi}}\int_{-\infty}^{\infty}\exp\left(-\frac{\tau_0^{\,2}}{4}\omega^2-\frac{j}{2}\ddot{\Phi}\omega^2-\frac{j}{6}\dddot{\Phi}\omega^3+j\omega t\right)d\omega \tag{3-20a}$$

$$r_2(t) = \frac{A_0\left|H(\omega)\right|\tau_0}{4\sqrt{\pi}}\int_{-\infty}^{\infty}\exp\left[-\frac{\tau_0^{\,2}}{4}\omega^2-\frac{j}{2}\ddot{\Phi}\omega^2-\frac{j}{6}\dddot{\Phi}\omega^3+j\omega(t-\tau_0)\right]d\omega \tag{3-20b}$$

An analytic solution of the above integrals can be obtained in terms of Airy function [191]. It is known that although the incident pulse $y(t)$ is un-chirped, the output optical pulse from the

dispersive element, $r(t)$, becomes chirped (with phase modulation). Then $r_1(t)$ and $r_2(t)$ can be rewritten as

$$r_i(t) = |r_i(t)| \exp[j\phi_i(t)] \qquad (i = 1, 2) \tag{3-21}$$

where $\phi_i(t)$ is the time-dependent phase term of $r_i(t)$. Accordingly, the instantaneous optical carrier frequency of the chirped optical pulses is time-dependent as well, which is given by

$$f_i(t) = \frac{1}{2\pi}\frac{d\phi_i(t)}{dt} \qquad (i = 1, 2) \tag{3-22}$$

The two chirped optical pulses $r_1(t)$ and $r_2(t)$ are then sent to a high speed PD, where the interference between these two pulses occurs. The electrical current at the output of the photodetector $I(t)$ is proportional to the intensity of the input electrical field, which is expressed as

$$I(t) \propto |r(t)|^2 = |r_1(t)|^2 + |r_2(t)|^2 + 2|r_1(t)||r_2(t)|\cos[\phi_1(t) - \phi_2(t)] \tag{3-23}$$

It can be seen from (3-23) that the first and second terms on the right-hand side are the low-frequency components, whereas the third term is the high-frequency component with an instantaneous RF frequency given by

$$f_{RF}(t) = \frac{1}{2\pi}\frac{d}{dt}[\phi_1(t) - \phi_2(t)] = f_1(t) - f_2(t) \tag{3-24}$$

Therefore, the beating between the two chirped optical pulses $r_1(t)$ and $r_2(t)$ leads to the generation of a chirped microwave pulse with an instantaneous RF carrier frequency determined

by the instantaneous optical carrier frequency difference of the two optical pulses. According to the above analysis, both the pulse envelope and instantaneous RF carrier frequency of the generated chirped microwave pulse can be computed by using equations (3-20)–(3-24).

In order to investigate the direct relationship between the grating dispersion and the frequency profile of the generated chirped microwave pulse, an approximate model focusing on the instantaneous RF carrier frequency of the generated microwave pulse is developed based on frequency-to-time mapping.

It is known that the transfer function of a two-tap Sagnac loop filter is given by

$$\tilde{S}(\omega) = \tilde{F}\left[s(t)\right] = 1 + \cos(\omega\tau_0) \tag{3-25}$$

where $\tilde{F}(\bullet)$ denotes the Fourier transform operation. Then the optical power spectrum of the spectrum-shaped pulse at the output of the filter can be expressed as

$$\tilde{Y}(\omega) = \tilde{X}(\omega)\tilde{S}(\omega) = \exp\left(-\frac{{\tau_0}^2}{4}\omega^2\right)\left[1 + \cos(\omega\tau_0)\right] \tag{3-26}$$

After the spectrum-shaped optical pulse propagates through the dispersive device, where the second- and third-order dispersion are both considered, the spectrum $\tilde{Y}(\omega)$ is mapped into a temporal waveform $r(t)$. Thanks to the high-order dispersion, the frequency-to-time conversion is no longer linear. The nonlinear mapping relationship from the frequency domain to time domain is derived from the group delay response of the dispersive element and is given by [201]

$$\omega(t) = \frac{-\ddot{\Phi} \pm \sqrt{\ddot{\Phi}^2 + 2\dddot{\Phi}t}}{\dddot{\Phi}} \tag{3-27}$$

where the ± sign is due to the positive or negative dispersion. Note that (3-27) only gives the nonlinear mapping relationship with the dispersion terms up to the third-order. A general nonlinear frequency-to-time mapping relationship when considering all higher-order dispersion terms has been investigated [202].

Then the mapped temporal waveform is obtained from (3-26) and (3-27),

$$\begin{aligned} |r(t)| &\propto \tilde{Y}(\omega)|_{\omega=\frac{-\Phi\pm\sqrt{\Phi^2+2\Phi t}}{\Phi}} \\ &= \frac{1}{2}\exp\left[-\frac{{\tau_0}^2}{4}\left(\frac{-\ddot{\Phi}\pm\sqrt{\ddot{\Phi}^2+2\dddot{\Phi}t}}{\dddot{\Phi}}\right)^2\right]\times\left[1+\cos\left(\frac{\sqrt{\ddot{\Phi}^2+2\dddot{\Phi}t}}{\dddot{\Phi}}\tau_0\pm\frac{\ddot{\Phi}}{\dddot{\Phi}}\tau_0\right)\right] \end{aligned} \tag{3-28}$$

From (3-28), we can find that the instantaneous RF angular frequency of the generated electrical pulse is obtained by

$$\omega_{RF}(t)=\frac{d}{dt}\left(\frac{\sqrt{\ddot{\Phi}^2+2\dddot{\Phi}t}}{\dddot{\Phi}}\tau_0\pm\frac{\ddot{\Phi}}{\dddot{\Phi}}\tau_0\right)=\frac{\tau_0}{\sqrt{\ddot{\Phi}^2+2\dddot{\Phi}t}} \tag{3-29}$$

It can be obviously seen from (3-29) that the generated microwave pulse is nonlinearly chirped. If the dispersion coefficients satisfy that $|(2\dddot{\Phi})/\ddot{\Phi}^2|<<1$, (3-29) can be well approximated according to the binomial theorem

$$\omega_{RF}(t)\cong\frac{\tau_0}{\ddot{\Phi}}-\frac{\dddot{\Phi}\tau_0}{|\ddot{\Phi}|^3}t \tag{3-30}$$

The central frequency of the generated chirped pulse can now be calculated by letting $t=0$ in (3-30), which is $\omega_{RF0}=\omega_{RF}(0)\cong\tau_0/|\ddot{\Phi}|$. As can be seen the central frequency is only dependent upon the second-order dispersion $\ddot{\Phi}$. On the other hand, the instantaneous frequency

chirp rate, which is given by $R_{RF} = d\omega_{RF}(t)/dt \cong -\dddot{\Phi}\tau_0 / \left|\ddot{\Phi}\right|^3$, is determined by both the second- and the high-order dispersion.

III. *Numerical Simulation*

To evaluate the approximate model given in (3-29), numerical simulations are performed based on equations (3-20)–(3-24). In the simulations, the input optical pulsewidth is 550 fs and the FSR of the Sagnac loop filter is chosen to be 0.8 nm, which corresponds to a time-delay difference of $\tau_0 = 63.6$ ps. In the first example, only the second-order dispersion of $\ddot{\Phi} = 320$ ps^2 is considered. After propagating through the dispersive device, the two optical pulses are linearly chirped with the same chirp rate, as shown in Fig. 3.19(a). As a result, the beating of the two delayed and equally chirped optical pulses leads to the generation of an microwave pulse with a constant RF carrier frequency of 31.6 GHz, as shown in Fig. 3.19(b), which matches well with the prediction given by (3-29) for the case of $\dddot{\Phi} = 0$.

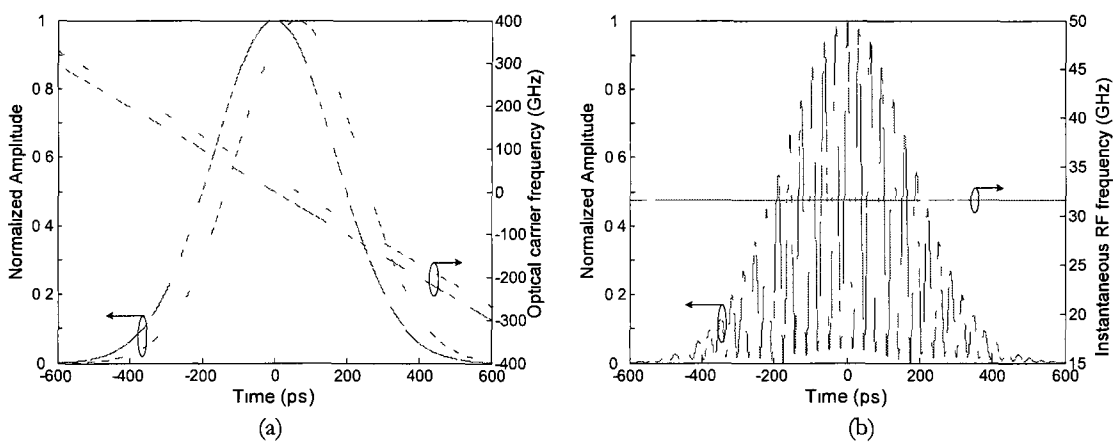

Fig. 3.19. Simulation results for a chirped microwave pulse generation system using a dispersive device with the second-order dispersion only. (a) Envelope and optical instantaneous carrier frequency of the two chirped optical pulses {solid line: $r_1(t)$, dotted line: $r_2(t)$}; (b) Amplitude and RF carrier frequency of the generated microwave pulse.

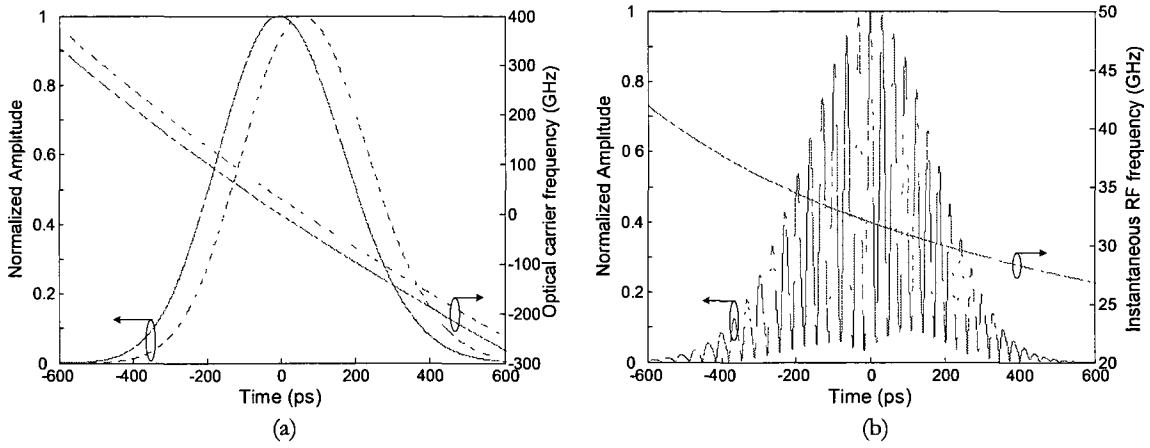

Fig. 3.20. Simulation results for a chirped microwave pulse generation system using a dispersive device with both the second- and third-order dispersion. (a) Envelope and optical instantaneous carrier frequency of the two chirped optical pulses {solid line: $r_1(t)$, dotted line: $r_2(t)$}; (b) Amplitude and RF carrier frequency of the generated chirped microwave pulse.

In the second example, both the second- and third-order dispersion are considered. We choose the third-order dispersion $\dddot{\Phi}$ to be 35 ps^3, while keeping the second-order dispersion $\ddot{\Phi}$ to be 320 ps^2. The simulation results are shown in Fig. 3.20. Due to the third-order dispersion, the two incident optical pulses are nonlinearly chirped after propagating through the dispersive device, as shown in Fig. 3.20(a). Therefore, the beating between the two delayed and nonlinearly chirped optical pulses leads to the generation of a chirped microwave pulse with the RF carrier frequency given by (3-24). Simulation results about the generated electrical pulse are shown in Fig. 3.20(b). In this case, the central frequency is around 31.7 GHz and the instantaneous RF frequency varies from 25.4 to 46.5 GHz within the main pulsewidth, which is in good agreement with the prediction given by (3-29) as well. The envelope of the generated electrical pulse has a shape close to a Gaussian pulse, but with a slight asymmetry. Simulations show that with a larger third-order dispersion, the pulse envelope becomes more asymmetrical. A detailed analysis on the pulse-shape asymmetry due to higher order dispersion can be found in [203] and [204].

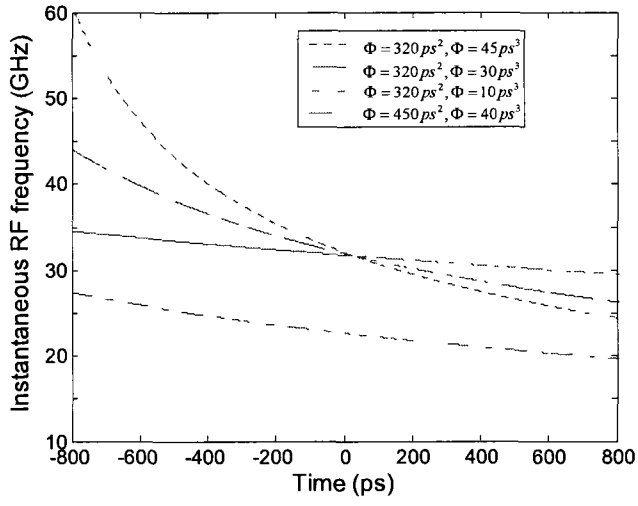

Fig. 3.21. Instantaneous RF carrier frequency of the generated chirped pulses under different second- and third-order dispersion.

Fig. 3.21 shows the simulation results of the instantaneous RF carrier frequency of the generated chirped microwave pulses under different second- and third-order dispersion. As can be seen from Fig. 3.21, by selecting a dispersive device with suitable second- and third-order dispersion, the chirped microwave pulse with the required central frequency and chirp rate can be generated. It is worth noting that a linear frequency chirping is not always necessary in a pulse compression system. In fact, the frequency modulation can be of almost any form, provided that the matched filter in the receiver is properly designed to match the transmitted chirped pulse.

IV. *NL-CFBG*

In the proposed system, a dispersive device with tunable high-order dispersion provides the possibility of tailoring the frequency characteristics of the generated chirped microwave pulses. Such tunable high-order dispersion is realized by using a properly designed NL-CFBG, in which the group-delay response varies nonlinearly with respect to the optical wavelength. NL-

CFBGs have been widely used to compensate for high-order chromatic dispersion and polarization mode dispersion in high speed optical communications systems [205-207]. NL-CFBGs were usually fabricated using a nonlinearly chirped phase mask [205-206] or a linearly chirped phase mask with a properly controlled exposure time during the fabrication to introduce a nonlinear chirp [205]. These fabrication techniques are either expensive or complicated. It is, therefore, highly desirable to develop a simple and low-cost technique for the NL-CFBG fabrication.

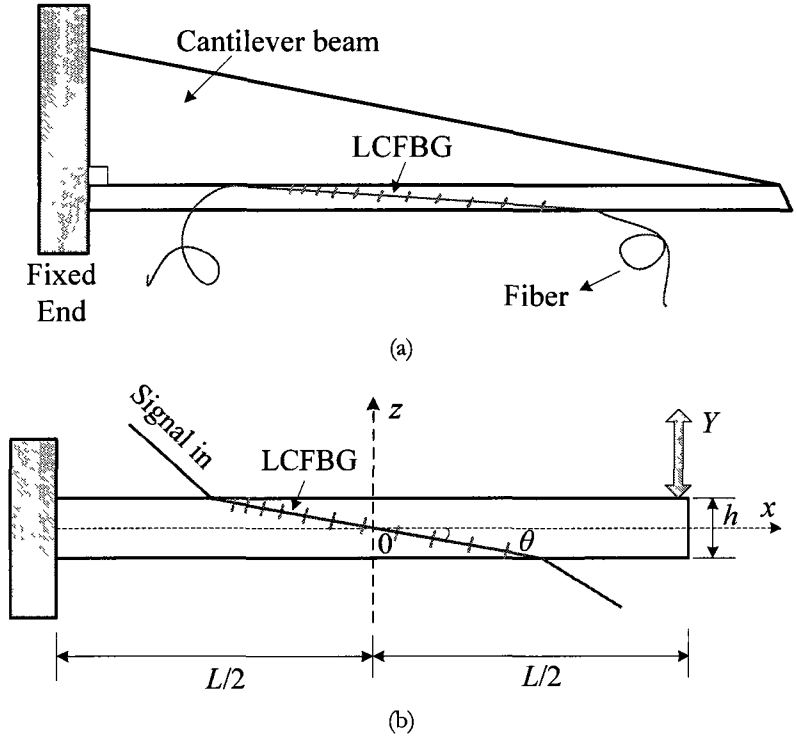

Fig. 3.22. Schematic diagram showing the NL-CFBG generation using strain-gradient beam tuning technique. (a) Right-angled triangle cantilever beam. (b) Bending of the grating with the beam. LCFBG: linearly chirped fiber Bragg grating.

In research work, we propose a simple and efficient method to introduce large nonlinear chirp to a regular LCFBG based on strain-gradient beam tuning technique. Fig. 3.22 shows the schematic diagram of the NL-CFBG fabrication technique. As can be seen from Fig. 3.22(a), an

LCFBG is glued in an inclined direction onto the lateral side of a right-angled triangular cantilever beam. When a mechanical force is applied to the free end of the beam, as shown in Fig. 3.22(b), a linear strain gradient is generated, which leads to the generation of a NL-CFBG. In Fig. 3.22(b), the x-axis is on the neutral layer of the cantilever beam, L is the beam length, h is the thickness of the beam, θ is the angle between the grating axis and the beam neutral surface, and Y is the applied displacement at the free end of the beam. The center of the grating is consistent with the neutral layer on the side cross section. This ideal situation will be always considered in the following analysis.

When the beam is bent by deflecting the free end while keeping the other end fixed, the introduced axial strain gradient along the grating can be expressed as [208]

$$\varepsilon_{axis}(l) = \frac{1}{2}\kappa l \sin(2\theta) = \frac{Y \sin(2\theta)}{L^2} l \tag{3-31}$$

where κ is the beam curvature, l is the grating length between the given point and the center point of grating. Assume that θ is approximately constant, which is true if the beam displacement is small relative to the length of beam. It can be seen from (3-31) that, the linear strain is produced along the grating when deflecting the beam. Suppose that the deflection is upward ($Y > 0$), then the strain on the neutral layer of the beam is zero; half of the grating (the section of $0 < x < L/2$) is under varying tension strain, whereas the other half (the section of $-L/2 < x < 0$) suffers a varying compression strain. The symmetrical strain distribution ensures that the central wavelength of the grating may keep closely fixed during the beam tuning process.

When an LCFBG is mounted on the side surface of the beam, the developed linear strain gradient is transferred to physically change the grating pitch according to the strain-optic effect. The grating pitch variance $\Delta\Lambda$ is expressed as

$$\Delta\Lambda(l) = (1-p_e)\varepsilon_{axis}(l)\Lambda(l) = (1-p_e)\frac{Y\sin(2\theta)}{L^2}(\Lambda_C + R_\Lambda l)l \tag{3-32}$$

where p_e is the effective photo-elastic constant (~0.22) of the fiber material, Λ_C is the central grating pitch, and R_Λ is the chirp rate of the grating pitch.

According to the well-known Bragg condition [69], the Bragg wavelength distribution $\lambda_B(l)$ as a function of distance along the fiber axis under linear strain gradient is expressed as [209]

$$\begin{aligned} \lambda_B(l) &= \lambda_{B_C} + K_1 l + K_2 l^2 \\ K_1 &= R_\lambda + \lambda_{B_C}\frac{Y\sin(2\theta)}{L^2}(1-p_e) \\ K_2 &= R_\lambda \frac{Y\sin(2\theta)}{L^2}(1-p_e) \end{aligned} \tag{3-33}$$

where λ_{B_C} is the center Bragg wavelength of the LCFBG and R_λ (in nm/mm) is the wavelength chirp rate of the original grating. It is shown that the Bragg wavelength distribution is a quadratic function of the distance l, instead of a linear function as in an LCFBG. Consequently, a NL-CFBG with a nonlinear group delay is fabricated directly from a regular LCFBG by applying a linear strain gradient.

Fig. 3.23 shows the calculated group delays of the NL-CFBG with different displacements according to the method presented in this research work. In our simulation, the length of the cantilever beam is chosen to be 150 mm, and the grating angle is $\theta = 15^0$. An initial LCFBG

with a grating length of 50 mm, a center Bragg wavelength of $\lambda_{Bc} = 1556$ nm, and a linear chirp rate of $R_\lambda = 0.24$ nm/mm is considered. Without loss of generality, we assume that the grating reflects a longer wavelength at the input end and a shorter wavelength at the back end, therefore, the grating has negative second-order dispersion. In fact, for an initially unchirped optical incident pulse, dispersion-induced broadening and phase modulation of the pulse does not depend on the sign of the second-order dispersion coefficient $\ddot{\Phi}$ [191].

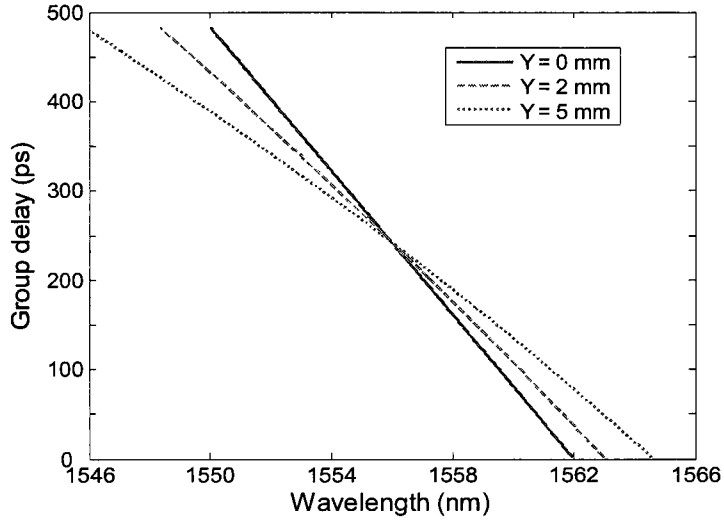

Fig. 3.23. Simulation results: group delay characteristics of the generated NL-CFBG at different beam displacements.

It is obviously shown in Fig. 3.23 that the nonlinear chirp characteristics of the NL-CFBG can be easily controlled by adjusting one parameter only, namely, the beam deflection Y. For example, for the case of displacement $Y = 2$ mm, the equivalent second- and third-order dispersion coefficients of the generated NL-CFBG at 1556 nm are $\ddot{\Phi} = 265.4$ ps^2 and $\dddot{\Phi} = 24.7$ ps^3, respectively. If the displacement is increased to 5 mm, the second- and third-order dispersion coefficients will become $\ddot{\Phi} = 209.4$ ps2 and $\dddot{\Phi} = 29.6$ ps3 at 1556 nm.

There is a trade-off between the nonlinearity and second-order dispersion: larger group delay nonlinearity and a broader spectral bandwidth can be realized when a larger displacement is applied, but a decreased second-order dispersion level would be resulted. By properly choosing the displacement Y, the NL-CFBG can provide a sufficiently large second-order dispersion, a suitable nonlinear group delay and bandwidth for the application in generating chirped microwave pulses, as described in this research work.

V. *Experiment*

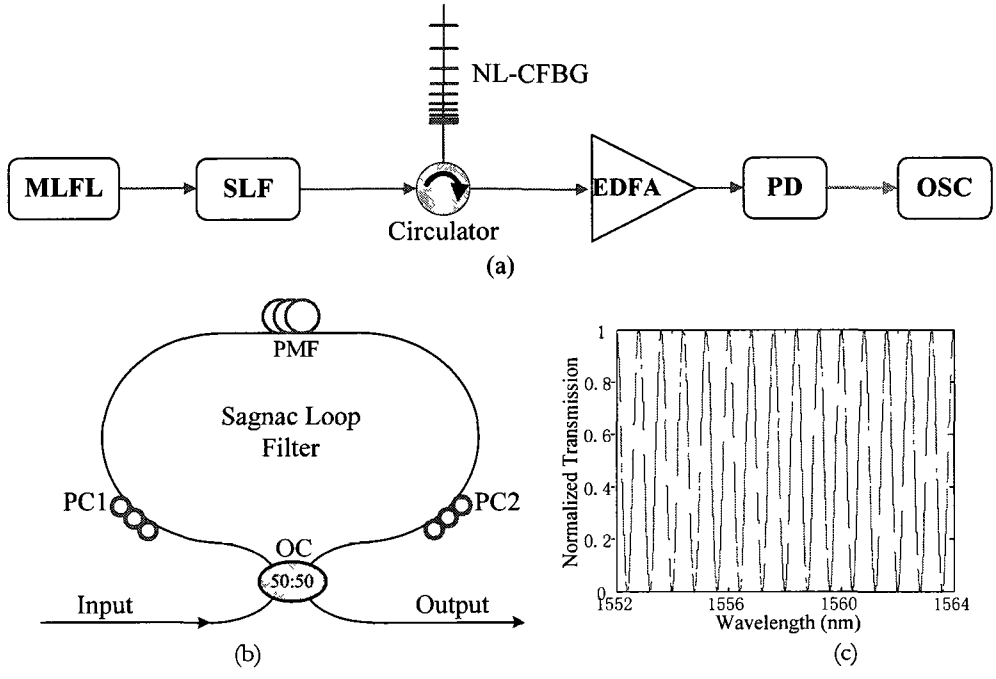

Fig. 3.24. Experimental setup of the proposed chirped microwave pulse generation system based on nonlinear frequency-to-time mapping. (a) System configuration; (b) the two-tap SLF; (c) the normalized transmission response of the SLF. (MLFL: mode-locked fiber laser, SLF: Sagnac loop filter, NL-CFBG: nonlinearly chirped fiber Bragg grating, EDFA: erbium-doped fiber amplifier, PD: photodetector, OC: optical coupler, PC: polarization controller, PMF: polarization maintaining fiber, OSC: oscilloscope.)

An experiment is carried out to verify the proposed approach for chirped microwave pulses generation. The experimental setup of the proposed system is shown in Fig. 3.24(a). An MLFL is used to generate a broadband transform-limited ultrashort Gaussian pulse. A two-tap Sagnac

loop filter, which consists of a length of polarization maintaining fiber (PMF) and two PCs, as shown in Fig. 3.24(b), serves as an optical spectral filter. The Sagnac loop filter has a uniform sinusoidal spectral response, with the simulated result shown in Fig. 3.24(c). The FSR is determined by the length and the birefringence of the polarization maintaining fiber. A NL-CFBG is used as a dispersive device with both the second- and third-order dispersion, which is fabricated based on our proposed beam-bending technique, to perform the nonlinear frequency-to-time mapping. As a result, a chirped microwave pulse is obtained at the output of a high-speed photodetector.

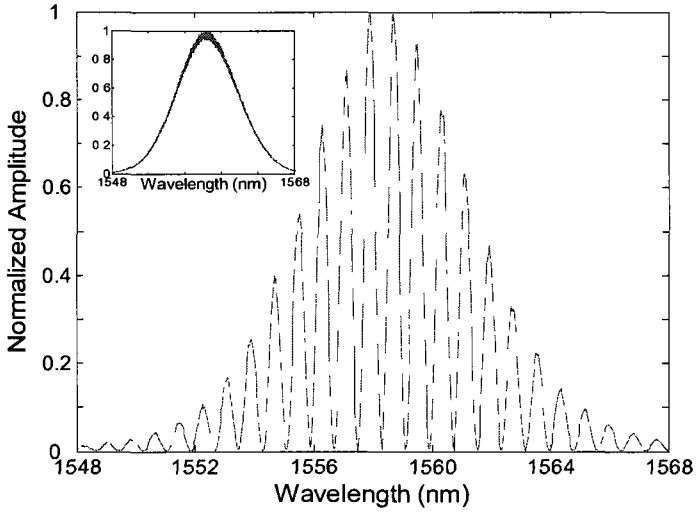

Fig. 3.25. Measured optical spectrum of the shaped optical pulse. The inset shows the spectrum of input optical pulse before spectral shaping.

In the experiment, a transform-limited Gaussian pulse with a FWHM of 550 fs generated from the MLFL is used as the input optical pulse. The central wavelength of the ultrashort pulse is 1558.5 nm, and the 3-dB spectral bandwidth is 8 nm, as shown in the inset of Fig. 3.25. The FSR of the Sagnac loop filter is set as 0.8 nm. After the spectral shaping by the filter, we obtain

a spectrum-shaped pulse with its spectrum shown in Fig. 3.25. It can be seen that a uniform sinusoidal spectrum is obtained after the spectral shaping.

The performance of the fabricated NL-CFBG is measured first. In order to cover the main spectral bandwidth of the broadband femtosecond laser source, a regular linearly chirped fiber Bragg grating with a linear chirp rate of 0.24 nm/mm, grating length of 50 mm, and center Bragg wavelength of 1556 nm is used to generate a NL-CFBG based on the strain-gradient beam tuning technique, as described in the previous section.

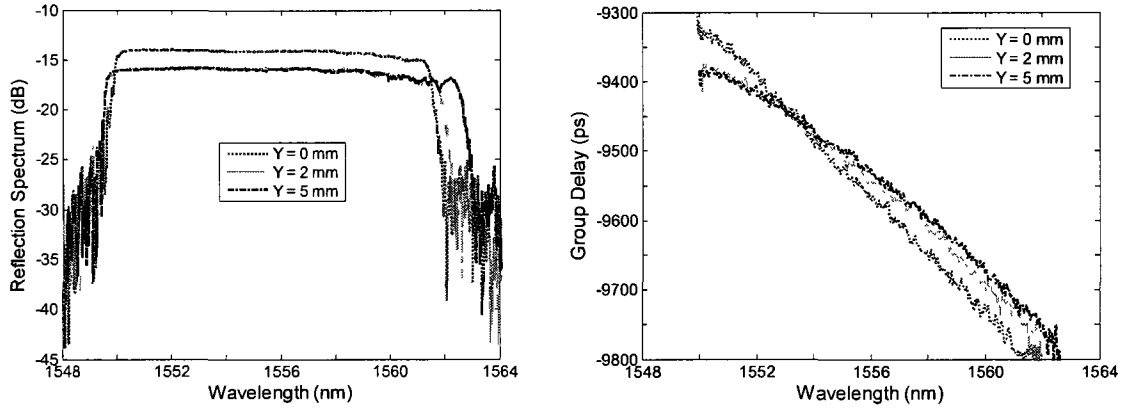

Fig. 3.26. Measured results: (a) reflection spectra and (b) group delay responses of the generated NL-CFBG under different beam deflections. (dotted line: zero deflection; solid line: 2 mm deflection; dash-dot line: 5 mm deflection.)

Fig. 3.26 shows the measured reflection spectra and group delay responses of the produced NL-CFBG under different beam free-end deflections. It can be seen from Fig. 3.26(a) that the 3-dB spectral bandwidth can be tuned from 11.6 nm (with zero displacement) to 13.2 nm (with 5 mm displacement). Since the center wavelength of the fabricated LCFBG is shorter than that of the input optical pulse, in order to cover the spectrum of the input pulse as much as possible, the grating center point is intentionally mismatched with the beam neutral layer: a major part of the grating experiences the tension strain and a minor part of the grating experiences the

compression strain. As a result, the central wavelength of the produced NL-CFBG is slightly shifted to a longer wavelength when bending the beam. In the meantime, a nonlinear group-delay distribution with respect to the wavelength is realized as well, as shown in Fig. 3.26(b).We can find that a larger nonlinearity of the group delay response and a broader spectral bandwidth can be achieved in the NL-CFBG when a larger displacement is applied, which is consistent with the theoretical analysis in the previous section.

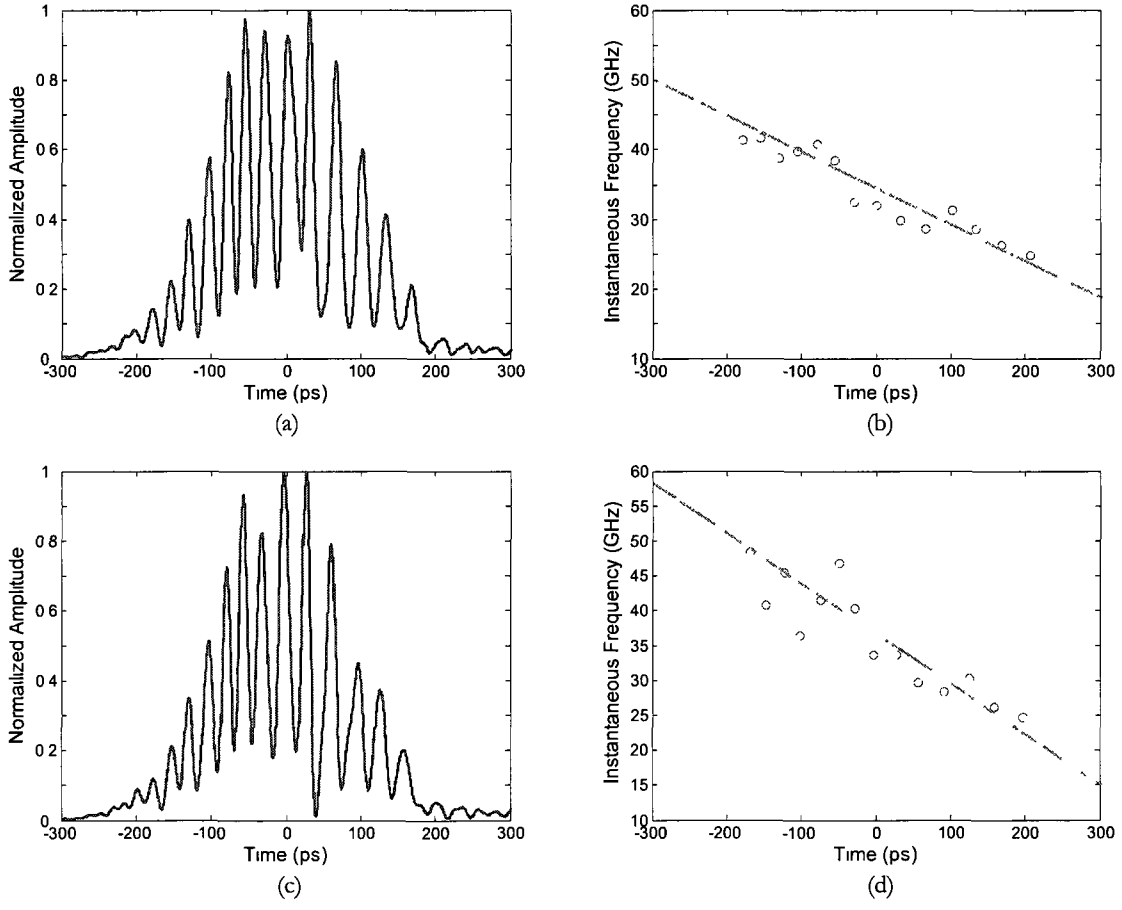

Fig. 3.27. Experimental results. (a) Pulse profile and (b) instantaneous frequency in the case of 2-mm beam deflection. (c) Pulse profile and (d) instantaneous frequency in the case of 5-mm beam deflection. {Circle in (b) and (d): obtained from experimental results, dashed line in (b) and (d): theoretical prediction by (3-30).}

The experimental results are shown in Fig. 3.27. The generated waveforms are measured using a high-speed sampling oscilloscope, 5 times averaging is performed. Both the pulse profile and

instantaneous carrier frequency versus time are plotted in the figure. In the first example, the applied beam deflection is 2 mm. According to the measured group-delay result, the equivalent second- and third-order dispersion coefficients $\ddot{\Phi}$ and $\dddot{\Phi}$ at 1558.5 nm are 295.1 ps^2 and 20.9 ps^3, respectively. Thanks to the nonlinear frequency-to-time mapping in the produced NL-CFBG, a chirped microwave pulse is generated.

As can be seen from Fig. 3.27 (a), the FWHM of the generated pulse envelope is around 243 ps, which is measured by a high-speed sampling oscilloscope (Agilent 86100C). Fig. 3.27(b) shows the instantaneous RF carrier frequency within the main pulsewidth, which can be calculated by Hilbert transform [188]. Here, for simplicity, the instantaneous carrier frequency is approximated by the reciprocal of the time period of pulse trace, as plotted in the open-circle curve. The dotted curve illustrates the theoretical prediction given by (3-30). In this case, the frequency profile of the generated microwave pulse is quasi-linear and the instantaneous carrier frequency changes from 25 to 43 GHz, which corresponds to an equivalent frequency chirp rate of 0.053 GHz/ps.

In the second case, the beam displacement is increased to 5 mm, which leads to the equivalent second- and third-order dispersion coefficients of $\ddot{\Phi} = 278.1$ ps^2 and $\dddot{\Phi} = 23.7$ ps^3 at 1558.5 nm. As a result, the FWHM of the generated pulse envelope is around 218 ps; the instantaneous RF carrier frequency varies from 24 to 49 GHz, which corresponds to a chirp rate of 0.074 GHz/ps. The measured pulse profile and instantaneous frequency are shown in Fig. 3.27(c) and (d). The dotted curve in Fig. 3.27(d) also illustrates the theoretical prediction given by (3-30). One may notice that the measured instantaneous frequency does not match the theoretical prediction at some time points. This discrepancy is resulted from the abnormal strain induced dispersion

variation in the NL-CFBG when applying the beam deflection. One solution to reduce the error is to use a beam with a more smooth surface and more stable strain distribution.

From the above experimental results, we can find that, with a larger beam deflection, the fabricated NL-CFBG will possess smaller second-order dispersion, but higher third-order dispersion. As a result, the generated waveform will have a higher central frequency and a larger chirp rate. The system shows its high efficiency of tuning the frequency profile of the generated microwave waveform by simply controlling the applied beam deflection.

In a pulsed microwave radar system, the chirped microwave pulses at a receiver end should be compressed, which is usually realized via correlation or matched filtering. Fig. 3.28 shows the correlations between the generated microwave pulses with different chirp rates and the matched reference pulses according to (3-4). In the above two cases (2- and 5-mm beam deflections), the FWHMs of the obtained autocorrelation envelopes are around 49 and 42 ps, respectively. By comparison with the results in Fig. 3.27, pulse compression ratios of 4.15 and 5.2 are achieved.

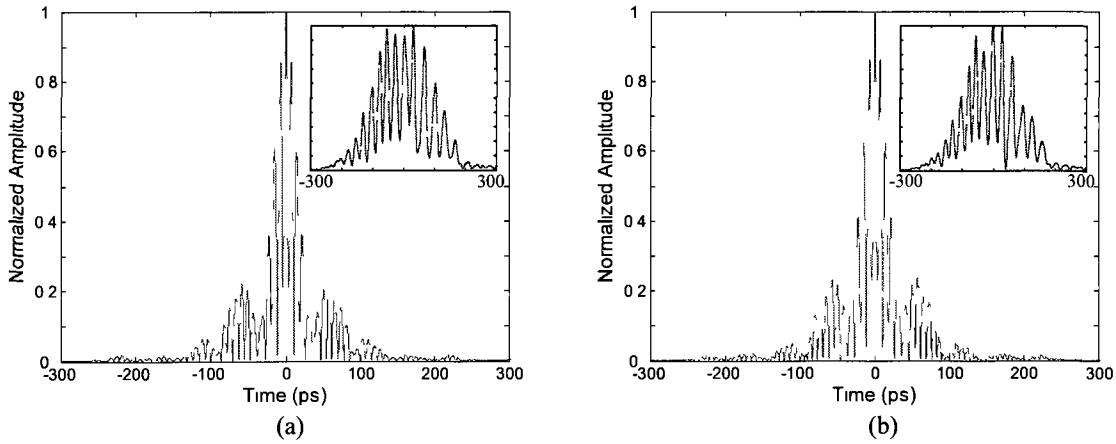

Fig. 3.28. Autocorrelation waveforms of the generated chirped microwave pulses. (a) Beam displacement is 2 mm. (b) Beam displacement is 5 mm. Insets: generated chirped microwave pulse.

Despite that the realized pulse compression ratio is not very high due to the small amount of cycles within the pulse envelope and the limited high-order dispersion in our NL-CFBG, the nonlinear dispersion induced microwave pulse chirping is observed and verified. The experimental results also agree well with the theoretical predictions. In order to achieve a higher pulse compression ratio for practical applications, an optical spectral filter with narrower FSR should be used to generate more cycles within the pulse envelope, and a longer grating should be fabricated to satisfy the requirement of large high-order dispersion and wide bandwidth.

VI. *Discussion*

According to the principle of dispersion-induced frequency-to-time mapping, the generated temporal waveform should have the same shape with the shaped optical spectrum, as shown in Fig. 3.25. From the experimental results shown in Fig. 3.27(a) and (c), however, it is found that the measured time-domain waveforms have a limited modulation depth compared with the shaped optical spectrum. Similar effects have also been found in [200] and [183]. Their analysis indicated that the reduced modulation depth could be caused due to the nonflat frequency response of the photodetector or the environmental changes during the measurement, which could slightly change the interference pattern and cause a decrease of the modulation depth.

In order to find a more intrinsic mechanism that leads to the degradation in the modulation depth of the generated microwave waveforms, some simulations based on the theoretical model presented in this research work are performed. Fig. 3.29 shows the simulation results, where the FSR of the Sagnac loop filter is chosen as 0.8 nm, or an equivalent time-delay difference of $\tau_0 = 63.6$ ps. Several cases with different second-order dispersion are considered. For simplicity,

the third-order dispersion is not taken into account since it has negligible contributions to the poor modulation depth, but only slightly distorts the shape of the generated waveform.

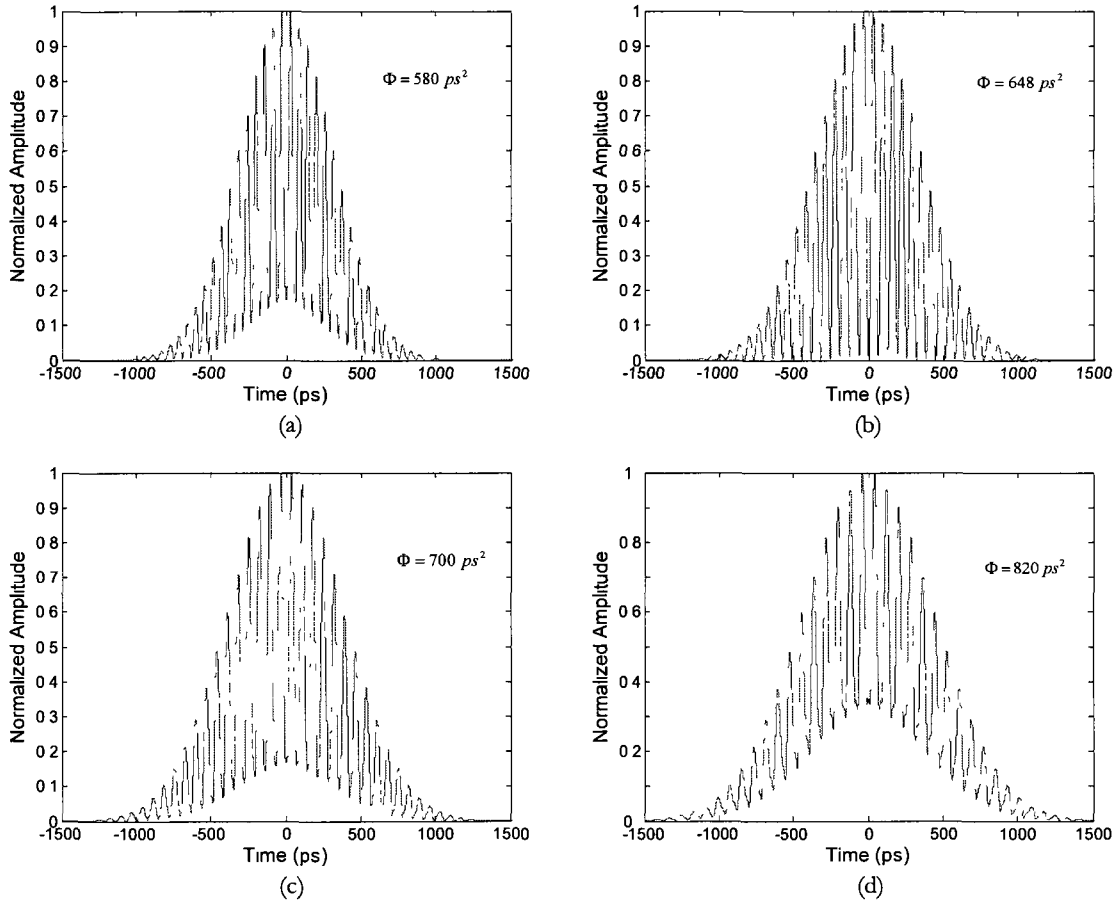

Fig. 3.29. Generated microwave waveforms with different modulation depth under different second-order dispersion of (a) 580, (b) 648, (c) 700, and (d) 820 ps^2.

From Fig. 3.29 we can find that for two incident optical pulses with a given time-delay difference τ_0, only a certain value of dispersion can ideally convert the shaped optical spectrum to a temporal waveform with a good modulation depth, as shown in Fig. 3.29(b). A larger or smaller value of dispersion will lead to a poor modulation depth in the central part of the generated waveform, as shown in Fig. 3.29(a) and (c). The modulation depth degradation will become more serious if a much larger dispersion is applied, as illustrated in Fig. 3.29(d). This

may be explained by considering the interference effect of two optical pulses. It is known that a stable interference pattern with good interference visibility can be obtained only if the phase difference reaches π and the amplitudes of the two pulses are identical at certain time points. In the dispersion-induced frequency-to-time mapping system, the phase difference and the relative amplitude difference between two optical pulses depend not only on the time-delay difference τ_0, but also on the total dispersion experienced by the optical pulses. As a result, for a given τ_0, the above ideal interference conditions can be satisfied only at a certain value of dispersion.

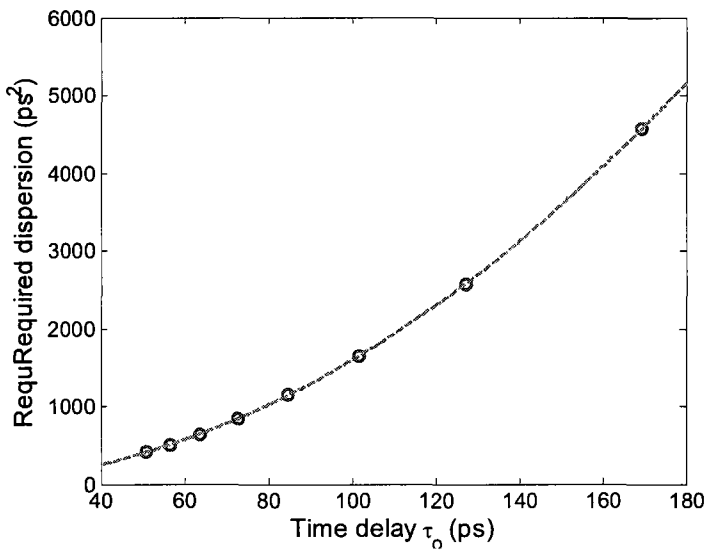

Fig. 3.30. Required second-order dispersion to generate a temporal waveform with an optimal modulation depth at different time delays. (Circle: simulation results, dashed line: quadratic fitting result).

Further simulations are performed to find the relationship between the time-delay difference τ_0 and the required second-order dispersion for realizing an optimal modulation depth. Fig. 3.30 shows the simulation results. A quadratic relationship between the second-order dispersion $\ddot{\Phi}$ and the time-delay difference τ_0 is found as follows:

$$\ddot{\Phi}(\tau_0) = 0.159\tau_0^2 + 0.026\tau_0 + 1.91 \qquad (3\text{-}34)$$

which gives us a good prediction for the selection of the required dispersion in designing a chirped microwave pulse generation system.

It is also worth pointing out that an approximate model is used to analyze the higher-order dispersion induced nonlinear frequency-to-time mapping. This approximate model is valid for dispersive element with moderate value of higher-order dispersion and is verified by both simulation and experimental results. A comprehensive study on the nonlinear frequency-to-time mapping in a dispersive element involving arbitrary high-order dispersion has been reported recently [149].

VII. *Conclusion*

A detailed theoretical and experimental study on the generation of chirped microwave pulse with tunable chirp rate based on optical spectral shaping and nonlinear frequency-to-time mapping was performed in this research work. In the system, the spectral shaping was implemented using a two-tap Sagnac loop filter with a uniform sinusoidal spectral response. The nonlinear frequency-to-time mapping was realized by applying the spectrum-shaped pulse to a NL-CFBG with both second- and third-order dispersion. The NL-CFBG was fabricated from a regular linearly chirped fiber Bragg grating using a simple beam-bending technique. By properly controlling the second- and third-order dispersion in the NL-CFBG, the chirped microwave pulse with required central frequency and chirp rate could be generated.

A detailed theoretical analysis to describe the generation of chirped millimeter-wave pulses was developed. The direct relationship between the dispersion and the frequency profile of the generated chirped pulse was revealed by an approximate model. An experiment was performed

to verify the proposed approach. Chirped microwave pulses with a central frequency of around 35 GHz and instantaneous frequency chirp rates of 0.053 and 0.074 GHz/ps were generated.

A major advantage of the proposed approach is that the frequency characteristics of the generated chirped microwave pulse could be easily tailored by adjusting the parameters of the system. The demonstrated approach offers a solution to the generation of high-frequency electrical pulse with large tunable chirp rate for applications in high-speed communications and modern radar systems.

3.1.3. FBG as a multifunctional device for both spectral shaping and frequency-to-time mapping

This section is a revised version of the following published paper.

Article title: Simultaneous optical spectral shaping and wavelength-to-time mapping for photonic microwave arbitrary waveform generation

Authors: Chao Wang, and Jianping Yao

Published in IEEE Photonics Technology Letters, vol.21, no. 12, pp. 793-795, Jun. 2009.

As we have presented in Section 3.1.1 and 3.1.2, several different FBG-based configurations to achieve optical spectral shaping and frequency-to-time mapping have been proposed and demonstrated. Since the optical spectral shaping and the frequency-to-time mapping are achieved using two separate devices, the system becomes complicated, costly and with high loss. Therefore, it is desirable to find a multifunctional fiber-optics device to achieve both spectral shaping and frequency-to-time mapping processes for photonic microwave arbitrary waveform

generation. The use of an LCFBG may provide a promising solution. First, we can arbitrarily control the spectral response of the LCFBG by properly designing the refractive index modulation profile. In addition, the inherent linear group delay response of the LCFBG can perfectly perform the dispersion-induced linear frequency-to-time mapping. In this section, photonic microwave arbitrary waveform generation using a single LCFBG to achieve both spectral shaping and frequency-to-time mapping is investigated.

I. *Introduction*

SS-FTM-based microwave arbitrary waveform generation has been successfully demonstrated in the optical domain using an optical spectral shaper followed by a frequency-to-time mapper. As shown in Fig. 3.2, by properly designing the spectral response of the optical spectral shaper, a microwave waveform with the shape identical to that of the shaped optical spectrum is obtained. In this research work, for the first time to the best of our knowledge, we propose an FBG-based all-fiber technique to implement microwave arbitrary waveform generation based on simultaneous optical spectral shaping and frequency-to-time mapping in a single LCFBG. The LCFBG is designed to have a magnitude response corresponding to the shape of the target microwave waveform for spectral shaping and a linear group delay response for frequency-to-time mapping. Compared with the previous photonic microwave arbitrary waveform generation systems in [26, 37, 39, 122], the presented system provides the advantages of smaller size and simplified structure. Moreover, the LCFBG can have a broad operation bandwidth, which is suitable for broadband optical pulse shaping. A simple and effective technique to synthesize the LCFBG with an arbitrary reflection spectral response based on an accurate mapping of the refractive index apodization to the grating reflection response is proposed. Since amplitude-only refractive index modulation is required, the designed LCFBG can be easily fabricated.

II. *System Configuration*

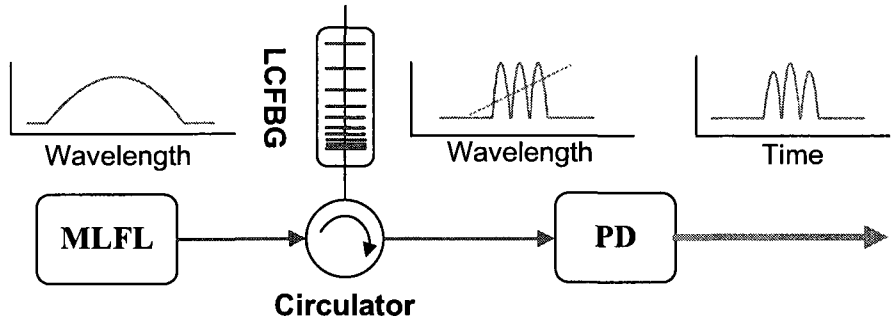

Fig. 3.31. Schematic diagram showing the proposed microwave arbitrary waveform generator using a single LCFBG. MLFL: mode-locked fiber laser, LCFBG: linearly chirped fiber Bragg grating, PD: photo detector.

A diagram showing the proposed photonic microwave arbitrary waveform generation system is illustrated in Fig. 3.31. A transform-limited ultrashort optical pulse from the MLFL is sent to a specially designed LCFBG working in the reflection mode. The LCFBG, which has a magnitude response corresponding to a scaled version of the target temporal waveform, is used to shape the power spectrum of the input optical pulse. At the same time, due to the inherent linear group delay response, the LCFBG also performs the dispersion-induced frequency-to-time mapping. A microwave waveform with its shape identical to that of a shaped optical power spectrum is then generated at the output of a high speed PD. Compared with the conventional microwave waveform generation system, as shown in Fig. 3.2, the proposed system is significantly simplified.

III. *LCFBG Design*

The key component in the proposed system is the LCFBG, which should be designed to have a magnitude as well as a phase response that can fulfill the requirements for both arbitrary spectral shaping and dispersion-induced frequency-to-time mapping. Thanks to the inherent linear group delay response, an LCFBG can always act as a linear frequency-to-time mapper.

Therefore, the focus of our work is to synthesize the grating refractive index modulation profile from the target grating magnitude response.

The grating synthesis problem is complicated, especially compared to the well-known direct problem of computing the reflection spectrum from a known grating structure. The simplest approach for solving grating synthesis problem was based on the first-order Born approximation where a Fourier transform relationship exists between the grating magnitude response and the refractive index modulation function [155], but it has limitations when used in the design of high-reflectivity gratings. Other numerical methods include the GLM inverse scattering algorithm [156] and the discrete layer peeling synthesis method [157]. However, these methods are only applied in the design of uniform-period or small chirped fiber gratings. In addition, these methods usually require the designed gratings to have both complex amplitude apodization and phase modulation profiles. Therefore, they are not suitable for practical design of strongly chirped FBG. In this research work, we present a simple and effective method to synthesize a highly-reflective and strongly chirped FBG with nearly arbitrary reflection magnitude response. Since amplitude-only index modulation is required, the designed LCFBG can be easily realized with the state-of-the-art FBG fabrication technology.

It was reported in [210] that when an LCFBG has a large dispersion, the grating apodization profile can be linearly mapped to its spectral response. Our recent study shows that the mapping relationship is unique, but not always linear, depending on the grating parameters such as the refractive index modulation coefficient, the grating chirp rate, and the bandwidth. The proposed LCFBG design technique is based upon an assumption that for an LCFBG with a large chirp coefficient C (in nm/cm), a unique mapping relationship exists between the reflection magnitude response and the refractive index modulation function.

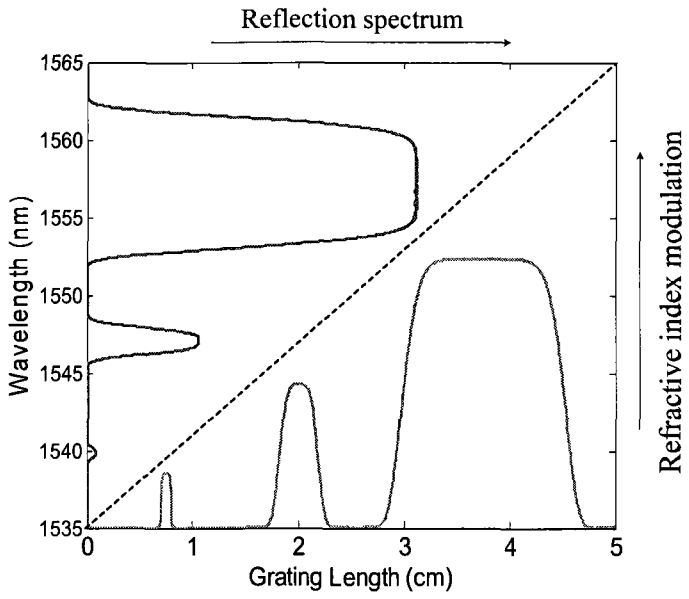

Fig. 3.32. Refractive index modulation and reflection spectrum for a strongly chirped fiber Bragg grating.

Fig. 3.32 shows the index modulation and magnitude reflection response relationship for a strongly chirped FBG (C=2.4 nm/cm), which is calculated by use of the piecewise-uniform matrix approach [154]. From Fig. 3.32 we can see that the reflectivity of each wavelength is determined mainly by the refractive index modulation in a very small corresponding local segment of the grating. Therefore, the index modulation function of a given LCFBG can be uniquely mapped to the grating reflection magnitude response. According to our simulation, the above assumption is always valid for an LCFBG with a chirp coefficient C>1 nm/cm [152].

Based on the above description of grating synthesis problem, we can first set up the mapping relationship between the refractive index modulation profile and the grating magnitude response by applying a linearly increasing index modulation function to a calibration grating with the use of a linearly chirped phase mask and then measuring the grating reflection response. A linearly increasing index modulation function is constructed, which is expressed as [152]

$$\Delta n_L(z) = \Delta n_{\max} \frac{z}{L} \exp\left(j \frac{2\pi z}{\Lambda_0} \right) \exp\left[-j \frac{2\pi C (z - L/2)^2}{\Lambda_0^2} \right] \tag{3-35}$$

where Λ_0 is the grating period at the center of the LCFBG, L is the total length of the LCFBG, and z is the lateral position along the grating ($0 \le z \le L$). By properly choosing the maximum index modulation coefficient $\Delta n_{\max}$, we can imprint the index modulation function in (3-35) into the calibration grating using a given linearly chirped phase mask with a known length and chirp coefficient. Then the reflection spectrum $R_{cali}(\lambda)$ of the fabricated calibration grating is measured. By uniformly dividing the grating into N short and consecutive segments with the positions z_i ($1 \le i \le N$), we can get the sampled reflection spectrum $R_{cali}(\lambda_i)$ thanks to the unique mapping relationship between $\Delta n_L(z_i)$ and $R_{cali}(\lambda_i)$. The number of segments N should be properly selected according to the achievable system resolution and the error tolerance.

For a target grating reflection spectrum $R_{target}(\lambda)$, we can compare it with the calibration grating response $R_{cali}(\lambda_i)$ wavelength by wavelength and then determine the desired index modulation function $\Delta n_D(z_i)$ by querying the linear index modulation function $\Delta n_L(z_i)$ segment by segment. Therefore, by applying the amplitude-only index modulation $\Delta n_D(z_i)$ under the same experimental condition, a desired LCFBG with the target reflection spectrum can be easily fabricated with the current FBG fabrication technology.

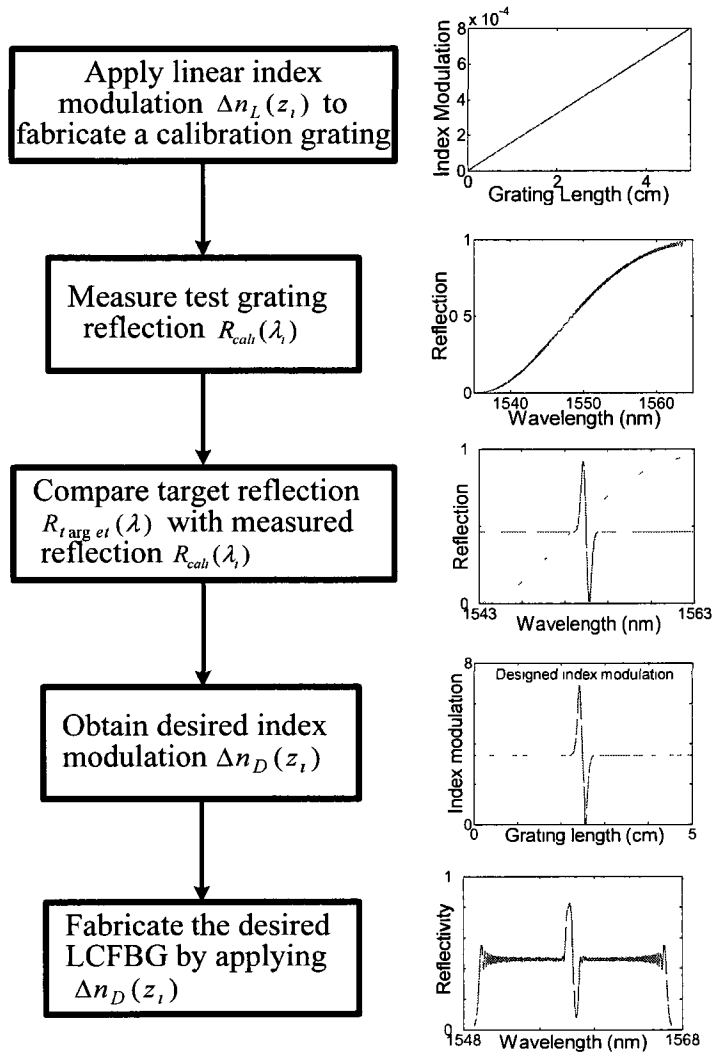

Fig. 3.33. Flow chart for the design and fabrication of an LCFBG with arbitrary magnitude response.

The LCFBG design and fabrication process can be described using the flow chart shown in Fig. 3.33. Simulation results for each design step are also plotted to numerically verify the proposed approach. In the simulation, the maximum index modulation of $\Delta n_{\max} = 0.0008$, grating chirp rate of $C = 2.4$ nm/cm, grating length of $L = 5$ cm, and the center grating period of Λ_0=535.96 nm are chosen. The designed LCFBG has a target reflection spectrum corresponding to a UWB monocycle pulse [124].

IV. *Experiment*

An experiment based on the setup shown in Fig. 3.31 is then carried out to verify the proposed approach. The MLFL is a commercial passive mode-locked fiber laser source that can generate an ultrashort pulse train with a repetition rate of 48.6 MHz, a pulsewidth of 550 fs, a 3-dB spectral bandwidth of 8 nm, and an average power of 5 dBm.

Two LCFBGs are first designed following the procedure shown in Fig. 3.33. The gratings are then fabricated by a frequency-doubled argon–ion laser operating at 244 nm using a linearly chirped phase mask. Due to the nonlinear response of the fiber to ultraviolet (UV) light, one needs to first measure the nonlinear response of the glass and then compensate the nonlinearity with a customized exposure function to produce the desired index modulation function. In fact, for a strong index modulation $\Delta n_{\max} \geq 0.0008$, the linear approximation of fiber response to UV energy is well satisfied [211].

The two fabricated gratings both have a length of 5 cm and a chirp rate of 2.4 nm/cm. To ensure high energy efficiency, the fabricated LCFBGs have a strong reflection as high as 98%. The center wavelength of the LCFBGs is 1558.1 nm, which is selected to match the center wavelength of the input optical pulse. The reflection spectra and the group delay responses of the fabricated LCFBGs are both shown in Fig. 3.34, which are measured using an optical vector analyzer (OVA, LUNA CTe) with a wavelength resolution of 1 pm.

The first LCFBG has a reflection spectrum corresponding to a chirped pulse waveform, as shown in Fig. 3.34(a), and the second LCFBG has a reflection spectrum corresponding to a UWB monocycle pulse, as shown in Fig. 3.34(b). It can be seen from Fig. 3.34 that, no matter what the index modulation is, the linear group delay responses are always maintained.

Therefore, the fabricated LCFBG can be also used to act as a frequency-to-time mapper to convert the shaped optical spectrum to the target temporal waveform.

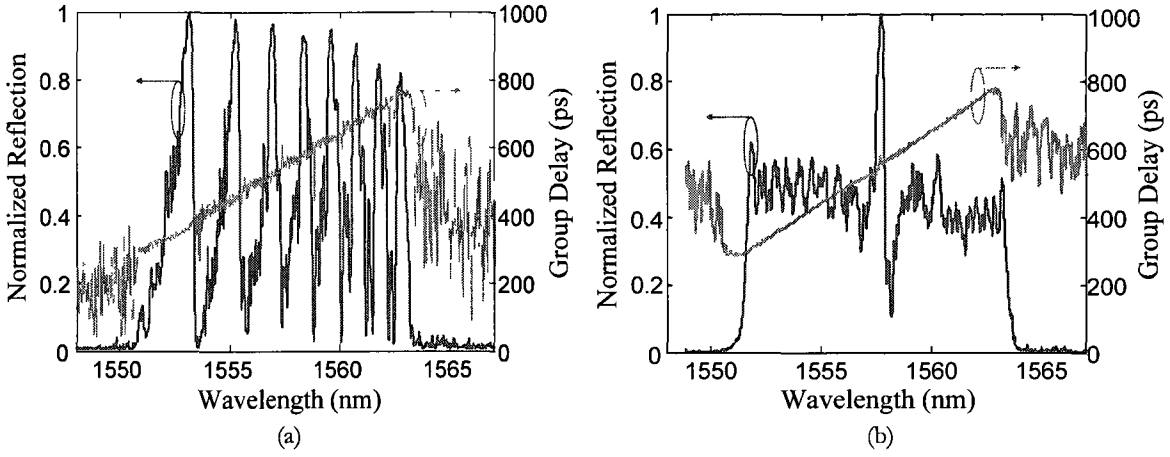

Fig. 3.34. Measured reflection spectra and group delay responses of the fabricated LCFBGs for (a) chirped microwave pulse generation and (b) UWB monocycle pulse generation.

The two LCFBGs are then incorporated, respectively, into the experimental system shown in Fig. 3.31, to generate the desired temporal waveforms. The generated waveforms are measured both in the frequency domain using the OVA and in the time domain using a 63-GHz sampling oscilloscope (OSC). Fig. 3.35(a) shows the shaped optical power spectrum by the first LCFBG. Thanks to the simultaneous frequency-to-time mapping in the LCFBG, a linearly chirped microwave pulse is generated and measured using a high-speed sampling oscilloscope, with the result shown in Fig. 3.35(b) (5 times averaging is performed). Fig. 3.35(c) shows the shaped optical spectrum by the second LCFBG. The generated temporal waveform, which is a UWB monocycle pulse with a pulse width of 90 ps, is shown in Fig. 3.35(d).

Note that the electrical spectrum of the generated UWB pulse doesn't fit the spectrum mask regulated by the US Federal Communications Commission (FCC) for indoor wireless communications. To generate a UWB pulse that meets the spectrum requirement regulated by

FCC, the monocycle pulse should have a pulsewidth of about 180 ps [124]. One solution to achieve the desired pulsewidth is to utilize an LCFBG with a larger dispersion (or equivalently a smaller chirp rate of 1.2 nm/cm). For practical applications, the optically generated UWB pulse train can be modulated by a binary sequence using an optical intensity modulator with ON–OFF keying (OOK) modulation.

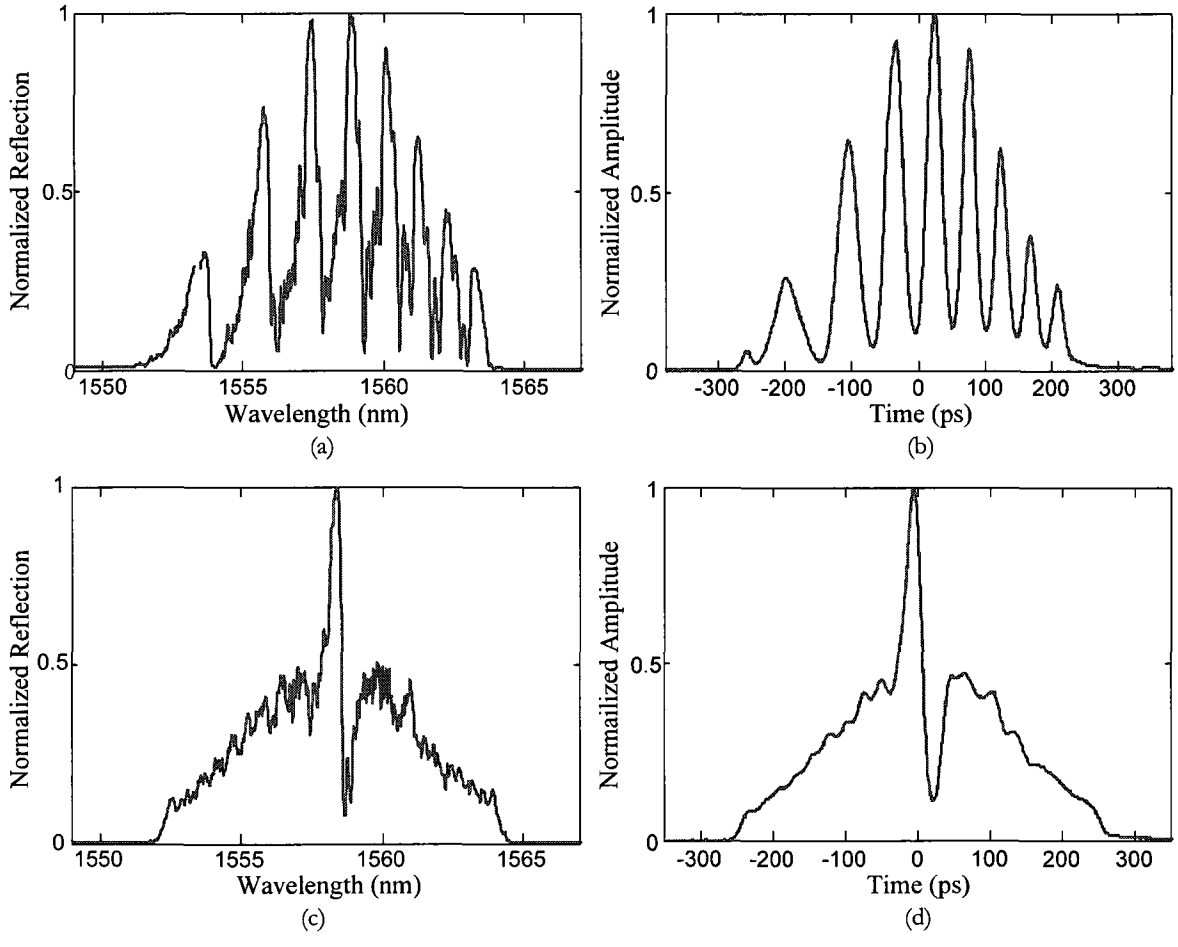

Fig. 3.35. Arbitrary waveform generation results. (a) Shaped spectrum by an LCFBG for chirped microwave pulse generation. (b) The generated chirped microwave pulse. (c) Shaped spectrum by a second LCFBG for UWB monocycle pulse generation. (d) The generated UWB monocycle pulse.

As can be seen from Fig. 3.35, the generated temporal waveform has almost an identical shape to the shaped optical spectrum, which verifies that the linear frequency-to-time mapping is

perfectly achieved by the LCFBGs. Note that the temporal waveform has a smoother trace compared to the optical spectrum, which is due to the limited bandwidth of the PD and OSC.

V. *Conclusion*

In this section, we have proposed and experimentally demonstrated a novel approach to achieving photonic microwave arbitrary waveform generation using a single specially designed LCFBG to simultaneously perform both the optical spectral shaping and the frequency-to-time mapping. A simple and efficient technique to design an LCFBG with an arbitrary magnitude response and a linear group delay response was proposed based on an accurate mapping of the grating magnitude response to the refractive index modulation function. Amplitude-only index modulation is required to produce the designed LCFBGs. Two LCFBGs were designed and fabricated. The use of the LCFBGs for the generation of a chirped microwave pulse and a UWB monocycle pulse was experimentally demonstrated. Compared with the systems in [37] and [39], the main limitation of the technique for practical applications is that the system is not reconfigurable. A potential solution to improve the reconfigurability is to use a strain-gradient beam tuning technique [132].

3.1.4. FBG as a multifunctional device for spectral shaping, frequency-to-time mapping and time shifting

This section is a revised version of the following published paper.

Article title: Large time-bandwidth product microwave arbitrary waveform generation using a spatially discrete chirped fiber Bragg grating

Authors: Chao Wang, and Jianping Yao

Published in IEEE/OSA Journal of Lightwave Technology, vol. 28, no. 11, pp.1652-1660, Jun. 2010.

In Section 3.1.3, a properly designed LCFBG with an arbitrary magnitude response and a linear group delay response has been proposed to achieve both the optical spectral shaping and the frequency-to-time mapping for photonic microwave arbitrary waveform generation. In fact, an LCFBG can provide not only linear but also discrete (jumped) group delay. In the latter case, discrete time shifts, which are caused by the jumped group delay, can be introduced to the mapped temporal waveform. Therefore, an additional flexibility is created for microwave arbitrary waveform generation. In this section, a spatially-discrete chirped fiber Bragg grating (SD-CFBG) with jumped group delay response is proposed. An approach using the SD-CFBG to achieve microwave arbitrary waveform generation based on optical pulse shaping is investigated. Compared to the LCFBG used in Section 3.1.3, the SD-CFBG provides one extra feature: the mapped temporal waveform can be further time shifted. A large TBWP arbitrary microwave waveform can be generated based on simultaneous spectral slicing, frequency-to-time mapping, and temporal shifting of the input optical pulse in the SD-CFBG.

I. *Introduction*

Microwave pulses with a large TBWP have been extensively employed in modern radar systems to improve the range resolution while maintaining a large detection distance [127]. To achieve a large TBWP, the transmitted microwave waveforms are usually frequency-chirped or phase coded. Photonically assisted techniques have been intensively investigated recently to

generate large TBWP microwave waveforms in the optical domain based on coherent optical pulse shaping.

For example, a phase-coded microwave pulse can be generated by beating two dispersed optical pulses in an unbalanced MZI with an optical phase modulator incorporated in one arm of the MZI structure [212]. The same concept can also be applied to the generation of a frequency-chirped microwave pulse [133, 183]. The linearly chirped microwave pulse is generated by beating two time-delayed chirped optical pulses at a PD, and the two time-delayed optical pulses are dispersed by two LCFBGs with different dispersion [183] or a single NL-CFBG [133]. A frequency-chirped microwave pulse can also be generated based on optical sinusoidal filtering of an ultrashort optical pulse followed by nonlinear frequency-to-time mapping [132, 201, 213]. The nonlinear frequency-to-time mapping is realized in a dispersive element with high-order dispersion. If a fiber-optic spectral filter with a varying FSR, which was termed a chirped FSR in [130], is used to perform spectral shaping, a dispersion device with only the second-order dispersion is required to generate a chirped microwave pulse based on linear frequency-to-time mapping [130-131]. More recently, an approach to generating a chirped microwave pulse using a photonic microwave delay-line filter with a quadratic phase response was reported [214]. By passing a broadband chirp-free microwave pulse through the microwave delay-line filter with a quadratic phase response, a chirped microwave pulse is generated. The photonic microwave delay-line filter with a quadratic phase response can be realized using a regular uniformly-spaced delay-line filter, but the tap coefficients should be complex-valued, making it hard to implement in the optical domain. A much simpler approach to achieving a quadratic phase response is to use a delay-line filter with nonuniformly spaced taps, in which the complex coefficients are equivalently generated by nonuniform time delays [214].

The photonically assisted phase-coded and frequency-chirped microwave pulse generation systems summarized above were implemented using multiple optical devices with each performing a different function; the systems were thus complicated, costly with high coupling losses. In this research work, we propose, for the first time to the best of our knowledge, a novel all-fiber technique to implement large TBWP arbitrary microwave waveform generation based on optical pulse shaping using an SD-CFBG. The SD-CFBG consists of multiple spatially separated sub-gratings that function to perform simultaneously spectral slicing, frequency-to-time mapping, and temporal shifting. When a broadband transform-limited optical pulse is sent to the SD-CFBG, which is operating in the reflection mode, the spectrum of the optical pulse is sliced, mapped to the time domain, and then temporally delayed, leading to the generation of an optical pulse burst with a custom-designed amplitude profile and time spacing. With the help of a bandwidth-limited PD, a smooth frequency-chirped or phase-coded microwave pulse is generated. The SD-CFBG is fabricated using a linearly chirped phase mask by axially shifting the fiber to introduce a spatial spacing between two adjacent sub-gratings during the fabrication process. By properly designing the fiber shifting function, a large TBWP microwave pulse with the desired frequency chirping or phase coding is generated.

Note that the generation of a custom-designed optical pulse burst from a single input optical pulse by using a multi-mirror interferometer has been reported in [215]. The similar architectures have been successfully applied for coherent arbitrary optical pulse shaping [68] and arbitrary microwave waveform generation based on incoherent optical pulse processing [38, 216]. The key limitation in the above systems is the complexity of the interferometer, such as a multi-stage Michelson interferometer used in [68] and a fiber Bragg grating sampling array used in [38]. Compared with the above optical pulse burst generation systems, the presented system

has a significantly simplified structure (only one single SD-CFBG is used for optical pulse burst generation), which features smaller size, lower loss, better stability and higher potential for integration.

II. *Principle*

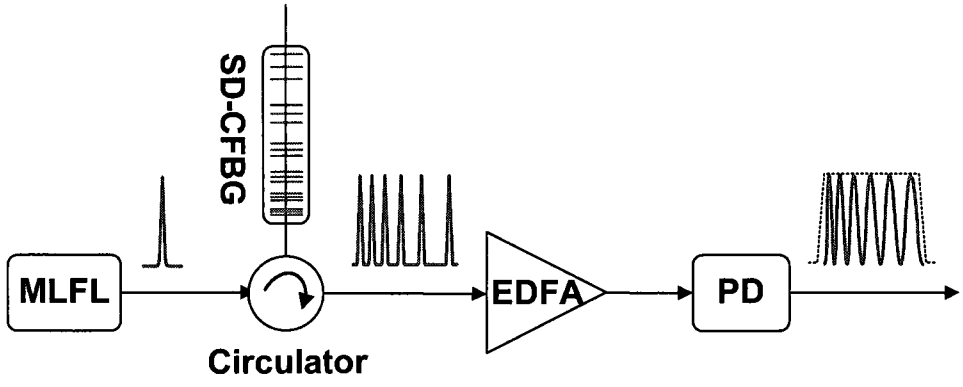

Fig. 3.36. A large TBWP microwave pulse generator using an SD-CFBG. MLFL: mode-locked fiber laser, SD-CFBG: spatially discrete chirped fiber Bragg grating, EDFA: Erbium-doped fiber amplifier, PD: photodetector.

The proposed large TBWP microwave pulse generation system using an SD-CFBG is shown in Fig. 3.36. A broadband ultrashort optical pulse from the MLFL is sent to the SD-CFBG, which is working in the reflection mode. Thanks to the simultaneous spectral slicing, frequency-to-time mapping and temporal shifting performed by the SD-CFBG, an optical pulse burst with the desired time spacing is generated from the single input optical pulse. With the help of a bandwidth-limited PD, a smooth frequency-chirped or phase-coded microwave pulse is generated thanks to the equivalent low-pass filtering process at the PD. By properly controlling the time spacing between the individual seed pulses, arbitrary large TBWP microwave pulses with the desired frequency chirping or phase coding can be generated.

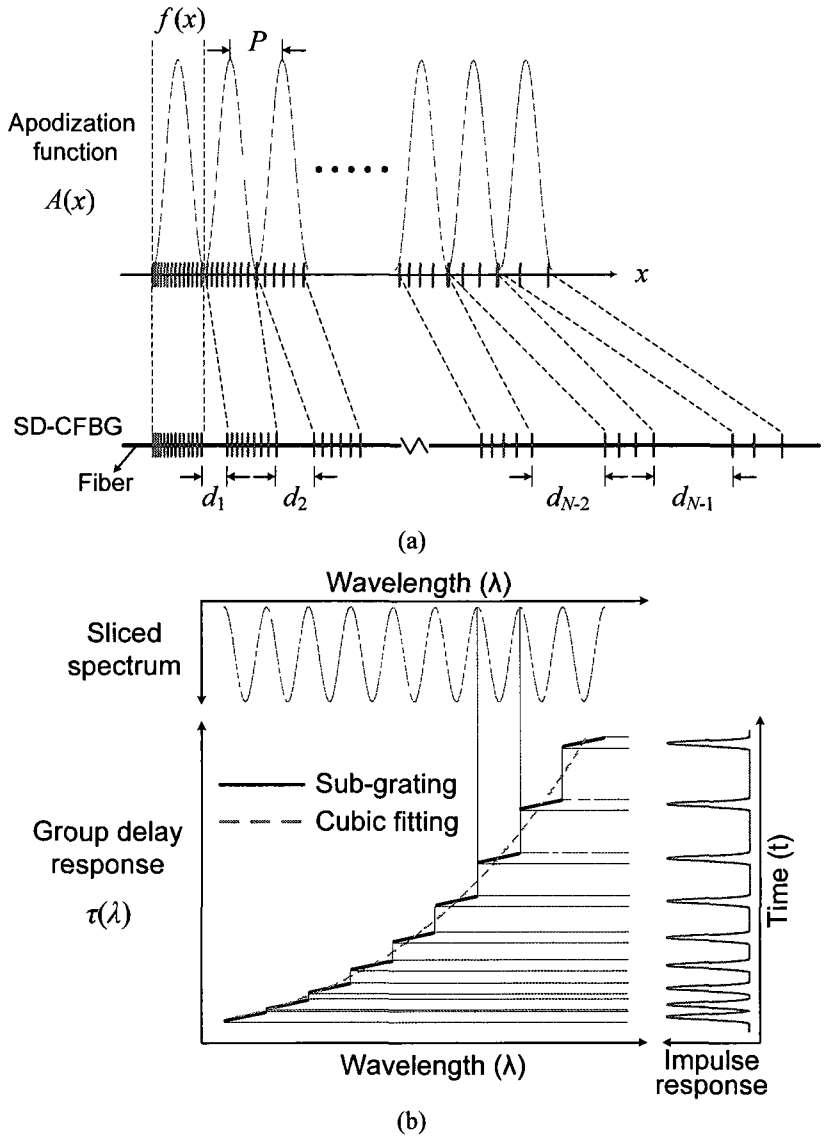

Fig. 3.37. Illustration of the design and fabrication of an SD-CFBG. (a) An SD-CFBG implemented based on axial fiber shifting during the fabrication process. (b) The group delay response and the impulse response of the produced SD-CFBG.

The key device in the proposed microwave pulse generation system is the SD-CFBG. A diagram showing the principle of the proposed SD-CFBG is illustrated in Fig. 3.37(a). The SD-CFBG is produced by first dividing a linearly chirped refractive index modulation function that is continuous and periodic along the fiber axial direction into N seed modulation functions that have identical length and identical index apodization profile, and then imprinting these N seed

index apodization functions into N spatially separated sub-gratings with a properly designed separation function to achieve the required group delay response for the SD-CFBG. The sub-grating separation function is implemented by axially shifting the photon-sensitive fiber to introduce a spatial spacing between two adjacent sub-gratings during the grating fabrication process.

To produce the SD-CFBG, as shown in Fig. 3.37(a), a linearly chirped refractive index modulation function is first constructed, which is continuous along the fiber axial direction and is expressed as

$$\Delta n(x) = \Delta n_{\max} A(x) \exp\left(-j\frac{\pi C}{\Lambda_0^2}x^2\right) \times \exp\left(j\frac{2\pi}{\Lambda_0}x\right), \quad 0 \le x \le L \tag{3-36}$$

where $\Delta n_{\max}$ is the maximum refractive index modulation, Λ_0 is the fundamental period of the grating and C (nm/mm) is the chirp rate of the produced grating. Here we consider that the refractive index modulation occurs over a length of L. $A(x)$ describes the normalized index apodization function, which is continuous and periodic with a constant period of P,

$$A(x) = \sum_{k=0}^{N-1} f(x - kP) \tag{3-37}$$

where $f(x)$ is the seed index apodization function, i.e., a Gaussian function, within one period of the apodization function, as illustrated in Fig. 3.37(a). It is known that when a linearly chirped FBG has a high enough dispersion, its index apodization profile can be mapped to the grating reflection spectral response thanks to the space-to-frequency mapping relationship in a weak LCFBG [210]. Therefore, a spectral comb filter can be obtained due to the periodic index

apodization function $A(x)$ introduced to the SD-CFBG. The obtained comb filter can be used to slice the spectrum of the input ultrashort optical pulse.

The continuous linearly chirped index modulation function in (3-36) is then imprinted into a photosensitive fiber through UV illumination using a linearly chirped phase mask. During the grating fabrication, the fiber is axially shifted with a small offset of d_k ($k = 1, 2, \ldots, N\text{-}1$, where N is the number of the sub-gratings) after the kth sub-grating is written with the index apodization function $f(x - kP)$. Therefore, an SD-CFBG consisting of N spatially separate sub-gratings is obtained, as shown in Fig. 3.37(a).

The group delay response of the SD-CFBG can then be expressed as

$$\tau(\Delta\lambda) = \frac{\Delta\lambda}{C} \times \frac{2n_{eff}}{c} + \sum_{k=1}^{M} d_k \times \frac{2n_{eff}}{c} \tag{3-38}$$

where $\Delta\lambda$ denotes the wavelength offset from the starting wavelength, n_{eff} is the effective mode index of the fiber core, c is the light speed in vacuum, and M is the number of the involved fiber shifts within the bandwidth of $\Delta\lambda$. The first term in (3-38) is the original linear group delay contributed by the linear phase mask, and the second term represents the user-defined group delay response introduced by the fiber shifting. Therefore, the entire group delay response of the produced SD-CFBG is discontinuous with N linear segments and $N-1$ jumps. The bandwidth of each linear segment is given by $\delta\lambda = C \times P$. The height of the kth jump is determined by the corresponding spacing d_k. The selection of the heights of the jumps provides the flexibility to design an SD-CFBG with an arbitrary discrete group delay response. For example, if the fiber shifting function d_k is increasing quadratically, a fitted group delay

response that is a cubic function of wavelength can be achieved, which is shown as the dashed line in Fig. 3.37(b).

When a broadband transform-limited (chirp-free) optical pulse is sent to the SD-CFBG, which is operating in the reflection mode, the spectrum of the optical pulse is first sliced due to the multiple sub-grating responses, as shown in Fig. 3.37(b). The linear group delay response within each sub-grating channel is then used to perform the dispersion-induced frequency-to-time mapping, which leads to the generation of a comb temporal waveform. Finally, the mapped comb waveform is temporally delayed due to the user-defined group delay jumps in the SD-CFBG, resulting in an optical pulse burst with the desired time spacing between individual seed pulses. Therefore, thanks to the simultaneous spectral slicing, frequency-to-time mapping and temporal shifting by the single SD-CFBG, an optical pulse burst consisting of N seed pulses with the pulse spacing determined by the fiber shifting function d_k is generated from a single input optical pulse.

It is important to note that even though the frequency-to-time mapping is a coherent process, the proposed microwave pulse generation system is still operating in the incoherent scheme. The word 'incoherent' refers to the fact that only the amplitude (not the phase) of the generated optical pulse burst is involved in the pulse shifting and combining process. This is because each seed optical pulse comes from different frequency component of the input broadband optical pulse. There is no interference between different seed pulses. Thus only the intensity of the pulse burst is considered in our theoretical treatment. Mathematically, the output optical pulse burst is expressed as

$$r(t) = w(t) \times \left\{ s_0(t) + \sum_{k=1}^{N-1} s_0 \left[t - \left(kP + \sum_{1}^{k} d_k \right) \frac{2n_{eff}}{c} \right] \right\} \tag{3-39}$$

where $s_0(t)$ is the seed pulse, which is obtained according to the space-to-frequency-to-time mapping in the SD-CFBG [210],

$$s_0(t) \propto g(t) * \left[f(x) \right]_{x=C/(2n_{eff}) \times t} \tag{3-40}$$

where $g(t)$ is the temporal envelope of the input transform-limited optical pulse. As shown in (3-40), the seed pulse $s_0(t)$ is determined by the input optical pulse $g(t)$, the seed index apodization function $f(x)$, and the grating chirp rate C. Note that the generated optical pulse burst is modulated by a slowly varying envelope $w(t)$, which is determined by the input optical spectrum due to the dispersion-induced frequency-to-time mapping. Since the nonlinear group delay response is applied according to (3-38), even though the input optical pulse has a symmetric spectrum, the envelope function $w(t)$ is usually asymmetric due to the pulse shape change by high-order dispersion [191]. This may also be interpreted as the sampled nonlinear frequency-to-time mapping, relative to the continuous nonlinear frequency-to-time mapping [132], where continuous nonlinear group delay response is applied. The generated optical pulse burst $r(t)$ is then amplified and directed to a high-speed PD for incoherent detection. A properly shaped microwave waveform is obtained at the output of the PD. Since the PD has a limited bandwidth, the smooth microwave form is resulted [8, 38, 216].

The instantaneous frequency of the generated microwave pulse is inversely proportional to the seed pulse spacing. The sampled instantaneous microwave frequency f_k, which is determined by both the index apodization period P and the sub-grating spacing d_k, can be expressed as

$$f_k = \frac{1}{P + d_k} \times \frac{c}{2n_{eff}} \tag{3-41}$$

where P determines the initial instantaneous microwave frequency (the frequency offset) and d_k controls the frequency chirping profile. Thus we can conclude that by properly selecting the period of the index apodization function and designing the fiber shifting function, a large TBWP microwave waveform with the desired frequency chirping or phase coding can be generated.

III. *Experiment*

In this section, several examples to show the generation of different types of chirped microwave pulses using the proposed technique are experimentally demonstrated. We also show that the proposed system can be easily adapted to realize phase-coded microwave pulse generation. Chirped and phase-coded microwave pulses have been widely applied for many important scientific and industrial applications, such as in modern radar systems to increase the range resolution and in broadband communications systems to increase the signal-to-noise ratio (SNR).

In our demonstrations, a periodic index apodization function $A(x)$ with a constant period of P and a seed apodization function $f(x)$ with a Gaussian profile are always applied. The desired frequency chirping is then achieved by properly controlling the fiber shifting function d_k.

In the first example, we demonstrate the generation of a linearly frequency modulated (LFM) or linearly chirped microwave pulse, which is the first and still the most commonly used microwave waveform in modern radar systems due to the generation simplicity [217]. Photonic generation of linearly chirped microwave pulses has been intensively investigated and many different techniques have been proposed. In our proposed system, to generate a linearly chirped microwave pulse, according to (3-39), a linearly increasing shifting function d_k is required.

The key device in the large TBWP microwave pulse generation system is the SD-CFBG. In our experiment, the SD-CFBG is fabricated in a hydrogen-loaded single-mode fiber by a frequency-doubled argon-ion laser (Coherent FreD 300C) operating at 244 nm using a 50-mm long linearly chirped phase-mask with a chirp rate of $C = 0.24$ nm/mm. The refractive index modulation has a maximum index change of $\Delta n_{\max} = 3.5 \times 10^{-4}$. A strong reflection (the maximum reflectivity is around 90%) is achieved to ensure a high energetic efficiency. The produced grating has a center wavelength of 1558.3 nm, which is again selected to match the center wavelength of the input transform-limited optical pulse. The desired linear fiber shifting is accurately performed during the grating fabrication process by a computer-controlled high-precision translation stage that has a resolution of 1 μm. In the demonstration, the index apodization period is set at $P = 2.78$ mm and the fiber shifting function d_k is selected to be linearly increasing from 0.1 to 2.6 mm, which would lead to the generation of a linearly chirped microwave pulse with 19 cycles.

The group delay response of the fabricated SD-CFBG is first measured using an OVA (LUNA Technologies), with the result shown in Fig. 3.38. It can be seen that a nonlinear (quadratic) group delay response is obtained, which matches well with the theoretical prediction given by

(3-38). A quadratic curve fitting result is also plotted in dashed line. The measured group delay response contains 18 jumps, which, however, are not clearly visible due to the very narrow bandwidth of each segment. One may notice that some group delay peaks are also observed, which are generated from the reflection spectral notches caused by the optical resonance between two adjacent sub-gratings in the SD-CFBG. Due to the very low power at the spectral notches, the group delay response cannot be accurately measured at these notch wavelengths. In fact, such group delay peaks have no impact on the time-domain optical pulse shaping due to the incoherent feature of the system. This issue will be further discussed later.

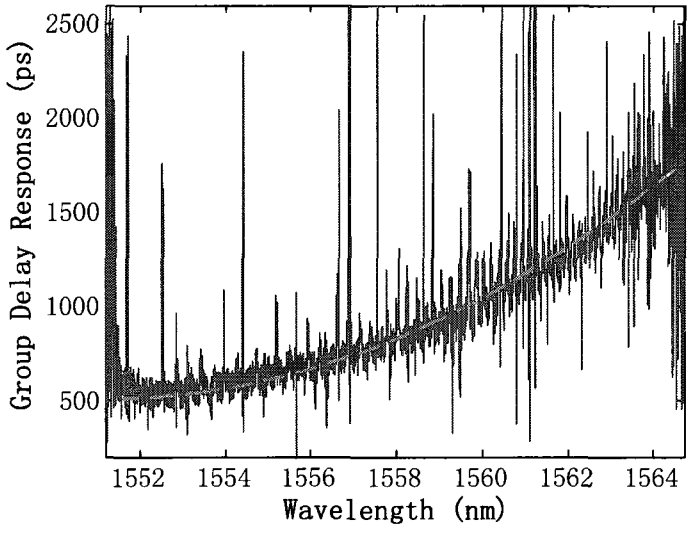

Fig. 3.38. Experiment result: the measured group delay response of the fabricated SD-CFBG for linearly chirped microwave pulse generation. The dashed line shows the quadratic fitting result.

The fabricated SD-CFBG is then incorporated into the experimental system shown in Fig. 3.36, to generate the linearly chirped microwave pulse. In the experiment, the broadband ultrashort optical pulse from the MLFL is first sent to the fabricated SD-CFBG, which is working in the reflection mode. The SD-CFBG is functioning to slice the spectrum of the input optical pulse, to implement frequency-to-time mapping, and to temporally shift the mapped optical seed pulses. A PD with a bandwidth of 45 GHz is used to perform the optical to electrical conversion. Due

to the limited bandwidth of the PD, a smooth microwave pulse would be generated. The generated microwave waveform is measured in the time domain using a 53-GHz-bandwidth digital sampling oscilloscope (Agilent 86100C). A broadband DC block is also used to eliminate the dc component in the generated microwave pulse. The measured result is shown in Fig. 3.39 (5 times averaging is performed). As can be seen, a chirped microwave waveform is generated. The instantaneous frequency of the generated microwave pulse is also plotted in Fig. 3.39 in circles, which is obtained by calculating the reciprocal of the seed pulse spacing. A linear curve fitting for the measured instantaneous frequency is also performed, which is shown in Fig. 3.39 as dashed line. It is shown that a linearly chirped microwave pulse is generated. The instantaneous frequency is linearly decreasing from 38 to 17 GHz within the main pulse lobe, with an equivalent frequency chirp rate of 26.25 GHz/ns. According to the experimental results, a TBWP of 16.8 is achieved for the generated linearly chirped microwave pulse.

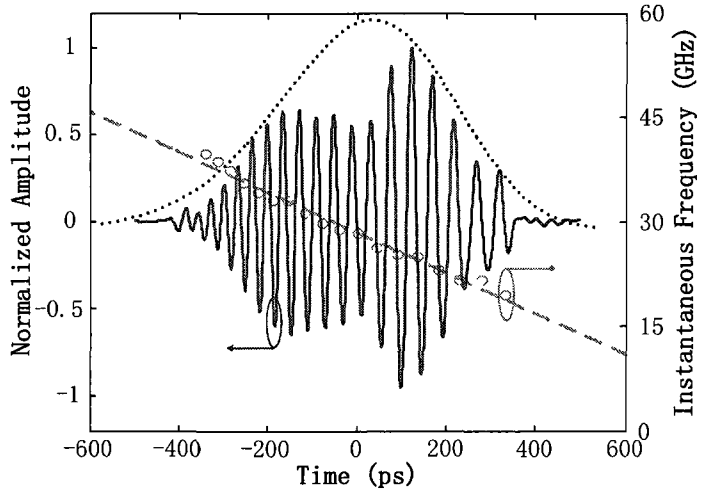

Fig. 3.39. Experimental result: the generated linearly chirped microwave pulse (solid line) and the instantaneous frequency (circle line). Dashed line: linear curve fitting of the instantaneous frequency. Dotted line: the calculated pulse envelope.

Given the quadratic group delay response in (3-38), the waveform envelope $w(t)$ is also numerically calculated by using the Fourier transform method [191], with the result plotted in Fig. 3.39 as dotted line. Note that the generated pulse envelope does not exactly fit the simulated profile, which is mainly due to the non-ideal (non-flat) spectral response of the SD-CFBG.

In a radar system, a chirped or phase-coded microwave pulse is usually compressed through matched filtering or autocorrelation at the radar receiver end. Fig. 3.40 shows the calculated correlation between the generated linearly chirped microwave pulse and the ideal reference pulse. The autocorrelation peak has a FWHM of 60 ps. Considering the FWHM of the generated chirped microwave pulse is 795 ps as shown in Fig. 3.39, a pulse compression ratio of 13.2 is achieved. It is also shown in Fig. 3.40 that a peak-to-sidelobe ratio (PSR) of 7.7 is realized.

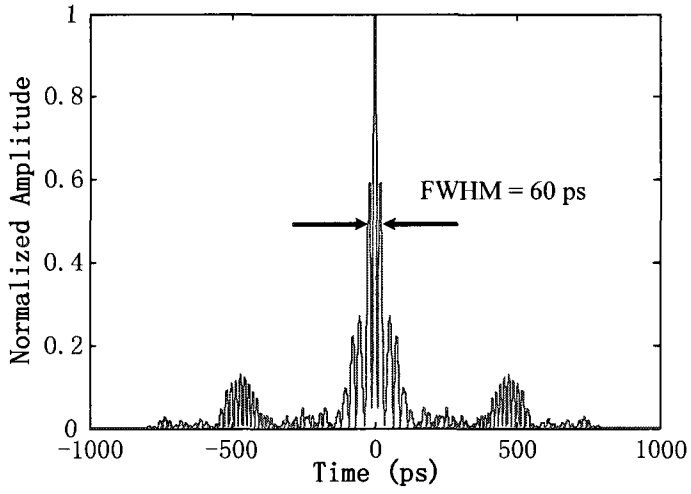

Fig. 3.40. Calculated autocorrelation of the generated linearly chirped microwave pulse.

It is worth noting that a linear frequency chirping is not always the only frequency modulation scheme in a microwave radar system. In fact, the frequency chirping can be of any form,

provided that the matched filter in the receiver end is designed to match the chirped microwave pulse. The presented approach can also be used to generate other types of chirped microwave waveforms, such as nonlinearly chirped and step-chirped microwave pulses by properly designing the fiber shifting function d_k. These waveforms can also find wide applications in modern radar systems [217].

In the second example, nonlinear chirped microwave pulse generation is investigated. Although linearly chirped microwave pulses are widely used in pulsed radar systems thanks to the generation simplicity, the autocorrelation of a linearly chirped microwave pulse at a radar receiver usually has relatively high sidelobes which are not expected, especially in an environment with multiple targets and clutter. This problem can be alleviated by using microwave pulses with nonlinear frequency chirping [217].

To generate a nonlinearly chirped microwave pulse, i.e., with quadratic frequency chirping, using the proposed approach, a quadratic fiber shifting function d_k is required according to (3-41). In the second example, the index apodization period is set at $P = 2.63$ mm and the fiber shifting function d_k is selected to be quadratically increasing from 0.1 to 4.5 mm, which would lead to the generation of a nonlinearly (quadratically) chirped microwave pulse with 20 cycles.

A second SD-CFBG is fabricated using the same linearly chirped phase mask. The group delay response of the fabricated grating is measured and shown in Fig. 3.41. A nonlinear (cubic) group delay response containing 19 jumps is obtained, which agrees well with the theoretical prediction given by (3-38). The cubic fitting curve is also plotted in dashed line.

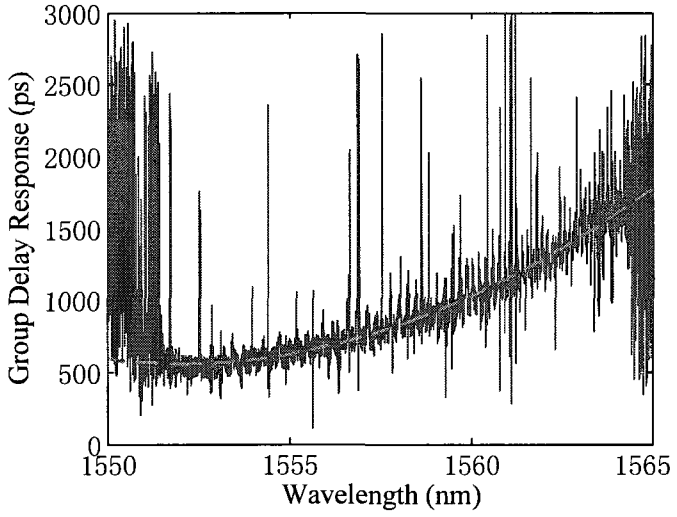

Fig. 3.41. Experiment result: the measured group delay response of the fabricated SD-CFBG for nonlinearly chirped microwave pulse generation. The dashed line shows the cubic curve fitting result.

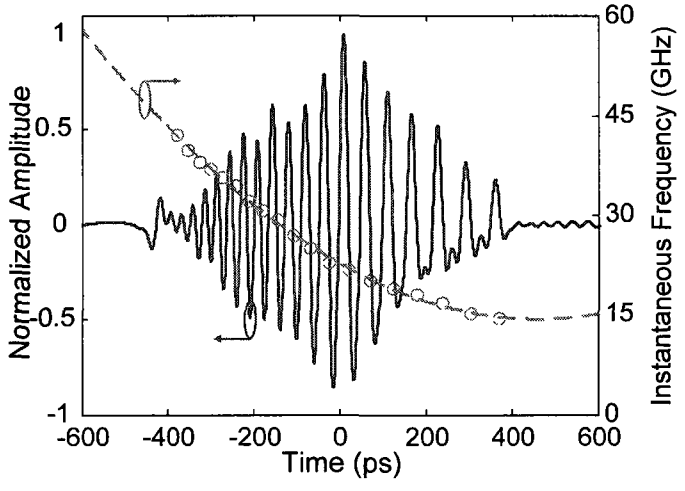

Fig. 3.42. Experimental result: the generated nonlinearly chirped microwave pulse (solid line) and the instantaneous frequency (circle line). Dashed line: quadratic curve fitting of the instantaneous frequency.

Fig. 3.42 shows the generated nonlinearly chirped microwave pulse by use of the second SD-CFBG. The instantaneous frequency of the generated microwave pulse is also shown in circles in Fig. 3.42, with the quadratic fitting result shown as the dashed line. As can be seen a nonlinearly chirped microwave pulse with an FWHM of 808 ps is generated. The instantaneous frequency is quadratically decreasing from 43 to 14 GHz. The chirp rate of the generated

microwave pulse is decreasing from 93.6 to 11.2 GHz/ns. The TBWP of the generated microwave pulse is calculated to be 23.2.

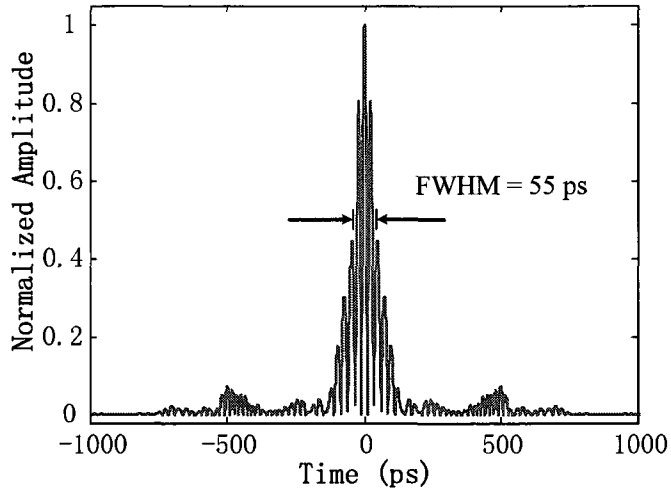

Fig. 3.43. Calculated autocorrelation of the generated nonlinearly chirped microwave pulse.

Fig. 3.43 shows the calculated autocorrelation of the generated nonlinearly chirped microwave pulse with its reference. The autocorrelation peak has an FWHM of 55 ps. Considering the FWHM of the generated chirped microwave pulse is 808 ps, as shown in Fig. 3.42, a pulse compression ratio of 14.7 is obtained. It is also shown in Fig. 3.43 that the achieved PSR is 14.3, which is much higher than that when a linearly chirped microwave pulse is employed in the first example. The sidelobe level can be further suppressed by finely controlling the envelope of the generated microwave pulse.

In the third example, we apply the proposed approach to generate step-chirped microwave pulse. Stepped frequency modulation or microwave frequency-hopping technique has been widely used in radar systems and wireless communications systems due to the advantages of high resistance to narrowband interference, low probability of interception and coexistence with other communications schemes.

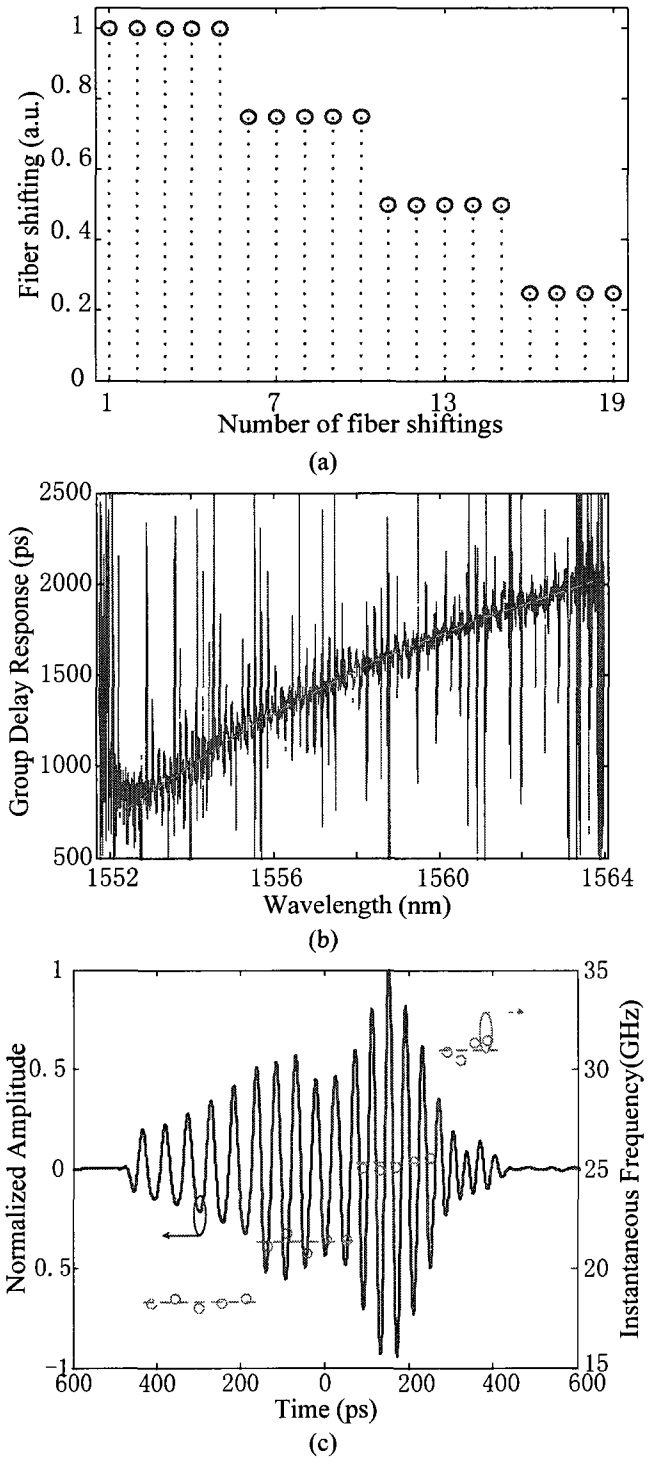

Fig. 3.44. Step-chirped microwave pulse generation. (a) The designed fiber shifting function. (b) The measured group delay response of the fabricated SD-CFBG. (c) The generated step-chirped microwave pulse (solid line) and the instantaneous frequency (circle line). Dashed line: discrete linear fitting of the instantaneous frequency.

To generate a step-chirped microwave pulse, the fiber shifting function d_k should be a step function. Same as the second example, the index apodization period is set at $P = 2.63$ mm to generate a microwave pulse with 20 cycles. A four-level stepped fiber shifting function ($d_k = 0.7$, 1.4, 2.1 and 2.8 mm) is designed, as shown in Fig. 3.44(a), which would lead to the generation of a step-chirped microwave pulse with four different carrier frequencies. An SD-CFBG is then fabricated with the designed fiber shifting function that is implemented by shifting the fiber with four different d_k during the grating fabrication process. Fig. 3.44(b) shows the measured group delay response of the fabricated SD-CFBG. As expected, the entire group delay response consists of four discrete linear group delay responses with four different slopes. The fabricated SD-CFBG is then incorporated in the microwave pulse generation system shown in Fig. 3.36. Again, thanks to the simultaneous spectral slicing, frequency-to-time mapping and temporal shifting in the SD-CFBG, a step-chirped microwave pulse with four carrier frequencies at 18, 21.8, 25.6 and 31 GHz and three frequency jumps within the main pulse lobe is obtained at the output of the PD, as shown in Fig. 3.44(c).

Phase coding is another technique to increase the signal TBWP. Phase-coded microwave pulses have been widely adopted in radar and code division multiple access (CDMA) systems [48]. The proposed technique can be easily adapted for phase-coded microwave pulse generation.

According to (3-39), the reflected signal from the SD-CFBG is an optical pulse burst with the pulse spacing determined by the fiber shifting function. If the fiber shifting function has uniform spacing, i.e., d_k is a constant for different k, then an optical pulse burst with identical temporal spacing is resulted. To implement phase modulation, a simple solution is to use a fiber shifting function with non-uniform spacing. It was demonstrated recently by Dai and Yao that

arbitrary phase modulation can be implemented based on pulse position modulation [216]. If a fiber shifting function is properly designed, the position of the seed pulses is modulated. With the help a microwave bandpass filter, a phase-coded microwave waveform would be generated from the pulse-position-modulated optical pulse burst [216].

IV. *Discussion*

In the proposed optical pulse shaping system, an optical pulse burst is generated from a single input optical pulse thanks to the simultaneous spectral slicing, frequency-to-time mapping and temporal shifting by a single SD-CFBG. By controlling the temporal pulse spacing, the generation of an arbitrary large TBWP microwave pulse with different types of frequency chirping has been demonstrated. In addition to the generation of chirped or phase-coded microwave waveforms, the proposed technique can also be used to generate other microwave waveforms. For example, an arbitrary microwave waveform can be synthesized by incoherently superposing a set of seed optical pulses with the proper temporal spacing. This concept has been proved for coherent arbitrary optical pulse shaping [68]. Compared with the approach in [68], the proposed photonic microwave waveform generation system has the key advantage that the pulse shaping process is incoherent, making the process insensitive to the environmental fluctuations. In addition, the ability in performing individual amplitude modulation of each seed optical pulse can also be achieved by controlling the seed index apodization function $f_k(x)$, which would provide an additional flexibility in microwave arbitrary waveform generation.

In order to convert a specific optical pulse burst into a smooth microwave waveform, a bandwidth-limited PD is employed, which functions equivalently as a low-pass filter. In addition, a broadband DC block is also used to eliminate the baseband component in the

generated chirped microwave pulse. In fact, this is equivalent to using a microwave bandpass filter to select the spectral channel of interest from a multichannel spectral response of a pulse-position-modulated pulse burst, as was first reported in [216]. To perform optical pulse shaping and microwave bandpass filtering in an all-optical fashion, the microwave bandpass filter can be a photonic microwave delay-line filter implemented in the optical domain [4].

In the measured group delay responses of the fabricated SD-CFBGs, as shown in Figs. 3.38, 3.41 and 3.44(b), some group delay peaks are observed. These group delay peaks are measurement errors due to the very low power at the reflection spectral notches [130]. The spectral notches are caused by optical resonance between adjacent sub-gratings in the SD-CFBG. In our proposed SD-CFBG design, two adjacent sub-gratings spatially separated along the fiber form a multi-cavity Fabry-Perot resonator. Ideally, if the sub-gratings have completely separate (no overlapping) spectral responses, no optical resonance would be generated, and a clean comb filter response with a smooth group delay response will be obtained, as illustrated in Fig. 3.37(b). In practice, however, the spectral crosstalk between the adjacent channels will lead to obvious optical resonance.

The reflection spectral response and the group delay response of the SD-CFBG used for nonlinearly chirped microwave pulse generation are measured, which are shown in Fig. 3.45. A strong optical resonance is observed in the reflection spectrum. It can be seen that the group delay peaks are all resulted from the spectral notches. A smaller FSR is observed for a longer wavelength, where a longer cavity length (longer fiber shifting) is set. It is important to note that the group delay peaks due to the optical resonance have negligible impact on the time-domain optical pulse shaping because the optical power reflected from these resonance notches is

negligible. There is no interference between the adjacent seed pulses in the incoherent scheme. This has been verified by the experimental results, as shown in Figs. 3.39, 3.42 and 3.44(c).

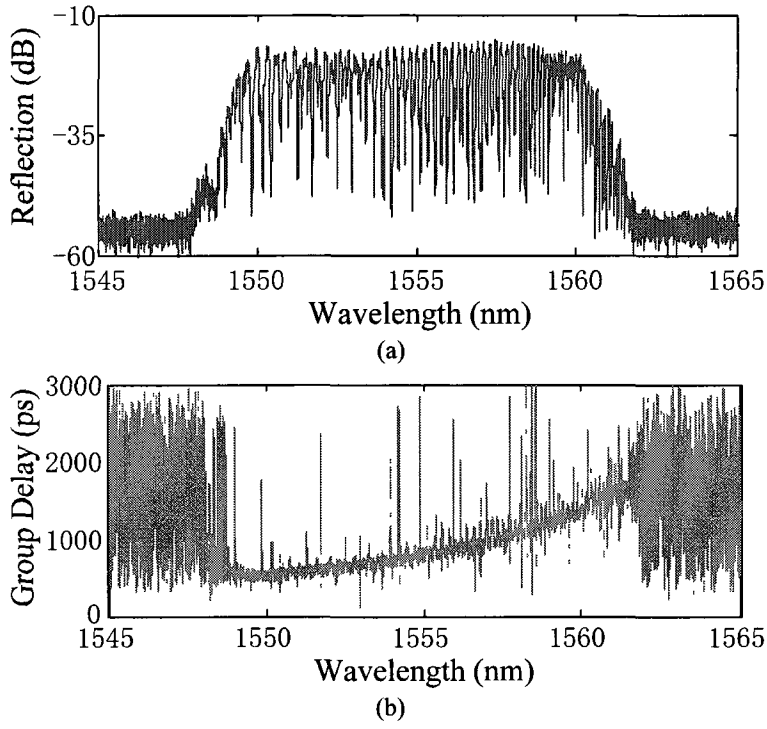

Fig. 3.45. (a) Measured reflection spectral response and (b) the group delay response of the fabricated SD-CFBG for nonlinearly microwave pulse generation.

3.2 Photonic microwave arbitrary waveform generation based on Fourier-transform optical pulse shaping

As shown in Fig. 3.1, photonic microwave arbitrary waveform generation is usually implemented based on optical pulse shaping. Fourier synthesis, also called Fourier-transform pulse shaping, is one of the most commonly used techniques for ultrashort optical pulse shaping [42]. In this Section, photonic microwave arbitrary waveform generation based on Fourier-transform optical pulse shaping is investigated. Fourier-transform optical pulse shaping can be implemented in either the time domain or the frequency domain. Photonic microwave arbitrary

waveform generation based on the time-domain Fourier-transform pulse shaping is first discussed in Section 3.2.1. Then we study the frequency-domain Fourier-transform pulse shaping for photonic microwave arbitrary waveform generation in Section 3.2.2.

3.2.1. Time-domain Fourier-transform pulse shaping for microwave arbitrary waveform generation

Time-domain Fourier-transform optical pulse shaping is first investigated, which is also known as temporal pulse shaping (TPS). A microwave arbitrary waveform can be generated in the time domain using a TPS system. In this section, the principle of a typical balanced TPS system is first described. Photonic generation of a high-frequency microwave waveform by use of an unbalanced TPS system is then studied.

3.2.1.1. Typical balanced temporal pulse shaping system

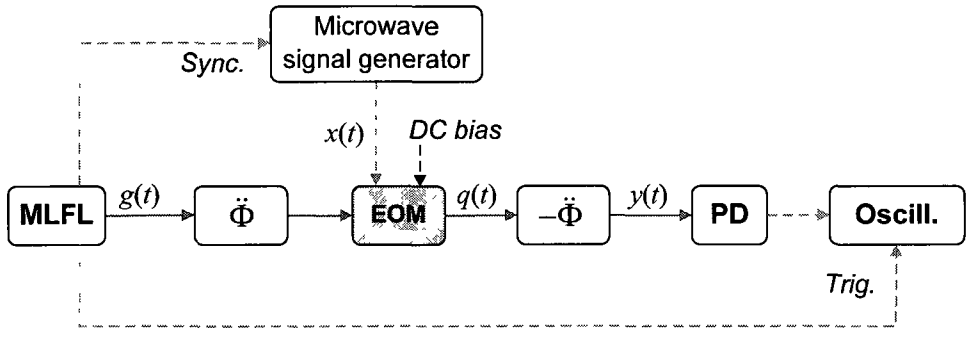

Fig. 3.46. Schematic diagram of a typical temporal pulse shaping system for microwave arbitrary waveform generation. MLFL: mode-locked fiber laser; EOM: electro-optic modulator; PD: photodetector.

The schematic diagram of a typical balanced TPS system for microwave arbitrary waveform generation is shown in Fig. 3.46. The typical TPS system consists of two conjugate dispersive elements and an electro-optic modulator (EOM) that is placed between the two dispersive elements. In the system, an ultrashort optical pulse is temporally stretched by the first dispersive

element. The dispersed pulse is then modulated in the time domain by a low-frequency RF signal $x(t)$ at the EOM. The dispersed and modulated optical pulse is finally completely compressed by the second dispersive element with opposite dispersion.

For an ideal input ultrashort pulse, i.e. Dirac delta function $\delta(t)$, the output signal of the system $y(t)$ is the scaled version of Fourier transform of the RF signal applied to the EOM. Considering the pulse width of the input signal $g(t)$ is usually not zero in practice, the temporal signal at the output of the typical TPS system can be obtained from the following convolution [20]

$$y(t) = \frac{1}{\ddot{\Phi}} g(t) * \tilde{X}\left(\frac{t}{\ddot{\Phi}}\right) \tag{3-42}$$

where $\ddot{\Phi}$ (in ps^2) is the dispersion of the dispersive element, * denotes the convolution operation and $\tilde{X}(\bullet)$ is the Fourier transform of the RF signal $x(t)$.

Photonic generation of microwave waveforms based on optical pulse shaping using a TPS system has been intensively investigated [13-15, 17-22, 218-219]. The key advantage of this TPS technique is that an ultra-fast microwave pulse can be generated using a relatively slow microwave driving signal.

3.2.1.2. Microwave waveform generation based on frequency multiplication using an unbalanced temporal pulse shaping system

This section is a revised version of the following published paper.

Article title: Continuously tunable photonic microwave frequency multiplication by use of an unbalanced temporal pulse shaping system

Authors: Chao Wang, Ming Li, and Jianping Yao

Published in IEEE Photonics Technology Letters, vol. 22, no. 17, pp. 1285-1287, Sep. 2010.

In this section, photonic generation of a high-frequency microwave pulse based on microwave frequency multiplication using an unbalanced temporal pulse shaping (UB-TPS) system is investigated. The proposed UB-TPS system consists of a Mach-Zehnder modulator (MZM) and two dispersive elements (DEs) having opposite dispersion, but non-identical in magnitude. The entire system can be modeled as a typical balanced TPS system for a real-time Fourier transformation followed by a residual DE for a second real-time Fourier transformation.

I. *Introduction*

High-frequency pulsed microwave signals have found important applications such as in radar systems [217] and microwave tomography [129]. Techniques to generate microwave pulses based on optical spectral shaping and frequency-to-time mapping have been discussed in previous sections. Another interesting method to generate a high frequency microwave pulse is to multiply the carrier frequency of a low-frequency microwave drive signal based on temporal pulse shaping. For example, frequency division or multiplication of a pulsed microwave signal has been reported through dispersively stretching or compression of a highly chirped optical pulse that is modulated by the microwave drive signal [220]. The main limitation of the approach in [220] is that the maximum microwave frequency that can be multiplied is limited (input bandwidth limitation) due to the dispersion-induced power penalty using optical double-sideband (DSB) modulation, similar to the power penalty in a DSB-modulation-based analog fiber link [221]. Although the use of optical single-sideband (SSB) modulation can eliminate

this penalty [222], it may increase the complexity of the system. In addition, SSB modulation is only achievable within a small bandwidth due to the limited bandwidth of a 90^{o} RF phase shifter, which is not expected for broadband and tunable microwave frequency multiplication. Recently, Azana et al. demonstrated an approach that was used to overcome the bandwidth limitation by exploiting a general temporal self-imaging effect in the optical fiber for frequency multiplication of a pulsed microwave signal [223]. Since the focused image of the microwave drive signal can only be obtained under specific dispersion conditions (so called integer Talbot conditions), the multiplication factor can be tuned only at specific values. Thus microwave pulses with only specific carrier frequencies can be generated from a given input microwave drive signal.

In this research work, we propose and experimentally demonstrate an optical approach to generating high frequency microwave pulses based on frequency multiplication with a high and continuously tunable multiplication factor. The technique is implemented using an UB-TPS system that incorporates two DEs having opposite dispersion, but non-identical in magnitude. The entire system is equivalent to a typical balanced TPS system with a pair of complementary DEs [20] for real-time Fourier transformation followed by a residual DE with its dispersion being the offset of the dispersion of the two DEs, to achieve a second real-time Fourier transform. The frequency multiplication factor is only determined by the dispersion of the two DEs. The limited bandwidth of the technique in [220] is eliminated by using optical intensity modulation that is biased at the minimum transmission point to achieve carrier suppression. Therefore, the approach is well suited for broadband operation. Moreover, since no specific dispersion conditions are required, the frequency multiplication factor can be continuously

tunable by changing the dispersion. Therefore, a pulsed microwave signal with a high and tunable carrier frequency can be generated.

II. *Principle*

A schematic diagram showing the proposed unbalanced TPS system is illustrated in Fig. 3.47. The system consists of an MLFL, two conjugate DEs, which can be two LCFBGs or two dispersive fibers with different dispersion coefficients, and an MZM. The two DEs can be modeled as LTI systems with transfer functions given by [191]

$$H_i(\omega) = \exp\left(-j\ddot{\Phi}_i\omega^2/2\right) \tag{3-43}$$

where i=1, 2, $\ddot{\Phi}_1$ and $\ddot{\Phi}_2$ (in ps^2) are, respectively, the dispersion coefficients of the two DEs.

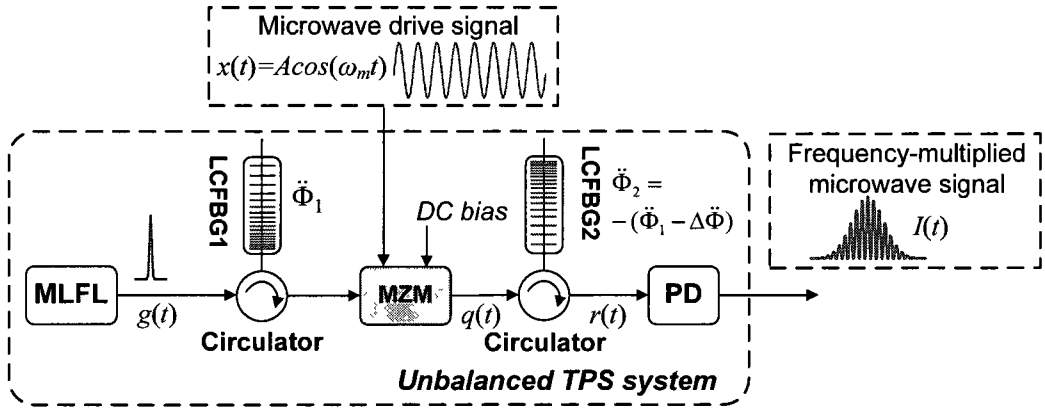

Fig. 3.47. Schematic diagram of an unbalanced TPS system for microwave pulse generation based on frequency multiplication. MLFL: mode-locked fiber laser, LCFBG: linearly chirped fiber Bragg grating, MZM: Mach-Zehnder modulator, PD: photodetector.

In the proposed UB-TPS system, the values of the dispersion should satisfy $\ddot{\Phi}_1\ddot{\Phi}_2 < 0$, and $\left|\ddot{\Phi}_1\right| \neq \left|\ddot{\Phi}_2\right|$. Therefore the transfer function of the second DE can be rewritten as $H_2(\omega) = \exp(j\ddot{\Phi}_1\omega^2/2)\exp(-j\Delta\ddot{\Phi}\omega^2/2)$, where $\Delta\ddot{\Phi} = \ddot{\Phi}_1 + \ddot{\Phi}_2$ is defined as the residual

dispersion. Therefore, the entire UB-TPS system can be modeled as a typical balanced TPS system with a pair of complementary DEs having dispersion coefficients of $\ddot{\Phi}_1$ and $-\ddot{\Phi}_1$, followed by a residual DE with a transfer function of $H_\Delta(\omega) = \exp(-j\Delta\ddot{\Phi}\omega^2/2)$, as shown in Fig. 3.48.

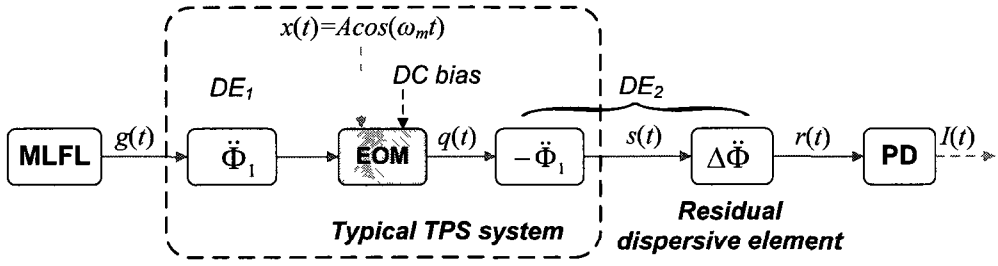

Fig. 3.48. The unbalanced TPS system can be modeled as a typical TPS system followed by a residual dispersion element. MLFL: mode-locked fiber laser, LCFBG: linearly chirped fiber Bragg grating, MZM: Mach-Zehnder modulator, PD: photodetector.

Assume that the modulating RF signal applied to the MZM is a sinusoidal signal $x(t) = A\cos(\omega_m t)$, where A and ω_m are the amplitude and angular frequency of the electrical drive signal, respectively. The intensity modulation in the MZM can be expressed as [224]

$$\begin{aligned} e_{IM}(t) &= \frac{1}{2}\exp\left\{i\left[\phi_0 + x(t)\right]\right\} + \frac{1}{2}\exp\left\{-i\left[\phi_0 + x(t)\right]\right\} \\ &= \cos\left[\frac{\phi_0 + x(t)}{2}\right] \end{aligned} \tag{3-44}$$

where ϕ_0 is a constant phase shift determined by the constant DC-bias voltage. Equation (3-44) can be expanded in Bessel series by

$$e_{IM}(t) = \cos\left[\frac{\phi_0 + x(t)}{2}\right] = \cos\left(\frac{\phi_0}{2}\right) J_0(\beta) + \sum_{n=1}^{\infty} a_n J_n(\beta) \cos(n\omega_m t),$$

$$a_n = \begin{cases} 2 \times \cos\left(\frac{\phi_0}{2}\right) \times (-1)^{\frac{n}{2}}, & n \text{ is even} \\ -2 \times \sin\left(\frac{\phi_0}{2}\right) \times (-1)^{\frac{n+1}{2}}, & n \text{ is odd} \end{cases} \qquad (3\text{-}45)$$

where $J_n(\beta)$ is a Bessel function of the first kind of order n with argument of β, and $\beta = A/2$ is the phase modulation index. We can see that the intensity modulation in the MZM will introduce the first-order and higher order optical sidebands, with the amplitude distribution of these sidebands determined by the variation of Bessel functions parameterized by β.

In our proposed approach, a different modulation scheme is employed – double-sideband modulation with suppressed carrier (DSB-SC), where the DC bias of the MZM is tuned to have $\phi_0 = \pi$. This is equivalent that the MZM is dc-biased at the minimum transmission point to suppress the optical carrier. Therefore the optical carrier and all the even-order optical sidebands will vanish, as indicated in (3-45). In addition, under the small signal modulation condition, all optical sidebands above the second order have an amplitude low enough to be ignored. Therefore the intensity modulation can be rewritten as

$$e_{IM}(t) \cong 2 \times J_1(\beta) \cos(\omega_m t) \qquad (3\text{-}46)$$

Theoretically, we can assume that the ultrashort optical pulse from the MLFL is a transform-limited Gaussian pulse that is expressed as $g(t) = \exp(-t^2 / \tau_0^2)$, where τ_0 is half pulse width at 1/e maximum. Its Fourier transform is given by $\tilde{G}(\omega) = \tilde{F}[g(t)] = \sqrt{\pi}\tau_0 \exp(-\tau_0^2 \omega^2 / 4)$. The input optical pulse is dispersed by passing through the first DE. The temporally stretched pulse

is then modulated by the microwave drive signal in the MZM. The Fourier transform of the signal $q(t)$ at the output of the MZM can be expressed as

$$\tilde{Q}(\omega)=\frac{1}{2\pi}\left[\tilde{G}(\omega)H_1(\omega)\right]*\tilde{E}_{IM}(\omega) \tag{3-47}$$

where $\tilde{E}_{IM}(\omega)=J_1(\beta)[\delta(\omega-\omega_m)+\delta(\omega+\omega_m)]$ is the Fourier transform of the intensity modulation function $e_{IM}(t)$. Assume that the dispersion of the first DE is large enough to satisfy that $\left|\tau_0^2/\ddot{\Phi}_1\right|<<1$ and the microwave drive signal $x(t)$ is faster than the dispersed optical pulse stretched by the first DE, i.e., $\omega_m >> 2\pi/(\Delta\omega_{opt}\ddot{\Phi}_1)$, where $\Delta\omega_{opt}$ is the optical bandwidth of the input pulse $g(t)$. Then by employing a similar mathematical treatment as in [25], equation (3-47) can be approximated as (Fraunhofer approximation)

$$\tilde{Q}(\omega)\cong\tilde{G}(\omega)\exp\left(-j\ddot{\Phi}_1\omega^2\right)e_{IM}(t)\Big|_{t=\ddot{\Phi}_1\omega} \tag{3-48}$$

The dispersed and modulated pulse $q(t)$ is then sent to the second DE, which can be theoretically modeled as the combination of two sub-DEs as shown in Fig. 3.48. Let $s(t)$ be the output signal of the typical TPS system, which can be obtained by passing $q(t)$ through the first part of the second DE. Therefore, the spectrum of the output signal of the typical TPS system can be expressed as

$$\begin{aligned}\tilde{S}(\omega)&\cong\tilde{Q}(\omega)\times\exp\left(j\ddot{\Phi}_1\omega^2\right)=\tilde{G}(\omega)e_{IM}(t)\Big|_{t=\ddot{\Phi}_1\omega}\\&=2J_1(\beta)\tilde{G}(\omega)\cos\left(\omega_m T\right)_1\end{aligned} \tag{3-49}$$

where $T_1=\left|\omega_m\ddot{\Phi}_1\right|/2\pi$. Then the corresponding temporal output signal is given by

$$s(t) = \frac{1}{\left|\ddot{\Phi}_1\right|} g(t) * \tilde{E}_{IM}(\omega)\Big|_{t=\ddot{\Phi}_1\omega} = S_0\left[g(t-T_1) + g(t+T_1)\right] \tag{3-50}$$

where $S_0 = J_1(\beta)/\left|\ddot{\Phi}_1\right|$ is a time-independent constant. Therefore two time-delayed replicas of the input pulse are generated at the output of the typical TPS system, which correspond to the two first-order optical sidebands of the suppressed-carrier modulation.

Then the electrical field at the output of the entire unbalanced TPS system, $r(t)$, is obtained by propagating $s(t)$ through the residual DE. If the dispersion of the residual DE is large enough such that $\left|\Delta\ddot{\Phi}\right| \geq T_1^2/2$ is satisfied, then the output signal can be approximated by the real-time FT of $s(t)$ in the residual DE [25]

$$r(t) \approx \exp\left[-jt^2/\left(2\Delta\ddot{\Phi}\right)\right] S(\omega)\Big|_{\omega=t/\Delta\ddot{\Phi}} = \exp\left[-jt^2/\left(2\Delta\ddot{\Phi}\right)\right] 2J_1(\beta) G\left(t/\Delta\ddot{\Phi}\right)\cos\left(2\pi t T_1/\Delta\ddot{\Phi}\right) \tag{3-51}$$

Finally, the current at the output of the PD is proportional to the intensity of the input electrical field, which is given by

$$I(t) \propto \left|r(t)\right|^2 = K\exp\left(-\frac{t^2}{\tau^2}\right) \times \left[1 + \cos\left(2\pi \frac{2T_1}{\Delta\ddot{\Phi}} t\right)\right] \tag{3-52}$$

where $K = J_1^{\,2}(\beta)\pi\tau_0^{\,2}$ is a time-independent constant, and $\tau = \sqrt{2}\Delta\ddot{\Phi}/\tau_0$ is the temporal duration of the generated microwave pulse. Therefore, a frequency-multiplied microwave signal is generated, which is a pulsed microwave signal with a Gaussian envelope. Its microwave carrier frequency is given by

$$\omega_{RF} = \left|2T_1 / \Delta\ddot{\Phi}\right| = \omega_m \left|2\ddot{\Phi}_1 / \Delta\ddot{\Phi}\right| \tag{3-53}$$

From (3-53) we reach a conclusion that a high-frequency microwave pulse is generated from the low-frequency microwave drive signal based on unbalanced temporal pulse shaping. The frequency multiplication factor $M = \omega_{RF} / \omega_m = 2\left|\ddot{\Phi}_1 / \Delta\ddot{\Phi}\right|$ is determined by both the stretching dispersion $\ddot{\Phi}_1$ and the residual dispersion $\Delta\ddot{\Phi}$. The key significance of the proposed approach is that the frequency multiplication can be continuously tunable by changing the dispersion of the DEs, while only a discrete multiplication factor can be achieved in [223] with the values of dispersion that satisfy the Talbot effect condition. In addition, the proposed approach offers an additional two-fold improvement in frequency multiplication thanks to the use of DSB-SC modulation as compared with the previous approach in [223] where DSB modulation was employed.

III. *Simulation*

The proposed approach is first evaluated by numerical simulations. In the calculations, we assume the sinusoidal modulating signal has a frequency of f_m = 5 GHz. The phase modulation index β is selected as 0.35 rad. The dispersion coefficients are $\ddot{\Phi}_1$ = 2640 ps^2 and $\ddot{\Phi}_2$ = -2904 ps^2. Based on (3-53), a frequency multiplication factor of 20 should be achieved.

The simulation results are shown in Fig. 3.49. Fig. 3.49(a) shows the signal $s(t)$ at the output of the typical TPS system. Two short pulses separated by a time shift of $2T_1$ are observed, as predicted by (3-50). The inset gives a zoom-in view of the input pulse (dashed line) and one of the output pulses (solid line). Both the pulses are properly time shifted. We can see that the

output pulses are the replica of the input optical pulse. The optical spectrum of the two output pulses is shown in Fig. 3.49(b). The output signal from the typical TPS system is then passing through the residual DE. Fig. 3.49(c) shows the microwave signal at the output of the entire system. As expected, a pulsed microwave signal, which has a Gaussian envelope with a temporal duration of 180 ps and a carrier frequency of 100 GHz, is generated. The corresponding frequency multiplication factor is 20, which matches well with the theoretical prediction given by (3-52) and (3-53). In addition, by comparing the results in Fig. 3.49(b) and (c), the real-time Fourier transform operation in the residual DE is also confirmed.

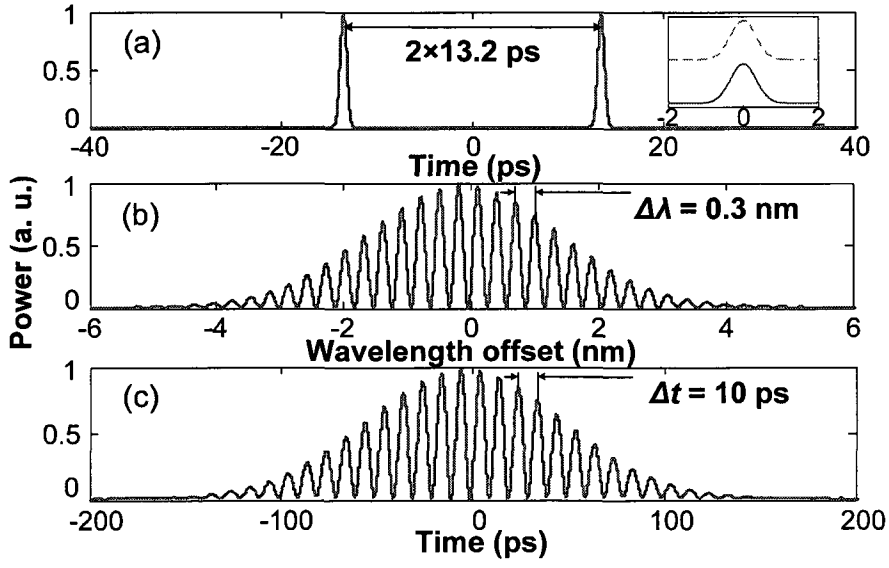

Fig. 3.49. Simulation results. (a) Output signal from the typical TPS system. (b) The optical spectrum of the signal in (a). (c) The frequency-multiplied microwave signal at the output of the entire system.

To verify the capability of the proposed system in eliminating the dispersion-induced power penalty in [220], an additional simulation is performed, in which the input RF signal at three different frequencies of 10, 12, or 16 GHz for both DSB and DSB-SC modulation schemes is considered. As can be seen from Fig. 3.50, the dispersion-induced power penalty, which occurs in DSB modulation at 12 and 16 GHz, does not exist in DSB-SC modulation. Therefore, the

input bandwidth limitation, which occurs in DSB modulation, is eliminated by applying DSB-SC modulation.

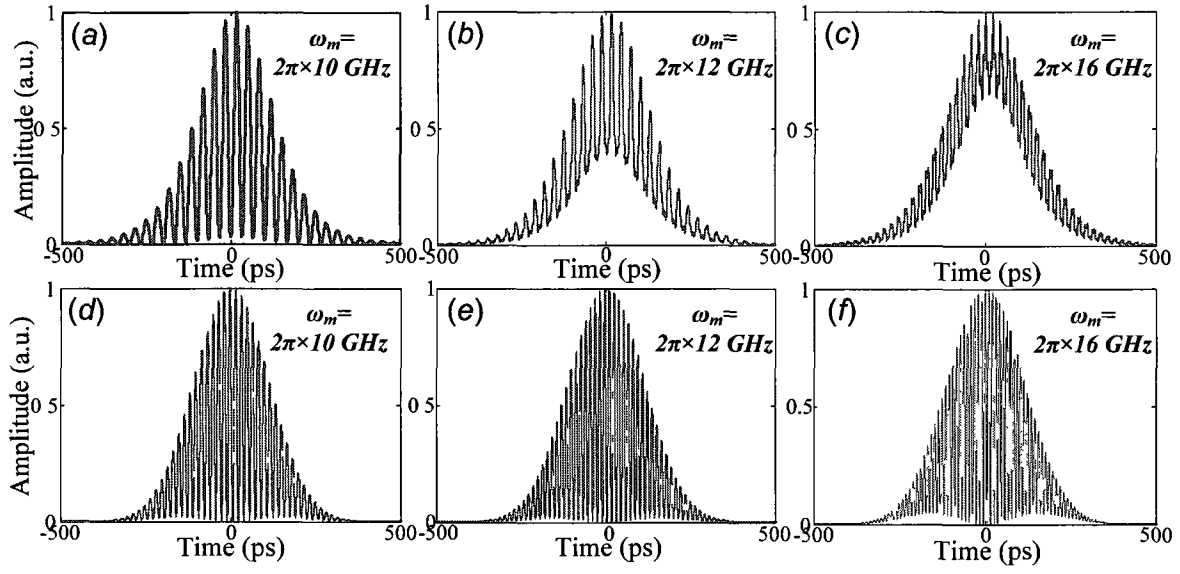

Fig. 3.50. Simulated output microwave pulses from the unbalanced TPS systems based on DSB modulation {(a), (b), (c)} and DSB-SC modulation {(d), (e), (f)}.

IV. *Experiment*

A proof-of-concept experiment based on the setup shown in Fig. 3.47 is then carried out. The ultrashort optical pulse from the MLFL has a pulse width of 550 fs and a 3-dB bandwidth of 8 nm. The MZM is biased at the minimum transmission point to achieve carrier suppression. A 6.1 km DCF with a dispersion of $\ddot{\Phi}_1 = 7624$ ps^2, and SMFs with different dispersion values are used as the first DE and the second DE, respectively.

The generated microwave waveforms are measured both in the time and frequency domains, with the results shown in Fig. 3.51. Note that all the time domain measurements are implemented using a real-time oscilloscope, no averaging is performed. Experimental parameters and results are summarized in Table 3.1. The system capability in tunable frequency

multiplication is verified. The experimental results agree well the theoretical results values given by (3-53). Note that the generated frequencies are relatively low, which are limited due to the low operation bandwidth of the used real-time oscilloscope.

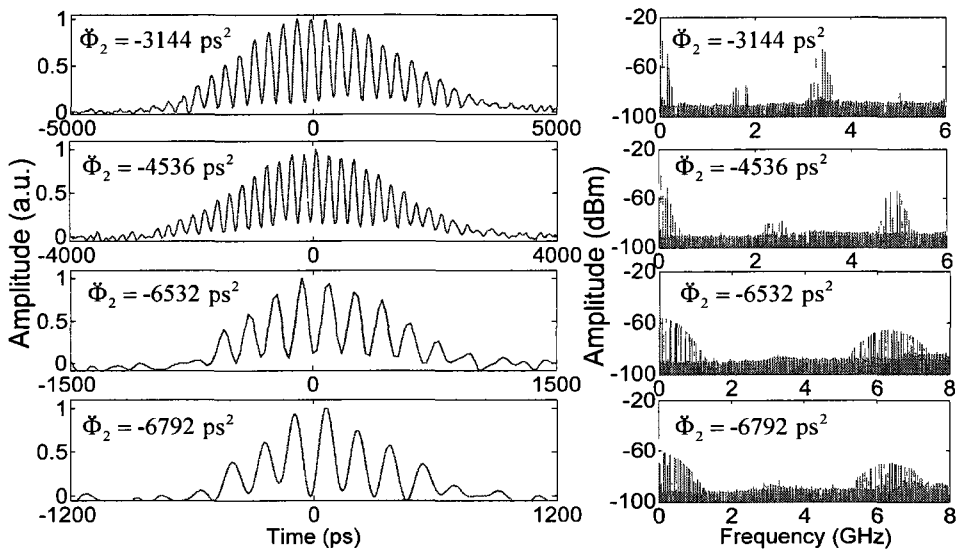

Fig. 3.51. Experimentally generated frequency-multiplied microwave pulses with different multiplication factors.

TABEL 3.1. EXPERIMENTAL PARAMETERS AND RESULTS

$\ddot{\Phi}_2$ (ps^2)	f_m (GHz)	f_{RF} (GHz)	M (measured /theoretical)	τ (ps)
-3144	1	3.38	3.38/3.40	2450
-4536	1	4.91	4.91/4.94	1700
-6532	0.45	6.31	14.02/13.96	725
-6792	0.35	6.34	18.11/18.32	550

V. *Discussions*

The multiplication factor is given by $M = \omega_{RF} / \omega_m = 2\left|\ddot{\Phi}_1 / \Delta\ddot{\Phi}\right|$. For a fixed input modulation frequency, ω_m, the multiplication factor can be increased by decreasing the residual dispersion

$\Delta\ddot{\Phi}$. Note that the residual dispersion must be kept sufficiently large to perform the second real-time Fourier transform, $\left|\Delta\ddot{\Phi}\right| \geq T_1^2/2$, where $T_1 = \left|\omega_m \ddot{\Phi}_1\right|/2\pi$, thus we have $M \leq 4\ddot{\Phi}_1 / T_1^2 = \frac{4\times(2\pi)^2}{\ddot{\Phi}_1 \omega_m \omega_m}$. It is also worth pointing out that, the microwave drive signal must be much faster than the dispersed optical pulse stretched by the input dispersion, $\ddot{\Phi}_1$, i.e., $T_0 = \frac{\Delta\omega_{opt}\ddot{\Phi}_1}{2\pi} \geq \frac{2\pi N}{\omega_m}$, where $\Delta\omega_{opt}$ is the optical bandwidth of the input pulse, T_0 is the time duration of the input dispersed optical pulse, N is the minimum number of cycles in the modulated optical pulse. Therefore, we have $\frac{1}{\ddot{\Phi}_1 \omega_m} \leq \frac{\Delta\omega_{opt}}{(2\pi)^2 N}$, and thus the frequency multiplication factor can be expressed as

$$M \leq 4\Delta\omega_{opt} / (N\omega_m) \tag{3-54}$$

We can find that for a microwave pulse with a given number of cycles, N, a higher frequency multiplication factor can be obtained for a lower-frequency microwave drive signal. Finally, the multiplied microwave pulse can be expressed as

$$\omega_{RF} = M\omega_m \leq \frac{4\Delta\omega_{opt}}{N} \tag{3-55}$$

Theoretically, the highest multiplied frequency that can be achieved is only limited by the input optical bandwidth. The frequency multiplication is practically limited by the operation bandwidth of the PD.

It is also worth noting that decreasing the residual dispersion $\Delta\ddot{\Phi}$ may increase the frequency multiplication factor according to (3-53), but also reduces the temporal duration of the output

microwave pulse according to (3-52), as shown in Fig. 3.51. Therefore, a tradeoff exists between the frequency multiplication factor and the output pulse duration. To provide more design guidelines, more simulations are performed. Fig. 3.52 shows the frequency multiplication factor and the output pulse duration as a function of the residual dispersion for a given stretching dispersion value (5280 ps^2), a modulation frequency (1 GHz) and an input optical pulse width. By employing an input optical pulse with a shorter pulse width, we can achieve a higher multiplication factor while maintaining a suitable output pulse duration.

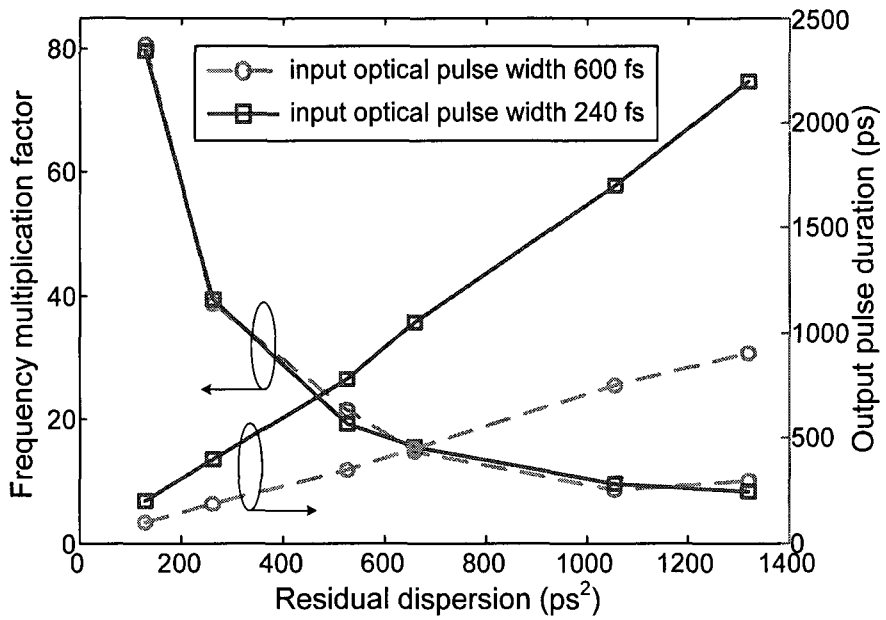

Fig. 3.52. Calculated frequency multiplication factor and output pulse duration as a function of the residual dispersion.

In our analysis, only GVD ($\ddot{\Phi}$) are considered. This treatment is valid for a moderate length of dispersive fiber (SMF, < 70 km) and is verified by both simulations and experiments. For a longer dispersive fiber, the TOD ($\dddot{\Phi}$) has to be taken into account. In this scenario, a dispersion element with both GVD and TOD can be described by the transfer function

$$H_1(\omega) = H_{GVD1}(\omega) H_{TOD1}(\omega) \tag{3-56}$$

where $H_{GVD1}(\omega) = \exp(-j\ddot{\Phi}_1\omega^2/2)$, and $H_{GVD1}(\omega) = \exp(-j\dddot{\Phi}_1\omega^3/6)$. For simplicity, we can assume that the input optical pulse is an ideal Dirac delta function. Then the spectrum of the dispersed and modulated signal $q(t)$ at the output of the MZM can be expressed as

$$\begin{aligned}
\tilde{Q}(\omega) &= H_1(\omega) * \tilde{E}_{IM}(\omega) \\
&= \int_{-\infty}^{\infty} \tilde{E}_{IM}(u) \exp\left[-j\frac{\ddot{\Phi}_1(\omega-u)^2}{2}\right] \exp\left[-j\frac{\dddot{\Phi}_1(\omega-u)^3}{6}\right] du \\
&= \int_{-\infty}^{\infty} \tilde{E}_{PM}(u) \exp\left(-j\frac{\ddot{\Phi}_1\omega^2}{2}\right) \exp\left(-j\frac{\ddot{\Phi}_1 u^2}{2}\right) \exp\left(j\ddot{\Phi}_1\omega u\right) \\
&\qquad \times \exp\left(-j\frac{\dddot{\Phi}_1 u^3}{6}\right) \exp\left(j\frac{\dddot{\Phi}_1 u^2\omega}{2}\right) \exp\left(-j\frac{\dddot{\Phi}_1 u\omega^2}{2}\right) \exp\left(j\frac{\dddot{\Phi}_1\omega^3}{6}\right) du \\
&= \exp\left(-j\frac{\ddot{\Phi}_1\omega^2}{2}\right) \exp\left(j\frac{\dddot{\Phi}_1\omega^3}{6}\right) \int_{-\infty}^{\infty} \tilde{E}_{IM}(u) \exp\left(-j\frac{\ddot{\Phi}_1 u^2}{2}\right) \exp\left(j\ddot{\Phi}_1\omega u\right) \\
&\qquad \times \exp\left(-j\frac{\dddot{\Phi}_1 u^3}{6}\right) \exp\left(j\frac{\dddot{\Phi}_1 u^2\omega}{2}\right) \exp\left(-j\frac{\dddot{\Phi}_1 u\omega^2}{2}\right) du
\end{aligned} \tag{3-57}$$

Considering that the bandwidth of the microwave drive signal is small, i.e., $u < 10\ GHz$, we can assume that $\ddot{\Phi}_1 u^2/2 << 1$ and $\dddot{\Phi}_1 u^3/6 << 1$. This assumption is valid if the DE has a moderate value of dispersion, i.e., 10-km SMF with dispersion coefficients of $\ddot{\Phi} = 1320\ ps^2$, $\dddot{\Phi} = 18\ ps^3$. In addition, the integral term $\exp(-j\dddot{\Phi}_1 u\omega^2/2)du$ can also be ignored if TOD of the applied DE is small. According to these considerations, (3-57) can be simplified as

$$\begin{aligned}
\tilde{Q}(\omega) &= \exp\left(-j\frac{\ddot{\Phi}_1\omega^2}{2}\right) \exp\left(j\frac{\dddot{\Phi}_1\omega^3}{6}\right) \\
&\qquad \times \int_{-\infty}^{\infty} \tilde{E}_{IM}(u) \exp\left(j\ddot{\Phi}_1\omega u\right) \exp\left(j\frac{\dddot{\Phi}_1 u^2\omega}{2}\right) du
\end{aligned} \tag{3-58}$$

Considering $\tilde{E}_{IM}(\omega) = J_1(\beta)[\delta(\omega-\omega_m)+\delta(\omega+\omega_m)]$, we have

$$\begin{aligned}\tilde{Q}(\omega) &= J_1(\beta)\exp\left(-j\frac{\ddot{\Phi}_1\omega^2}{2}\right)\exp\left(j\frac{\dddot{\Phi}_1\omega^3}{6}\right)\\ &\times\left\{\exp\left(j\ddot{\Phi}_1\omega\omega_m\right)\exp\left[j\frac{\dddot{\Phi}_1(\omega_m)^2\omega}{2}\right]+\exp\left(-j\ddot{\Phi}_1\omega\omega_m\right)\exp\left[j\frac{\dddot{\Phi}_1(-\omega_m)^2\omega}{2}\right]\right\} \quad (3\text{-}59)\\ &= 2J_1(\beta)\exp\left(-j\frac{\ddot{\Phi}_1\omega^2}{2}\right)\exp\left(j\frac{\dddot{\Phi}_1\omega^3}{6}\right)\exp\left(j\frac{\dddot{\Phi}_1\omega_m^2\omega}{2}\right)\cos\left(\ddot{\Phi}_1\omega\omega_m\right)\end{aligned}$$

Therefore, the spectrum of the output signal of the typical TPS system can be rewritten as

$$\tilde{S}(\omega) = \tilde{Q}(\omega)H_1^*(\omega) = 2J_1(\beta)\exp\left(-j\frac{\dddot{\Phi}_\Delta\omega^3}{6}\right)\exp\left(j\frac{\dddot{\Phi}_1\omega_m^2\omega}{2}\right)\cos\left(\ddot{\Phi}_1\omega\omega_m\right) \quad (3\text{-}60)$$

where $\dddot{\Phi}_\Delta$ is the mismatched third-order dispersion in the typical TPS system. Take into account that the input optical pulse $g(t)$ has a nonzero pulse width, the output signal from the typical TPS system is then expressed as

$$\begin{aligned}s_{TOD}(t) &= g(t) * F^{-1}\left[\tilde{S}(\omega)\right]\\ &= 2\left(\ddot{\Phi}_\Delta\right)^{-1/3}J_1(\beta)\left[g\left(t-T_1-\ddot{\Phi}_1\omega_m^2/2\right)+g\left(t+T_1-\ddot{\Phi}_1\omega_m^2/2\right)\right]*\left[\sqrt{t}Y_{1/3}(Z)\right]\end{aligned} \quad (3\text{-}61)$$

where $Y_{1/3}(Z)$ is the 1/3 order Bessel function of the second kind, and $Z = (\dddot{\Phi}_\Delta)^{-1/2}t^{3/2}$ is its argument. According to (3-61), the signal at the output of the typical TPS system still consists of two pulses. However, the pulses are not exactly the replicas of the original input pulse. They are time shifted, differently weighted and dispersed. The simulation result is shown in Fig. 3.53. Dispersion values are selected as $\ddot{\Phi} = 1320\ \text{ps}^2$, $\dddot{\Phi}_\Delta = 0.45\ \text{ps}^3$.

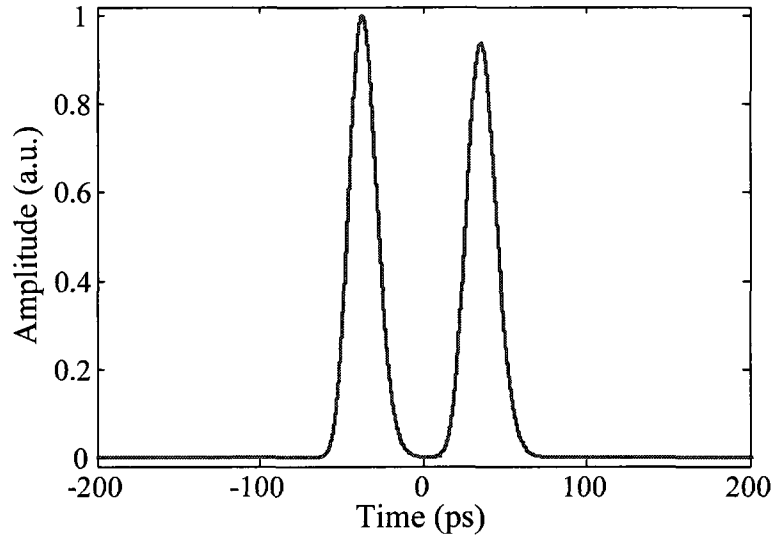

Fig. 3.53. Simulation result. The output signal of the typical TPS system with both the GVD and TOD.

After passing through the residual DE, a chirped microwave pulse would be generated due to the higher-order dispersion induced nonlinear real time Fourier transform [132]. Since the frequency of the microwave drive signal can be tuned, the proposed system may find application in configurable chirped microwave pulse generation.

In the proof-of-concept experiment, the employed DCFs and SMFs have different dispersion to obtain different frequency multiplication factors. To achieve a real continuously tunable frequency multiplication, the DEs with continuously tunable dispersion are required. In fact, the dispersion of an LCFBG can be continuously tunable in a bandwidth up to 10 nm or more by using the simply supported beam tuning technique [225].

VI. Conclusion

In conclusion, a novel approach to generation high-frequency microwave pulses based on continuously tunable frequency multiplication in an unbalanced TPS system has been proposed and demonstrated. The entire system is equivalent to a typical TPS system for a real-time

Fourier transform followed by a residual DE for a second real-time Fourier transform. The approach provides a potential solution to generate high-frequency pulsed microwave signals for applications such as in radar and microwave tomography.

3.2.2. Frequency-domain Fourier-transform pulse shaping for microwave arbitrary waveform generation

This section is a revised version of the following published paper.

Article title: Fourier transform ultrashort optical pulse shaping using a single chirped fiber Bragg grating

Authors: Chao Wang, and Jianping Yao

Published in IEEE Photonics Technology Letters, vol. 21, no. 19, pp. 1375-1377, Oct. 2009.

Fourier-transform optical pulse shaping can also be implemented in the frequency-domain using an optical spectral filter and two complementary DEs. In the pulse shaping system, the optical spectral filter is usually located between the two DEs to shape the spectrum of a dispersed optical pulse by the first DE. The spectrum-shaped pulse is then completely compressed by the second DE.

A simplified frequency-domain Fourier-transform optical pulse shaping using a single LCFBG is investigated and experimentally demonstrated in this section. The LCFBG in the system performs three functions: temporally stretching the input ultrashort pulse, shaping the pulse spectrum, and temporally compressing the spectrum-shaped pulse. The impulse response of the entire pulse shaping system is equal to the Fourier transform of the square of grating power

reflectivity function. By appropriately designing the grating reflection response, a temporal waveform in the sub-picosecond regime can be accurately synthesized. The use of a single LCFBG guarantees an exact cancellation of the dispersion, making the pulse shaping system have a better pulse shaping accuracy with a simplified structure.

I. *Introduction*

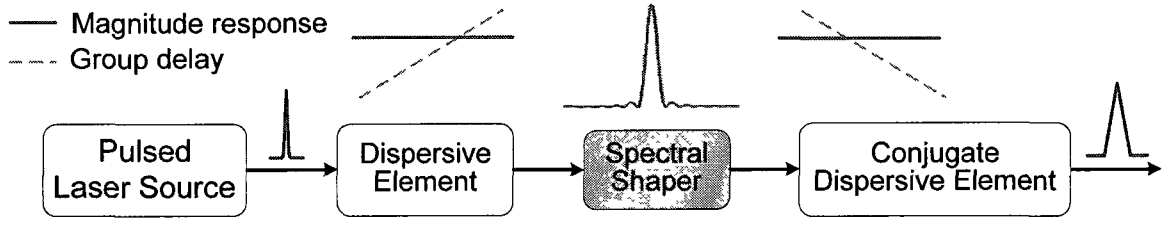

Fig. 3.54. Schematic diagram of a conventional frequency-domain Fourier-transform optical pulse shaping system.

Ultrashort optical pulse shaping has been intensively studied in recent years for a number of scientific and engineering applications, including high-speed optical telecommunications, fast optical computing systems, coherent quantum optics, modern instrumentation and microwave arbitrary waveform generation. Fourier synthesis, also known as Fourier transform pulse shaping, is one of the most commonly used techniques for optical pulse shaping in the sub-picosecond regime [42]. In a frequency-domain Fourier-transform pulse shaping system, as shown in Fig. 3.54, a pair of diffractive or dispersive elements is employed to decompose and compose the spectral content of the original input optical pulse; and a spectral shaping device is incorporated between the two conjugate dispersive elements to realize optical spectral shaping in the Fourier domain. For example, an optical spectral shaper with a Sinc-squared magnitude response can be employed to achieve spectral shaping for the generation of a triangular waveform, as shown in Fig. 3.54.

The Fourier-transform optical spectral shaping can be implemented using free-space optical devices, such as a programmable liquid crystal modulator (LCM) [226]. On the other hand, Fourier transform pulse shaping can also be implemented using fiber-optics devices. For example, two LCFBGs have been used to perform frequency-domain Fourier-transform pulse shaping, with the first LCFBG serving as a spectral shaper and the other as a dispersion compensator [227]. To cancel completely the dispersion introduced by the first LCFBG, the second LCFBG must be precisely fabricated to have an exact opposite chirp, which would increase significantly the fabrication complexity and cost. In addition, the LCFBGs in [227] were designed based on the weak coupling (Born) approximation [210], making the LCFBGs have a very low energy efficiency.

In this research work, we propose and experimentally demonstrate a novel Fourier-transform optical pulse shaper that uses only a single LCFBG. In the proposed system, an input ultrashort optical pulse is first temporally stretched by the LCFBG, and then completely compressed by the same LCFBG by directing the dispersed optical pulse into the LCFBG from an opposite direction. Therefore, a perfect dispersion cancellation is obtained. At the same time, the LCFBG also acts as an optical spectral shaper which is designed to have a user-defined spectral reflection response according to the target temporal waveform. The impulse response of the entire system is equal to the Fourier transform of the square of the LCFBG power reflectivity function.

The key device in the system is the LCFBG, which should be designed to have a strict linear group delay response and a user-defined reflection magnitude response. In this research work, we propose to use a simple and effective method based on an accurate mapping of the grating reflection response to the refractive index apodization to synthesize and produce the required

LCFBG, as have been discussed in Section 3.1.3. It is different from the design based on the Born approximation, the method here can make the grating have a high reflectivity, leading to an improved energy efficiency. Since an amplitude-only index apodization is required, the LCFBG can be easily realized with the current phase-mask-based FBG fabrication technology.

II. *Principle*

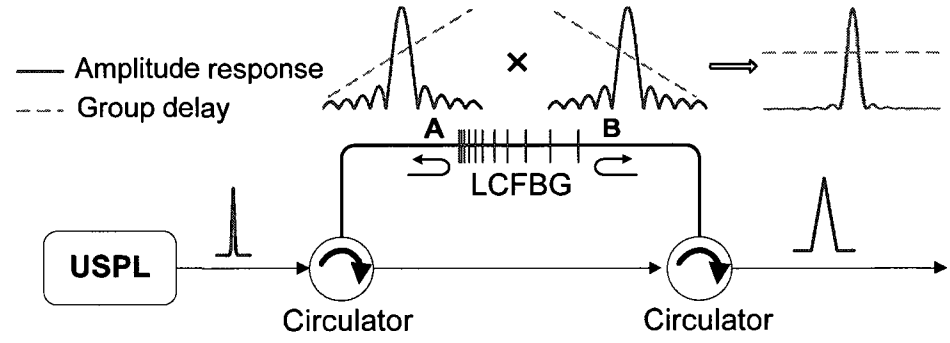

Fig. 3. 55. Schematic diagram of the proposed Fourier-transform optical pulse shaping system using a single LCFBG. USPL: ultra-short pulsed laser, LCFBG: linearly chirped fiber Bragg grating.

A schematic diagram showing the proposed Fourier-transform optical pulse shaping system is illustrated in Fig. 3.55. The system consists of a single LCFBG and two three-port optical circulators. The two ports of the LCFBG (A and B) are connected by the circulators, to route the input optical pulse to enter the LCFBG from the two ports successively. Mathematically, the LCFBG can be modeled as a LTI system with a transfer function given by $H_A(\omega) = |H_A(\omega)| \exp[j\Phi_A(\omega)]$ if the input pulse enters the LCFBG from port A and is then reflected by the LCFBG. Under the second-order dispersion approximation, which is always true for an LCFBG with very low higher order dispersion, the transfer function becomes

$$H_A(\omega) = R(\omega) \exp\left(-j\ddot{\Phi}_A \omega^2 / 2\right) \tag{3-62}$$

where ω is the offset frequency from the optical central frequency ω_0, $R(\omega)$ is the grating power reflectivity, and $\ddot{\Phi}_A = d^2\Phi_A/d\omega^2\,|_{\omega=0}$ is the second-order dispersion at the frequency ω_0. Similarly, the LCFBG has a transfer function $H_B(\omega)$ if the input optical pulse enters the LCFBG from port B and is then reflected by the LCFBG,

$$H_B(\omega) = R(\omega)\exp\left(-j\ddot{\Phi}_B\omega^2/2\right) \tag{3-63}$$

where $\ddot{\Phi}_B = d^2\Phi_B/d\omega^2\,|_{\omega=0}$ is again the second-order dispersion at the frequency ω_0. Thanks to the linear group delay response of the LCFBG, we have $\ddot{\Phi}_A = -\ddot{\Phi}_B$. Therefore, the impulse response of the entire system is given by

$$h(t) = \tilde{F}\left[H_A(\omega)H_B(\omega)\right] = \tilde{F}\left[R^2(\omega)\right] \tag{3-64}$$

where $\tilde{F}(\cdot)$ denotes the Fourier transform operation. As can be seen the impulse response of the entire system is equal to the Fourier transform of the square of the grating power reflectivity.

For a temporal waveform $y(t)$ to be synthesized, the desired grating power reflectivity function is determined by

$$R(\omega) = \sqrt{Y(\omega)/G(\omega)} \tag{3-65}$$

where $Y(\omega)$ and $G(\omega)$ are the Fourier transforms of the target output waveform $y(t)$ and the input optical pulse $g(t)$, respectively.

An accurate grating synthesis technique is required to synthesize the grating refractive index modulation profile from the desired LCFBG power reflectivity function given by (3-65). It was

reported in [227] that when an LCFBG has a large dispersion, the grating apodization profile can be linearly mapped to its spectral response. Our recent study shows that the mapping relationship is unique, but not always linear, depending on the grating parameters such as the refractive index modulation coefficient, the grating chirp rate, and the bandwidth [134]. In this research work, the desired LCFBG is synthesized and produced using a simple and effective technique based on an accurate mapping of the grating reflection response to the refractive index apodization as discussed in Section 3.1.3, which offers a better accuracy as compared to the approach in [227]. In addition, since the weak-coupling condition is not required in the design, the produced LCFBG can have a high reflectivity, leading to improved energy efficiency

III. *Experiment*

To prove the concept, an experiment to generate an optical triangular waveform is carried out. In our design, the optical input pulse is assumed to be an ideal Dirac impulse function with $G(\omega) \approx 1$. The target temporal waveform $y(t)$ is a triangular pulse with a FWHM of 2 ps. Therefore, the desired LCFBG power reflectivity function, according to (3-65), is given by

$$R(\omega) = \sqrt{Y(\omega)/G(\omega)} = \sqrt{Y(\omega)} \propto \left| Sinc\left(\frac{\omega}{B}\right) \right| \tag{3-66}$$

where B is the spectral bandwidth of the LCFBG, which has a value of $2\pi \times 0.25$ THz (2 nm).

The LCFBG with the desired reflection response given by (3-66) is first designed by applying the grating synthesis technique described above. The grating is then fabricated using a linearly chirped phase mask. The fabricated LCFBG has a length of 5 cm, a chirp rate of 2.4 nm/cm, and a strong reflection (the maximum reflectivity is around 90%). The center wavelength of the

LCFBG is selected to match the central wavelength of the input optical pulse. The reflection spectrum and the group delay response of the fabricated LCFBG are measured using an optical vector analyzer (OVA, LUNA Technologies). The measured reflection profile matches well with the desired reflection profile, as shown in Fig. 3.56(a). The linearity of the group delay response is also achieved, as shown in Fig. 3.56(b).

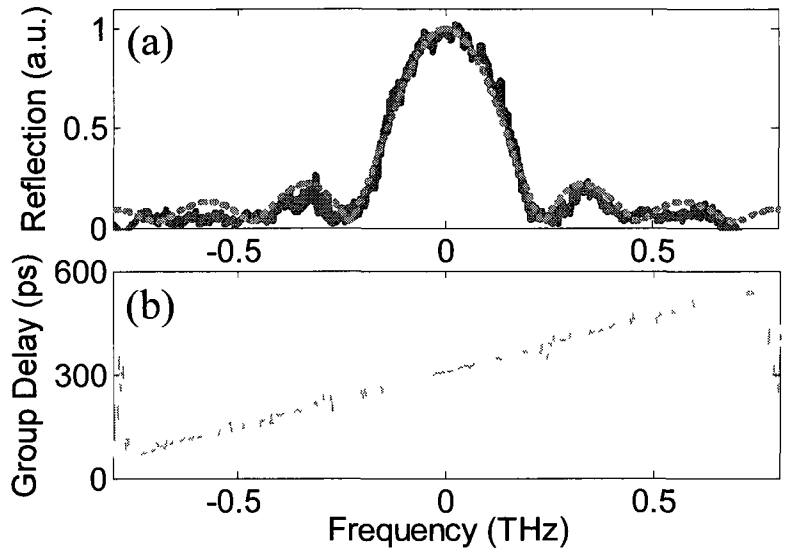

Fig. 3.56. The reflection spectrum and the group delay response of the fabricated LCFBG. Solid line: measured spectrum; dotted line: desired spectrum.

The fabricated LCFBG is then incorporated into the experimental setup shown in Fig. 3.55, to perform the spectral shaping of the input ultrashort optical pulse. The system performance is measured both in the frequency domain and the time domain using the OVA. The measured spectral response of the entire system, including the magnitude response and the group delay response, is shown in Fig. 3.57. A system magnitude response corresponding to $|Sinc(\omega / B)|$ is obtained, as shown in Fig. 3.57(a). The desired magnitude response is also shown in dotted line in Fig. 3.57(a) for comparison. A constant system group delay response is observed, as shown

in Fig. 3.57(b), which verifies a perfect dispersion cancellation. Note that bidirectional propagation in the LCFBG can be used to compensate the second-order dispersion only. The group delay ripples (GDRs) cannot be compensated. The GDRs in the LCFBG may also have an impact on the pulse shaping accuracy. A comprehensive study on the tolerances of an optical pulse compression system against the GDR can be found in [228].

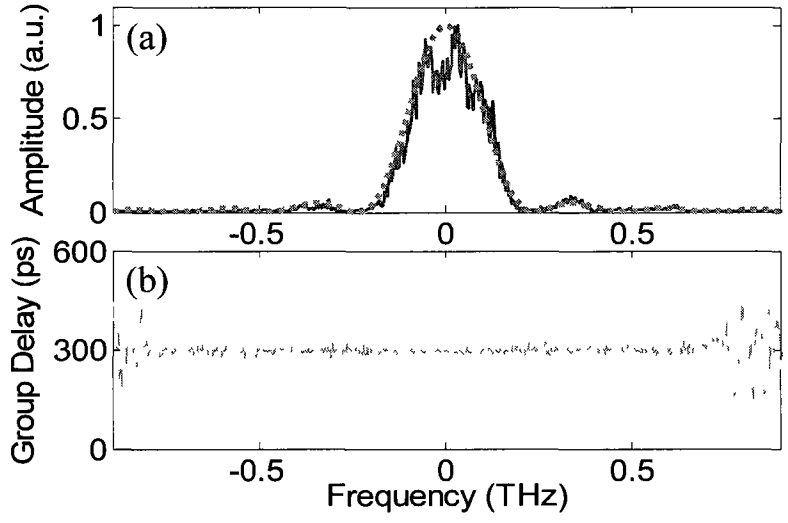

Fig 3.57. The magnitude and group delay response of the entire pulse shaping system. Solid line: measured magnitude response; dotted line: desired magnitude response.

Fig. 3.58 shows the system impulse response measured by the OVA. Due to the limited temporal resolution of the OVA, the details of the impulse response are not fully shown. To evaluate the performance of the proposed system for ultrashort optical pulse shaping more accurately, the measured system spectral response, including its magnitude response and phase response, is used to calculate the system impulse response, with the calculated result shown in Fig. 3.59. A triangular-shape impulse response with more details is obtained. The errors in the pulse shaping are resulted from the inaccuracy of the LCFBG magnitude response, which can be improved by refining the fabrication process.

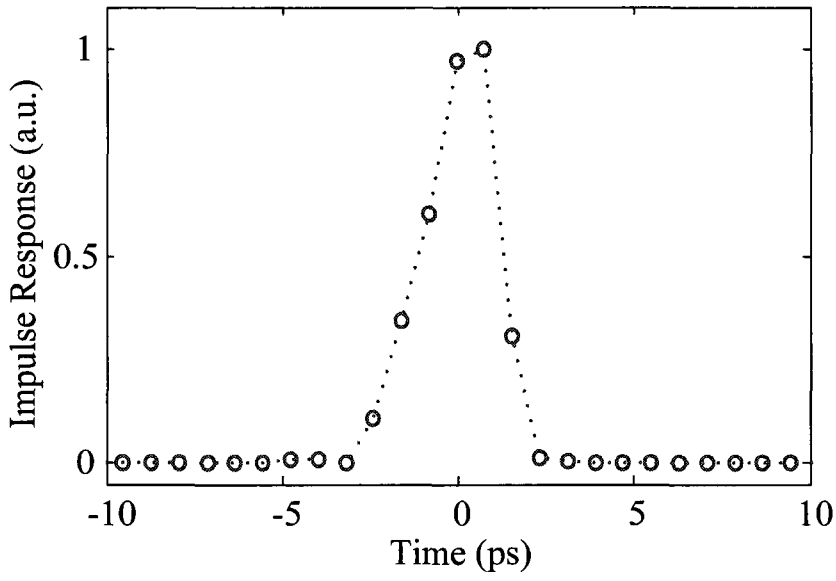

Fig. 3.58. Measured impulse response of the entire pulse shaping system.

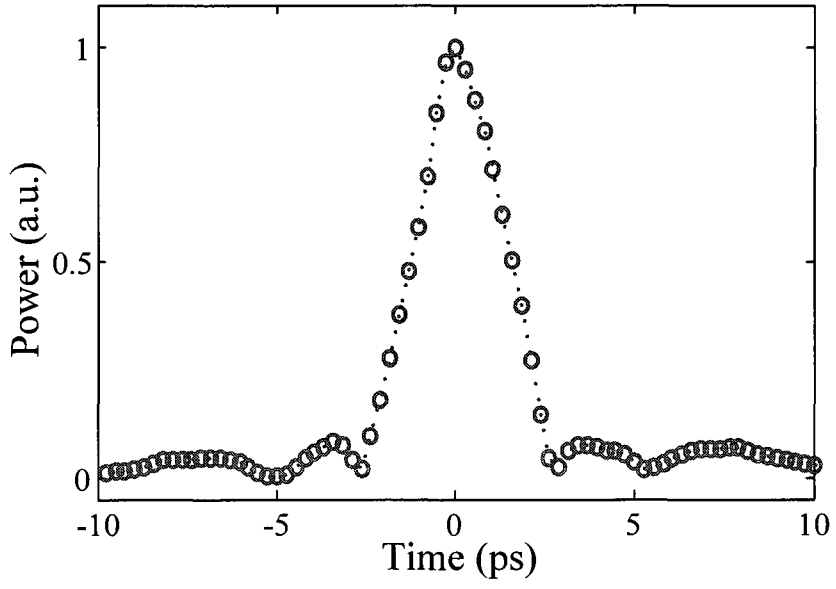

Fig. 3.59. Synthesized triangular pulse (calculated using the measured LCFBG magnitude and group delay response).

Note that in the synthesis of the triangular pulse, the input optical pulse was assumed to be a Dirac impulse function. For pulse shaping with a higher accuracy, the non-zero input pulse

width should be taken into consideration, then the LCFBG should be designed with a target reflection power spectrum given by $\sqrt{Y(\omega)/G(\omega)}$.

It is also worth noting that since the grating is not 100% reflective, the spectral leakage of the input signal may also generate unwanted temporal waveforms. Since the unwanted waveforms are temporally separated with the wanted temporal waveform, the target waveform can be extracted using specific time windows.

IV. *Conclusion*

A novel technique to implement frequency-domain Fourier-transform optical pulse shaping using a single LCFBG was proposed and experimentally demonstrated. The LCFBG in the system was functioning as a spectral shaper and at the same time as a conjugate dispersive element pair to perform pulse stretching and pulse compression. The use of a single LCFBG guarantees an exact cancellation of the dispersion, making the pulse shaping system have a simplified structure with a better pulse shaping accuracy. An experiment to demonstrate the generation of a triangular pulse with an FWHM of 2 ps was performed.

CHAPTER 4 PHOTONIC PROCESSING OF MICROWAVE ARBITRARY WAVEFORMS USING FBGS

FBG-based photonic microwave arbitrary waveform generation techniques have been intensively investigated in Chapter 3. High-frequency and broadband microwave waveforms have been generated using photonically assisted techniques. On the other hand, it is also desirable that the optically generated microwave waveforms can be processed in the optical domain, to take advantage of the high speed and broad bandwidth offered by optics.

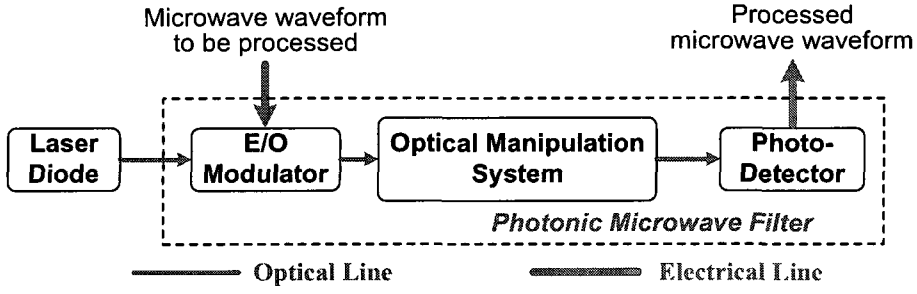

Fig. 4.1. General diagram of a photonic microwave filter for microwave waveform processing.

A photonic microwave filter is usually used to process a microwave waveform in the optical domain. A photonic microwave filter is a photonic structure, the object of which is to replace a standard microwave filter structure used in a RF system. The advantages of the photonic microwave filter include wide bandwidth, tunability, electromagnetic immunity, etc. Fig. 4.1 shows the general structure of a photonic microwave filter for microwave waveform processing. A laser diode (LD) or an LD array is employed as the optical carrier(s). The microwave to optical conversion is realized by directly or externally modulating the optical carrier. The input

microwave signal to be processed is then conveyed by the optical carrier and fed to a proper optical manipulation system, where the composite signal is processed in the optical domain. At the output of the system, the processed microwave signal is recovered by means of various optical receivers, such as a photodetector. In order to obtain desirable microwave filter response, the optical manipulation system is to be properly designed. Two different types of photonic microwave filters are investigated in this chapter: 1) photonic microwave multi-tap delay-line filter, and 2) photonic microwave filter based on optical filter response to microwave filter response conversion. Matched filtering of microwave arbitrary waveforms using both photonic microwave filters is demonstrated.

4.1. Photonic microwave multi-tap delay-line filter for microwave waveform processing

4.1.1. Principle of photonic microwave multi-tap delay-line filter

In the last few years, extensive efforts have been devoted to the design and implementation of photonic microwave filters with different structures to realize different filtering characteristics. Photonic microwave multi-tap delay-line filter is the most investigated technique for microwave signal filtering. Comprehensive overviews of photonic microwave delay-line filters have been published recently [73, 229]. In this section, a brief introduction to the principle of photonic microwave delay-line filter is presented.

Fig. 4.2 shows a diagram of a generic photonic microwave multi-tap delay-line filter with a finite impulse response (FIR). The system consists of an optical source, which is usually incoherent, an electro-optical modulator, a tapped delay-line structure, and a photodetector. The

optical carrier(s), after being modulated by the input microwave signal $x(t)$ at the modulator, is sent to the tapped delay-line device, where it is split into several channels with different time delays kT and tap coefficients (weights) α_k and then combined incoherently at the photodetector. The filtered microwave signal $y(t)$ is obtained at the output of the photodetector. It is worth noting that the optical source can be a single-wavelength optical source, a laser diode array, or a sliced broadband optical source; the tapping device can be an optical splitter, a uniform FBG array or an AWG, and the time delay component can be fiber delay lines, a chirped FBG or a length of dispersive fiber.

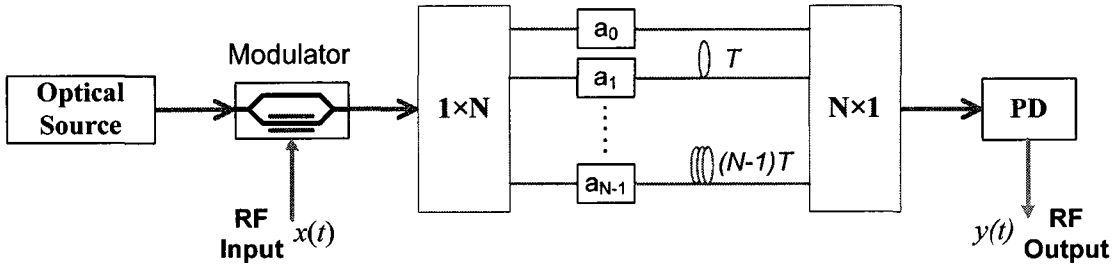

Fig. 4.2. A diagram showing a generic photonic microwave delay-line filter with a finite impulse response.

Provided that the nonlinear effects in the system are small and negligible, the entire system can be considered as a LTI system functioning as a microwave filter. According to the multi-tap delay-line structure shown in Fig. 4.2, the impulse response of the photonic microwave filter can be expressed as

$$h(t)=\sum_{k=0}^{N-1}\alpha_k\delta(t-kT) \tag{4-1}$$

where N is the number of the taps, α_k is the coefficient of the kth tap and T represents the constant time delay difference between the two adjacent taps. Then the transfer function of the microwave filter can be obtained from the Fourier transform of impulse response.

$$H(\omega) = \tilde{F}\left[h(t)\right] = \sum_{k=0}^{N-1} \alpha_k \exp(-jk\omega T) \tag{4-2}$$

where ω denotes the RF angular frequency. We can define a coefficient profile $a(t)$, which is given by

$$\begin{aligned} &a(kT) = \alpha_k \\ &a(t) = 0 \ \ (t < 0 \ or \ t \geq NT) \end{aligned} \tag{4-3}$$

Therefore the frequency response $H(\omega)$ can be rewritten as

$$H(\omega) = \frac{\Omega}{2\pi} \sum_m A(\omega - m\Omega) \tag{4-4}$$

where $A(\omega)$ is the Fourier transform of the coefficient profile $a(t)$. From (4-4) we can find that the transfer function of a regular photonic microwave filter is spectrally periodic with a period given by $\Omega = 2\pi / T$, which is known as the filter free spectral range (FSR).

4.1.2. Nonuniformly-spaced photonic microwave multi-tap delay-line filter for arbitrary microwave waveform matched filtering

I. *Introduction*

In a regular uniformly-spaced photonic microwave multi-tap delay-line filter, the time delay difference between the two adjacent taps is constant. The phase response of the filter with real tap coefficients is usually linear according to (4-4). Linear-phase filter is preferred in many applications in microwave signal processing. However, in some advanced microwave signal

processing applications, such as chirped microwave pulse generation or compression, a microwave filter with a nonlinear phase response is usually required [138, 214].

Complex tap coefficients are usually required in a uniformly-spaced FIR filter to achieve a sophisticated phase response. Various techniques to implement a photonic microwave FIR filter with complex coefficients have been proposed and demonstrated. For example, a complex tap coefficient can be generated using a system consisting of three PDs and two broadband phase-shifted microwave couplers [230]. In [91], a hybrid optical/electrical system consisting of two Mach-Zehnder modulators and a broadband 90° electronic phase shifter was proposed to achieve complex tap coefficients for a photonic microwave delay-line filter. Recently, an all-optical system to implement a complex tap coefficient was proposed by changing the phase of the microwave signal realized based on a combined use of optical single-sideband modulation and stimulated Brillouin scattering [231-232]. We can find that these filters usually have a complicated structure, which may limit their potential for practical applications.

Most recently, a novel technique to design and implement a photonic microwave delay-line FIR filter with a nonlinear phase response based on nonuniformly-spaced structure has been proposed and demonstrated [233-234]. In the proposed system, a nonuniform sampling technique is applied to generate equivalent complex tap coefficients. Since the actual tap coefficients are all-positive, a simple implementation is ensured. The major limitation of the technique is that a group of CW tunable laser sources are required, since the number of the filter taps is equal to the number of optical wavelengths. The use of a tunable laser array makes the system bulky and costly.

In fact, a multiwavelength erbium-doped fiber laser (EDFL) or a spectrum-sliced broadband optical source can be employed as the optical source in the photonic microwave delay-line filter to provide multiple taps. An EDFL for stable lasing of large number of multiwavelength has been intensively investigated [235-236]. Regular uniformly-spaced photonic microwave delay-line filters using a multiwavelength EDFL [235] and a spectrum-sliced broadband optical source [237-238] have been proposed and demonstrated. Since a single optical source is used in the photonic microwave filter, the system is more compact with greatly reduced cost. On the other hand, since the wavelength spacing in the multiwavelength EDFL or the sliced broadband spectrum is usually identical, to achieve equivalent complex tap coefficients for the photonic microwave filter, a nonuniform tapped delay-line device providing user-defined weights and time delays for different taps is required. In this section, our efforts will be directed to the investigation of the use of an SD-CFBG as the nonuniform delay-line device.

II. *Principle*

According to the analysis in Section 4.1.1, the frequency response of a regular uniformly-spaced delay-line FIR filter has multiple channels with each channel having the same spectral response $A(\omega)$. The tap coefficient profile is just the inverse Fourier transform of the desired spectral response in each channel.

As proposed in [234], if the time delay difference between the adjacent taps is nonuniform, the Fourier transform relationship does not exist between the tap coefficients profile and the frequency response of each channel. In this scenario, the impulse response of a nonuniformly-spaced FIR filter can be expressed as

$$h_{non}(t)=\sum_{k=0}^{N-1}\beta_k\delta(t-\tau_k) \tag{4-5}$$

where β_k and τ_k are the tap coefficient and time delay of the kth tap, respectively. The time delay and tap coefficient of each tap can be obtained by modifying the constant time delay difference and the tap coefficient of the regular uniformly-spaced FIR filter with a time delay shifting function $f(t)$ [234],

$$\tau_k = kT - f(\tau_k) \tag{4-6a}$$

$$\beta_k = \left|\frac{a(\tau_k)}{1+f'(\tau_k)}\right| \tag{4-6b}$$

In fact, the nonuniform time delay function $f(t)$ provides a phase modulation to the real tap coefficient profile $a(t)$. Accordingly, the frequency response of the nonuniformly-spaced FIR filter is given by

$$H_{non}(\omega)=\frac{\Omega}{2\pi}\sum_m B_m(\omega-m\Omega) \tag{4-7a}$$

$$B_m(\omega)=\tilde{F}\left\{a(t)\exp\left[jm\Omega f(t)\right]\right\} \tag{4-7b}$$

From (4-7) we can find that the nonuniformly-spaced FIR filter still has a multichannel frequency response. However, the responses of individual channels are no longer identical. By properly designing the tap coefficient profile $a(t)$, the nonuniform time delay shifting function $f(t)$, and the channel order m, an arbitrary bandpass frequency response can be realized at the mth channel with all-positive coefficients via nonuniform tap delay shifting.

The research efforts here will be focused on the design and implementation of a nonuniformly-spaced microwave delay-line FIR filter with the desired bandpass response using an SD-CFBG. Fig 4.3 shows a diagram of a nonuniformly-spaced photonic microwave delay-line FIR filter using an SD-CFBG as the nonuniform delay-line device.

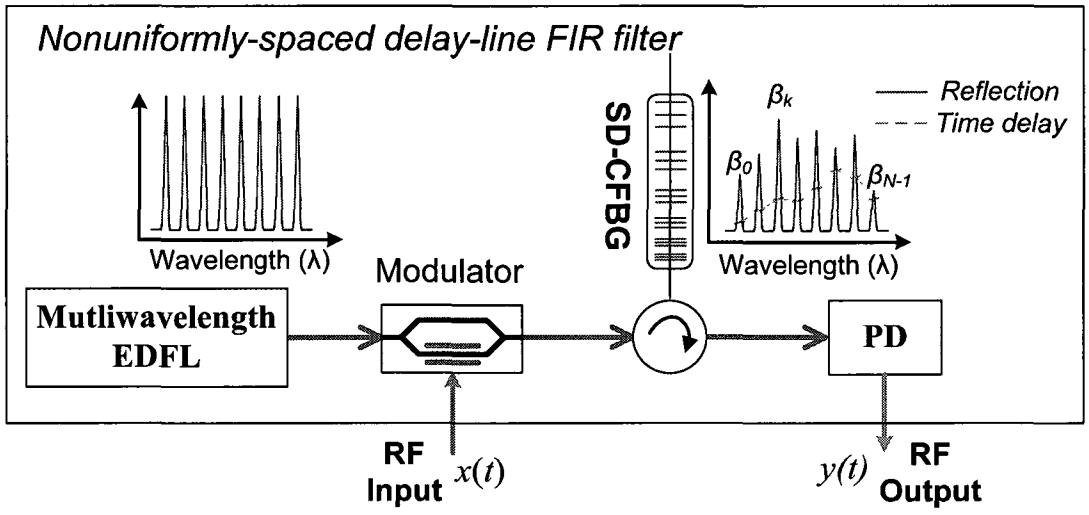

Fig. 4.3. A diagram showing a nonuniformly-spaced photonic microwave delay-line filter by using an SD-CFBG. EDFL: erbium-doped fiber laser, SD-CFBG: spatially-discrete chirped fiber Bragg grating, PD: photodetector.

We start the design of the nonuniformly-spaced FIR filter from the desired bandpass frequency response $A(\omega)$ (with both magnitude and phase responses). First, by calculating the inverse Fourier transform of the desired bandpass response $A(\omega)$, we can obtain the tap coefficients profile $a(t)$, which can be complex valued with the amplitude $|a(t)|$ and the phase $\theta(t)$, of the regular uniformly-spaced FIR filter. Second, choose the order of channel m, which could be any non-zero value. Then the nonuniform time delay shifting function can be obtained as [234]

$$f(t)=\frac{\theta(t)}{m\Omega} \tag{4-8}$$

Finally, the tap coefficient and time delay of the nonuniformly-spaced FIR filter can be obtained from $a(t)$ and $f(t)$ according to (4-6). The frequency response of the mth channel of the produced nonuniformly-spaced FIR microwave filter $B_m(\omega - m\Omega)$ will provide the desired bandpass frequency response.

If a multiwavelength optical source with identical wavelength spacing is used to provide multiple filter taps, a nonuniform delay-line device is required to provide the user-defined tap coefficients and time delays.

As we have discussed in Section 3.1.4, an SD-CFBG can be designed to have multi-channel spectral response and provide user-defined time delays for individual channels. Therefore, the SD-CFBG can be employed in the nonuniformly-spaced FIR delay-line filter as the tapped delay-line device. According to (3-38), the time delay of the kth tap introduced by the SD-CFBG can be expressed as

$$\tau_k = k\frac{\lambda_\Delta}{C} \times \frac{2n_{eff}}{c} + \sum_{i=1}^{k} d_i \times \frac{2n_{eff}}{c} \tag{4-9}$$

where λ_Δ is the constant wavelength spacing between the adjacent reflection channels of the SD-CFBG, n_{eff} is the effective refractive index of the fiber core, c is the light speed in vacuum, C is the chirp rate of the grating, and d_i is the fiber shifting function [135]. By comparing (4-9) with (4-6a), we can determine the SD-CFBG parameters from the required FIR filter parameters, such as the filter FSR Ω, and the nonuniform time shifting function $f(t)$

$$\lambda_\Delta = T\frac{C \times c}{2n_{eff}} \tag{4-10a}$$

$$\sum_{i=1}^{k} d_i \times \frac{2n_{eff}}{c} = -f(\tau_k) \qquad (4\text{-}10b)$$

Moreover, the SD-CFBG can be also designed to arbitrarily control the reflectivity of each channel to achieve the required tap coefficients of nonuniformly-spaced FIR filter according to (4-6b). Therefore, the SD-CFBG can be employed in the nonuniformly-spaced photonic microwave delay-line filter as a tapped delay-line device to achieve the arbitrary magnitude and phase response.

III. *Results*

The nonuniformly-spaced microwave delay-line filter using an SD-CFBG is investigated by numerical simulations. As an example, a bandpass microwave filter with a flat-top magnitude response and a quadratic phase response (linear time delay response) is designed and analyzed, which can be applied in chirped microwave pulse generation [214] and compression [138].

In the simulation, we assume that the desired bandpass filter has a central frequency of f_0 = 10 GHz, and a FWHM bandwidth of 5 GHz. We also assume that the slope of the time delay response is -0.5 ns/GHz. Fig. 4.4 shows the desired magnitude and time delay response of the bandpass filter of interest.

Based on the filter design procedure described above, a nonuniformly-spaced FIR filter with all-positive tap coefficients is designed. The designed filter has 25 taps. The tap coefficients β_k and the time delays τ_k are calculated based on (4-6), with the results plotted in Fig. 4.5. We can see that the tap coefficients are all positive and the time delays are nonuniformly spaced (the time delays is no longer a linear function of tap numbers).

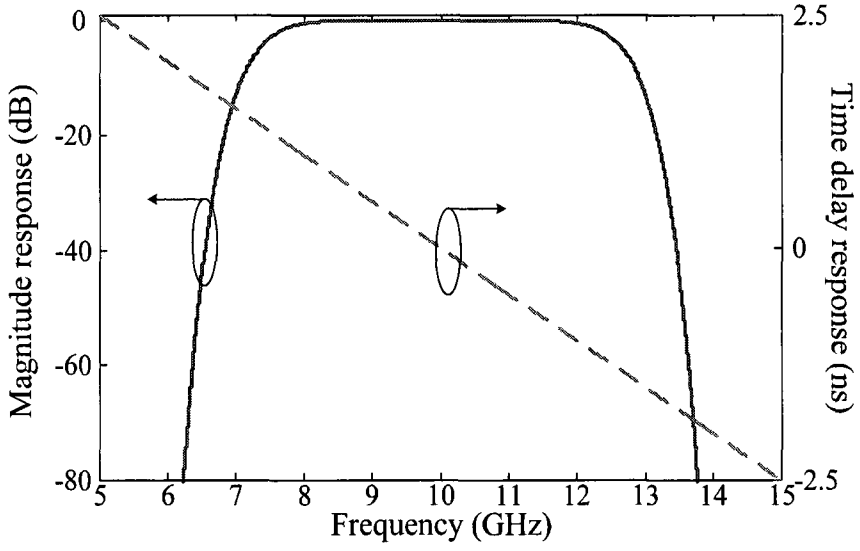

Fig. 4.4. The frequency response of the desired bandpass filter.

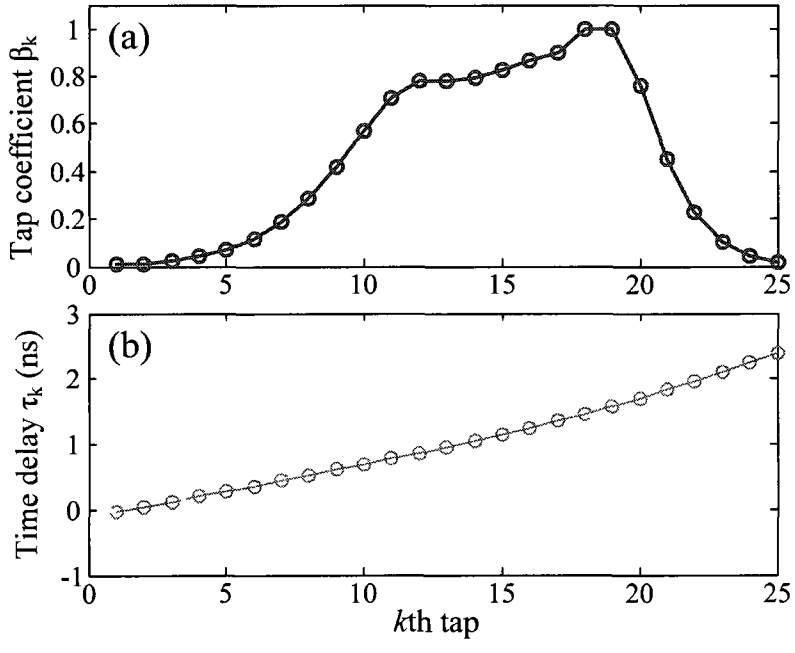

Fig. 4.5. The tap coefficients (a) and time delays (b) of the designed nonuniformly-spaced FIR filter.

It is worth pointing out that the channel order m can be any non-zero value. Here $m = 1$ (first-order channel) is selected. Then frequency response of the designed filter can be calculated by the Fourier transform of (4-5),

$$H_{non}(\omega) = \tilde{F}[h_{non}(t)] = \sum_k \beta_k \exp(-j\tau_k \omega) \tag{4-11}$$

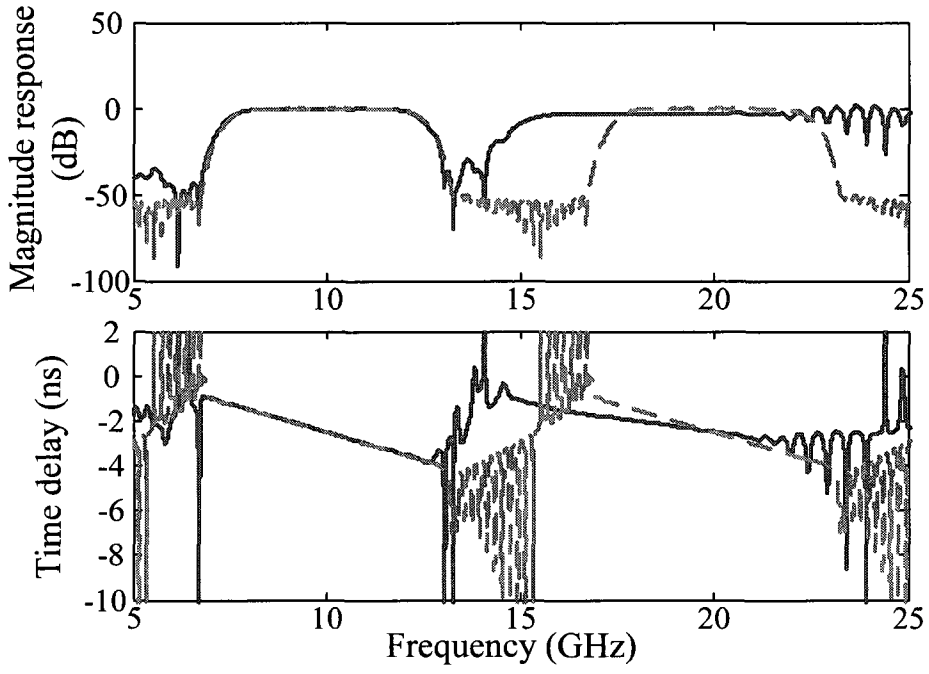

Fig. 4.6. The calculated frequency responses (both magnitude and time delay) of the nonuniformly-spaced FIR filter (solid lines) and the regular uniformly-spaced FIR filter (dashed lines)

The calculated frequency responses are shown in Fig. 4.6. The desired magnitude and time delay phase responses are obtained in the first-order channel. The frequency responses of a regular uniformly-spaced delay-line FIR filter that is designed to realize the same bandpass response are also plotted in Fig. 4.6 in dashed lines for comparison. We can see that for the regular FIR filter, the frequency responses at different channels are identical. However, a nonuniformly-spaced FIR filter has different frequency responses at different channels. In the first-order channel, the two filters have the identical frequency responses, in both magnitude and phase.

In this research work, a multiwavelength optical source with identical wavelength spacing is used to provide multiple filter taps. Then an SD-CFBG is designed and employed as the tapped delay-line device to achieve the required tap coefficients and nonuniform time delays. We assume that the wavelength spacing is λ_Δ = 0.5 nm. To achieve 25 filter taps, a chirped phase mask with a bandwidth of 13 nm is required to fabricate the grating. The fiber shifting function d_i is calculated according to (4-10) and the grating refractive index modulation function is determined by the required tap coefficients according to (4-6).

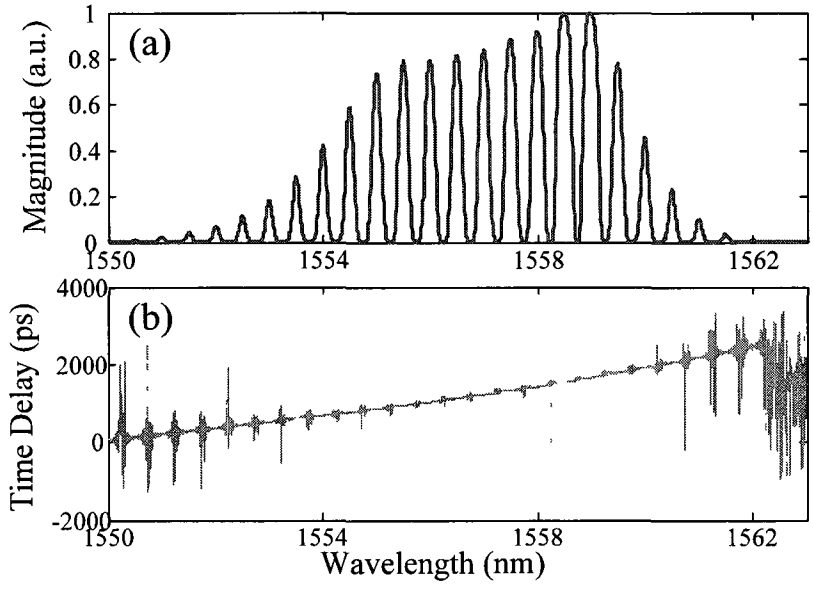

Fig. 4.7. (a) Simulated reflection spectral response and (b) the group delay response of the designed SD-CFBG.

Fig. 4.7 shows the reflection spectral response and the group delay response of the designed SD-CFBG. We can see that multichannel response with the desired reflectivity and wavelength spacing is obtained. By properly designing the fiber shifting function, a discrete (jumped) group delay response is also achieved. By comparing with Fig. 4.5, the required tap coefficients and nonuniform time delays are obtained by the single SD-CFBG. Therefore, a nonuniformly-

spaced FIR filter with flat-top magnitude response and quadratic phase response (linear time delay response) can be implemented using a multiwavelength optical source and the designed SD-CFBG.

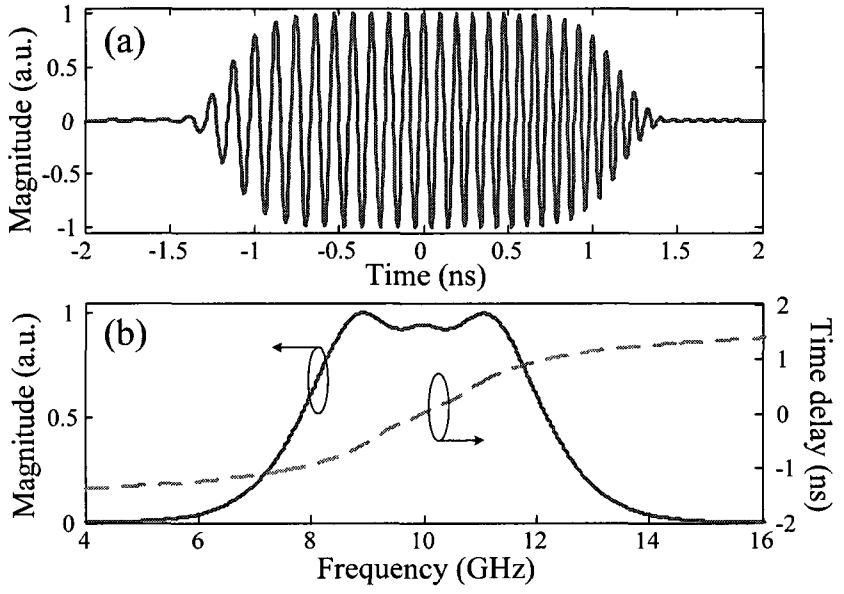

Fig. 4.8. (a) The temporal shape and (b) the spectrum of the input linearly chirped microwave pulse to be compressed.

The compression of a linearly chirped microwave pulse using the designed nonuniformly-spaced FIR filter with a flat-top magnitude response and a quadratic phase response is also investigated. Consider a linearly chirped super-Gaussian microwave pulse with a FWHM of 2.5 ns and a chirp rate of 0.5 GHz/ns. The temporal waveform and the spectrum of the input linearly chirped microwave pulse are plotted in Fig. 4.8(a) and (b), respectively. The designed nonuniformly-spaced photonic microwave delay-line filter has a nonlinear phase response that is opposite to the chirp profile of the input chirped microwave pulse. Therefore, when the input chirped microwave pulse is passing through the microwave filter, the pulse is compressed. Fig.

4.9 shows the compressed microwave pulse at the output of the designed photonic microwave filter. A compression ratio of 10 is achieved.

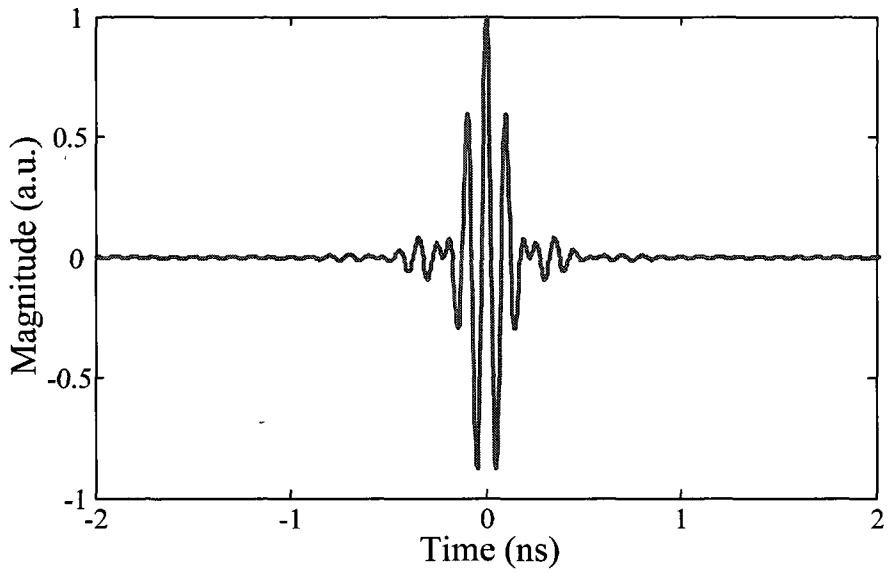

Fig. 4.9. The compressed pulse at the output of the designed photonic microwave filter.

IV. *Conclusion*

A nonuniformly-spaced photonic microwave delay-line filter using an SD-CFBG was investigated in this research work. The SD-CFBG was designed to have a multichannel reflection spectral response and a discrete (jumped) group delay response. The produced SD-CFBG was employed in the photonic microwave filter to simultaneously control the tap coefficients and the time delays. A nonuniformly-spaced photonic microwave delay-line filter with flat top magnitude response and quadratic phase response using an SD-CFBG was designed. The application of the designed filter in chirped microwave pulse compression was also investigated. Instead of using a tunable laser array and a coil of dispersive fiber [233], the use of a multiwavelength optical source and an SD-CFBG in the nonuniformly-spaced photonic microwave makes the system simplified with a greatly reduced cost.

4.2. Photonic microwave filter based on optical filter response to microwave filter response conversion.

This section is a revised version of the following published paper.

Article title: Chirped microwave pulse compression using a photonic microwave filter with a nonlinear phase response

Authors: Chao Wang, and Jianping Yao

Published in IEEE Transactions on Microwave Theory and Techniques, vol. 57, no. 2, pp. 496-504, Feb. 2009.

The major limitation of the microwave waveform processing technique presented in Section 4.1 is that a multiwavelength source is required to build the multi-tap delay-line filter, since the tap number of the filter is determined by the number of optical wavelengths, which may make the system bulky and costly. In this section, a photonic microwave filter with a used-defined filter response using only a single optical wavelength based on optical filter response to microwave filter response conversion is proposed and experimentally demonstrated.

I. *Introduction*

The proposed photonic microwave filter is implemented based on optical filter response to microwave filter response conversion by using a SSB modulator and an FBG. The FBG acts as an optical spectral filter that is designed to have user-defined magnitude and phase response. The optical filter response is then transferred to the response of the photonic microwave filter through SSB modulation and heterodyne detection at a high-speed photodetector. Therefore, by

appropriately designing the spectral characteristics of the FBG, a photonic microwave filter with the desired magnitude and phase response is realized. In this section, the principle of the proposed photonic microwave filter is first described. Its application in chirped microwave pulse compression is investigated in much detail. Numerical simulation and experimental demonstration are both performed to verify the proposed approach.

II. *Principle*

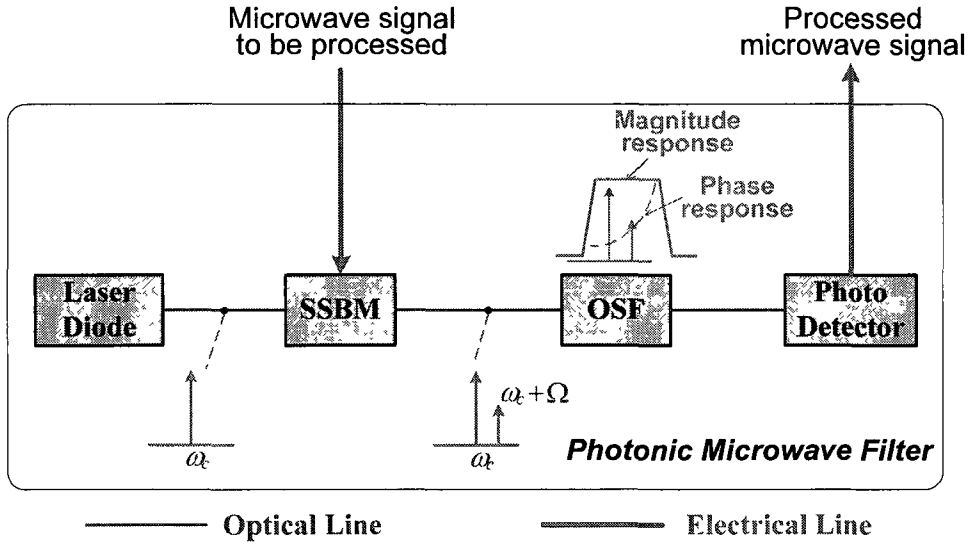

Fig. 4.10. Schematic diagram of the proposed photonic microwave filter based on optical filter response to microwave filter response conversion. SSBM: single-sideband modulator; OSF: optical spectral filter.

The schematic diagram of the proposed photonic microwave filter based on optical filter response to microwave filter response conversion is shown in Fig. 4.10. In the system, a CW light from an LD is fiber coupled to an optical single-sideband modulator (SSBM), which is driven by an input microwave waveform to be processed. The modulated optical field has a single-sideband format. The carrier and one sideband are then sent to an optical spectral filter (OSF) where different magnitude and phase responses are applied to the carrier and the sideband. The magnitude spectra of the optical field components and optical filter response are

also schematically illustrated in Fig. 4.10. The output microwave signal is recovered via the heterodyne beating between the carrier and the sideband at a high-speed PD.

We start our analysis by assuming that the input microwave signal has a single RF angular frequency Ω, which is also appropriate for comparison with the swept-frequency measurements performed in the experimental demonstration. If the optical carrier with a angular frequency ω_c is modulated by the microwave signal in the single-sideband modulator, under small-signal modulation conditions, the single sideband intensity modulation can be regarded as a narrowband linear modulation, and the spectrum of the modulated optical signal has two major frequency components: the optical carrier ω_c and one first-order sideband $\omega_c + \Omega$. The single-sideband modulated optical field can then be described by

$$E_{SSB}(t) = A\exp(j\omega_c t) + B\exp[j(\omega_c + \Omega)t] \tag{4-12}$$

where A and B denote the amplitudes of the optical carrier and the single sideband, which are determined by the DC bias of the modulator and the power of input microwave signal. Without loss of generality, the upper sideband $\omega_c + \Omega$ is chosen in our treatment.

An optical filter with a transfer function of $\rho(\omega) = |\rho(\omega)|\exp[j\theta(\omega)]$ is then used to modify the amplitudes and phases of the optical carrier and the sideband. The optical field at the output of the filter is given by

$$\begin{aligned} E_{SSB}(t) = &|\rho(\omega_c)|A\exp\left[j\omega_c t + j\theta(\omega_c)\right] \\ &+|\rho(\omega_c + \Omega)|B\exp\left[j(\omega_c + \Omega)t + j\theta(\omega_c + \Omega)\right] \end{aligned} \tag{4-13}$$

where $|\rho(\omega)|$ and $\theta(\omega)$ represent the frequency-dependent magnitude and phase response of the optical filter, respectively.

The electrical current at the output of the photodetector is proportional to the intensity of the input electrical field, which is given by

$$I(t) \propto \left|E_{SSB}(t)\right|^2 = \frac{1}{2}\left|\rho(\omega_c)\right|^2 A^2 + \frac{1}{2}\left|\rho(\omega_c+\Omega)\right|^2 B^2 + \left|(\omega_c)\right|\left|\rho(\omega_c+\Omega)\right| AB\cos\left[\Omega t + \theta(\omega_c+\Omega) - \theta(\omega_c)\right] \tag{4-14}$$

Note that all high-order harmonic components are ignored in (4-14) considering the fact that the high-order harmonic components will be filtered out due to the limited bandwidth of the photodetector. It can be seen from (4-14) that the first and second terms on the right-hand side are dc components, and the third term is the recovered microwave signal.

Considering that the input microwave signal is $\cos(\Omega t)$, we can easily get the transfer function of the system by comparing the recovered signal with the input microwave signal.

$$\left|H(\Omega)\right| \propto \left|\rho(\omega_c)\right|\left|\rho(\omega_c+\Omega)\right| \tag{4-15a}$$

$$\Psi(\Omega) = \theta(\omega_c+\Omega) - \theta(\omega_c) \tag{4-15b}$$

where $|H(\Omega)|$ and $\Psi(\Omega)$ are, respectively, the magnitude and the phase responses of the developed photonic microwave filter. From (4-15a) we can see that the magnitude response of the microwave filter is only determined by the magnitude response of the optical filter. The phase response of the microwave filter, from (4b), is thus the optical phase difference between the optical carrier and the sideband in the optical phase filter. Therefore, by appropriately design

the magnitude response and the phase or group delay characteristics of the optical phase filter, we are able to create a photonically implemented microwave filter with a desired magnitude and phase response.

III. *Photonic microwave matched filter for chirped microwave pulse compression*

III.1. Introduction to chirped microwave pulse compression

Microwave pulse compression technique using frequency-chirped pulses has been widely used in modern radar systems to improve the radar range resolution [217]. Pulse compression is usually implemented at the radar receiver end via correlation or matched filtering. To implement pulse compression for a high-frequency and broadband chirped microwave pulse, optical techniques would be utilized.

In this section, chirped microwave pulse compression using the presented photonic microwave filter with a nonlinear phase response is investigated. In the proposed system, a photonic microwave filter with a nonlinear phase response that is opposite to the chirp profile of the input chirped microwave pulse is used. When the input pulse is passing through the microwave filter, the pulse is compressed. The principle is similar to dispersion compensation in an optical communication system, where a chirped FBG with an opposite chromatic dispersion is used to compress an optical pulse that is dispersed due to the dispersion of the fiber link [239].

III.2. Design of a photonic microwave filter for chirped microwave pulse compression

To compress a chirped microwave pulse, the microwave filter should have a nonlinear phase response that is opposite to the chirp profile of the input microwave pulse. The group delay introduced by the microwave filter can be obtained from the filter phase response by

$$\tau_{RF}(\Omega)=\frac{d\Psi(\Omega)}{d\Omega} \tag{4-16}$$

In other words, the microwave filter can be regarded as a dispersive microwave device, which has a group delay response or a chromatic dispersion that is opposite to that of the input chirped microwave signal, leading to the microwave pulse compression. The operation is similar to optical pulse compression by dispersion compensation in an optical communication system [239].

As a simple example, we consider the compression of a linearly frequency-modulated (or linearly chirped) microwave signal, which is the most commonly used pulsed signal in modern radar systems [127]. Mathematically, an amplitude-normalized linearly chirped microwave pulse with a Gaussian envelope can be expressed as

$$s(t)=\exp\left(-\frac{t^2}{2T_0^2}\right)\exp\left[j\left(\Omega_0 t+\frac{ut^2}{2}\right)\right] \tag{4-17}$$

where T_0 is the width of the pulse at the $1/e$ maximum, Ω_0 is the central microwave angular frequency, $|u|=B/T_0$ is the signal frequency chirp parameter, B is the overall frequency bandwidth. The reason we select a Gaussian pulse rather than a normal rectangular pulse is that a Gaussian pulse has inherently low correlation sidelobes.

The frequency domain expression of the linearly chirped Gaussian signal can be obtained by the following Fourier transform,

$$\tilde{S}(\Omega)=\tilde{F}\left[s(t)\right]=\left(\frac{2\pi T_0^2}{1-jP}\right)^{1/2}\exp\left[-\frac{(\Omega-\Omega_0)^2 T_0^2}{2(1-jP)}\right] \tag{4-18}$$

where $\widetilde{F}(\cdot)$ denotes the Fourier transform operation. Here for simplicity, we introduce a new notation $P = uT_0^2$, which is the time-bandwidth product of the linearly chirped microwave signal.

It is known that the group delay of the linearly chirped microwave signal is a linear function with respect to the instantaneous microwave frequency. According to (4-16), to compress the linearly chirped microwave signal, a microwave filter with an opposite linear group delay response, or equivalently, a quadratic phase response is required. According to (4-15b), this can be obtained by setting the optical phase filter with a quadratic phase response. A detailed analysis on the design of the optical filter with the required phase response for the linearly chirped microwave pulse compression will be discussed later in this section. Here we firstly consider a microwave filter with a quadratic phase response, given by

$$\Psi(\Omega) = D_2\Omega^2 + D_1\Omega + D_0 \tag{4-19}$$

where D_0 is a constant phase shift, $D_1 = d\Psi/d\Omega$ is a frequency-independent group delay introduced by the filter, and $D_2 = d^2\Psi/d\Omega^2$ is the dispersion parameter of the microwave filter. Since the first two terms (D_0 and D_1) will not affect the operation of the pulse compression, only the third term (D_2) will be considered here.

The transfer function of the microwave filter with only the third term in (4-19) being considered is given as $H(\Omega) = |H(\Omega)|\exp[jD_2\Omega^2]$. When the linearly chirped signal is passing through the filter, we have the filtered microwave signal, $r(t)$, which is given by

$$r(t) = \tilde{F}^{-1}\left[\tilde{S}(\Omega)H(\Omega)\right]$$
$$= \frac{\left|\rho(\omega_c)\right|^2 T_0}{\left[T_0^2 - jD_2(1-jP)\right]^{1/2}} \times \exp\left\{-\frac{(1-jP)t^2}{2\left[T_0^2 - jD_2(1-jP)\right]} + j\Omega_0 t\right\} \tag{4-20}$$

Therefore, the filtered microwave signal maintains its Gaussian shape but with a compressed pulse width. Let T_1 represent the pulse width of the signal after passing through the microwave filter. Then the pulse compression ratio γ is given by

$$\gamma = \frac{T_0}{T_1} = \left[\left(1 - \frac{D_2 P}{T_0^2}\right)^2 + \left(\frac{D_2}{T_0^2}\right)^2\right]^{-1/2} \tag{4-21}$$

According to (4-21), the compression only occurs when the microwave filter has an opposite dispersion with respect to that of the input chirped microwave pulse, i.e., $D_2 u > 0$. The pulse reaches the maximum compression when the chirp of the input pulse is completely cancelled by the dispersion of the filter. Mathematically, for an input chirped microwave signal with a given chirp, the maximum compression factor occurs when the following condition is satisfied,

$$D_{2opt} = \frac{P}{1+P^2} T_0^2 \tag{4-22}$$

where D_{2opt} (in ns^2) denotes the optimal microwave filter dispersion parameter required for a maximal compression of a linearly chirped microwave pulse with a time-bandwidth product P and a pulse-width T_0. Equation (4-22) gives us a guideline for the design of a microwave filter with an optimal phase response for a given linearly chirped microwave pulse. According to (4-22), the maximum compression ratio can be calculated by

$$\gamma_{\max} = \left(1 + P^2\right)^{1/2} \tag{4-23}$$

For $P >> 1$, which is always true for a highly chirped microwave pulse, we have $\gamma_{\max} \cong P$. This demonstrates that the maximum compression ratio is equal to the time-bandwidth product of the input linearly chirped microwave signal. Therefore, the technique presented here has an equivalent compression performance to that of a complex matched filter, which is widely used in radar systems [217].

III.3. Different types of microwave matched filters

It is worth pointing out that not only the filter phase response but also the filter magnitude response may determine the filter performance for chirped microwave pulse compression. Among the many filter performance measures [240], the pulse compression ratio (PCR), the signal-to-noise ratio (SNR), and the sidelobe suppression ratio (SSR) are the three most important measures that define the performance of a matched filter.

Given an input signal $s(t)$ embedded in an additive Gaussian white noise $n(t)$, the output signal $y(t)$ of the filter is given by $y(t) = h(t) * [s(t) + n(t)]$, where $*$ denotes the convolution operation.

It is known that the use of a classical complex matched filter (CMF) would optimize the SNR for pulse compression [217]. Mathematically, a CMF is defined as

$$H_{CMF}(\Omega) = S^*(\Omega) = |S(\Omega)| \exp\left\{-i\Phi\left[S(\Omega)\right]\right\} \tag{4-24}$$

where $S(\Omega)$ is the Fourier transform of $s(t)$, $\Phi[S(\Omega)]$ is the phase term of $S(\Omega)$. If only the phase information is kept, the CMF becomes a phase-only filter (POF), with its transfer function is given by

$$H_{POF}(\Omega)=\frac{S^*(\Omega)}{|S(\Omega)|}=\exp\{-i\Phi[S(\Omega)]\} \tag{4-25}$$

An inverse filter provides the narrowest output pulse; therefore, the PCR can be maximized. The key difficulty in using an inverse filter for pulse compression is its extremely high sensitivity to noise. A solution to the problem is to modify the filter design, to introduce a filter with a good trade-off between the noise robustness and the PCR [217]. A modified inverse filter (MIF) can then be expressed as

$$H_{MIF}(\Omega)=\frac{K}{|S(\Omega)|+Q}\exp\{-i\Phi[S(\Omega)]\} \tag{4-26}$$

where K and Q are two non-zero constants which are selected to optimize the correlation performance. Q is also useful in designing the filter to avoid taking an inverse of a zero-value.

Note that all the three matched filters have the same phase response, which is complementary to the phase information of the input signal $s(t)$ and can be determined by (4-19) and (4-22). Different amplitude modulation schemes are required to implement the desired matched filters.

III.4. Design of FBG as an optical spectral filter

In the proposed system, an FBG is employed as the optical spectral filter as shown in Fig. 4.10. The FBG is designed to have a phase response, which is transferred to the microwave filter with

the desired phase response for chirped microwave pulse compression, according to (4-15b). As a simple example, to realize pulse compression of a linearly chirped microwave signal shown in (4-17), the microwave filter with a linear group delay is required, according to (4-16). Equation (4-16) can then be rewritten as

$$\begin{aligned}\tau_{RF}(\Omega) &= \frac{d\Psi(\Omega)}{d\Omega} = \lim_{\Delta\Omega\to 0}\frac{\theta(\omega_c+\Omega+\Delta\Omega)-\theta(\omega_c+\Omega)}{\Delta\Omega} \\ &= \left.\frac{d\theta(\omega)}{d\omega}\right|_{\omega_c+\Omega} = \tau(\omega_c+\Omega)\end{aligned} \tag{4-27}$$

where $\tau(\omega_c+\Omega)$ is the frequency-dependent optical group delay experienced by the remaining sideband $\omega_c+\Omega$ in the FBG filter.

According to (4-27), the FBG with a highly linear optical group-delay response within a narrow bandwidth from ω_c to $\omega_c+\Omega$ would enable the implementation of a microwave filter with a linear group-delay response. To efficiently compress the input linearly chirped microwave pulse, the optical group delay response, or the optical dispersion of the FBG must be properly designed according to the characteristics of the input microwave pulse, such as the chirp parameter u and the frequency bandwidth B, to satisfy the desired microwave filter dispersion coefficient given by (4-22). According to (4-27), the required optical dispersion parameter d (in ps/nm) of the FBG is determined by the input microwave pulse chirp profile, and is expressed as

$$d = -\frac{c}{2\pi\lambda_c^{\,2}n}\frac{T_0}{B} = -\frac{c}{2\pi\lambda_c^{\,2}n}\frac{1}{u} \tag{4-28}$$

where λ_c is the optical carrier wavelength, n is the refractive index of the FBG, T_0 is the width of the input pulse, B is the pulse bandwidth, $|u| = B/T_0$ is the signal frequency chirp parameter.

On the other hand, the magnitude response of the matched filter, as described by (4-24), (4-25) or (4-26), can be implemented by designing the magnitude response of the FBG according to (4-15a). In the fabrication of the FBG, a properly designed refractive index modulation function will enable to achieve the desired amplitude transmission. Such an FBG reconstruction problem can be solved by inverse scattering algorithms, such as the DLP algorithm [115]. Therefore, a single optical component (an FBG) enables both the phase and amplitude modulations. The use of the FBG in a system with SSB modulation and heterodyne detection would achieve a photonic microwave matched filter with the required phase and magnitude responses.

IV. *Simulation results*

The proposed approach is first verified by numerical simulations, in which the compression of a linearly chirped microwave pulse with a rectangular envelope is considered. The central frequency of the chirped microwave pulse is $\Omega_0 = 2\pi \times 40$ GHz, the pulse width is $T_0 = 4$ ns, and the bandwidth is $B = 20$ GHz. Therefore the TBWP of the pulse is 80, and the chirp rate of the pulse is $u = 5$ GHz/ns. To compress this chirped microwave pulse, the grating should have a chromatic dispersion of $d = -2700$ ps/nm according to (4-28).

The spectrum of the input pulse shown in Fig. 4.11 is obtained by the Fourier transform (magnitude only). To cover the whole bandwidth of the input pulse (around 30 GHz), an LCFBG with a bandwidth greater than 0.24 nm is required.

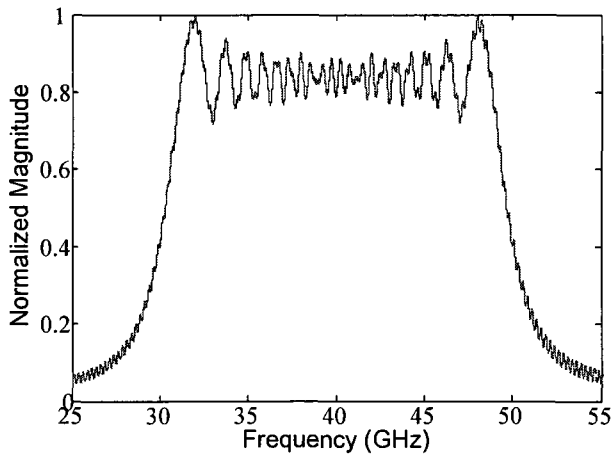

Fig. 4.11. Normalized magnitude spectrum of the linearly chirped microwave pulse with a TBWP of 80.

If no amplitude modulation is needed, the developed microwave filter is a POF, which is implemented by using an LCFBG with a linear group delay response and a flat magnitude response. Fig. 4.12(a) shows the design of an LCFBG using the DLP algorithm for the implementation of the POF. In the simulations, a 30-cm long LCFBG having a dispersion of -2700 ps/nm and a bandwidth of 0.4 nm is considered.

To implement a CMF, the LCFBG should have a magnitude response that is identical to that of the input signal. The grating reconstruction is also calculated based on the DLP algorithm. A similar treatment is applied to the design of an LCFBG for the implementation of an MIF. In the simulation, $Q = 0.2$ is selected to overcome the indeterminate condition caused by taking an inverse of a zero value; $K = 0.15$ is selected to ensure that the filter gain is less than unity. The designs of the LCFBGs for the CMF and the MIF are shown in Fig. 4.12(b) and (c), respectively. In all the three cases, a large dispersion of -2700 ps/nm in the LCFBGs is needed. The LCFBGs should have a length as long as 30 cm, which can be realized with the current FBG fabrication technology. In fact, an LCFBG with a length up to 1 m has been demonstrated [241]. In addition, a long grating length would make it easier to control the magnitude response.

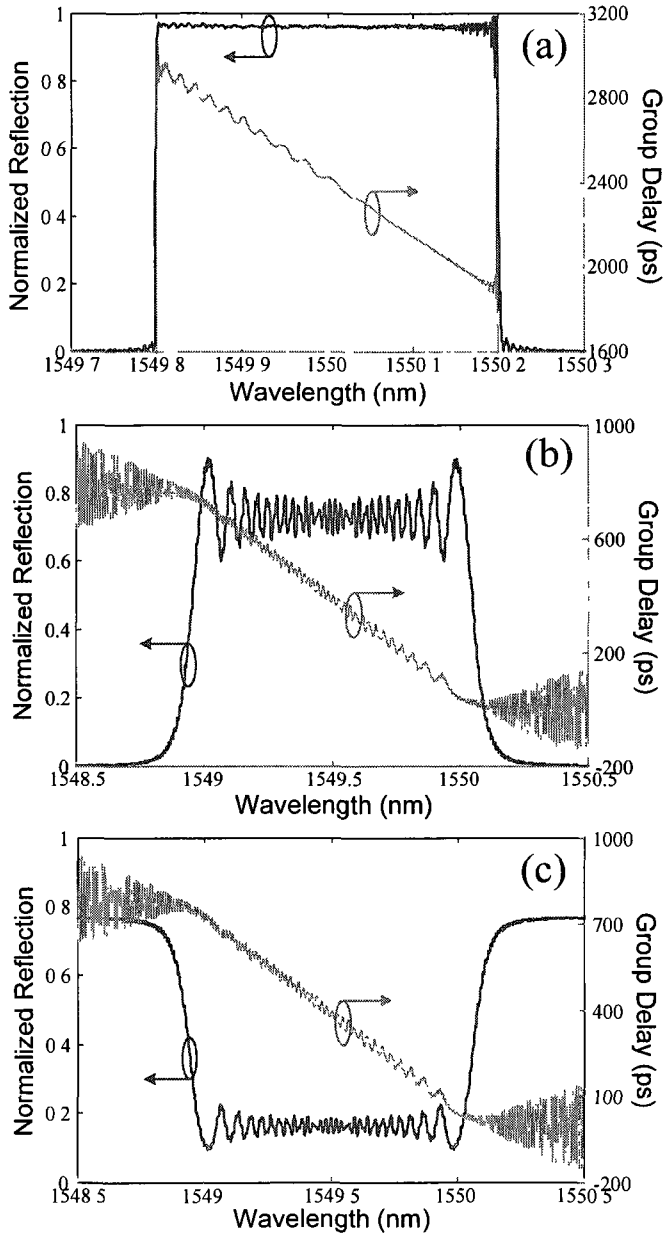

Fig. 4.12. Reflection magnitude response and group-delay response of the LCFBGs for the implementation of (a) a POF, (b) a CMF, and (c) an MIF.

By incorporating the produced LCFBGs into the system as shown in Fig. 4.10, microwave matched filters, including the POF, the CMF, and the MIF can then be realized. When a linearly chirped microwave pulse is passing through the filters, the pulse is compressed. Fig. 4.13(a) shows the compressed pulses at the outputs of the three matched filters. The performance

measures of both PCR and SSR for the filters are compared and listed in Table 4.1. It is shown that the CMF has a poor SSR and the MIF is the optimal filter for both the PCR and SSR.

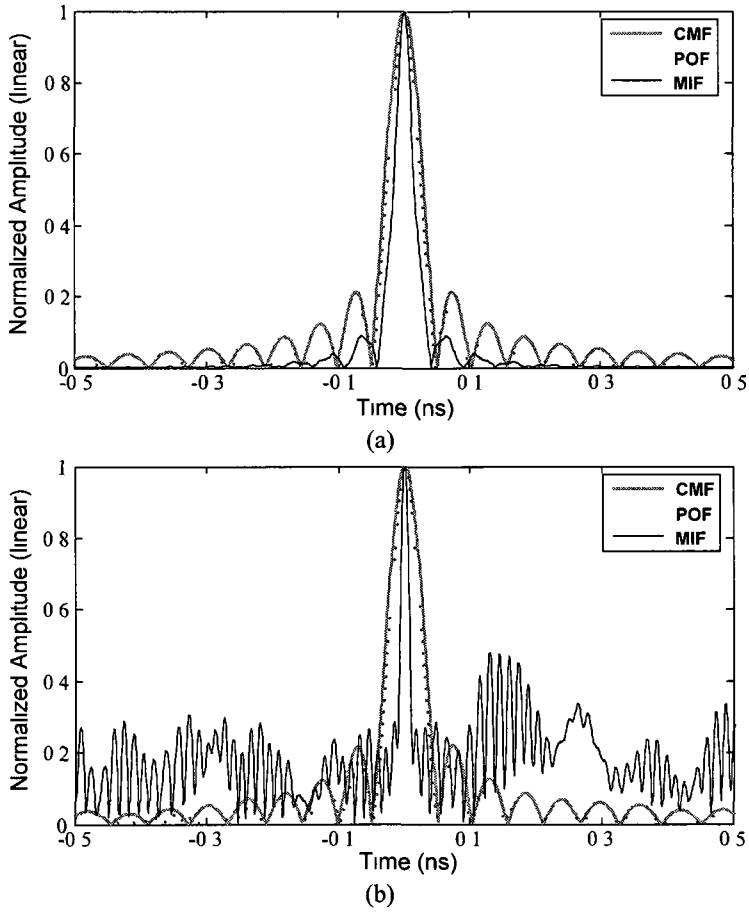

Fig 4 13 Correlations outputs of the three filters for (a) a noise-free chirped microwave pulse, and (b) a chirped microwave pulse with an additive white Gaussian noise (The correlation peak height is normalized)

To investigate the noise robustness of the filters, an additive white Gaussian noise is added to the linearly chirped microwave signal with an SNR of 30 dB. The compressed pulses at the outputs of the filters are shown in Fig. 4.13(b) A performance comparison is also listed in Table 4 1 It is obviously seen that a smooth correlation at the output of the CMF is maintained and hence the CMF provides the best output SNR. On the other hand, for the input signal with noise, the MIF presents a significantly deteriorated correlation performance. We can also find

that the POF exhibits a moderate performance when compared with the other two filters against all the three performance measures.

TABLE 4.1. PERFORMANCE MEASURES FOR DIFFERENT FILTERS

Filters	Filter Performances				
	PCR (noise free)	***PCR (noisy)***	***SSR (noise free)***	***SSR (noisy)***	***Noise Robustness***
CMF	67	65.5	6.71 dB	6.67 dB	optimal
POF	77	73.9	7.87 dB	7.82 dB	good
MIF	121	-	10.45 dB	-	poor

V. *Experimental results*

V.1. Experimental setup

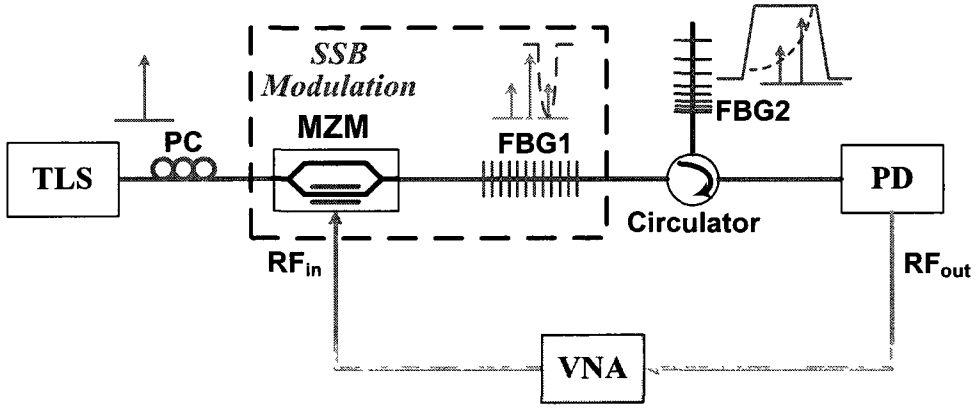

Fig. 4.14. Experimental setup of the proposed system. TLS: tunable laser source; PC: polarization controller; MZM: Mach-Zehnder modulator; FBG: fiber Bragg grating; VNA: vector network analyzer; PD: photodetector.

A proof-of-concept experiment is then carried out to verify the proposed technique. The experimental setup shown in Fig. 4.14 is built, which consists of a tunable laser source, an MZM, two FBGs, and a high-speed photodetector. The tunable laser source has a wavelength tunable range from 1520 to 1620 nm and a wavelength resolution of 1 pm, which is used as the

optical source to produce a CW optical carrier. A polarization controller connected before the MZM is used to adjust the polarization state of the optical carrier to the MZM, to minimize the polarization-dependent loss. The swept-frequency microwave signal generated by a vector network analyzer (VNA) is applied to the MZM via its RF port. At the output of the MZM, the modulated optical signal consisting of an optical carrier and two sidebands is generated.

To realize single-sideband modulation, a narrow band FBG, FBG1, with very high reflectivity is used as an optical bandstop filter to suppress one sideband while transmitting both the optical carrier and the other sideband without introducing any additional magnitude and phase distortions. Although single-sideband modulation using a dual-drive modulator and a microwave phase shifter has been developed [242], our double-sideband modulation + bandstop FBG approach is a promising alternative with the features of low cost and easy to implement. Experimental result shows that a sideband suppression ratio as high as 50 dB is realized by using a regular MZM and a strong narrow band FBG. The second FBG, FBG2, is properly designed to have a phase response to introduce magnitude and phase changes to both the optical carrier and the remaining single sideband. The microwave signal is then recovered via heterodyne detection at the high-speed photodetector. The frequency response of the photonically implemented microwave filter is characterized by the VNA.

V.2. Phase-only matched filter

In the proposed system as shown in Fig. 4.14, FBG2 can be designed to have a unity magnitude response across the entire passband; therefore the photonically implemented microwave filter is operating as a phase-only matched filter according to (4-25). In practice, the phase-only filter (POF) is the easiest filter to implement since no amplitude modulation is needed. In fact, our

proposed technique enables both the amplitude and phase modulations; therefore other types of filters, such as complex matched filter and modified inverse filter, can also be implemented using this technique. The primary motivation behind the use of phase-only filter is not only the implementation simplicity, but also the better performance as discussed in simulation part, such as higher power efficiency as well as a narrower output peak when compared with the use of a complex matched filter [139].

V.3. FBG as an optical spectral filter

Consider an input linearly chirped microwave pulse having a bandwidth $B = 3$ GHz, a chirp parameter u = -0.8 GHz/ns, which corresponds to a TBWP of 11.25. Therefore, according to (4-28), FBG2 should have a large chromatic dispersion of d = 16770 ps/nm in a 0.024-nm bandwidth. This requirement can be met by using a uniform FBG. Fig. 4.15 shows the reflection spectrum and the group delay response of a fabricated uniform FBG. Both the simulation and experiment results are shown in Fig. 4.15 for comparison. The simulation results, which are obtained by solving the coupled mode equations using the piecewise-uniform matrix approach [154], are shown as dashed lines. Based on the simulation, a uniform FBG with a length of 50 mm, a refractive index modulation of 0.00008, and a central wavelength of 1556.08 nm is then fabricated using a frequency-doubled Argon-Ion laser operating at 244 nm. The measured results are plotted in Fig. 4.15 as solid lines. From Fig. 4.15(b), we can see that in the spectrum down-ramp region (enclosed by a dotted rectangle, around 0.018-nm bandwidth), nearly linear group delay difference of 240 ps is achieved, which is equivalent to an optical dispersion of 13610 ps/nm. As an optical phase filter, the FBG is preferred to have a unity magnitude response. Although the magnitude spectrum is falling off rapidly within the dashed

rectangle, it only has impact on the envelope of the compressed pulse. It is the group delay response that determines the microwave filter performance for pulse compression.

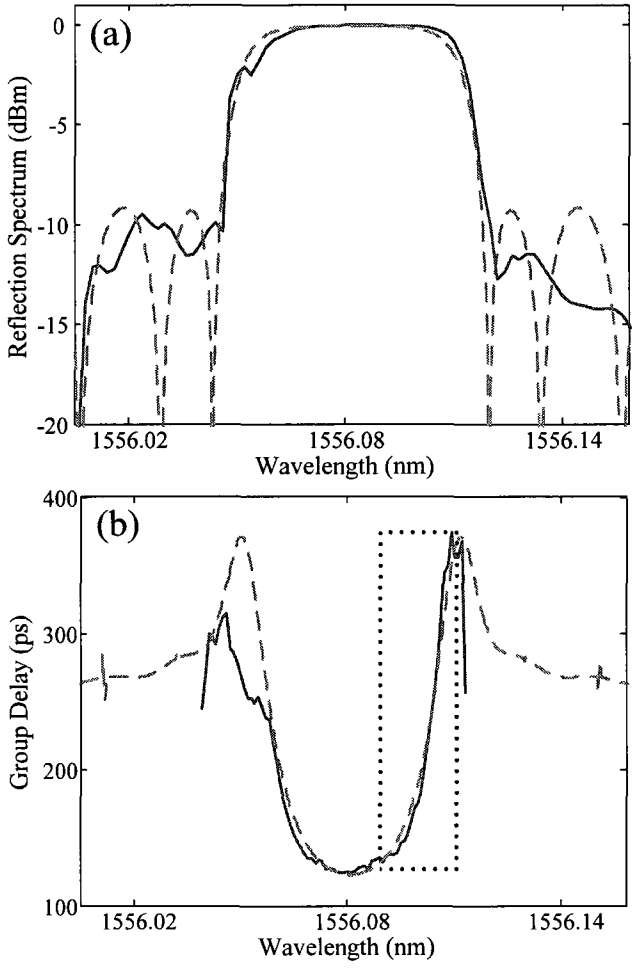

Fig. 4.15. Designed FBG for the implementation of the optical phase filtering. (a) Reflection spectra, (b) group delay responses. (Solid lines: experimental results; dashed lines: simulation results)

Such an FBG with the properly designed group delay response can then be used to build a photonic microwave filter with a quadratic phase response for linearly chirped microwave pulse compression. Note that the realized optical dispersion is not exactly identical to the designed dispersion value. The optical dispersion mismatch may reduce the filter performance for microwave pulse compression, which will be discussed laser.

V.4. Microwave filter with a nonlinear phase response

A microwave filter is experimentally demonstrated using the FBG presented above based on the setup shown in Fig. 4.14. The wavelength of the optical carrier is set at $\lambda_c = 1556.15$ nm. The first FBG, FBG1, which is used as an optical notch filter to filter out one sideband, has a center wavelength of 1556.23 nm, a 3-dB bandwidth of 0.04 nm, and a sideband suppression ratio more than 50 dB. The other FBG, FBG2, designed as an optical phase filter, has a center wavelength of 1556.10 nm and a 3-dB bandwidth of 0.067 nm. The measured transmission spectrum of FBG1, the reflection spectrum of FBG2, as well as the spectrum of the single-sideband modulated optical signal, are all shown in Fig. 4.16, where the microwave modulating frequency is $\Omega = 2\pi \times 4$ GHz. In our implementation, the upper sideband (with shorter wavelength) is selected. Note that, however, in general, either one of the two sidebands can be chosen.

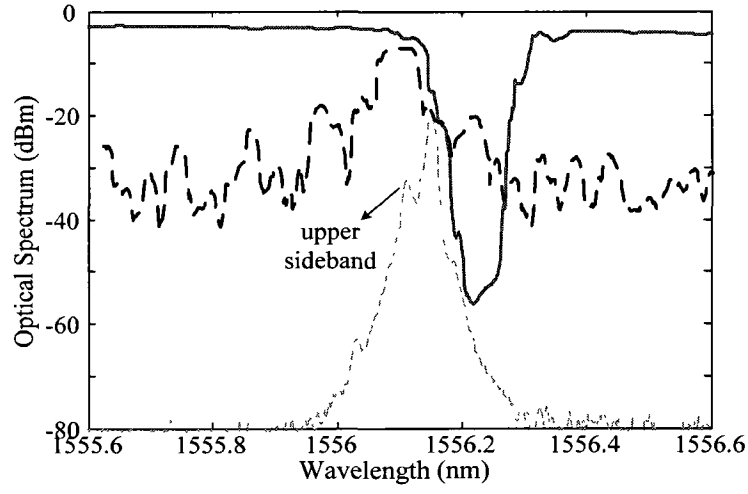

Fig. 4.16. Experimental results: optical spectra of the gratings and the optical signals. (Solid line: transmission of FBG1; dashed line: reflection of FBG2; dotted line: single-sideband modulated optical signal).

Both the magnitude and phase responses of the implemented microwave filter are measured using the VNA by sweeping the microwave modulating frequency from 2 to 5 GHz while

keeping the output RF power of 5 dBm. The operational frequency range is mainly limited by the narrow operational bandwidth of the optical spectral filter (FBG2). One solution to eliminate this limitation is to develop an optical phase filter with a broader operational bandwidth. This will be discussed in more detail later.

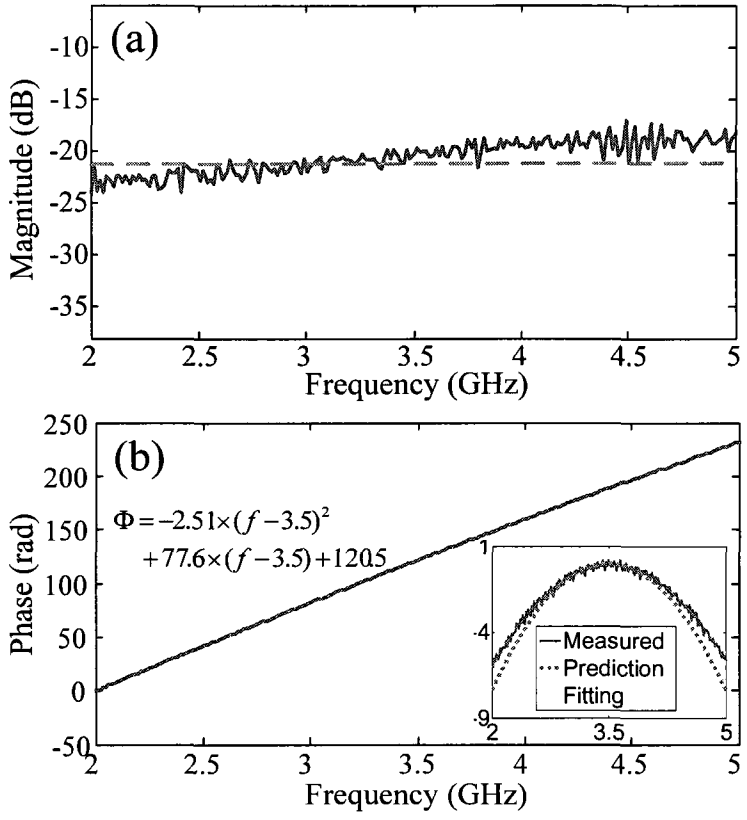

Fig. 4.17. Experimental results: frequency response of the microwave filter. (a) Magnitude transmission response (Solid line: measured response; dashed line: desired response); (b) measured phase response. Inset: parabolic phase response after subtracting the linear phase component (Dashed line: quadratic curve-fitting; dotted line: theoretical prediction).

Fig. 4.17(a) shows the measured magnitude response of the implemented microwave filter. As we have discussed before, the desired microwave filter is a phase-only filter with a flat magnitude response, as shown via the dashed line in Fig. 4.17(a). The measured magnitude response has a good flatness with variations limited within 4 dB. The variations in magnitude response are mainly resulted from the three sources: the electrical-optical conversion at the

MZM, the optical-electrical conversion at the photodetector, and the nonflat magnitude response of the optical filter (FBG2). A theoretical analysis on the impact of optical filter magnitude response variations on a linearly chirped microwave pulse when passing through a photonic system has been reported in [243].

The measured phase response of the microwave filter is plotted in Fig. 4.17(b). The polynomial curve-fitting shows that the phase response is nearly quadratic. Based on the fitting result, the microwave dispersion parameter of the microwave filter can be calculated as

$$D_2 = \frac{d^2\Phi}{d\omega^2} = \frac{1}{(2\pi)^2}\frac{d^2\Phi}{df^2} = -\frac{5.02}{(2\pi)^2} \text{ (ns}^2\text{)} \qquad (4\text{-}29)$$

Note that the microwave filter has a strong linear phase response in addition to the desired quadratic phase response, which means that a large frequency-independent group delay is introduced in the filter. To show the nonlinear phase response more clearly, the linear phase component $\Phi = 77.6f - 151.1$ can be removed from the entire measured phase response. A parabolic phase response is thus obtained after subtracting the linear phase, as shown in the inset of Fig. 4.17(b). A quadratic curve-fitting is also shown via the dashed line. The phase variation is limited within around 0.4 rad. The theoretical prediction of the phase response by (4-22) is also plotted as dotted line in the inset for comparison. Note that the difference between the phase response of the implemented microwave filter and that of the desired filter mainly comes from the optical dispersion mismatch in FBG2, as described before.

V.5. Linearly chirped microwave pulse compression

The compression of a linearly chirped microwave pulse using the implemented microwave filter with a quadratic phase response is investigated. Consider again the linearly chirped Gaussian microwave pulse with a bandwidth $B = 3$ GHz and a chirp parameter $u = -0.8$ GHz/ns. The original temporal waveform $s(t)$ with a pulsewidth $T_0 = 3.75$ ns is plotted as a dotted line in Fig. 4.18.

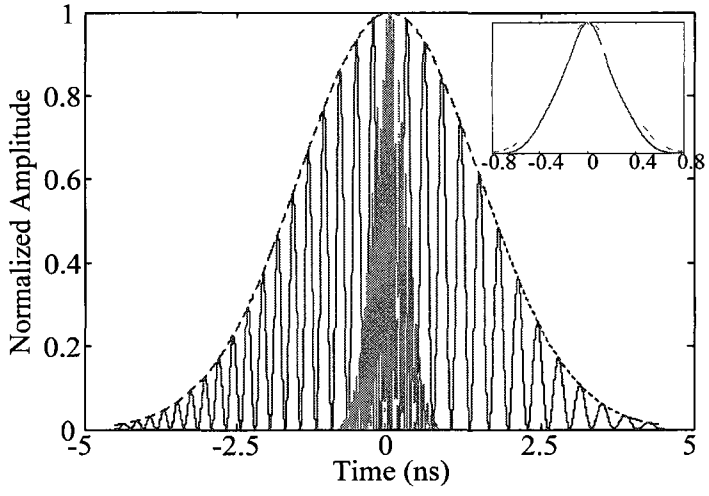

Fig. 4.18. Temporal waveforms. (Blue dotted line: original microwave pulse; red solid line: compressed microwave pulse). Inset: zoom-in view of the envelopes of the compressed microwave pulses.

The compressed microwave signal $r(t)$ is obtained at the output of the microwave filter, which is given by

$$r(t) = \tilde{F}^{-1}\left[\tilde{S}(\Omega)H(\Omega)\right] \tag{4-30}$$

where $H(\Omega)$ is the transfer function (both amplitude and phase) of the implemented microwave filter, $\tilde{S}(\Omega)$ is the Fourier transform of the input signal $s(t)$ and $\tilde{F}^{-1}(\bullet)$ denotes the inverse Fourier transform operation.

The compressed microwave pulse calculated based on (4-30) is also shown as a solid line in Fig. 4.18. A pulse compression ratio of 5.62 is achieved. Both the desired and achieved system performances are summarized in Table 4.2 for comparison.

TABLE 4.2. COMPARISON OF SYSTEM PERFORMANCES

System Performances	Desired Value	Achieved Value
Optical Filter Dispersion (ps/nm)	16770	13610
Microwave Filter Dispersion (ns^2)	0.1678	0.1273
Microwave Filter Phase Response Variation (rad)	0	0.4
Microwave Filter Magnitude Response Variation (dB)	0	4
Microwave Pulse Compression Ratio	11.25 (TBWP of the input pulse)	5.62

We can see that the compression ratio is slightly smaller than the time-bandwidth product of the input microwave pulse due to the mismatch between the phase response of the microwave filter and that of the input microwave pulse. Based on (4-22), the optimal microwave filter dispersion parameter should be $D_{2opt} = 0.1678$ ns^2. On the other hand, the realized microwave filter dispersion parameter is $D_2 = 0.1273$ ns^2. The microwave dispersion parameter mismatch is due to the optical dispersion mismatch as discussed above. The design of an optical phase filter with more accurate group delay response would enable an improved compression performance. The inset of Fig. 4.18 provides a zoom-in view of the compressed microwave pulse envelope (via a solid line). The envelope of compressed Gaussian microwave pulse by an ideal phase-only filter is also plotted for comparison (via a dashed line). Note that the microwave filter magnitude

response perturbations have no obvious impact on the pulse compression (even a slight improvement on the compression ratio).

VI. *Discussion*

VI.1. Bandwidth extension

In this research work, a proof-of-concept experiment is carried out, which works within a relative narrow bandwidth (a few gigahertz), limited by the bandwidth of the optical phase filter. For many practical applications, high-frequency and broadband linearly chirped microwave pulses are usually required to be compressed. In addition, the magnitude response variations are found in the demonstrated microwave filter. Therefore, a broadband optical phase filter with a linear group-delay response and a flatter magnitude response will be required to achieve true phase-only filtering for high-frequency linearly chirped microwave pulse compression. One solution to the problem is to construct a long-length linearly chirped FBG, which can provide a large linear group delay. Moreover, the linearly chirped FBG with a properly designed index modulation function would ensure the microwave filter to have a unity magnitude transmission response. Such a grating reconstruction problem can be numerically solved by using the inverse scattering algorithms, such as the DLP algorithm [115].

As an example, to build a microwave filter with a quadratic phase response for the compression of a linearly chirped microwave pulse with a bandwidth of 50 GHz, and a chirp parameter $u = -2.86$ GHz/ns, the linearly chirped FBG should have an optical dispersion of $d = 5000$ ps/nm, a bandwidth of 0.4 nm, and a grating length as long as 30 cm. Since the facility currently available in the laboratory cannot fabricate such a long grating, the potential of the proposed technique for broadband operation is supported by simulations. Fig. 4.19 shows the simulation

results of a linearly chirped FBG designed by using the DLP algorithm. Both the linear group delay and unity magnitude response are obtained. In fact, such a long grating can be easily realized with the current FBG fabrication technology. Recently, a linearly chirped FBG with a length up to 1 m has been demonstrated [241], which can be used to compress a chirped microwave pulse with a bandwidth as large as 165 GHz for the same given chirp parameter.

For an optical filter with large bandwidth, the operation frequency of the system is practically limited only by the bandwidth of the optical-electrical conversion devices, such as photodetector and the modulator. For example, to compress a chirped microwave pulse with its highest frequency of 50 GHz, both the photodetector and the modulator must have a bandwidth of 50 GHz.

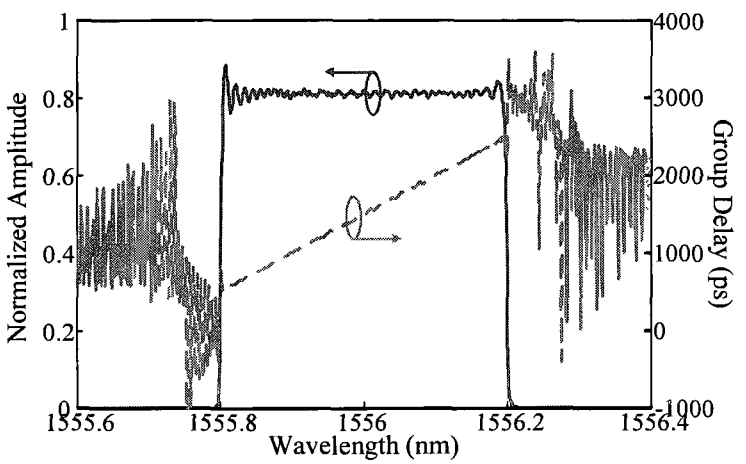

Fig. 4.19. Simulation results: reflection spectrum and group delay of a broadband linearly chirped FBG.

VI.2. Compression of nonlinearly chirped microwave pulse

In our study, only a linearly chirped microwave signal is considered since it is the most commonly used pulsed signal for most of the applications. It is worth noting that a linear frequency chirping is not always necessary in a microwave pulse compression system. In fact,

the frequency modulation can be of any form, provided that the compression filter in the receiver end is designed to match the phase of the microwave pulse to be compressed.

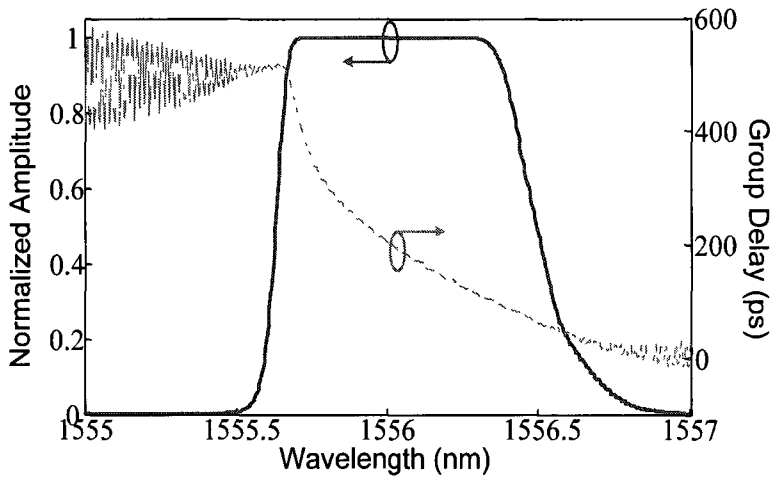

Fig. 4.20. Simulated reflection spectrum and group delay responses of a broadband nonlinearly chirped FBG.

Here we consider the compression of a nonlinearly chirped microwave pulsed signal. The use of a nonlinearly frequency modulated signal for pulse compression has the advantage of a reduced sidelobe level if the input pulse is compressed [244]. According to the expressions in (4-16) and (4-27), to compress a nonlinearly (quadratically) chirped microwave signal by using a phase-only matched filter, an optical phase filter with a quadratic group-delay response, or equivalently, a cubic phase response is required. In addition, the optical phase filter should have a broad bandwidth and a unity magnitude response. The DLP algorithm is again utilized to reconstruct the desired FBG in the numerical simulation. A nonlinearly chirped FBG with a quadratic group delay is obtained, with the reflection spectrum and group delay response being shown in Fig. 4.20. A simple way to fabricate such a nonlinearly chirped FBG is to use a custom-designed nonlinearly chirped phase mask [206], but at a higher cost. A low-cost solution is to generate a nonlinearly chirped FBG from a regular linearly chirped FBG by applying a strain to the grating using the strain-gradient beam tuning technique [132].

VII. Conclusion

We have proposed and demonstrated a photonic microwave filter with a nonlinear phase response for chirped microwave pulse compression. The proposed microwave filter was realized based on SSB modulation and heterodyne detection at a high-speed photodetector, to transfer the optical filter response to the response of the microwave filter. The key component in the proposed system is an FBG, which was employed as the optical filter with a user-defined nonlinear phase response. The key advantage is that the system requires only a single optical wavelength and can be implemented using pure fiber-optic components, which has the high potential for integration.

A detailed theoretical analysis on the photonic microwave filter design and its application in chirped microwave pulse compression was developed. A photonic microwave filter having a quadratic phase response with a bandwidth of 3 GHz was experimentally generated. The compression of a linearly chirped microwave pulse using the implemented microwave filter was investigated. A pulse compression ratio of 5.62 was demonstrated. To achieve a higher pulse compression ratio for a highly chirped microwave pulse, an optical filter with more accurately controlled phase response and a broader bandwidth is required. Potential solutions were discussed and demonstrated by numerical simulations.

The demonstrated approach offers an optical solution to the compression of a high-frequency chirped microwave signal for applications in modern radar and other civil and defence systems.

CHAPTER 5 SUMMARY AND FUTURE WORK

5.1. Summary

In this thesis, the research efforts have been focused on the investigation of innovative optical techniques to generating and processing high-frequency and large-bandwidth microwave arbitrary waveforms using advanced FBGs.

Photonic generation of microwave arbitrary waveforms based on coherent optical pulse shaping using advanced FBGs was first studied. Two different methods for photonic microwave arbitrary waveform generation were investigated and experimentally demonstrated. One method was based on optical spectral shaping and dispersion-induced frequency-to-time mapping. Advanced FBGs have been employed in the systems as optical spectral filters for optical spectral shaping, dispersive elements for frequency-to-time mapping and multifunctional devices for both spectral shaping and frequency-to-time mapping. The other method for photonic microwave arbitrary waveform generation was realized based on Fourier-transform optical pulse shaping. Both time-domain and frequency-domain Fourier-transform optical pulse shaping has been investigated. Advanced FBGs have been employed in the systems as optical spectral filters and dispersive elements.

Photonic processing of microwave arbitrary waveforms using advanced FBGs was also investigated. Two different photonic microwave filters were demonstrated to achieve matched filtering of microwave arbitrary waveforms. One filter uses nonuniform sampling technique to achieve equivalent complex tap coefficients for all-positive microwave delay-line filter, while

the other filter was realized based on optical filter response to microwave filter response conversion. In the first filter, a spatially-discrete chirped FBG was employed to arbitrarily control the tap coefficients and the time delays, and in the second filter, an FBG with the desired magnitude and phase response was used as the optical filter.

In conclusion, the unique filtering properties and versatility as an in-fiber device of an FBG have been illustrated by its use in a variety of microwave photonics applications. Different types of FBGs were designed and fabricated, which have played very important roles in the proposed microwave arbitrary waveform generation and processing systems, with the advantages of small size, low loss, low cost, good stability, and high compatibility with other well-developed fiber-optic devices.

5.2. Future work

In this thesis, various FBGs have been fabricated and incorporated into the proposed systems to achieve microwave arbitrary waveform generation and processing. The FBGs were designed based on amplitude-only refractive index modulation, which may eliminate the difficulty in fabrication. However, the realizable grating responses are also limited. With the help of precisely controlled piezoelectric moving devices, arbitrary refractive index modulation including some phase-shifts can be obtained. FBGs with the complex refractive index modulation to achieve nearly arbitrary spectral responses (both magnitude and phase responses) will be designed and fabricated. Their applications in the microwave arbitrary waveform generation and processing will be further investigated.

In addition, compared with the photonic microwave arbitrary waveform generation and processing techniques using free-space optical devices, such as spatial lightwave modulators, the FBG-based methods have the key limitation of poor reconfigurability since the spectral response of an FBG is hard to be altered once it is fabricated. In practice, a reconfigurable FBG-based microwave waveform generation and processing system would be more desirable. To overcome this limitation, the filtering properties of FBGs must be tunable by some means. In fact, grating tuning can be implemented by fiber stretching using piezoelectric devices [205] or by thermal control using a divided thin-film heater [245]. Further study on the reconfigurable microwave arbitrary waveform generation and processing based on FBG tuning will be performed in the future work.

Finally, discrete optical devices, such as high-speed electro-optical modulator and photodetectors have been used in the proposed microwave arbitrary waveform generation and processing systems. The whole system becomes costly, even though the FBG itself has a very low cost. A solution to reduce the system cost is to use photonic integrated circuits (PICs). A silicon-based PIC was recently demonstrated to generate microwave arbitrary waveforms with a center frequency up to 60 GHz based on optical spectral shaping and frequency-to-time mapping [246]. The generated microwave waveform can be reconfigured at millisecond to microsecond speeds. Further research would be carried out to investigate integrated photonic microwave waveform generation and processing systems using PIC technique. Bragg gratings would be imprinted in the silicon waveguide chip to achieve the desired spectral characteristics.

LIST OF REFERENCE

[1] A. J. Seeds, "Microwave photonics," *IEEE Trans. Microw. Theory Tech.,* vol. 50, no. 3, pp. 877-887, Mar. 2002.

[2] A. J. Seeds and K. J. Williams, "Microwave photonics," *J. Lightwave Technol.,* vol. 24, no. 12, pp. 4628-4641, Dec. 2006.

[3] J. Capmany and D. Novak, "Microwave photonics combines two worlds," *Nature Photon.,* vol. 1, no. 6, pp. 319-330, Jun. 2007.

[4] J. P. Yao, "Microwave Photonics," *J. Lightwave Technol.,* vol. 27, no. 1-4, pp. 314-335, Jan-Feb. 2009.

[5] C. Wang, H. Chi, and J. Yao, "Photonic generation and processing of millimeter-wave arbitrary waveforms," in *IEEE Lasers and Electro-Optics Society, 2008. LEOS 2008. 21st Annual Meeting of the*, Newport Beach, CA, USA, 2008, pp. 346-347.

[6] B. Jalali, P. Kelkar, and V. Saxena, "Photonic arbitrary waveform generator," in *Lasers and Electro-Optics Society, 2001. LEOS 2001. The 14th Annual Meeting of the IEEE,* 2001, pp. 253-254 vol.1.

[7] D. E. Leaird and A. M. Weiner, "Femtosecond direct space-to-time pulse shaping," *IEEE J. Quantum Electron.,* vol. 37, no. 4, pp. 494-504, Apr. 2001.

[8] J. D. McKinney, D. E. Leaird, and A. M. Weiner, "Millimeter-wave arbitrary waveform generation with a direct space-to-time pulse shaper," *Opt. Lett.,* vol. 27, no. 15, pp. 1345-1347, Aug 1. 2002.

[9] J. D. McKinney, D. S. Seo, D. E. Leaird, and A. M. Weiner, "Photonically assisted generation of arbitrary millimeter-wave and microwave electromagnetic waveforms via direct space-to-time optical pulse shaping," *J. Lightwave Technol.,* vol. 21, no. 12, pp. 3020-3028, Dec. 2003.

[10] D. E. Leaird and A. M. Weiner, "Femtosecond direct space-to-time pulse shaping in an integrated-optic configuration," *Opt. Lett.,* vol. 29, no. 13, pp. 1551-1553, Jul. 2004.

[11] S. J. Xiao, J. D. McKinney, and A. M. Weiner, "Photonic microwave arbitrary waveform generation using a virtually imaged phased-array (VIPA) direct space-to-time pulse shaper," *IEEE Photon. Technol. Lett.,* vol. 16, no. 8, pp. 1936-1938, Aug. 2004.

[12] J. D. McKinney, D. S. Seo, and A. M. Weiner, "Photonically assisted generation of continuous arbitrary millimetre electromagnetic waveforms," *Electron. Lett.,* vol. 39, no. 3, pp. 309-311, Feb. 2003.

[13] J. P. Heritage and A. M. Weiner, "Optical systems and methods based upon temporal stretching, modulation and recompression of ultrashort pulses," United States Patent, No. 4928316, 1990.

[14] J. Azana, N. K. Berger, B. Levit, and B. Fischer, "Reconfigurable generation of high-repetition-rate optical pulse sequences based on time-domain phase-only filtering," *Opt. Lett.,* vol. 30, no. 23, pp. 3228-3230, Dec 1. 2005.

[15] R. E. Saperstein, N. Alic, D. Panasenko, R. Rokitski, and Y. Fainman, "Time-domain waveform processing by chromatic dispersion for temporal shaping of optical pulses," *J. Opt. Soc. Am. B,* vol. 22, no. 11, pp. 2427-2436, Nov. 2005.

[16] B. Xia and L. R. Chen, "A direct temporal domain approach for pulse-repetition rate multiplication with arbitrary envelope shaping," *IEEE J. Sel. Topics Quantum Electron.,* vol. 11, no. 1, pp. 165-172, Jan-Feb. 2005.

[17] J. Azana, N. K. Berger, B. Levit, and B. Fischer, "Broadband arbitrary waveform generation based on microwave frequency upshifting in optical fibers," *J. Lightwave Technol.,* vol. 24, no. 7, pp. 2663-2675, Jul. 2006.

[18] V. Torres-Company, M. Fernandez-Alonso, J. Lancis, J. C. Barreiro, and P. Andres, "Millimeter-wave and microwave signal generation by low-bandwidth electro-optic phase modulation," *Opt. Express,* vol. 14, no. 21, pp. 9617-9626, Oct 16. 2006.

[19] H. Chi and J. Yao, "Waveform distortions due to second-order dispersion and dispersion mismatches in a temporal pulse-shaping system," *J. Lightwave Technol.,* vol. 25, no. 11, pp. 3528-3535, Nov. 2007.

[20] H. Chi and J. Yao, "Symmetrical waveform generation based on temporal pulse shaping using amplitude-only modulator," *Electron. Lett.,* vol. 43, no. 7, pp. 415-417, Mar 29. 2007.

[21] S. Thomas, A. Malacarne, F. Fresi, L. Potì, A. Bogoni, and J. Azaña, "Programmable fiber-based picosecond optical pulse shaper using time-domain binary phase-only linear filtering," *Opt. Lett.,* vol. 34, no. 4, pp. 545-547. 2009.

[22] S. Thomas, A. Malacarne, F. Fresi, L. Poti, and J. Azana, "Fiber-based programmable picosecond optical pulse shaper," *J. Lightwave Technol.,* vol. 28, no. 12, pp. 1832-1843. 2010.

[23] T. Jannson, "Real-Time Fourier Transformation in Dispersive Optical Fibers," *Opt. Lett.,* vol. 8, no. 4, pp. 232-234. 1983.

[24] J. Azana, L. R. Chen, M. A. Muriel, and P. W. E. Smith, "Experimental demonstration of real-time Fourier transformation using linearly chirped fibre Bragg gratings," *Electron. Lett.,* vol. 35, no. 25, pp. 2223-2224, Dec 9. 1999.

[25] M. A. Muriel, J. Azana, and A. Carballar, "Real-time Fourier transformer based on fiber gratings," *Opt. Lett.,* vol. 24, no. 1, pp. 1-3, Jan 1. 1999.

[26] J. Azana and M. A. Muriel, "Real-time optical spectrum analysis based on the time-space duality in chirped fiber gratings," *IEEE J. Quantum Electron.,* vol. 36, no. 5, pp. 517-526, May. 2000.

[27] J. Azana, M. A. Muriel, and A. Carballar, "Real-time Fourier transformer system using transmissive fiber gratings," *Fiber Integrated Opt.,* vol. 19, no. 4, pp. 439-453. 2000.

[28] J. Azana and M. A. Muriel, "Real-time Fourier transformations performed simultaneously over multiwavelength signals," *IEEE Photon. Technol. Lett.,* vol. 13, no. 1, pp. 55-57, Jan. 2001.

[29] F. X. Li and J. Azana, "Simplified system configuration of optical pulses for real-time Fourier transformation in amplitude and phase," *Opt. Commun.,* vol. 274, no. 1, pp. 59-65, Jun 1. 2007.

[30] Y. Park, T. J. Ahn, J. C. Kieffer, and J. Azana, "Optical frequency domain reflectometry based on real-time Fourier transformation," *Opt. Express,* vol. 15, no. 8, pp. 4597-4616, Apr 16. 2007.

[31] E. B. Treacy, "Optical Pulse Compression with Diffraction Gratings," *IEEE J. Quantum Electron.,* vol. Qe 5, no. 9, pp. 454-&. 1969.

[32] B. H. Kolner, "Space-Time Duality and the Theory of Temporal Imaging," *IEEE J. Quantum Electron.,* vol. 30, no. 8, pp. 1951-1963, Aug. 1994.

[33] A. Papoulis, "Pulse-Compression, Fiber Communications, and Diffraction - a Unified Approach," *J. Opt. Soc. Am. A,* vol. 11, no. 1, pp. 3-13, Jan. 1994.

[34] H. Kobayashi and I. P. Kaminow, "Duality relationships among "space," "time", and "wavelength" in all-optical networks," *J. Lightwave Technol.,* vol. 14, no. 3, pp. 344-351, Mar. 1996.

[35] B. H. Kolner and M. Nazarathy, "Temporal Imaging with a Time Lens," *Opt. Lett.,* vol. 14, no. 12, pp. 630-632, Jun. 1989.

[36] A. W. Lohmann and D. Mendlovic, "Temporal Filtering with Time Lenses," *Appl. Optics,* vol. 31, no. 29, pp. 6212-6219, Oct 10. 1992.

[37] J. Chou, Y. Han, and B. Jalali, "Adaptive RF-photonic arbitrary waveform generator," *IEEE Photon. Technol. Lett.,* vol. 15, no. 4, pp. 581-583, Apr. 2003.

[38] M. Y. Shen and R. A. Minasian, "Toward a high-speed arbitrary waveform generation by a novel photonic processing structure," *IEEE Photon. Technol. Lett.,* vol. 16, no. 4, pp. 1155-1157, Apr. 2004.

[39] I. S. Lin, J. D. McKinney, and A. M. Weiner, "Photonic synthesis of broadband microwave arbitrary waveforms applicable to ultra-wideband communication," *IEEE Microw. Wireless Compon. Lett.,* vol. 15, no. 4, pp. 226-228, Apr. 2005.

[40] A. M. Weiner, "Femtosecond pulse shaping using spatial light modulators," *Rev. Sci. Instrum.,* vol. 71, no. 5, pp. 1929-1960, May. 2000.

[41] J. P. Heritage, A. M. Weiner, and R. N. Thurston, "Picosecond Pulse Shaping by Spectral Phase and Amplitude Manipulation," *Opt. Lett.,* vol. 10, no. 12, pp. 609-611. 1985.

[42] A. M. Weiner, J. P. Heritage, and E. M. Kirschner, "High-Resolution Femtosecond Pulse Shaping," *J. Opt. Soc. Am. B,* vol. 5, no. 8, pp. 1563-1572, Aug. 1988.

[43] A. M. Weiner, D. E. Leaird, J. S. Patel, and J. R. Wullert, "Programmable Femtosecond Pulse Shaping by Use of a Multielement Liquid-Crystal Phase Modulator," *Opt. Lett.,* vol. 15, no. 6, pp. 326-328, Mar 15. 1990.

[44] A. M. Weiner, D. E. Leaird, J. S. Patel, and J. R. Wullert, "Programmable Shaping of Femtosecond Optical Pulses by Use of 128-Element Liquid-Crystal Phase Modulator," *IEEE J. Quantum Electron.,* vol. 28, no. 4, pp. 908-920, Apr. 1992.

[45] C. W. Hillegas, J. X. Tull, D. Goswami, D. Strickland, and W. S. Warren, "Femtosecond Laser-Pulse Shaping by Use of Microsecond Radiofrequency Pulses," *Opt. Lett.,* vol. 19, no. 10, pp. 737-739, May 15. 1994.

[46] M. A. Dugan, J. X. Tull, and W. S. Warren, "High-resolution acousto-optic shaping of unamplified and amplified femtosecond laser pulses," *J. Opt. Soc. Am. B,* vol. 14, no. 9, pp. 2348-2358, Sep. 1997.

[47] M. R. Fetterman, D. Goswami, D. Keusters, W. Yang, J. K. Rhee, and W. S. Warren, "Ultrafast pulse shaping: amplification and characterization," *Opt. Express,* vol. 3, no. 10, pp. 366-375, Nov 9. 1998.

[48] S. Etemad, T. Banwell, S. Galli, J. Jackel, R. Menendez, P. Toliver, J. Young, P. Delfyett, C. Price, and T. Turpin, "Optical-CDMA incorporating phase coding of coherent frequency bins: concept, simulation, experiment," in *Optical Fiber Communication Conference*, 2004, p. FG5.

[49] T. Yilmaz, C. M. DePriest, T. Turpin, J. H. Abeles, and P. J. Delfyett, "Toward a photonic arbitrary waveform generator using a modelocked external cavity semiconductor laser," *IEEE Photon. Technol. Lett.,* vol. 14, no. 11, pp. 1608-1610, Nov. 2002.

[50] Z. Jiang, D. S. Seo, D. E. Leaird, and A. M. Weiner, "Spectral line-by-line pulse shaping," *Opt. Lett.,* vol. 30, no. 12, pp. 1557-1559, Jun 15. 2005.

[51] Z. Jiang, D. E. Leaird, and A. M. Weiner, "Optical processing based on spectral line-by-line pulse shaping on a phase-modulated CW laser," *IEEE J. Quantum Electron.,* vol. 42, no. 7-8, pp. 657-666, Jul-Aug. 2006.

[52] Z. Jiang, D. E. Leaird, C. B. Huang, H. X. Miao, M. Kourogi, K. Imai, and A. M. Weiner, "Spectral line-by-line pulse shaping on an optical frequency comb generator," *IEEE J. Quantum Electron.,* vol. 43, no. 11-12, pp. 1163-1174, Nov-Dec. 2007.

[53] Z. Jiang, C. B. Huang, D. E. Leaird, and A. M. Weiner, "Spectral line-by-line pulse shaping for optical arbitrary pulse-train generation," *J. Opt. Soc. Am. B,* vol. 24, no. 9, pp. 2124-2128, Sep. 2007.

[54] Z. Jiang, D. E. Leaird, and A. M. Weiner, "Line-by-line pulse shaping control for optical arbitrary waveform generation," *Opt. Express,* vol. 13, no. 25, pp. 10431-10439, Dec 12. 2005.

[55] Z. Jiang, D. E. Leaird, and A. M. Weiner, "Optical arbitrary waveform generation and characterization using spectral line-by-line control," *J. Lightwave Technol.,* vol. 24, no. 7, pp. 2487-2494, Jul. 2006.

[56] C. B. Huang, Z. Jiang, D. E. Leaird, and A. M. Weiner, "The impact of optical comb stability on waveforms generated via spectral line-by-line pulse shaping," *Opt. Express,* vol. 14, no. 26, pp. 13164-13176, Dec 25. 2006.

[57] C. B. Huang, Z. Jiang, D. E. Leaird, J. Caraquitena, and A. M. Weiner, "Spectral line-by-line shaping for optical and microwave arbitrary waveform generations," *Laser Photonics Rev.,* vol. 2, no. 4, pp. 227-248, Aug. 2008.

[58] C. B. Huang, D. E. Leaird, and A. M. Weiner, "Time-multiplexed photonically enabled radio-frequency arbitrary waveform generation with 100 ps transitions," *Opt. Lett.,* vol. 32, no. 22, pp. 3242-3244, Nov 15. 2007.

[59] H. Takahashi, S. Suzuki, K. Kato, and I. Nishi, "Arrayed-Wave-Guide Grating for Wavelength Division Multi Demultiplexer with Nanometer Resolution," *Electron. Lett.,* vol. 26, no. 2, pp. 87-88, Jan 18. 1990.

[60] H. Takahashi, S. Suzuki, and I. Nishi, "Wavelength Multiplexer Based on Sio2-Ta2o5 Arrayed-Wave-Guide Grating," *J. Lightwave Technol.,* vol. 12, no. 6, pp. 989-995, Jun. 1994.

[61] T. Kurokawa, H. Tsuda, K. Okamoto, K. Naganuma, H. Takenouchi, Y. Inoue, and M. Ishii, "Time-space-conversion optical signal processing using arrayed-waveguide grating," *Electron. Lett.,* vol. 33, no. 22, pp. 1890-1891, Oct 23. 1997.

[62] H. Tsuda, K. Okamoto, T. Ishii, K. Naganuma, Y. Inoue, H. Takenouchi, and T. Kurokawa, "Second- and third-order dispersion compensator using a high-resolution arrayed-waveguide grating," *IEEE Photon. Technol. Lett.,* vol. 11, no. 5, pp. 569-571, May. 1999.

[63] S. Yegnanarayanan, P. D. Trinh, and B. Jalali, "Recirculating photonic filter: A wavelength-selective time delay for phased-array antennas and wavelength code-division multiple access," *Opt. Lett.,* vol. 21, no. 10, pp. 740-742, May 15. 1996.

[64] S. Yegnanarayanan and B. Jalali, "Wavelength-selective true time delay for optical control of phased-array antenna," *IEEE Photon. Technol. Lett.,* vol. 12, no. 8, pp. 1049-1051, Aug. 2000.

[65] N. K. Fontaine, R. P. Scott, J. Cao, A. Karalar, W. Jiang, K. Okamoto, J. P. Heritage, B. H. Kolner, and S. J. B. Yoo, "32 phase X 32 amplitude optical arbitrary waveform generation," *Opt. Lett.,* vol. 32, no. 7, pp. 865-867, Apr 1. 2007.

[66] N. K. Fontaine, R. P. Scott, C. X. Yang, D. J. Geisler, J. P. Heritage, K. Okamoto, and S. J. B. Yoo, "Compact 10 GHz loopback arrayed-waveguide grating for high-fidelity optical arbitrary waveform generation," *Opt. Lett.,* vol. 33, no. 15, pp. 1714-1716, Aug 1. 2008.

[67] M. Hyodo, K. S. Abedin, and N. Onodera, "Generation of arbitrary optical waveforms by Fourier synthesis using three continuous-wave semiconductor lasers," *Electron. Lett.,* vol. 36, no. 3, pp. 224-225, Feb 3. 2000.

[68] Y. Park, M. H. Asghari, T. J. Ahn, and J. Azana, "Transform-limited picosecond pulse shaping based on temporal coherence synthesization," *Opt. Express,* vol. 15, no. 15, pp. 9584-9599, Jul 23. 2007.

[69] R. Kashyap, *Fiber Bragg Gratings*. San Diego: Academic Press., 1999.

[70] C. R. Giles, "Lightwave applications of fiber Bragg gratings," *J. Lightwave Technol.,* vol. 15, no. 8, pp. 1391-1404, Aug. 1997.

[71] J. Capmany, D. Pastor, B. Ortega, J. L. Cruz, and M. V. Andres, "Applications of fiber Bragg gratings to microwave photonics (Invited paper)," *Fiber Integrated Opt.,* vol. 19, no. 4, pp. 483-494. 2000.

[72] R. A. Minasian, "Photonic signal processing of high-speed signals using fiber gratings," *Opt. Fiber Technolo.,* vol. 6, no. 2, pp. 91-108, Apr. 2000.

[73] R. A. Minasian, "Photonic signal processing of microwave signals," *IEEE Trans. Microw. Theory Tech.,* vol. 54, no. 2, pp. 832-846, Feb. 2006.

[74] K. Wilner and A. P. Vandenheuvel, "Fiberoptic Delay-Lines for Microwave Signal-Processing," *P Ieee,* vol. 64, no. 5, pp. 805-807. 1976.

[75] J. X. Chen, Y. Wu, J. Hodiak, and P. K. L. Yu, "A novel digitally tunable microwave-photonic notch filter using differential group-delay module," *IEEE Photon. Technol. Lett.,* vol. 15, no. 2, pp. 284-286, Feb. 2003.

[76] V. Polo, B. Vidal, J. L. Corral, and J. Marti, "Novel tunable photonic microwave filter based on laser arrays and N x N AWG-based delay lines," *IEEE Photon. Technol. Lett.,* vol. 15, no. 4, pp. 584-586, Apr. 2003.

[77] B. Vidal, V. Polo, J. L. Corral, and J. Marti, "Photonic microwave filter with tuning and reconfiguration capabilities using optical switches and dispersive media," *Electron. Lett.*, vol. 39, no. 6, pp. 547-549, Mar 20. 2003.

[78] D. B. Hunter, "Incoherent bipolar tap microwave photonic filter based on balanced bridge electro-optic modulator," *Electron. Lett.*, vol. 40, no. 14, pp. 856-858, Jul 8. 2004.

[79] J. Capmany, J. Mora, D. Pastor, and B. Ortega, "High-quality online-reconfigurable microwave photonic transversal filter with positive and negative coefficients," *IEEE Photon. Technol. Lett.*, vol. 17, no. 12, pp. 2730-2732, Dec. 2005.

[80] L. R. Chen and V. Page, "Tunable photonic microwave filter using semiconductor fibre laser," *Electron. Lett.*, vol. 41, no. 21, pp. 1183-1184, Oct 13. 2005.

[81] J. H. Lee, Y. M. Chang, Y. G. Han, H. Chung, and S. B. Lee, "Flexibly tunable microwave photonic FIR filter incorporating wavelength spacing programmable, arrayed micro-mirror based optical filter," *Electron. Lett.*, vol. 42, no. 14, pp. 812-814, Jul 6. 2006.

[82] J. Mora, A. Ortigosa-Blanch, D. Pastor, and J. Capmany, "Tunable microwave photonic filter free from baseband and carrier suppression effect not requiring single sideband modulation using a Mach-Zenhder configuration," *Opt. Express,* vol. 14, no. 17, pp. 7960-7965, Aug 21. 2006.

[83] J. Wang and J. P. Yao, "A tunable photonic microwave notch filter based on all-optical mixing," *IEEE Photon. Technol. Lett.*, vol. 18, no. 1-4, pp. 382-384, Jan-Feb. 2006.

[84] D. Chen, H. Fu, and S. He, "Novel microwave photonic filter based on a mode-locked fiber laser," *Laser Phys Lett,* vol. 4, no. 8, pp. 597-600, Aug. 2007.

[85] L. H. Cheng and S. Aditya, "A novel photonic microwave filter with infinite impulse response," *IEEE Photon. Technol. Lett.*, vol. 19, no. 17-20, pp. 1439-1441, Sep-Oct. 2007.

[86] G. D. Kim and S. S. Lee, "Photonic microwave channel selective filter incorporating a thermooptic switch based on tunable ring resonators," *IEEE Photon. Technol. Lett.*, vol. 19, no. 13-16, pp. 1008-1010, Jul-Aug. 2007.

[87] G. X. Ning and P. Shum, "Coherence-free microwave photonic notch filter with a single driver intensity modulator in a Sagnac fiber loop," *Appl. Optics,* vol. 46, no. 29, pp. 7179-7183, Oct 10. 2007.

[88] C. K. Oh, T. Y. Kim, and C. S. Park, "Reconfigurable photonic microwave bandpass filter with negative coefficients based on polarisation modulation," *Electron. Lett.,* vol. 43, no. 11, pp. 639-641, May 24. 2007.

[89] Q. Wang, J. P. Yao, and J. D. Bull, "Negative tap photonic microwave filter based on a Mach-Zehnder modulator and a tunable optical polarizer," *IEEE Photon. Technol. Lett.,* vol. 19, no. 21-24, pp. 1750-1752, Nov-Dec. 2007.

[90] Y. Yan, S. R. Blais, and J. P. Yao, "Tunable photonic microwave bandpass filter with negative coefficients implemented using an optical phase modulator and chirped fiber Bragg gratings," *J. Lightwave Technol.,* vol. 25, no. 11, pp. 3283-3288, Nov. 2007.

[91] Y. Yan and J. P. Yao, "A tunable photonic microwave filter with a complex coefficient using an optical RF phase shifter," *IEEE Photon. Technol. Lett.,* vol. 19, no. 17-20, pp. 1472-1474, Oct. 2007.

[92] J. P. Yao and Q. Wang, "Photonic microwave bandpass filter with negative coefficients using a polarization modulator," *IEEE Photon. Technol. Lett.,* vol. 19, no. 9-12, pp. 644-646, May-Jun. 2007.

[93] Y. Yan and J. Yao, "Photonic microwave handpass filter with improved dynamic range," *Opt. Lett.,* vol. 33, no. 15, pp. 1756-1758, Aug 1. 2008.

[94] K. Lee, J. H. Lee, and S. B. Lee, "Tunable photonic microwave notch filter using SOA-based single-longitudinal mode, dual-wavelength laser," *Opt. Express,* vol. 17, no. 15, pp. 13216-13221, Jul 20. 2009.

[95] X. Yi, T. X. H. Huang, and R. A. Minasian, "Microwave photonic filter with tunability, reconfigurability and bipolar taps," *Electron. Lett.,* vol. 45, no. 16, pp. 840-U51, Jul 30. 2009.

[96] X. K. Yi and R. A. Minasian, "New Spectrum-Sliced Microwave Photonic Filter for High-Frequency Signal Processing," *IEEE Photon. Technol. Lett.,* vol. 21, no. 1-4, pp. 230-232, Jan-Feb. 2009.

[97] W. Zhang, J. A. R. Williams, and I. Bennion, "Polarization synthesized optical transversal filter employing high birefringence fiber gratings," *IEEE Photon. Technol. Lett.,* vol. 13, no. 5, pp. 523-525, May. 2001.

[98] D. Pastor, J. Capmany, and B. Ortega, "Broad-band tunable microwave transversal notch filter based on tunable uniform fiber Bragg gratings as slicing filters," *IEEE Photon. Technol. Lett.,* vol. 13, no. 7, pp. 726-728, Jul. 2001.

[99] J. Marti, V. Polo, F. Ramos, and D. Moodie, "Photonic tunable microwave filters employing electroabsorption modulators and wideband chirped fibre gratings," *Electron. Lett.,* vol. 35, no. 4, pp. 305-306, Feb 18. 1999.

[100] J. Capmany, D. Pastor, and B. Ortega, "New and flexible fiber-optic delay-line filters using chirped Bragg gratings and laser arrays," *IEEE Trans. Microw. Theory Tech.,* vol. 47, no. 7, pp. 1321-1326, Jul. 1999.

[101] J. Marti, F. Ramos, and R. I. Laming, "Photonic microwave filter employing multimode optical sources and wideband chirped fibre gratings," *Electron. Lett.,* vol. 34, no. 18, pp. 1760-1761, Sep 3. 1998.

[102] D. B. Hunter and R. A. Minasian, "Photonic signal processing of microwave signals using an active-fiber Bragg-grating-pair structure," *IEEE Trans. Microw. Theory Tech.,* vol. 45, no. 8, pp. 1463-1466, Aug. 1997.

[103] D. B. Hunter and R. A. Minasian, "Microwave optical filters using in-fiber Bragg grating arrays," *Ieee Microw Guided W,* vol. 6, no. 2, pp. 103-105, Feb. 1996.

[104] D. B. Hunter and R. A. Minasian, "Reflectively Tapped Fiber Optic Transversal Filter Using in-Fiber Bragg Gratings," *Electron. Lett.,* vol. 31, no. 12, pp. 1010-1012, Jun 8. 1995.

[105] G. Yu, W. Zhang, and J. A. R. Williams, "High-performance microwave transversal filter using fiber Bragg grating arrays," *IEEE Photon. Technol. Lett.,* vol. 12, no. 9, pp. 1183-1185, Sep. 2000.

[106] X. K. Yi, C. Lu, X. F. Yang, W. D. Zhong, F. Wei, L. Ding, and Y. X. Wang, "Continuously tunable microwave-photonic filter design using high-birefringence linear chirped grating," *IEEE Photon. Technol. Lett.,* vol. 15, no. 5, pp. 754-756, May. 2003.

[107] F. Zeng, J. P. Yao, and S. J. Mihailov, "Fiber Bragg-grating-based all-optical microwave filter synthesis using genetic algorithm," *Opt. Eng.,* vol. 42, no. 8, pp. 2250-2256, Aug. 2003.

[108] G. Ning, S. Aditya, P. Shum, Y. D. Gong, J. H. Ng, and G. Teo, "Tunable photonic microwave filter with Hi-Bi chirped grating free from chromatic dispersion," *Electron. Lett.*, vol. 40, no. 16, pp. 999-1000, Aug 5. 2004.

[109] M. Delgado-Pinar, J. Mora, A. Diez, M. V. Andres, B. Ortega, and J. Capmany, "Tunable and reconfigurable microwave filter by use of a Bragg-grating-based acousto-optic superlattice modulator," *Opt. Lett.*, vol. 30, no. 1, pp. 8-10, Jan 1. 2005.

[110] G. Ning, S. Aditya, P. Shum, L. H. Cheng, Y. D. Gong, and C. Lu, "Tunable photonic microwave bandpass filter using phase modulation and a chirped fiber grating in a Sagnac loop," *IEEE Photon. Technol. Lett.*, vol. 17, no. 9, pp. 1935-1937, Sep. 2005.

[111] X. B. Yu, X. M. Zhang, H. Chi, and K. S. Chen, "Photonic microwave transversal filter employing a fiber-Bragg-grating-based multiple resonator," *Microwave Opt. Tech. Lett.*, vol. 44, no. 4, pp. 369-371, Feb 20. 2005.

[112] W. Zhang, I. Bennion, and J. A. R. Williams, "Chromatic dispersion effect in a microwave photonic filter using superstructured fiber Bragg grating and dispersive fiber," *Opt. Express,* vol. 13, no. 17, pp. 6429-6437, Aug 22. 2005.

[113] J. D. Taylor, L. R. Chen, and X. J. Gu, "Simple reconfigurable photonic microwave filter using an arrayed waveguide grating and fiber Bragg gratings," *IEEE Photon. Technol. Lett.*, vol. 19, no. 5-8, pp. 510-512, Mar-Apr. 2007.

[114] J. Q. Zhou, S. Aditya, P. Shum, L. Xia, and B. P. Parhusip, "Wide-range continuously tunable microwave photonic filter using high-birefringence linearly chirped fiber Bragg grating and polarization beamsplitters," *Opt. Eng.*, vol. 48, no. 1, pp. -, Jan. 2009.

[115] R. Feced, M. N. Zervas, and M. A. Muriel, "An efficient inverse scattering algorithm for the design of nonuniform fiber Bragg gratings," *IEEE J. Quantum Electron.*, vol. 35, no. 8, pp. 1105-1115, Aug. 1999.

[116] O. V. Belai, L. L. Frumin, E. V. Podivilov, and D. A. Shapiro, "Efficient numerical method of the fiber Bragg grating synthesis," *J. Opt. Soc. Am. B,* vol. 24, no. 7, pp. 1451-1457, Jul. 2007.

[117] A. Othonos, "Fiber Bragg gratings," *Rev. Sci. Instrum.*, vol. 68, no. 12, pp. 4309-4341, Dec. 1997.

[118] M. Gagne, L. Bojor, R. Maciejko, and R. Kashyap, "Novel custom fiber Bragg grating fabrication technique based on push-pull phase shifting interferometry," *Opt. Express,* vol. 16, no. 26, pp. 21550-21557, Dec 22. 2008.

[119] G. Meltz, W. W. Morey, and W. H. Glenn, "Formation of Bragg Gratings in Optical Fibers by a Transverse Holographic Method," *Opt. Lett.,* vol. 14, no. 15, pp. 823-825, Aug 1. 1989.

[120] L. Dong, J. L. Archambault, L. Reekie, P. S. J. Russell, and D. N. Payne, "Single-Pulse Bragg Gratings Written during Fiber Drawing," *Electron. Lett.,* vol. 29, no. 17, pp. 1577-1578, Aug 19. 1993.

[121] K. O. Hill, B. Malo, F. Bilodeau, D. C. Johnson, and J. Albert, "Bragg Gratings Fabricated in Monomode Photosensitive Optical-Fiber by Uv Exposure through a Phase Mask (Vol 62, Pg 1035, 1993)," *Appl. Phys. Lett.,* vol. 63, no. 3, pp. 424-424, Jul 19. 1993.

[122] C. Wang, F. Zeng, and J. P. Yao, "All-fiber ultrawideband pulse generation based on spectral-shaping and dispersion-induced frequency-to-time conversion," *IEEE Photon. Technol. Lett.,* vol. 19, no. 2-4, pp. 137-139, Feb. 2007.

[123] D. Porcino and W. Hirt, "Ultra-wideband radio technology: Potential and challenges ahead," *Ieee Commun Mag,* vol. 41, no. 7, pp. 66-74, Jul. 2003.

[124] J. P. Yao, F. Zeng, and Q. Wang, "Photonic generation of ultrawideband signals," *J. Lightwave Technol.,* vol. 25, no. 11, pp. 3219-3235, Nov. 2007.

[125] J. P. Yao, "Photonics for Ultrawideband Communications," *IEEE Microw. Mag.,* vol. 10, no. 4, pp. 82-95, Jun. 2009.

[126] C. Xiaomin and S. Kiaei, "Monocycle shapes for ultra wideband system," in *Circuits and Systems, 2002. ISCAS 2002. IEEE International Symposium on*, 2002, pp. I-597-I-600 vol.1.

[127] A. W. Rihaczek, *Principles of High-Resolution Radar*. Norwood, MA: Artech House, 1996.

[128] R. Skaug and J. F. Hjelmstad, *Spread Spectrum in Communication*. London, U.K.: Peter Peregrinus Ltd., 1985.

[129] M. Bertero, M. Miyakawa, P. Boccacci, F. Conte, K. Orikasa, and M. Furutani, "Image restoration in chirp-pulse microwave CT (CP-MCT)," *IEEE Trans. Bio-Med. Eng.*, vol. 47, no. 5, pp. 690-699, May. 2000.

[130] C. Wang and J. P. Yao, "Photonic generation of chirped microwave pulses using superimposed chirped fiber Bragg gratings," *IEEE Photon. Technol. Lett.*, vol. 20, no. 9-12, pp. 882-884, Jun. 2008.

[131] C. Wang and J. P. Yao, "Chirped Microwave Pulse Generation Based on Optical Spectral Shaping and Wavelength-to-Time Mapping Using a Sagnac Loop Mirror Incorporating a Chirped Fiber Bragg Grating," *J. Lightwave Technol.*, vol. 27, no. 16, pp. 3336-3341, Aug. 2009.

[132] C. Wang and J. P. Yao, "Photonic generation of chirped millimeter-wave pulses based on Nonlinear frequency-to-time mapping in a nonlinearly chirped fiber Bragg grating," *IEEE Trans. Microw. Theory Tech.*, vol. 56, no. 2, pp. 542-553, Feb. 2008.

[133] C. Wang and J. Yao, "All-optical electrical chirped pulse generation with tunable chirp rate based on a nonlinearly chirped fiber Bragg grating," in *Microwave Photonics, 2007 IEEE International Topical Meeting on*, Victoria, British Columbia, Canada, 2007, pp. 202-205.

[134] C. Wang and J. P. Yao, "Simultaneous optical spectral shaping and wavelength-to-time mapping for photonic microwave arbitrary waveform generation," *IEEE Photon. Technol. Lett.*, vol. 21, no. 9-12, pp. 793-795, Jun. 2009.

[135] C. Wang and J. Yao, "Large Time-Bandwidth Product Microwave Arbitrary Waveform Generation Using a Spatially Discrete Chirped Fiber Bragg Grating," *J. Lightwave Technol.*, vol. 28, no. 11, pp. 1652-1660, Jun. 2010.

[136] C. Wang, M. Li, and J. Yao, "Continuously Tunable Photonic Microwave Frequency Multiplication by Use of an Unbalanced Temporal Pulse Shaping System," *IEEE Photon. Technol. Lett.*, vol. 22, no. 17, pp. 1285-1287, Sep. 2010.

[137] C. Wang and J. P. Yao, "Fourier transform ultrashort optical pulse shaping using a single chirped fiber Bragg grating," *IEEE Photon. Technol. Lett.*, vol. 21, no. 19, pp. 1375-1377, Oct. 2009.

[138] C. Wang and J. P. Yao, "Chirped Microwave Pulse Compression Using a Photonic Microwave Filter With a Nonlinear Phase Response," *IEEE Trans. Microw. Theory Tech.*, vol. 57, no. 2, pp. 496-504, Feb. 2009.

[139] C. Wang and J. Yao, "Photonic microwave matched filters for chirped microwave pulse compression," in *Microwave Photonics, 2008. Jointly held with the 2008 Asia-Pacific Microwave Photonics Conference. MWP/APMP 2008. International Topicsl Meeting on*, Gold Coast City, Queensland, Australia, 2008, pp. 47-50.

[140] A. Papoulis, "Pulse compression, fiber communications, and diffraction: a unified approach," *J. Opt. Soc. Am. A,* vol. 11, no. 1, pp. 3-13, Jan. 1994.

[141] C.-P. Huang, H. C. Kapteyn, J. W. McIntosh, and M. M. Murnane, "Generation of transform-limited 32-fs pulses from a self-mode-locked Ti:sapphire laser," *Opt. Lett.*, vol. 17, no. 2, pp. 139-141. 1992.

[142] T. Kobayashi, H. Yao, K. Amano, Y. Fukushima, A. Morimoto, and T. Sueta, "Optical pulse compression using high-frequency electrooptic phase modulation," *IEEE J. Quantum Electron.*, vol. 24, no. 2, pp. 382-387. 1988.

[143] T. Komukai, T. Yamamoto, and S. Kawanishi, "Optical pulse generator using phase modulator and linearly chirped fiber Bragg gratings," *IEEE Photon. Technol. Lett.*, vol. 17, no. 8, pp. 1746-1748. 2005.

[144] V. Torres-Company, J. Lancis, and P. Andrés, "Incoherent frequency-to-time mapping: application to incoherent pulse shaping," *J. Opt. Soc. Am. A,* vol. 24, no. 3, pp. 888-894. 2007.

[145] V. Torres-Company, J. Lancis, P. Andres, and L. R. Chen, "20 GHz arbitrary radio-frequency waveform generator based on incoherent pulse shaping," *Opt. Express,* vol. 16, no. 26, pp. 21564-21569, Dec 22. 2008.

[146] C. Dorrer, "Statistical analysis of incoherent pulse shaping," *Opt. Express,* vol. 17, no. 5, pp. 3341-3352. 2009.

[147] R. Kashyap and M. de Lacerda Rocha, "On the group delay characteristics of chirped fibre Bragg gratings," *Opt. Commun.*, vol. 153, no. 1-3, pp. 19-22. 1998.

[148] H. Chi and J. Yao, "Chirped RF Pulse Generation Based on Optical Spectral Shaping and Wavelength-to-Time Mapping Using a Nonlinearly Chirped Fiber Bragg Grating," *J. Lightwave Technol.*, vol. 26, no. 10, pp. 1282-1287. 2008.

[149] H. Xia, C. Wang, S. Blais, and J. Yao, "Ultrafast and Precise Interrogation of Fiber Bragg Grating Sensor Based on Wavelength-to-Time Mapping Incorporating Higher Order Dispersion," *J. Lightwave Technol.,* vol. 28, no. 3, pp. 254-261. 2010.

[150] K. O. Hill and G. Meltz, "Fiber Bragg grating technology fundamentals and overview," *J. Lightwave Technol.,* vol. 15, no. 8, pp. 1263-1276. 1997.

[151] A. Yariv, "Coupled-mode theory for guided-wave optics," *IEEE J. Quantum Electron.,* vol. 9, no. 9, pp. 919-933. 1973.

[152] T. Erdogan, "Fiber grating spectra," *J. Lightwave Technol.,* vol. 15, no. 8, pp. 1277-1294, Aug. 1997.

[153] M. McCall, "On the application of coupled mode theory for modeling fiber Bragg gratings," *J. Lightwave Technol.,* vol. 18, no. 2, pp. 236-242, Feb. 2000.

[154] M. Yamada and K. Sakuda, "Analysis of almost-periodic distributed feedback slab waveguides via a fundamental matrix approach," *Appl. Opt.,* vol. 26, no. 16, pp. 3474-3478, Aug. 1987.

[155] K. A. Winick and J. E. Roman, "Design of corrugated waveguide filters by Fourier-transform techniques," *IEEE J. Quantum Electron.,* vol. 26, no. 11, pp. 1918-1929, Nov. 1990.

[156] E. Peral, J. Capmany, and J. Marti, "Iterative solution to the Gel'Fand-Levitan-Marchenko coupled equations and application to synthesis of fiber gratings," *IEEE J. Quantum Electron.,* vol. 32, no. 12, pp. 2078-2084, Dec. 1996.

[157] J. Skaar, L. G. Wang, and T. Erdogan, "On the synthesis of fiber Bragg gratings by layer peeling," *IEEE J. Quantum Electron.,* vol. 37, no. 2, pp. 165-173, Feb. 2001.

[158] J. Skaar, L. Wang, and T. Erdogan, "Synthesis of Thick Optical Thin-Film Filters with a Layer-Peeling Inverse-Scattering Algorithm," *Appl. Opt.,* vol. 40, no. 13, pp. 2183-2189. 2001.

[159] W. W. Morey, G. Meltz, and W. H. Glenn, "Holographically generated gratings in optical fibers," *Opt. Photon. News,* vol. 1, no. 7, pp. 14-16. 1990.

[160] K. O. Hill, B. Malo, K. A. Vineberg, F. Bilodeau, D. C. Johnson, and I. Skinner, "Efficient mode conversion in telecommunication fibre using externally written gratings," *Electron. Lett.,* vol. 26, no. 16, pp. 1270-1272. 1990.

[161] K. O. Hill, B. Malo, F. Bilodeau, D. C. Johnson, and J. Albert, "Bragg gratings fabricated in monomode photosensitive optical fiber by UV exposure through a phase mask," *Appl. Phys. Lett.*, vol. 62, no. 10, pp. 1035-1037. 1993.

[162] M. J. Cole, W. H. Loh, R. I. Laming, M. N. Zervas, and S. Barcelos, "Moving fibre/phase mask-scanning beam technique for enhanced flexibility in producing fibre gratings with uniform phase mask," *Electron. Lett.*, vol. 31, no. 17, pp. 1488-1490. 1995.

[163] H. Ito, T. Furuta, Y. Hirota, T. Ishibashi, A. Hirata, T. Nagatsuma, H. Matsuo, T. Noguchi, and M. Ishiguro, "Photonic millimetre-wave emission at 300 GHz using an antenna-integrated uni-travelling-carrier photodiode," *Electron. Lett.*, vol. 38, no. 17, pp. 989-990. 2002.

[164] M. Ghavami, L. B. Michael, and R. Kohno, *Ultra Wide-Band Signals and Systems in Communication Engineering*. West Sussex, England: Wiley, 2004.

[165] G. R. Aiello and G. D. Rogerson, "Ultra-wideband wireless systems," *IEEE Microw. Mag.*, vol. 4, no. 2, pp. 36-47, Jun. 2003.

[166] X. Chen and S. Kiaei, "Monocycle shapes for ultra wide-band system," in *IEEE Int. Symp. Circuits and Systems*, 2002, pp. 26-29.

[167] K. Marsden, H.-J. Lee, D. S. Ha, and H.-S. Lee, "Low Power CMOS Re-programmable Pulse Generator for UWB Systems," in *IEEE Conf. on Ultra Wideband Systems and Technologies*, Nov. 2003., pp. 443-447.

[168] Y. Jeong and S. Jung, "A CMOS Impulse Generator for UWB Wireless Communication System," in *Proc. of 2004 IEEE Int. Symp. Circuit and Systems*, May 2004, pp. IV-129 - IV-132.

[169] B. Jung, Y.-H. Tseng, J. Harvey, and R. Harjani, "Pulse Generator Design for UWB IR Communication System," in *IEEE Int. Symp. Circuits and Systems*, 2005, pp. 4381-4384.

[170] W. P. Lin and J. Y. Chen, "Implementation of a new ultrawide-band impulse system," *IEEE Photon. Technol. Lett.*, vol. 17, no. 11, pp. 2418-2420, Nov. 2005.

[171] F. Zeng and J. P. Yao, "An approach to ultrawideband pulse generation and distribution over optical fiber," *IEEE Photon. Technol. Lett.*, vol. 18, no. 5-8, pp. 823-825, Mar-Apr. 2006.

[172] M. Bolea, J. Mora, B. Ortega, and J. Capmany, "Optical UWB pulse generator using an N tap microwave photonic filter and phase inversion adaptable to different pulse modulation formats," *Opt. Express,* vol. 17, no. 7, pp. 5023-5032, Mar 30. 2009.

[173] J. Q. Li, S. N. Fu, K. Xu, J. T. Wu, J. T. Lin, M. Tang, and P. Shum, "Photonic ultrawideband monocycle pulse generation using a single electro-optic modulator," *Opt. Lett.,* vol. 33, no. 3, pp. 288-290, Feb 1. 2008.

[174] H. W. Chen, M. H. Chen, C. Y. Qiu, and S. Z. Xie, "A novel composite method for ultra-wideband doublet pulses generation," *IEEE Photon. Technol. Lett.,* vol. 19, no. 21-24, pp. 2021-2023, Nov-Dec. 2007.

[175] Q. Wang and H. Yao, "An electrically switchable optical ultrawideband pulse generator," *J. Lightwave Technol.,* vol. 25, no. 11, pp. 3626-3633, Nov. 2007.

[176] M. Abtahi, M. Mirshafiei, S. LaRochelle, and L. A. Rusch, "All-Optical 500-Mb/s UWB Transceiver: An Experimental Demonstration," *J. Lightwave Technol.,* vol. 26, no. 13-16, pp. 2795-2802, Jul-Aug. 2008.

[177] Y. C. Tong, L. Y. Chan, and H. K. Tsang, "Fibre dispersion or pulse spectrum measurement using a sampling oscilloscope," *Electron. Lett.,* vol. 33, no. 11, pp. 983-985, May 22. 1997.

[178] M. Abtahi, J. Magné, M. Mirshafiei, L. A. Rusch, and S. LaRochelle, "Generation of Power-Efficient FCC-Compliant UWB Waveforms Using FBGs: Analysis and Experiment," *J. Lightwave Technol.,* vol. 26, no. 5, pp. 628-635, Mar. 2008.

[179] M. Bertero, M. Miyakawa, P. Boccacci, F. Conte, K. Orikasa, and M. Furutani, "Image restoration in chirp-pulse microwave CT (CP-MCT)," *Biomedical Engineering, IEEE Transactions on,* vol. 47, no. 5, pp. 690-699, May. 2000.

[180] H. D. Griffiths and W. J. Bradford, "Digital generation of high time-bandwidth product linear FM waveforms for radar altimeters," *Radar and Signal Processing, IEE Proceedings F,* vol. 139, no. 2, pp. 160-169, Apr. 1992.

[181] F. W. Hopwood and R. A. Tracy, "Digital Generation of Wideband Linear FM Waveforms," in *Microwave Symposium Digest, 1980 MTT-S International*, 1980, pp. 111-113.

[182] K. Hyukjin and K. Bongkoo, "Linear frequency modulation of voltage-controlled oscillator using delay-line feedback," *Microwave and Wireless Components Letters, IEEE,* vol. 15, no. 6, pp. 431-433, Jun. 2005.

[183] A. Zeitouny, S. Stepanov, O. Levinson, and M. Horowitz, "Optical generation of linearly chirped microwave pulses using fiber Bragg gratings," *IEEE Photon. Technol. Lett.,* vol. 17, no. 3, pp. 660-662, Mar. 2005.

[184] L. Zhang, K. Sugden, I. Bennion, and A. Molony, "Wide-Stopband Chirped Fiber Moire Grating Transmission Filters," *Electron. Lett.,* vol. 31, no. 6, pp. 477-479, Mar 16. 1995.

[185] R. Slavik, S. Doucet, and S. LaRochelle, "High-performahce all-fiber Fabry-Perot filters with superimposed chirped Bragg gratings," *J. Lightwave Technol.,* vol. 21, no. 4, pp. 1059-1065, Apr. 2003.

[186] Y. G. Han, X. Y. Dong, C. S. Kim, M. Y. Jeong, and J. H. Lee, "Flexible all fiber Fabry-Perot filters based on superimposed chirped fiber Bragg gratings with continuous FSR tunability and its application to a multiwavelength fiber laser," *Opt. Express,* vol. 15, no. 6, pp. 2921-2926, Mar 19. 2007.

[187] J. Azana, P. Kockaert, R. Slavik, L. R. Chen, and S. LaRochelle, "Generation of a 100-GHz optical pulse train by pulse repetition-rate multiplication using superimposed fiber Bragg gratings," *IEEE Photon. Technol. Lett.,* vol. 15, no. 3, pp. 413-415, Mar. 2003.

[188] S. Mallet, *A Wavelet Tour of Signal Processing.* San Diego, CA: Academic, 1999.

[189] X. Shu, L. Yu, D. Zhao, L. Zhang, K. Sugden, and I. Bennion, "Transmission characteristics of Sagnac interferometers based on fiber Bragg gratings," *J. Opt. Soc. Am. B,* vol. 19, no. 11, pp. 2770-2780. 2002.

[190] X. Shu, S. Jiang, and D. Huang, "Fiber grating Sagnac loop and its multiwavelength-laser application," *IEEE Photon. Technol. Lett.,* vol. 12, no. 8, pp. 980-982, Aug. 2000.

[191] G. P. Agrawal, *Nonlinear Fiber Optics, 2nd ed.* NewYork: Academic Press, 1995.

[192] K. O. Hill, F. Bilodeau, B. Malo, T. Kitagawa, S. Thériault, D. C. Johnson, J. Albert, and K. Takiguchi, "Chirped in-fiber Bragg gratings for compensation of optical-fiber dispersion," *Opt. Lett.,* vol. 19, no. 17, pp. 1314-1316, Sep. 1994.

[193] L. Pei, S. S. Jian, F. P. Yan, T. G. Ning, and Z. Wang, "Long-haul WDM system through conventional single mode optical fiber with dispersion compensation by chirped fiber Bragg grating," *Opt. Commun.,* vol. 222, no. 1-6, pp. 169-178, Jul 1. 2003.

[194] B. J. Eggleton, B. Mikkelsen, G. Raybon, A. Ahuja, J. A. Rogers, P. S. Westbrook, T. N. Nielsen, S. Stulz, and K. Dreyer, "Tunable dispersion compensation in a 160-Gb/s TDM system by a voltage controlled chirped fiber Bragg grating," *IEEE Photon. Technol. Lett.,* vol. 12, no. 8, pp. 1022-1024, Aug. 2000.

[195] S. Lee, R. Khosravani, J. Peng, V. Grubsky, D. S. Starodubov, A. E. Willner, and J. Feinberg, "Adjustable compensation of polarization mode dispersion using a high-birefringence nonlinearly chirped fiber Bragg grating," *IEEE Photon. Technol. Lett.,* vol. 11, no. 10, pp. 1277-1279, Oct. 1999.

[196] S. Thibault, J. Lauzon, J. F. Cliche, J. Martin, M. A. Duguay, and M. Tetu, "Numerical-Analysis of the Optimal Length and Profile of a Linearly Chirped Fiber Bragg Grating for Dispersion Compensation," *Opt. Lett.,* vol. 20, no. 6, pp. 647-649, Mar 15. 1995.

[197] K. O. Hill, S. Theriault, B. Malo, F. Bilodeau, T. Kitagawa, D. C. Johnson, J. Albert, K. Takiguchi, T. Kataoka, and K. Hagimoto, "Chirped in-Fiber Bragg Grating Dispersion Compensators - Linearization of Dispersion Characteristic and Demonstration of Dispersion Compensation in 100-Km, 10-Gbit/S Optical-Fiber Link," *Electron. Lett.,* vol. 30, no. 21, pp. 1755-1756, Oct 13. 1994.

[198] J. A. R. Williams, I. Bennion, K. Sugden, and N. J. Doran, "Fiber Dispersion Compensation Using a Chirped in-Fiber Bragg Grating," *Electron. Lett.,* vol. 30, no. 12, pp. 985-987, Jun 9. 1994.

[199] X. F. Chen, Z. C. Deng, and J. P. Yao, "Photonic generation of microwave signal using a dual-wavelength single-longitudinal-mode fiber ring laser," *IEEE Trans. Microw. Theory Tech.,* vol. 54, no. 2, pp. 804-809, Feb. 2006.

[200] H. Chi, F. Zeng, and J. P. Yao, "Photonic generation of microwave signals based on pulse shaping," *IEEE Photon. Technol. Lett.,* vol. 19, no. 9-12, pp. 668-670, May-Jun. 2007.

[201] H. Chi and J. Yao, "All-fiber chirped microwave pulses generation based on spectral shaping and wavelength-to-time conversion," *IEEE Trans. Microw. Theory Tech.,* vol. 55, no. 9, pp. 1958-1963, Sep. 2007.

[202] H. Y. Xia and J. P. Yao, "Characterization of Subpicosecond Pulses Based on Temporal Interferometry With Real-Time Tracking of Higher Order Dispersion and Optical Time Delay," *J. Lightwave Technol.,* vol. 27, no. 22, pp. 5029-5037, Nov 15. 2009.

[203] M. Miyagi and S. Nishida, "Pulse spreading in a single-mode fiber due to third-order dispersion," *Appl. Opt.*, vol. 18, no. 5, pp. 678-682. 1979.

[204] M. Amemiya, "Pulse Broadening due to Higher Order Dispersion and its Transmission Limit," *J. Lightwave Technol.*, vol. 20, no. 4, p. 591. 2002.

[205] K. M. Feng, J. X. Chai, V. Grubsky, D. S. Starodubov, M. I. Hayee, S. Lee, X. Jiang, A. E. Willner, and J. Feinberg, "Dynamic dispersion compensation in a 10-Gb/s optical system using a novel voltage tuned nonlinearly chirped fiber Bragg grating," *IEEE Photon. Technol. Lett.*, vol. 11, no. 3, pp. 373-375, Mar. 1999.

[206] S. Lee, R. Khosravani, J. Peng, V. Grubsky, D. S. Starodubov, A. E. Willner, and J. Feinberg, "Adjustable compensation of polarization mode dispersion using a high-birefringence nonlinearly chirped fiber Bragg grating," *IEEE Photon. Technol. Lett.*, vol. 11, no. 10, pp. 1277-1279, Oct. 1999.

[207] Z. Pan, Y. W. Song, C. Yu, Y. Wang, Q. Yu, J. Popelek, H. Li, Y. Li, and A. E. Willner, "Tunable Chromatic Dispersion Compensation in 40-Gb/s Systems Using Nonlinearly Chirped Fiber Bragg Gratings," *J. Lightwave Technol.*, vol. 20, no. 12, p. 2239, Dec. 2002.

[208] X. Dong, P. Shum, N. Ngo, C. Chan, J. Ng, and C. Zhao, "A largely tunable CFBG-based dispersion compensator with fixed center wavelength," *Opt. Express,* vol. 11, no. 22, pp. 2970-2974, Nov. 2003.

[209] C. Wang and J. Yao, "All-optical electrical chirped pulse generation based on nonlinear wavelength-to-time conversion in a chirped fiber Bragg grating," in *Proc. SPIE*, 2007, pp. 67962K-5.

[210] J. Azana and L. R. Chen, "Synthesis of temporal optical waveforms by fiber Bragg gratings: a new approach based on space-to-frequency-to-time mapping," *J. Opt. Soc. Am. B,* vol. 19, no. 11, pp. 2758-2769, Nov. 2002.

[211] V. Grubsky, A. Skorucak, D. S. Starodubov, and J. Feinberg, "Fabrication of long-period fiber gratings with no harmonics," *IEEE Photon. Technol. Lett.*, vol. 11, no. 1, pp. 87-89, Jan. 1999.

[212] H. Chi and J. P. Yao, "An approach to photonic generation of high-frequency phase-coded RF pulses," *IEEE Photon. Technol. Lett.*, vol. 19, no. 9-12, pp. 768-770, May-Jun. 2007.

[213] H. Chi and J. P. Yao, "Chirped RF pulse generation based on optical spectral shaping and wavelength-to-time mapping using a nonlinearly chirped fiber Bragg grating," *J. Lightwave Technol.,* vol. 26, no. 9-12, pp. 1282-1287, May-Jun. 2008.

[214] Y. T. Dai and J. P. Yao, "Chirped Microwave Pulse Generation Using a Photonic Microwave Delay-Line Filter With a Quadratic Phase Response," *IEEE Photon. Technol. Lett.,* vol. 21, no. 9-12, pp. 569-571, May-Jun. 2009.

[215] V. Narayan and D. L. Macfarlane, "Bursts and Codes of Ultrashort Pulses," *IEEE Photon. Technol. Lett.,* vol. 5, no. 12, pp. 1465-1467, Dec. 1993.

[216] Y. Dai and J. P. Yao, "Arbitrary phase-modulated RF signal generation based on optical pulse position modulation," *J. Lightwave Technol.,* vol. 26, no. 17-20, pp. 3329-3336, Sep-Oct. 2008.

[217] N. Levanon and E. Mozeson, *Radar Signals*: Wiley-IEEE Press, 2004.

[218] W. J. Caputi, "Stretch - Time-Transformation Technique," *IEEE. Trans. Aero. Elec. Sys.,* vol. Aes7, no. 2, pp. 269-&. 1971.

[219] J. Azana, "Design specifications of time-domain spectral shaping optical system based on dispersion and temporal modulation," *Electron. Lett.,* vol. 39, no. 21, pp. 1530-1532. 2003.

[220] J. U. Kang, M. Y. Frankel, and R. D. Esman, "Demonstration of microwave frequency shifting by use of a highly chirped mode-locked fiber laser," *Opt. Lett.,* vol. 23, no. 15, pp. 1188-1190, Aug 1. 1998.

[221] Y. Han and B. Jalali, "Photonic time-stretched analog-to-digital converter: Fundamental concepts and practical considerations," *J. Lightwave Technol.,* vol. 21, no. 12, pp. 3085-3103, Dec. 2003.

[222] J. M. Fuster, D. Novak, A. Nirmalathas, and J. Marti, "Single-sideband modulation in photonic time-stretch analogue-to-digital conversion," *Electron. Lett.,* vol. 37, no. 1, pp. 67-68, Jan 4. 2001.

[223] J. Azana, N. K. Berger, B. Levit, V. Smulakovsky, and B. Fischer, "Frequency shifting of microwave signals by use of a general temporal self-imaging (Talbot) effect in optical fibers," *Opt. Lett.,* vol. 29, no. 24, pp. 2849-2851, Dec 15. 2004.

[224] G. H. Qi, J. P. Yao, J. Seregelyi, S. Paquet, and C. Belisle, "Generation and distribution of a wide-band continuously tunable millimeter-wave signal with an optical external

modulation technique," *IEEE Trans. Microw. Theory Tech.,* vol. 53, no. 10, pp. 3090-3097, Oct. 2005.

[225] Y. Q. Liu, J. L. Yang, and J. P. Yao, "Continuous true-time-delay beamforming for phased array antenna using a tunable chirped fiber grating delay line," *IEEE Photon. Technol. Lett.,* vol. 14, no. 8, pp. 1172-1174, Aug. 2002.

[226] A. M. Weiner, D. E. Leaird, J. S. Patel, and J. R. Wullert, II, "Programmable shaping of femtosecond optical pulses by use of 128-element liquid crystal phase modulator," *IEEE J. Quantum Electron.,* vol. 28, no. 4, pp. 908-920. 1992.

[227] M. A. Preciado, V. Garcia-Munoz, and M. A. Muriel, "Grating Design of Oppositely Chirped FBGs for Pulse Shaping," *IEEE Photon. Technol. Lett.,* vol. 19, no. 6, pp. 435-437. 2007.

[228] I. C. M. Littler, L. Fu, and B. J. Eggleton, "Effect of group delay ripple on picosecond pulse compression schemes," *Appl. Opt.,* vol. 44, no. 22, pp. 4702-4711. 2005.

[229] J. Capmany, B. Ortega, and D. Pastor, "A Tutorial on Microwave Photonic Filters," *J. Lightwave Technol.,* vol. 24, no. 1, pp. 201-209, Jan. 2006.

[230] Y. Ningsi and R. A. Minasian, "A novel tunable microwave optical notch filter," *IEEE Trans. Microw. Theory Tech.,* vol. 49, no. 10, pp. 2002-2005, Oct. 2001.

[231] A. Loayssa, J. Capmany, M. Sagues, and J. Mora, "Demonstration of incoherent microwave photonic filters with all-optical complex coefficients," *IEEE Photon. Technol. Lett.,* vol. 18, no. 16, pp. 1744-1746, Aug. 2006.

[232] M. Sagues, A. Loayssa, and J. Capmany, "Multitap Complex-Coefficient Incoherent Microwave Photonic Filters Based on Stimulated Brillouin Scattering," *IEEE Photon. Technol. Lett.,* vol. 19, no. 16, pp. 1194-1196, Jul. 2007.

[233] Y. T. Dai and J. P. Yao, "Nonuniformly-spaced photonic microwave delay-line filter," *Opt. Express,* vol. 16, no. 7, pp. 4713-4718, Mar. 2008.

[234] Y. Dai and J. P. Yao, "Nonuniformly spaced photonic microwave delay-line filters and applications," *IEEE Trans. Microw. Theory Tech.* accepted.

[235] X. H. Feng, C. Lu, H. Y. Tam, and P. K. A. Wai, "Reconfigurable microwave photonic filter using multiwavelength erbium-doped fiber laser," *IEEE Photon. Technol. Lett.,* vol. 19, no. 17-20, pp. 1334-1336, Sep-Oct. 2007.

[236] A. Bellemare, M. Karasek, M. Rochette, S. Lrochelle, and M. Tetu, "Room temperature multifrequency erbium-doped fiber lasers anchored on the ITU frequency grid," *J. Lightwave Technol.,* vol. 18, no. 6, pp. 825-831, Jun. 2000.

[237] J. Mora, B. Ortega, J. Capmany, J. L. Cruz, M. V. Andres, D. Pastor, and S. Sales, "Automatic tunable and reconfigurable fiberoptic microwave filters based on a broadband optical source sliced by uniform fiber Bragg gratings," *Opt. Express,* vol. 10, no. 22, pp. 1291-1298, Nov 04. 2002.

[238] X. K. Yi and R. A. Minasian, "Dispersion induced RF distortion of spectrum-sliced microwave-photonic filters," *IEEE Trans. Microw. Theory Tech.,* vol. 54, no. 2, pp. 880-886, Feb. 2006.

[239] R. L. Fork, C. H. B. Cruz, P. C. Becker, and C. V. Shank, "Compression of optical pulses to six femtoseconds by using cubic phase compensation," *Opt. Lett.,* vol. 12, no. 7, pp. 483-485, Jul. 1987.

[240] B. V. K. V. Kumar and L. Hassebrook, "Performance measures for correlation filters," *Appl. Opt.,* vol. 29, no. 20, pp. 2997-3006, Jul. 1990.

[241] M. Ibsen, M. K. Durkin, M. N. Zervas, A. B. Grudinin, and R. I. Laming, "Custom design of long chirped Bragg gratings: application to gain-flattening filter with incorporated dispersion compensation," *IEEE Photon. Technol. Lett.,* vol. 12, no. 5, pp. 498-500, May. 2000.

[242] M. Izutsu, S. Shikama, and T. Sueta, "Integrated optical SSB modulator/frequency shifter," *IEEE J. Quantum Electron.,* vol. 17, no. 11, pp. 2225-2227, Nov. 1981.

[243] R. Rotman, O. Raz, and M. Tur, "Analysis of a true time delay photonic beamformer for transmission of a linear frequency-modulated waveform," *J. Lightwave Technol.,* vol. 23, no. 12, pp. 4026-4036, Dec. 2005.

[244] M. Pollakowski and H. Ermert, "Chirp signal matching and signal power optimization in pulse-echo mode ultrasonic nondestructive testing," *Ultrasonics, Ferroelectrics and Frequency Control, IEEE Transactions on,* vol. 41, no. 5, pp. 655-659, Sep. 1994.

[245] S. Matsumoto, M. Takabayashi, K. Yoshiara, T. Sugihara, T. Miyazaki, and F. Kubota, "Tunable dispersion slope compensator with a chirped fiber grating and a divided thin-film heater for 160-Gb/s RZ transmissions," *IEEE Photon. Technol. Lett.,* vol. 16, no. 4, pp. 1095-1097, Apr. 2004.

[246] M. H. Khan, H. Shen, Y. Xuan, L. Zhao, S. Xiao, D. E. Leaird, A. M. Weiner, and M. Qi, "Ultrabroad-bandwidth arbitrary radiofrequency waveform generation with a silicon photonic chip-based spectral shaper," *Nature Photon.,* vol. 4, no. 2, pp. 117-122. 2010.

PUBLICATION LIST

Refereed journal papers

1 **C. Wang** and J. P. Yao, "Complete characterization of optical pulses based on temporal interferometry using an unbalanced temporal pulse shaping system," *IEEE/OSA Journal of Lightwave Technology*, accepted.

2 Z. Li, **C. Wang**, M. Li, H. Chi, X. Zhang and J. P. Yao, "Instantaneous microwave frequency measurement using a special fiber Bragg grating," *IEEE Microwave and Wireless Components Letters*, vol. 21, no. 1, pp. 52-54, Jan. 2011.

3 M. Li, **C. Wang**, W. Li and J. P. Yao, "An unbalanced temporal pulse shaping system for chirped microwave waveform generation," *IEEE Transactions on Microwave Theory and Techniques*, vol. 58, no. 11, pp. 2968-2975, Nov. 2010.

4 **C. Wang**, M. Li and J. P. Yao, "Continuously tunable photonic microwave frequency multiplication based on unbalanced temporal pulse shaping," *IEEE Photonics Technology Letters*, vol. 22, no. 17, pp. 1285-1287, Sep. 2010.

5 **C. Wang** and J. P. Yao, "Large time-bandwidth product microwave arbitrary waveform generation using a spatially discrete chirped fiber Bragg grating," *IEEE/OSA Journal of Lightwave Technology*, vol. 28, no. 11, pp.1652-1660, Jun. 2010.

6 M. H. Asghari, **C. Wang**, J. P. Yao and J. Azaña, "High-order passive photonic temporal integrators," *Optics Letters*, vol. 35, no. 8, pp. 1191-1193, Apr. 2010.

7 H. Xia, **C. Wang**, S. Blais, and J. P. Yao, "Ultrafast and precise interrogation of fiber Bragg grating sensor based on wavelength-to-time mapping incorporating higher-order dispersion," *IEEE/OSA Journal of Lightwave Technology*, vol. 28, no. 3, pp. 254-261, Feb. 2010.

8 **C. Wang** and J. P. Yao, "Fourier transform ultrashort optical pulse shaping using a single chirped fiber Bragg grating," *IEEE Photonics Technology Letters*, vol.21, no. 19, pp. 1375-1377, Oct. 2009.

9 S. Yang, **C. Wang**, H. Chi, X. Zhang, S. Zheng, X. Jin, and J. P. Yao, "Photonic analog-to-digital converter using Mach-Zehnder modulators having identical half-wave voltages with improved bit resolution," *Applied Optics*, vol. 48, no. 25, pp. 4458-4467, Aug. 2009.

10 **C. Wang** and J. P. Yao, "Chirped microwave pulse generation based on optical spectral shaping and wavelength-to-time mapping using a Sagnac-loop mirror incorporating a chirped fiber Bragg grating," *IEEE/OSA Journal of Lightwave Technology*, vol. 27, no. 16, pp. 3336-3341, Aug. 2009.

11 **C. Wang** and J. P. Yao, "Simultaneous Optical Spectral Shaping and Wavelength-to-Time Mapping for Photonic Microwave Arbitrary Waveform Generation," *IEEE Photonics Technology Letters*, vol.21, no. 12, pp. 793-795, Jun. 2009.

12 **C. Wang** and J. P. Yao, "Chirped microwave pulse compression using a photonic microwave filter with a nonlinear phase response," *IEEE Transactions on Microwave Theory and Techniques*, vol. 57, no. 2, pp. 496-504, Feb. 2009.

13 **C. Wang** and J. P. Yao, "Photonic generation of chirped microwave pulses using superimposed chirped fiber Bragg gratings," *IEEE Photonics Technology Letters*, vol. 20, no. 11, pp. 882-884, Jun. 2008.

14 **C. Wang** and J. P. Yao, "Photonic generation of chirped millimeter-wave pulses based on nonlinear frequency-to-time mapping in a nonlinearly chirped fiber Bragg grating," *IEEE Transactions on Microwave Theory and Techniques*, vol. 56, no. 2, pp. 542-553, Feb. 2008.

15 **C. Wang**, F. Zeng, and J. P. Yao, "All-fiber ultrawide band pulse generation based on spectral shaping and dispersion-induced frequency-to-time conversion," *IEEE Photonics Technology Letters*, vol. 19, no. 3, pp. 137-139, Feb. 2007.

Conference papers and talks

1 **C. Wang** and J. P. Yao, "Complete pulse characterization based on temporal interferometry using an unbalanced temporal pulse shaping system," *2010 International Topical Meeting on Microwave Photonics*, 5-9 Oct. 2010, Montreal, Canada. (**Best Student Paper Award**)

2 **C. Wang** and J. P. Yao, "Advanced fiber Bragg gratings for photonic generation and processing of arbitrary microwave waveforms," *2010 International Topical Meeting on Microwave Photonics*, 5-9 Oct. 2010, Montreal, Canada. (**Invited paper**)

3 **C. Wang** and J. P. Yao, "Superimposed oppositely chirped FBGs for ultrafast FBG sensor interrogation with significantly improved resolution," *2010 OSA Bragg Gratings, Photosensitivity, and Poling (BGPP) Topical Meeting*, 21-24 Jun. 2010, Karlsruhe, Germany, paper BThB6.

4 **C. Wang** and J. P. Yao, "Nonlinearly chirped microwave pulse generation using a spatially discrete chirped fiber Bragg grating," *2009 IEEE Microwave Photonics Conference*, 14-16 Oct. 2009, Valencia, Spain, paper Th4.27.

5 M. H. Asghari, **C. Wang**, J. P. Yao and J. Azana, "Demonstration of FBG-based first and second-order photonic temporal integrators with optimized energetic efficiencies," *2009 IEEE/Photonics Society Annual Meeting*, 4-8 Oct. 2009, Belek-Antalya, Turkey, paper ThK3.

6 **C. Wang** and J. P. Yao, "Microwave and millimeter-wave arbitrary waveform generation and processing using fiber-optics-based Techniques," *2009 Asia-Pacific Microwave Photonics Conference*, 22-25 Apr. 2009, Beijing, China. **(Best Student Paper Award)**

7 **C. Wang** and J. P. Yao, "Fourier-transform pulse shaping using a single chirped fiber Bragg grating," *2009 Asia-Pacific Microwave Photonics Conference*, 22-25 Apr. 2009, Beijing, China.

8 S. Pan, **C. Wang**, J. P. Yao, "Generation of a stable and frequency-tunable microwave signal using a polarization modulator and a wavelength-fixed notch filter," *2009 Optical Fiber Communication Conference & Exposition and the National Fiber Optic Engineers Conference (OFC/NFOEC)*, 22-26 Mar. 2009, San Diego, CA, USA, paper JWA51.

9 **C. Wang** and J. P. Yao, "Photonic generation and processing of millimeter-wave arbitrary waveforms," *2008 IEEE/LEOS Annual Meeting*, 9-13 Nov. 2008, Newport Beach, CA, USA, paper TuZ1. **(Invited paper)**

10 **C. Wang** and J. P. Yao, "Microwave arbitrary waveform generation based on optical spectral shaping and wavelength-to-time mapping using a chirped fiber Bragg grating," *1st Microsystems and Nanoelectronics Research Conference (MNRC 2008)*, 14-15 Oct. 2008, Ottawa, ON, Canada, pp.57-60.

11 **C. Wang** and J. P. Yao, "Photonic microwave matched filters for chirped microwave pulse compression," *2008 IEEE Microwave Photonics Conference*, 1-4 Oct. 2008, Gold Coast City, Queensland, Australia, pp. 47-50.

12 **C. Wang** and J. P. Yao, "All-optical electrical chirped pulse generation with tunable chirp rate based on a nonlinearly chirped fiber Bragg grating," *2007 IEEE Microwave Photonics Conference*, 3-5 Oct. 2007, Victoria, BC, Canada, pp. 202-205.

13 **C. Wang** and J. P. Yao, "All-optical high-frequency electrical chirped pulse generation using a nonlinearly chirped fiber Bragg grating," *2007 International Symposium on Signals, Systems and Electronics (ISSSE 2007)*, 30 Jul. - 2 Aug. 2007, Montreal, QC, Canada, pp. 625-628.

14 **C. Wang** and J. P. Yao, "All-optical electrical chirped pulse generation based on nonlinear wavelength-to-time conversion in a chirped fiber Bragg grating," *Photonics North 2007*, 4-7 Jun. 2007, Ottawa, ON, Canada, paper 67962K.

VITA

Chao Wang received the B.Eng. degree in Opto-electrical Engineering from Tianjin University, China, in July 2002, and the M.S. degree in Optics from Nankai University, China, in July 2005.

Chao Wang's research area, Microwave Photonics, is an interdisciplinary field that studies the interactions between microwave and lightwaves. During his Ph.D. work, Mr. Wang's research interests include photonic generation and processing of microwave arbitrary waveform, radio-over-fiber systems, coherent optical pulse shaping, optical signal processing, ultrafast optical sensor interrogation, advanced fiber Bragg gratings and their applications in microwave photonics systems. His research has applications for broadband wireless access systems, sensor networks, modern radar systems, satellite communications, and even biomedical imaging.

Mr. Wang is a student member of IEEE/PS, IEEE/MTT-S, OSA and SPIE. He has authored and co-authored 15 journal articles and 14 conference papers during his Ph.D. thesis work. He was the recipient of the Ontario Graduate Scholarship (2008-2009, for international students), the SPIE Scholarship in Optical Science & Engineering (2008), the Chinese Government Award for Outstanding Self-Financed Students Abroad (2009), the IEEE Photonics Society (formerly LEOS) Graduate Student Fellowship (2009), the Vanier Canada Graduate Scholarship (2009-2011), the IEEE Microwave Theory and Techniques Society Graduate Fellowship (2010) and the NSERC Postdoctoral Fellowship (2011-2012).